Chemical and Physical Phenomena Determining Carbon Gasification Reactivity

by

Robert Howard Hurt

B.S., Chemical Engineering
Michigan Technological University
(1982)

Submitted to the Department of Chemical Engineering
in Partial Fulfillment of the Requirements of the Degree of
Doctor of Philosophy

at the

Massachusetts Institute of Technology

August 1987

Signature of Author _____
Department of Chemical Engineering
August 21, 1987

Certified by _____
Adel F. Sarofim
Professor of Chemical Engineering
Thesis Supervisor

Certified by _____
John P. Longwell
Professor of Chemical Engineering
Thesis Supervisor

Accepted by _____
Robert C. Armstrong
Chairman, Committee on Graduate Students

CHEMICAL AND PHYSICAL PHENOMENA DETERMINING CARBON GASIFICATION REACTIVITY

by

ROBERT HOWARD HURT

Submitted to the Department of Chemical Engineering
on August 21, 1987 in partial fulfillment of the
requirements for the Degree of Doctor of Philosophy
in Chemical Engineering

Abstract. It was undertaken in this thesis to investigate the role of coal type, or maceral composition, of microporous surface area, and of reaction-induced carbon densification in carbon gasification. To accomplish this, low temperature gasification rates in oxygen and carbon dioxide were measured in a thermogravimetric analyzer for two synthetic carbons, various coal chars, and chars from several individual coal lithotypes. In addition, the carbons and chars at various stages of gasification conversion were microscopically examined and their pore structures characterized by vapor adsorption techniques.

It was found that microporous surface area participates in the gasification of pure carbons. Further, reactant penetration into microporous regions was complete for Spherocarb, a highly macroporous synthetic carbon with correspondingly small microporous regions. The accessible total surface area for Spherocarb is, then, the 636 m^2/gm measured by carbon dioxide adsorption, and the intrinsic rate of oxidation of this carbon in .21 atm. O_2 is given by:

$$\text{Rate } (gm/sec\text{-}m^2) = 3.0 \cdot 10^3 e^{-36/RT}$$

with R in kcal/gmol ^oK. There is some evidence, on the other hand, that restricted diffusion prevents complete reactant penetration into the microporous regions of a sucrose carbon which has limited macroporosity and thus large microporous regions.

It was also found that the rate of catalyzed gasification of impure carbons can bear no apparent relationship to measured surface area, depending instead on properties of the catalyst. The normalization of the rate of catalyzed gasification by microporous surface area is, in such a case, inappropriate, and the process of catalyzed gasification can not be treated as a total surface area evolution problem with an altered or adjustable intrinsic surface reactivity. Since chars from many naturally-occurring organic parent materials are rich in potentially catalytic inorganic matter, the use of surface area to normalize the gasification rates of many coal chars may be inappropriate.

Chars from individual macerals from a sub-bituminous coal had very different gasification reactivities, due to catalysis by differing amounts of naturally occurring, ion-exchanged inorganic matter. This effect is expected to be most important for low-rank coals with their high oxygen contents and correspondingly high ion-exchange capacities.

Finally, it was shown that kinetically-limited carbon gasification does not take place at constant particle diameter as heretofore widely assumed, but is accompanied by reaction-induced atomic rearrangements, which lead to densification and particle shrinkage.

Shrinkage has a major effect on pore structure evolution during Spherocarb gasification, and measured surface areas are in pronounced disagreement with the predictions of existing models which do not account for particle shrinkage. Models have been developed of gasification with concurrent densification which can account for much or all of the discrepency between data and constant volume models.

Thesis Supervisors: Dr. Adel F. Sarofim
Dr. John P. Longwell

Acknowledgements

I would like to thank Exxon Research and Enginineering Corporation and the National Science Foundation for support of this research and my graduate studies. There are many people in various capacities who have made technical contributions to this thesis. Foremost among them are my advisors Professors Adel Sarofim and Jack Longwell. Their insights were always valuable and their patience often remarkable. I would also like to acknowledge the technical contributions of and to thank the members of my committee, Professors Jack Howard and James Wei, my UROP students Larry Polleti, Andy Gengos, and Farzan Riza, and many others including Joe Floess, Ziyou Du, Dave Dudek, Tony Modestino, Matteo D'Amore, Tom Hastings, Lenny Sudenfield, Mim Rich, Chuck Mims, and Jenny Devaud.

Many other people, primarily fellow students, offered technical consultation, various other forms of assistance, and/or their friendship. Among this group I would like to thank John Nenniger for his generous help in the summer of '82; my office mates past and present, especially Andreas Kridiotis for his lack of furious activity, Mike Snow, Judy (Tex) Wornat for her southern congeniality, Karl Graham for his lessons on cattle nomenclature, and Joe Helbe for his untiring defense of the "Land of Fun"; Bob Didinato the German Italian American, and the Goethe Institute; the crew in the basement including Craig Vaughn, Tom and Daniel McKinnon, Fred and his wife; Larry, Kevin, Robert, Dennis, and Danny; and Andy Bommarius für seine Ratschläge.

I would like to thank my father and my parents-in-law for their encouragement and support, and my wife for her love, patience, and income.

Finally, I would like to dedicate this thesis to my mother, who thought that I should be an engineer before I knew what one was, but who was unable to see the completion of my studies.

To Patricia J. Hurt

TABLE OF CONTENTS

List of Figures

(excluding digest and appendices)

List of Tables

DOCTORAL THESIS DIGEST

CHEMICAL AND PHYSICAL PHENOMENA DETERMINING CARBON GASIFICATION REACTIVITY

by

ROBERT HOWARD HURT

THESIS SUPERVISORS: A.F. SAROFIM
J.P. LONGWELL

Doctoral Thesis Submitted to the Department of Chemical Engineering, Massachusetts Institute of Technology, Cambridge, MA 02139

August 7, 1987

D1. Introduction and Background

Carbon, as the term will often be used in this thesis, refers not to an entry in the periodic table, but to a class of solid materials containing primarily carbon, made by heating an organic substance in the absence of air.

Carbons participate in high temperature reactions with a variety of gaseous species, in which the solid carbon is consumed and new gaseous species are produced. These are the so-called gas reactions of carbon, and the set of gaseous reactants includes oxygen, carbon dioxide, hydrogen, and water vapor.

The gas reactions of carbon are fundamental to many commercial endeavors, including coal gasification and combustion, the production of activated carbon, and those applications in which carbon is used as an engineering material. The gasification reactivity of carbons is especially important in many gasification processes, determining equipment size and/or carbon conversion efficiency(D1). Under most conditions, the total time required for the gasification of a coal particle is dominated by the burn-out of the residual char remaining after devolatilization. The design of many gasifiers is thus carbon reactivity limited and, in fact, many gasifiers operate with significantly less than 100% carbon conversion despite strong economic incentives to use coal efficiently.

Because of its importance a large body of research on coal char gasification kinetics has accumulated, whose goal is to predict the effect of reactant gas composition, pressure, temperature, coal type,

char preparation and prior gasification history on the gasification rate and the product distribution.

D1.1 Problem statement.

This thesis concerns itself with several aspects of the relationship between carbon properties and carbon gasification reactivity. Reactivity in the carbon-oxygen system per unit internal surface area, corrected for external and pore diffusion limitations, has been shown to vary by as much as four orders of magnitude at a given temperature and oxygen partial pressure(D2). There is, at present, an inadequate understanding of the phenomena that determine the rate at which a given carbon will gasify.

Identification and fundamental understanding of the important phenomena could guide the design of gasification processes to enhance char reactivity, and thus improve performance. The fundamental approach should best start with phenomena determining the accessible surface area for gasification, from which a meaningful intrinsic rate can be calculated. This intrinsic rate would be a true property of the carbon surface, and could potentially be fundamentally related to (or at least correlated with) other properties of the carbon surface.

D1.2 The appropriate total surface area for gasification.

There is, at present, much uncertainty about the effective total surface area for gasification. It is well known that carbon surface areas measured by vapor adsorption techniques are often a strong function of the size of the adsorbate molecule. For example, large

discrepancies between areas measured by carbon dioxide and nitrogen are quite common, and Nandi et al.(D3) have presented good evidence that they are associated with the occurrence of restricted diffusion in carbon micropores.

Restricted diffusion occurs when the size of the pore approximates the size of the diffusing molecules. The diffusing molecules, then, are at all times under the influence of the potential energy field associated with the adjacent pore walls, and the rate of diffusion is slow, activated, and very sensitive to the size of the pores and the size and shape of the diffusing species(D4). Restricted diffusion is commonly observed for a variety of gases including nitrogen and carbon dioxide in both zeolites and coals or carbons(D4).

Because most of the surface area in high-area carbons lies in the micropores, the identification of the appropriate total surface area for gasification is equivalent to understanding the role of the microporous surface area. There is much confusion in the literature surrounding this topic, as well as a lack of experimental information.

Johnson(D5), for example, has cited evidence for micropore widening during gasification of coal chars, while Rist et al.(D6) observed a characteristic micropore diameter of 20 Å, independent of conversion. Dutta observed that the rates of gasification of his chars were proportional to the surface area lying in pores with diameters larger than 30 Å(D7), while there was evidence for micropore widening and thus microporous reaction during the gasification of an anthracite char(D8).

D1.3 The phenomenon of gasification induced carbon particle shrinkage.

Dudek(D9), in a parallel study at M.I.T., during single particle gasification experiments in an electrodynamic balance, has observed significant diameter reduction during air-oxidation of Spherocarb carbon particles under conditions where no preferential gasification on the external
surface is expected. The origin of this phenomenon was unknown at the outset, as were its implications to gasification behavior.

D1.4 The effect of coal type or maceral composition.

Another variable which may have an important influence on gasification reactivity is petrographic composition, or coal type. Type refers to the classification of a coal according to its vegetable matter composition at the start of coalification, in contrast to rank, which is a measure of the extent of coalification, or geologic age. All coals are composed of microscopic, optically homogeneous materials that have been called macerals (in an analogy to inorganic minerals). In addition, characteristic groupings of macerals occur, called lithotypes, which give coals their more or less pronounced macroscopic banding. It is the relative proportion and spatial arrangement of the different macerals and minerals which distinguishes coals by type(D10).

Whereas a correlation between coal rank and char gasification reactivity has been noted(D11), relatively little is known about the relationship between maceral composition (coal type) and reactivity.

D1.5 Thesis objectives.

This thesis addresses several aspects of the relationship between carbon reactivity and carbon properties. The first, which is summarized in section 3, is the identification of the accessible total surface area for carbon gasification. This is an endeavor which is important in the successful development of correlations of carbon reactivity, and in the development of gasification or pore structure models. The lack of knowledge of the appropriate area is, in addition, a major stumbling block to the measurement of meaningful intrinsic reactivities and thus the attainment of a more fundamental understanding of the factors determining carbon gasification reactivity. We hoped to identify the effective surface area for the gasification of several carbons, and, further, to understand the factors that determine the effective area for carbons in general.

Secondly, as summarized in section 4, it was undertaken in this thesis to investigate the phenomenon of gasification-induced carbon densification/shrinkage observed in this lab by Dudek(D9). The first goal was to find an explanation for the observed diameter reduction during gasification of Spherocarb carbon, the second to measure diameter reduction during the gasification of other chars, and the third to understand the influence of the phenomenon on surface areas, and to develop models of surface area evolution during gasification with concurrent shrinkage.

Finally, in section 5, we look at an important topic which has thus far received insufficient attention: the effect of coal type on coal char gasification reactivity. Our goal was to measure the

reactivities of chars from maceral concentrates separated from one coal to directly assess the importance of type to its gasification behavior, and hopefully to gain some insight into the role of coal type for other coals.

D2. Materials and Experimental Procedures

This thesis presents experimental results obtained for Spherocarb carbon and chars from a Utah sub-bituminous coal, Pittsburgh #8 high-volatile bituminous coal, a Montana lignite, reagent grade sucrose, and a sucrose and carbon black composite. Chars were made from the various organic parent materials by heat treatment in nitrogen in a small tube-furnace, at 1000 ^{o}C for one hour. Chars at various stages of gasification conversion were produced by reaction in a thermo-gravimetric analyzer or, for larger samples, in a small-tube furnace.

Many carbon particles at various stages of conversion were examined in this study by S.E.M. and by optical microscopy. A technique was developed, whereby an S.E.M. micrograph could be obtained of the fine features on the external surface of a given particle in a given orientation at several stages of conversion. This required that the particle be mounted in a holder that is stable and inert under gasification conditions, is preferably electrically conductive to improve the S.E.M. image, and can be mounted on an S.E.M. stub; and that the S.E.M. preparation does not destroy or contaminate the particle.

The successful particle mounting consisted of a 1 cm cube of

graphite, covered with platinum foil, with conical pits indented in the surface with a sharp instrument, into which the carbon particles of interest were lightly pressed. The graphite was observed to undergo little gasification in the T.G.A. under the conditions used, and the mounting produced a good S.E.M. image with relatively little charging. At least a complete hemisphere was visible for most particles, and enough (about 80%) of the particles maintained their original orientation upon handling to make the technique useful.

Nitrogen and carbon dioxide adsorption isotherms and adsorption equilibration times were measured for many of the carbons in a volumetric adsorption apparatus. The apparatus and procedures are similar to those described by Floess(D12). Adsorption isotherms of carbon dioxide were measured at 0 ^{o}C in an ice bath, and those of nitrogen at 77 ^{o}K in a liquid nitrogen bath. Surface areas were calculated from the carbon dioxide isotherms using the Dubinin-Polanyi equation, and from the nitrogen isotherms using the B.E.T. equation.

The rate of carbon dioxide uptake into initially evacuated carbon samples at an initial carbon dioxide pressure of approximately 5 torr was measured for several carbons.

Gasification rates were measured with a Cahn thermogravimetric analyzer (T.G.A.) by a procedure similar to that described by Floess(D12). The reaction rate was maintained below .2 mg/min to avoid the effects of external or intra-bed mass and heat transfer limitations(D12). Gasification reactivities were, in fact, found to be independent of bed size under several conditions tested here (each with a gasification rate <.2 mg/min).

3. The Role of Microporous Surface Area in Carbon Gasification

In this section we are concerned with identifying the accessible total surface area for gasification, which, as discussed in the introduction, is a logical starting point in the quest for an improved fundamental understanding of the factors that determine carbon gasification reactivity.

D3.1 Approach.

In this study, we attempted to understand the role of microporous surface area during the gasification of Spherocarb carbon, sucrose carbon, and various chars of the P.S.O.C. sub-bituminous coal. A number of experimental and analytical techniques were applied in this study which are capable of providing information on the role of microporosity in gasification.

A change in micropore dimensions is one indication of gasification within micropores and was detected here using information from vapor adsorption methods. A gasification mode in which reaction were confined to the surface of large pores, would result in macropore growth, which would potentially be visible upon examination of particle surface features before and after gasification. Individual fine features on the surfaces of carbon particles were therefore examined as a function of gasification conversion by the captive-particle S.E.M. technique.

The quantitative determination of the accessible surface area for gasification is equivalent to finding the reaction effectiveness factor η. The effect of particle size on the reactivities of several carbons

was measured, to provide information on the extent of reactant penetration and thus the reaction effectiveness factor. Finally, η was estimated from an analysis based on measured carbon dioxide diffusion times during vapor adsorption experiments.

D3.2 Results and Discussion.

D3.21 Data summary. In order to understand the role the microporous surface area in the gasification of the various carbons in this study, we consider the following distinguishing features of the experimental results.

1) The gasification rate of sucrose carbon in figure 3.5 is a function of particle size, under conditions for which a classical calculation of the effectiveness factor for Knudsen diffusion in 12.5 Å diameter pores (average pore size for a measured surface area of 800 m^2/gm, a measured porosity of .25, and a particle density of 1.0 gm/cc) with an assumed tortuosity factor of 5, and a measured porosity of .25 predicts essentially complete reactant penetration and thus no particle-size effect. The experimental determination of the effect of particle size on reactivity is a classical test for the extent of reactant penetration, and the results in figure 3.5 suggest that only a portion of the total surface area is available, and that carbon dioxide diffusion in sucrose micropores is significantly slower than Knudsen diffusion with a tortuosity factor of 5. The gasification rate of Spherocarb carbon was, on the other hand, essentially independent of particle

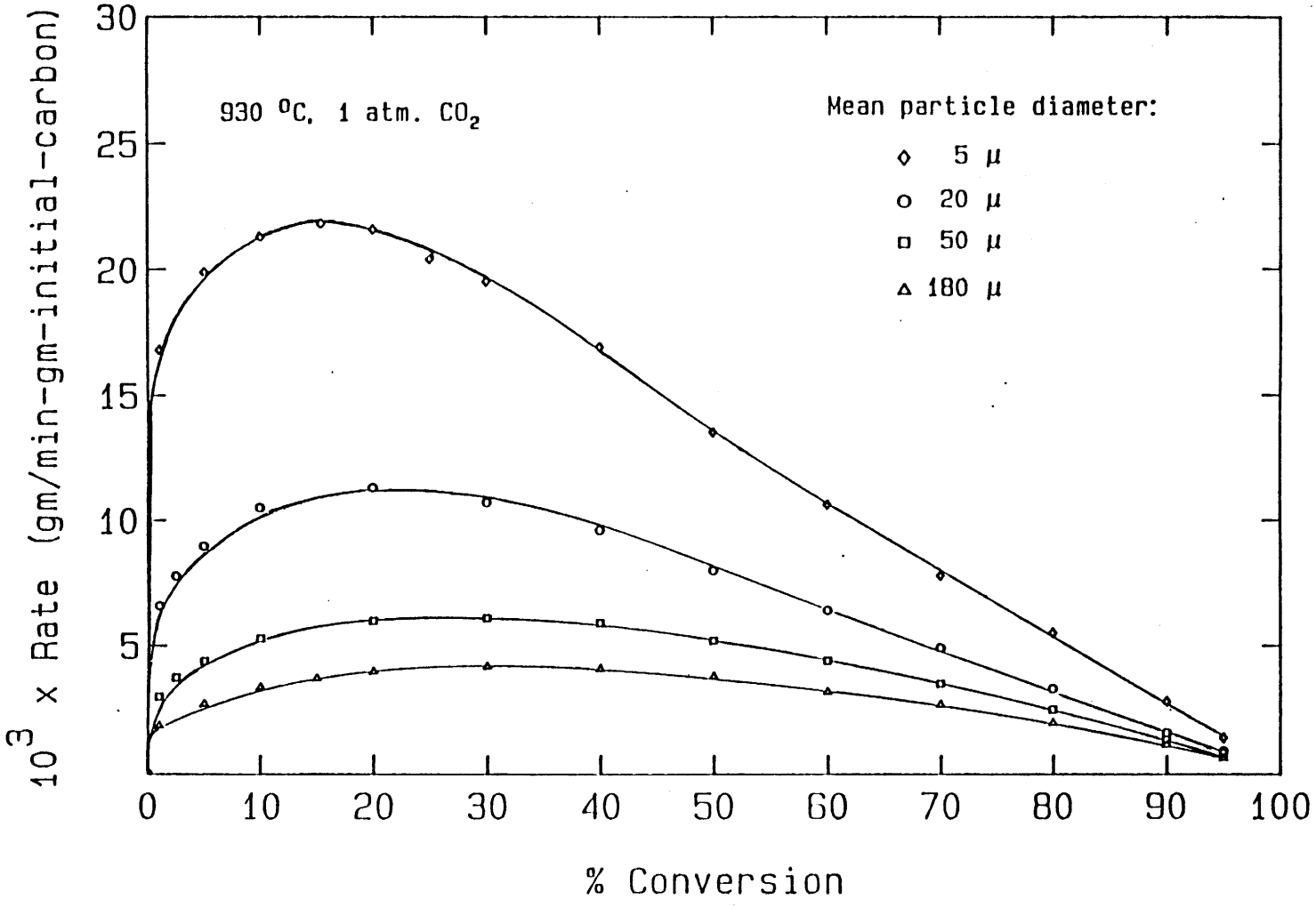

Figure 3.5

Gasification Reactivity of Sucrose Carbon

size in air, as shown in figure 3.2, and in a carbon dioxide/carbon monoxide mixture.

2) The gasification reactivity of the 1200 ^{o}C char from the acid-washed subbituminous coal bears no apparent relation to the char's total surface area, as seen in figure 3.16.

3) All features > 100 nm on the surfaces of sucrose and Spherocarb carbon particles are preserved during gasification, as seen in several sample photograhs in figure 3.1 taken using the captive-particle S.E.M. technique. There is evidence of uneven gasification of the external surface of the acid-washed sub-bituminous coal char, on the other hand, apparently in the form of production of approximately circular pits, as also seen in figure 3.1.

4) The Dubinin gradients in figure 3.11, which are qualitative indicators of micropore size, increase with conversion for the sucrose carbon, but are constant throughout conversion for the sub-bituminous coal chars.

5) The molecular sieve nature of sucrose carbon, as evidenced by the large difference between its nitrogen and carbon dioxide surface areas, is destroyed rapidly by gasification, as seen in figure 3.9. The sub-bituminous coal chars also exhibit a molecular sieve nature, which, however, is only gradually destroyed throughout conversion, as shown in figure 3.14.

6) The carbon dioxide adsorption equilibration time is much longer for unreacted sucrose carbon than for unreacted or partially reacted Spherocarb or for partially reacted sucrose carbon.

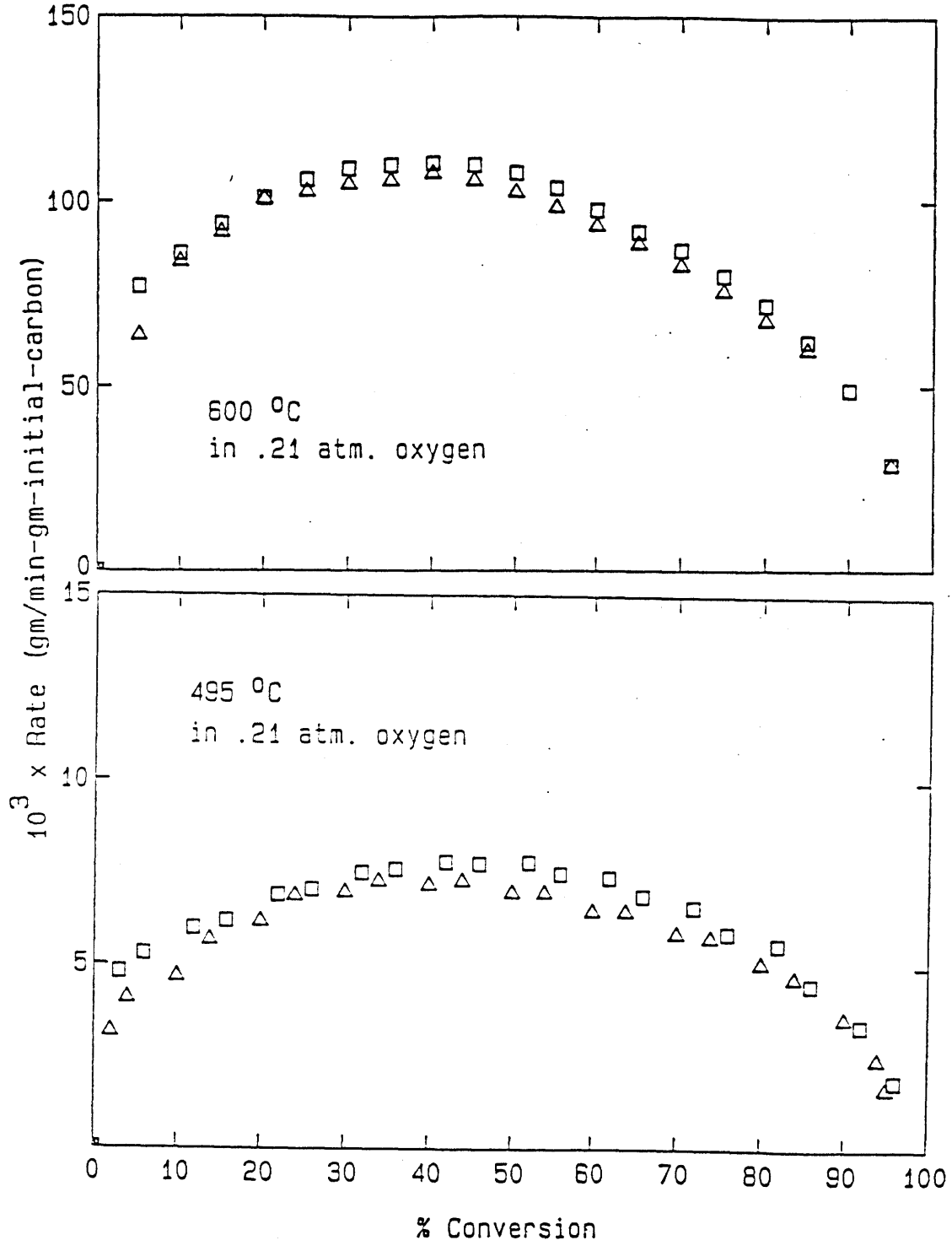

Figure 3.2
Oxidation Reactivity of Spherocarb

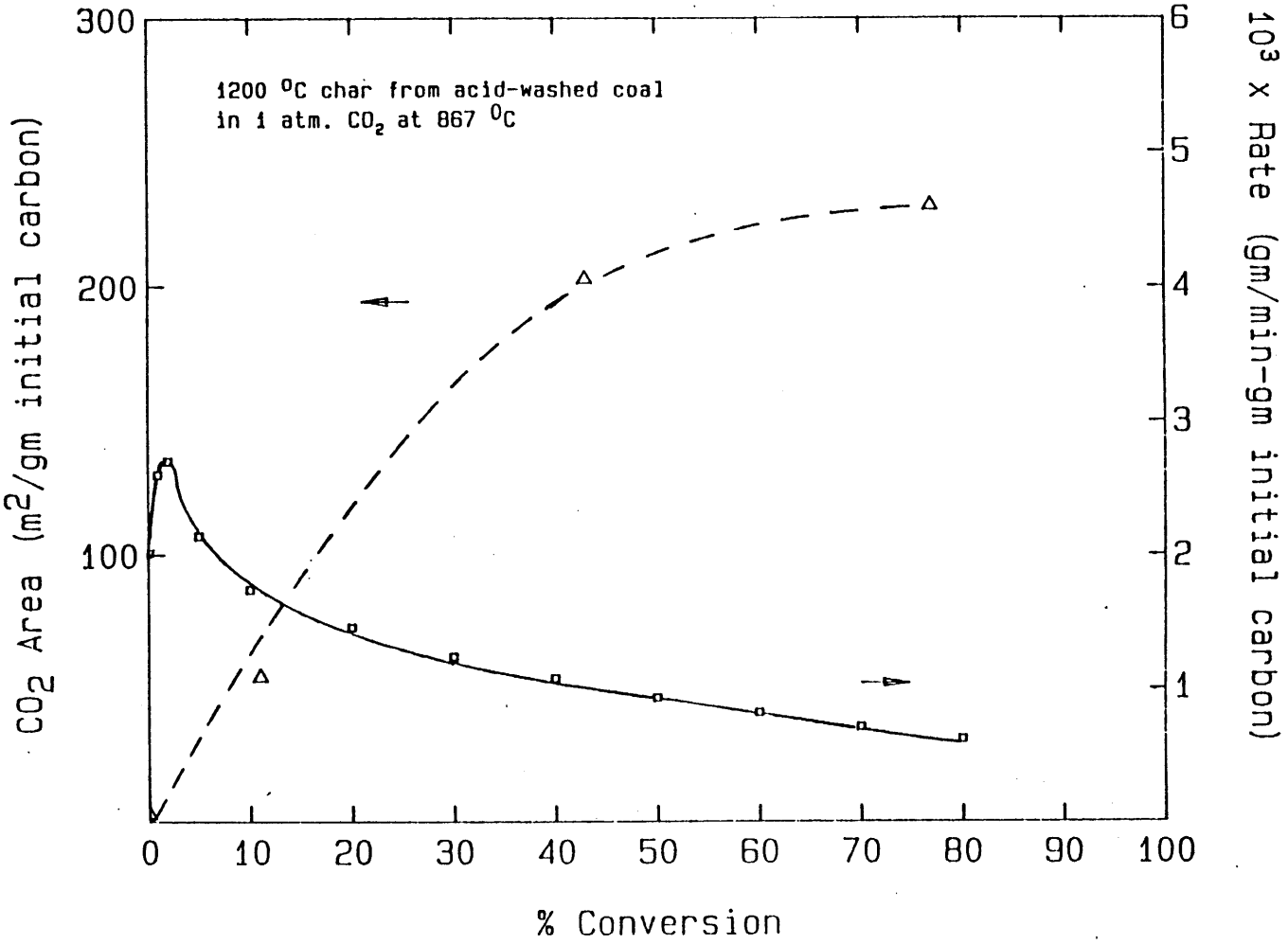

Figure 3.16

Reactivity and Area Evolution of High Temp. Coal Char

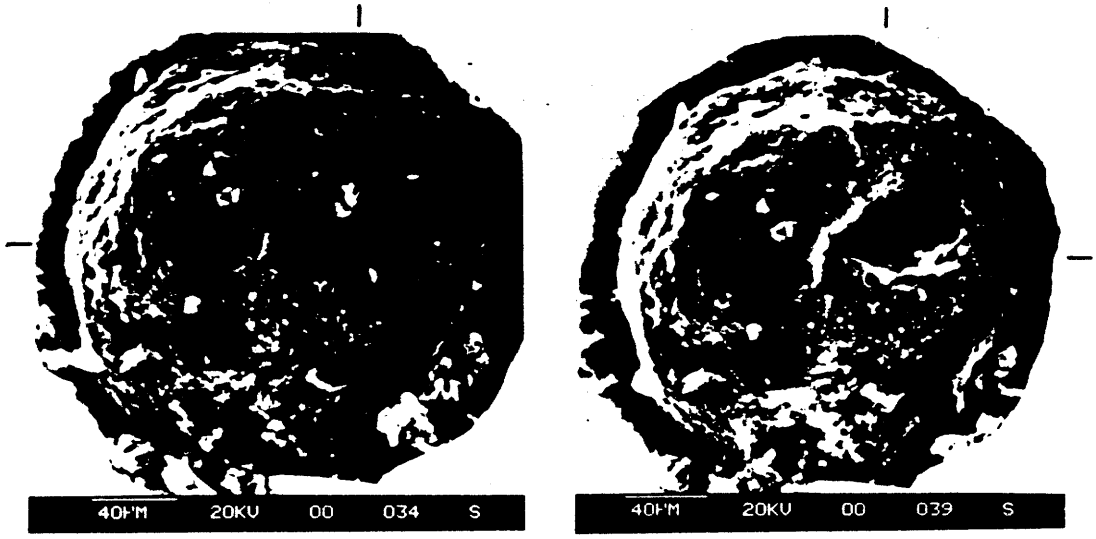

Unreacted

20% Conversion

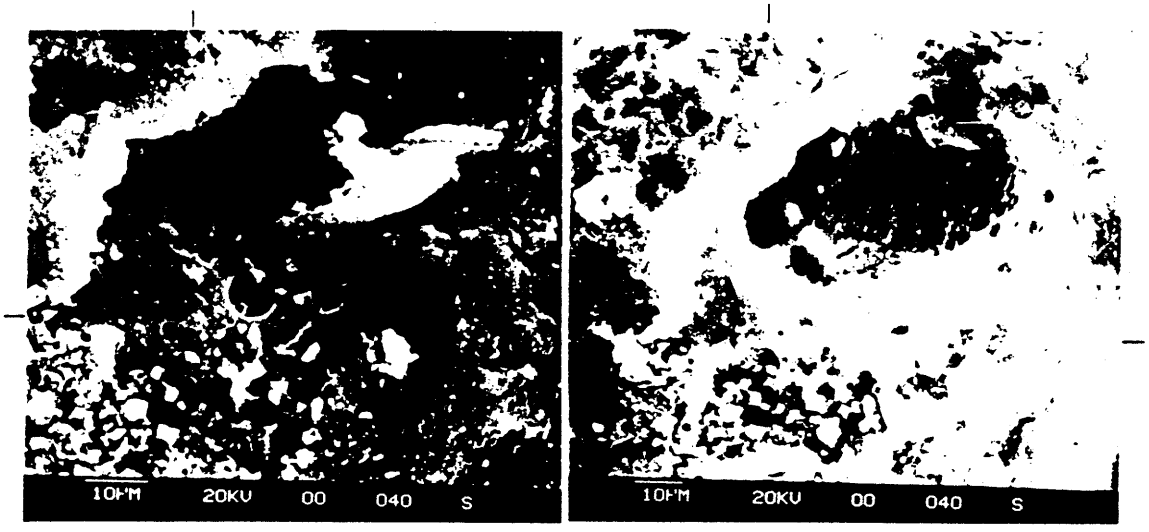

Unreacted

20%
Conversion

Spherocarb in .21 atm. O_2, 495 °C
Set of micrographs at increasing magnification

Figure 3.1 Photographs and S.E.M. Micrographs

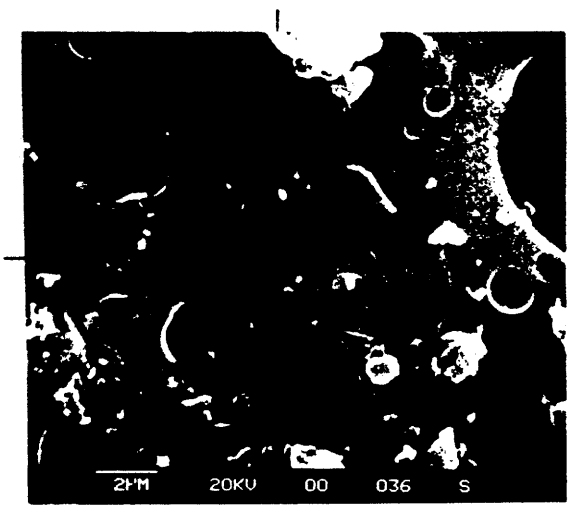

Unreacted

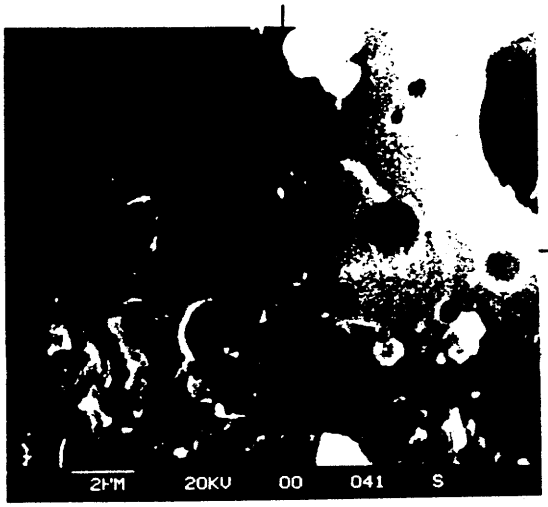

20%
Conversion

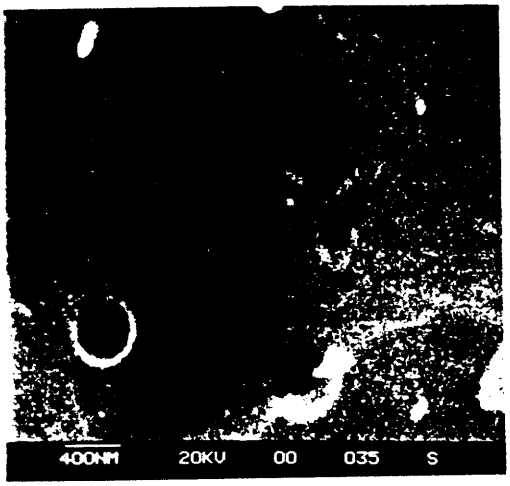

Unreacted

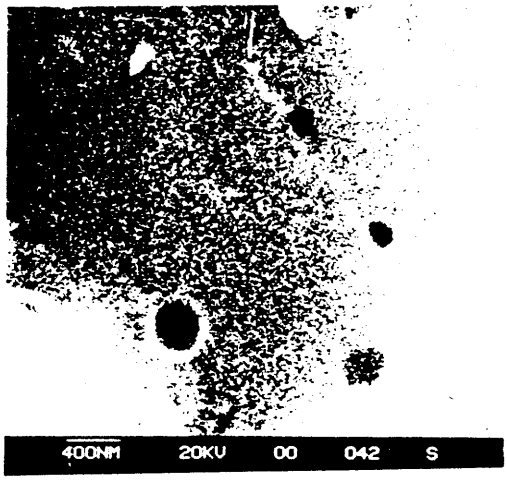

20% Conversion

Spherocarb in .21 atm. O_2, 495 °C
Set of micrographs at increasing magnification, continued

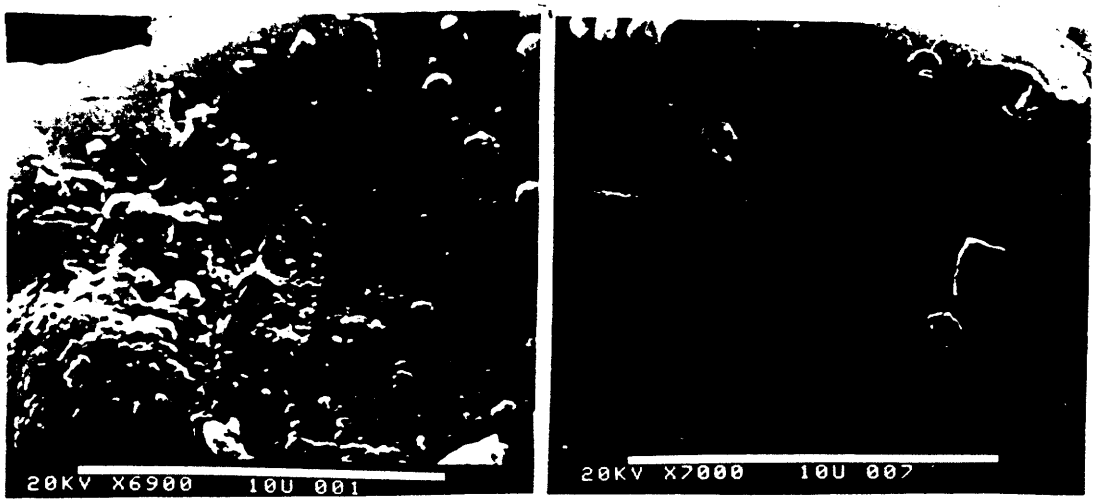

0% conversion

29% conversion

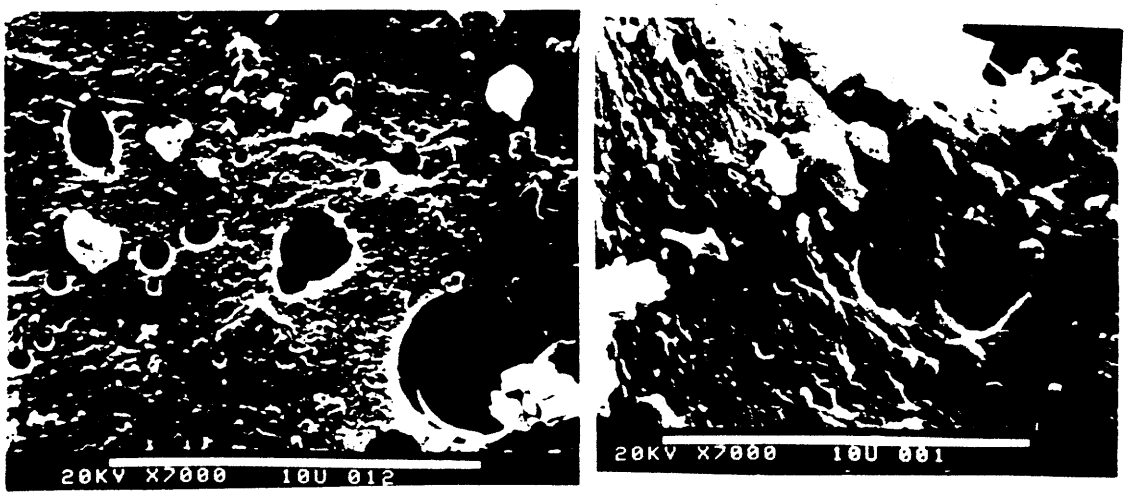

41% conversion

77% conversion

Acid-washed sub-bituminous coal char
in 1 atm. CO_2 at 860 ^{o}C

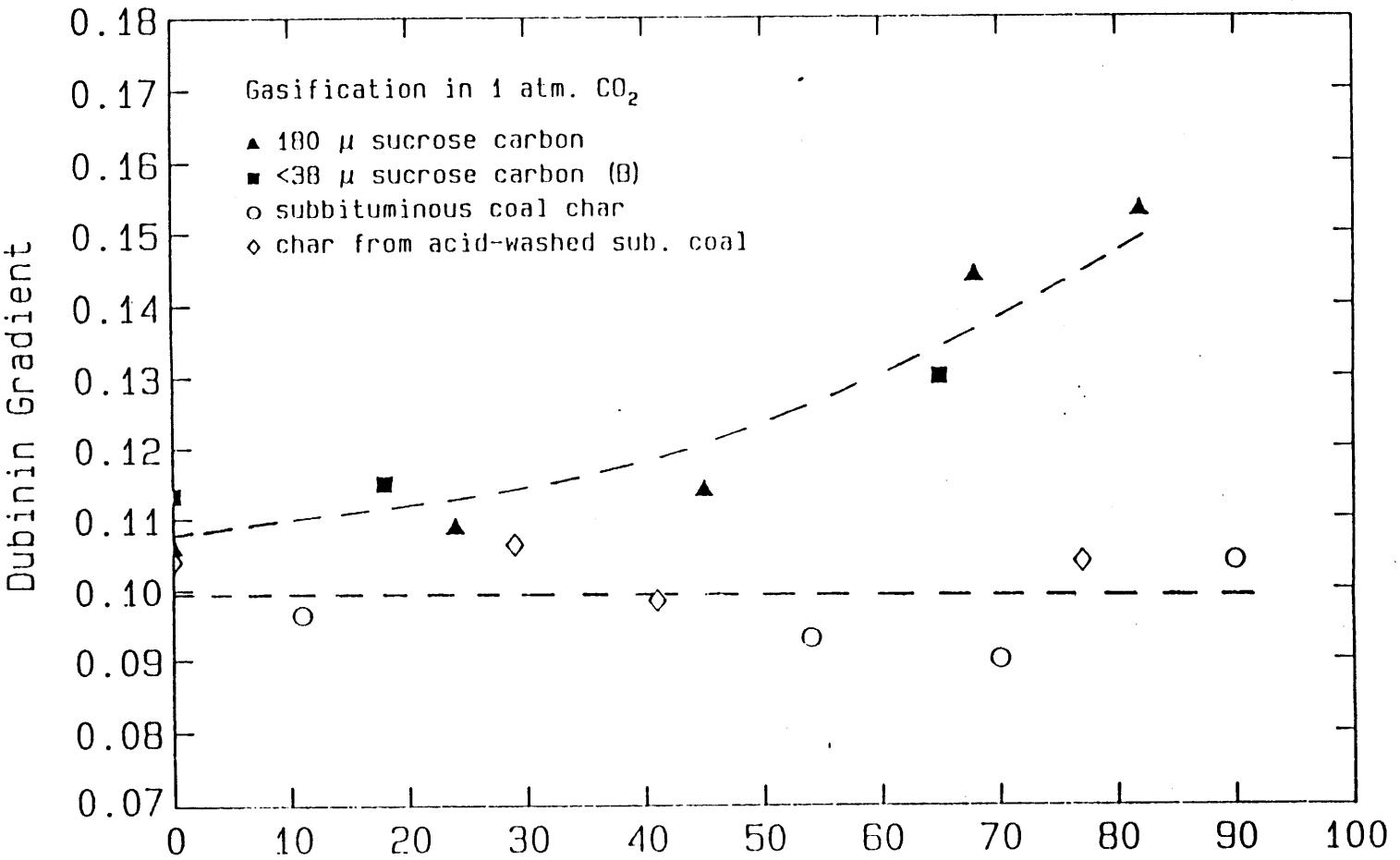

Figure 3.11

Effect of Conversion on the Dubinin Gradient

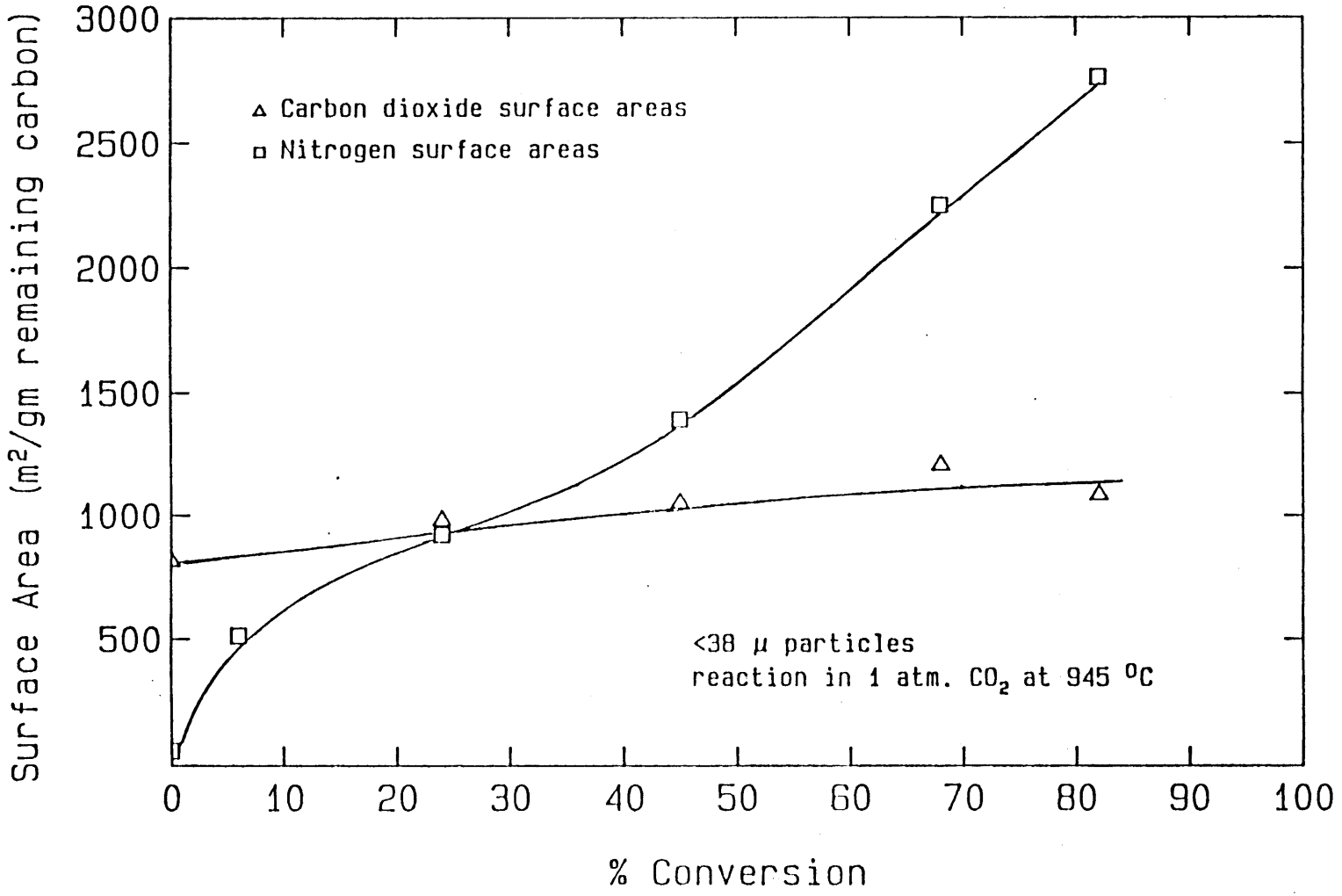

Figure 3.9
Sucrose Carbon Surface Area Evolution

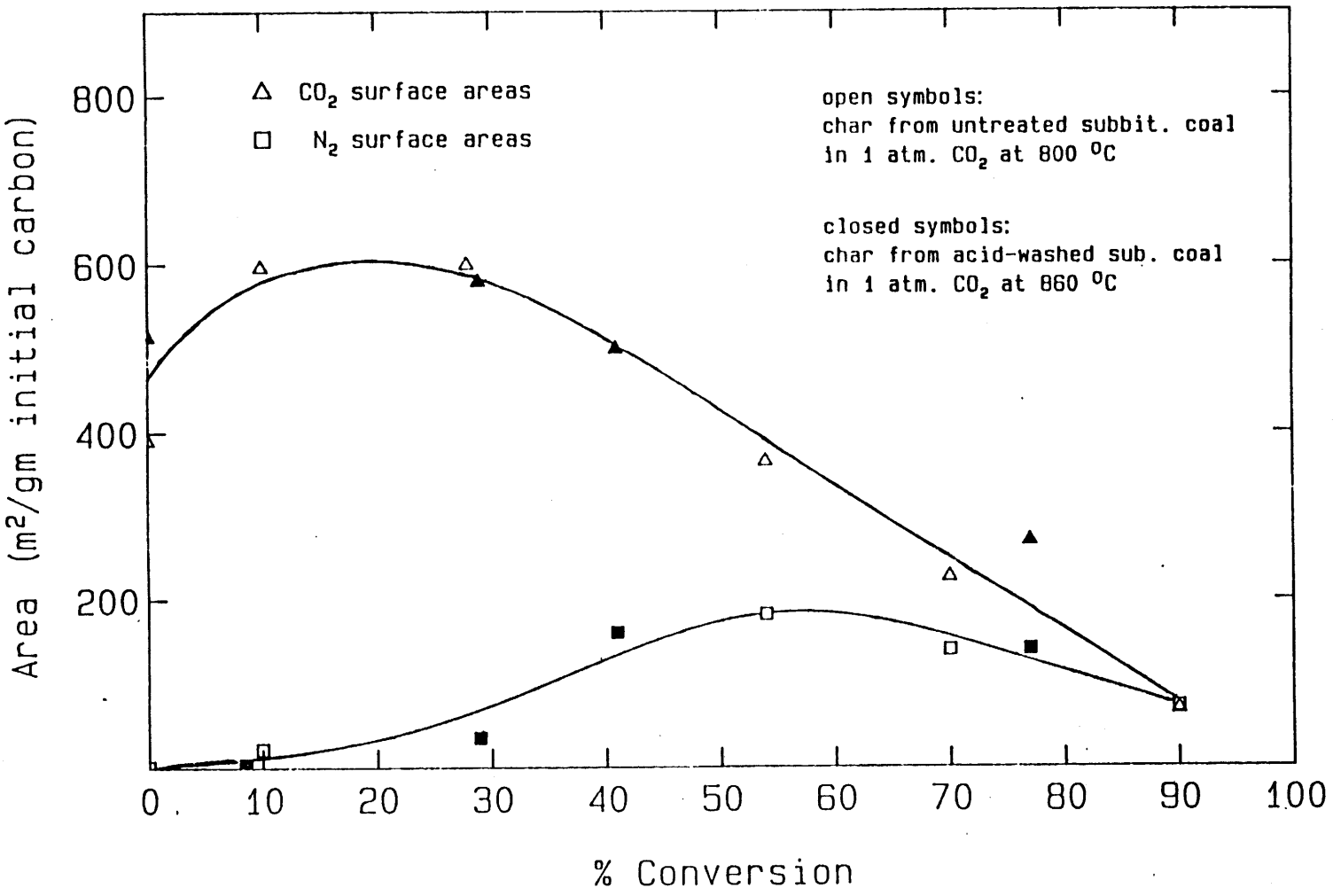

Figure 3.14
Coal Char Surface Area Development

In the following sections, we attempt to understand the role of microporous surface area for sucrose and Spherocarb carbons by considering possible diffusion limitations within microporous grains lying between larger pores. The coal chars, on the other hand, behave much differently from the two pure carbons, and the hypothesis is developed in the following sections that mineral matter catalysis determines the coal char behavior, including the role of the microporous surface area. In light of this, the coal chars and the pure carbons are discussed separately, after the following general discussion of the role of microporous diffusion limitations in gasification.

D3.22 Microporous diffusion limitations. Since diffusion of gasification reagents in carbon micropores may be in the restricted diffusion range and thus very much slower than molecular or Knudsen diffusion, there exists the possibility of diffusion limitations within microporous regions or "grains" lying between larger pores, under conditions where there are no diffusion limitations in the larger pores themselves. The severity of microporous diffusion limitations scales as L^2/D, where D is the local microporous diffusivity, a parameter which depends upon micropore size, and L is the characteristic size of the microporous regions, a parameter determined by the extent of carbon macroporosity.

Microporous diffusion limitations will give rise to an effect of particle size on reactivity, whose magnitude will depend upon the relative sizes of the microporous grains and the carbon particle. In the limit of very small microporous grains there will be no effect of

particle size, as fracture of the particle may be expected to occur without significant fracture of the small microporous grains in which the diffusion limitations actually lie. The particle size effect will be larger, however, for systems with less macroporosity, and thus with a larger characteristic grain radius. In the presence of severe microporous diffusion limitations, reactant penetration into microporous regions would be very limited, and the reaction front would be essentially confined to the surfaces of larger pores. Gasification in this mode would be accompanied by macropore growth, which would be potentially observable by microscopy. Gasification of highly microporous chars occuring within micropores, in contrast, would not be accompanied by observable macropore growth or by any other observable changes in the external particle surface. This is true because the extent of surface recession is of the same order as the characteristic distance between micropores, which can be shown to be of order 30 Å.

D3.23 The role of micropores in the gasification of the pure carbons. The preservation of even the finest surface features visible by S.E.M. during gasification of both Spherocarb and sucrose carbon indicates that the reaction is not confined to large-pore surfaces but occurs instead uniformly throughout the structure at this resolution, in pores invisible to S.E.M. Evidence for micropore widening during gasification, and thus additional evidence for reaction in micropores comes from the measurement of carbon dioxide and nitrogen surface areas for a set of sucrose carbons at various stages of gasification conversion. The rapid rise in nitrogen surface area (at almost constant carbon dioxide area) during gasification indicates that the

micropores are widening to become accessible to nitrogen at the temperatures of nitrogen adsorption experiments (77 ^{o}K), at which temperature restricted diffusion can be very slow. A second indication of micropore widening is the increase, during conversion, of the Dubinin gradient, a qualitative measure of micropore size derivable from carbon dioxide adsorption isotherms.

Another interesting feature of the sucrose char surface area evolution are the extrordinarily high nitrogen areas at high conversions, aprroximating the theoretical maximum surface area for isolated graphite planes, and in disagreement with the carbon dioxide areas. Nitrogen areas of this magnitude are thought not to be reliable, but, rather to indicate the presence of pore volume filling(D13).

We consider next whether reactant penetration is complete, and the gasification strictly kinetically limited, or if there are some finite microporous diffusion limitations.

D3.24 Estimation of η for sucrose carbon. An interesting feature of the sucrose reactivity data in figure 3.5 is that the effect of particle size is rather small between particle diameters of 180 and 50 μm, but increases substantially with further diameter reduction. This behavior is characteristic of the gasification of a carbon in which there are diffusion limitations within microporous grains that are significantly smaller than the particle itself.

We undertook to formulate the simplest possible model that incorporates the feature of diffusion limited microporous grains, in order to illustrate and quantify this concept. A sucrose carbon

particle is modeled as a collection of accessible but internally diffusion limited microporous grains which are spherical and have a monodisperse distribution of radii. Access to the microporous grains is provided by larger pores, which, in the case of sucrose carbon, may be the relatively few macropores(D12) and/or some fraction of the wider micro- and mesoporosity.

The observed gasification rate R_{obs} of such a particle of radius R_p is a function of the intrinsic reaction rate R_i, the effective microporous diffusivity D_m, and the grain radius R_g, which comprise the three parameters in this model. The observed rate is given by $R_{obs} = \eta R_i$, where η is calculated from R_i, R_g, and D_m according to the classical formulation. The model was completed by deriving an approximate expression for the effect of particle size reduction by grinding on grain size.

Figure 3.17 is a plot of the gasification reactivity at 20% conversion taken from Figure 3.5 for the four particle sizes, along with the predictions of the model generated using the optimum values of the parameters determined by nonlinear least-squares regression. The particle size effect is quite consistent with the model of accessible but internally diffusion limited microporous grains with a of radius of 27 μm.

The diffusivity from the model is between two and three orders of magnitude lower than the effective Knudsen diffusivity in 12.5 Å pores with a tortuosity factor of 5, and a porosity of 0.25, and is therefore in the restricted diffusion range.

The possibility exists that a grinding effect contributes to the

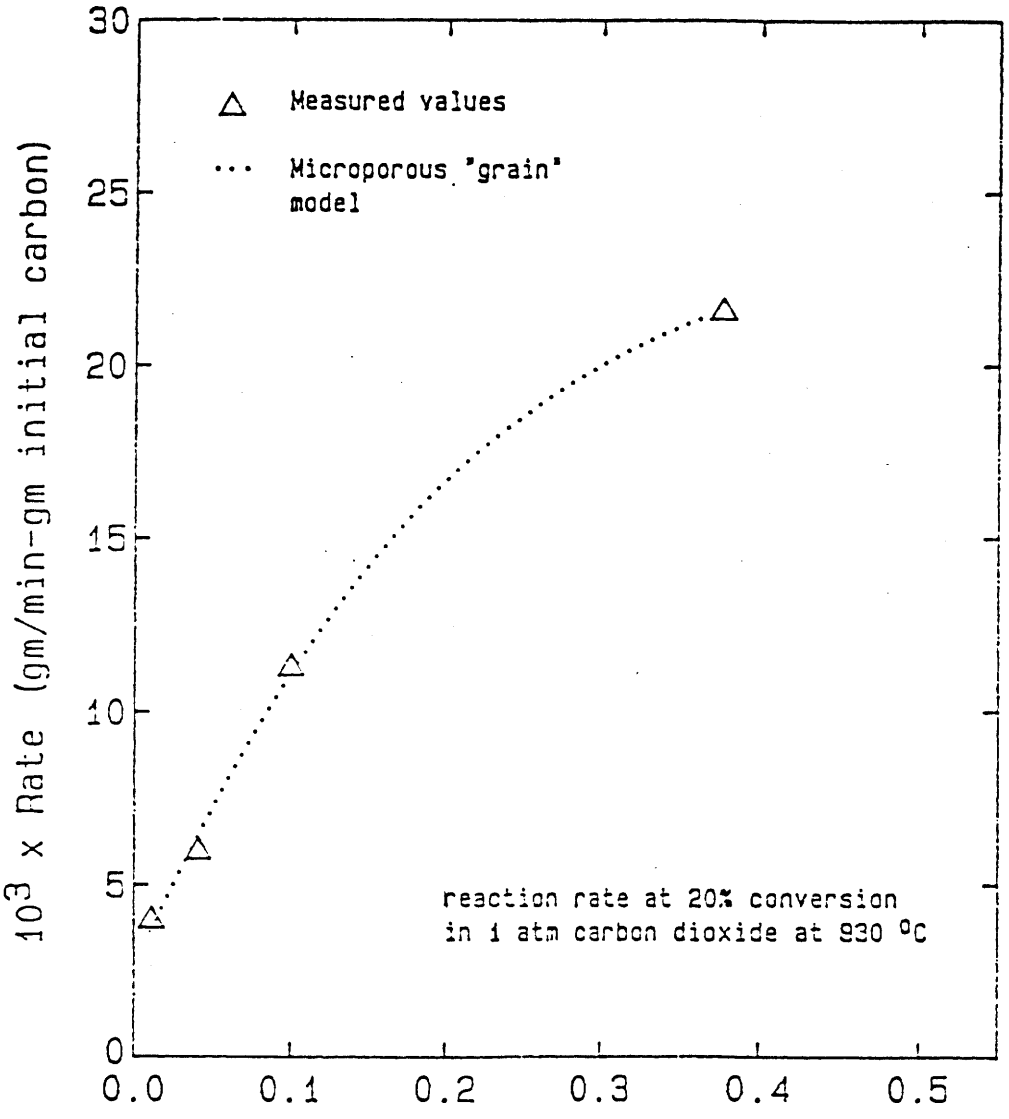

Figure 3.17

Effect of Particle Size on Sucrose Char Reactivity

increased reactivity of smaller particles, especially for the 5 μm fraction, which was intensively ground. The model parameters should therefore be regarded as setting an upper limit on the severity of diffusion limitations during sucrose gasification.

Carbon monoxide was found to inhibit the rate of carbon gasification in carbon dioxide, but the effect of particle size was the same in a carbon dioxide and carbon monoxide mixture as in pure carbon dioxide, indicating that the effect of particle size in pure carbon dioxide is not associated with carbon monoxide (reaction product) inhibition during otherwise kinetically limited gasification.

D3.25 Determination of η for Spherocarb carbon. The reactivity of Spherocarb carbon, unlike that of sucrose carbon, is essentially independent of particle size. This is a necessary but not sufficient condition for intrinsic gasification, due to the possibility of incomplete reactant penetration into microporous grains that are much smaller than the particle itself. Since the severity of diffusion limitations scales as L^2/D, however, it is <u>unlikely</u> that the gasification of a solid with very small microporous grains would be microporous-diffusion limited. It is, in fact, unlikely in the particular case of Spherocarb, in which the microporous grains must be small enough to ensure no particle size effect, and in which the local microporous diffusivity is expected to be as large or larger than that in sucrose carbon. (Spherocarb's initially high nitrogen area suggests wider micropores.) Nevertheless, the extent of reactant penetration into microporous regions in Spherocarb needs to be established, and in order to do so, we turn to measurements of diffusion times during vapor

adsorption experiments.

The adsorption of carbon dioxide in Spherocarb at 45% conversion was 87% complete after .95 seconds, yielding a characteristic diffusion time of 5.9 sec. This characteristic diffusion time was used in an analysis of microporous diffusion limitations for the Spherocarb oxygen reactions whose rates are plotted on the Arrhenius plot of figure 3.19. There is some uncertainty associated with the extrapolation of restricted diffusion coefficients to other conditions, and thus some uncertainty associated with this analysis, due to an incomplete understanding of the phenomenon of restricted diffusion(D14). We believe it to be a valuable analysis nevertheless, especially in connection with other analyses and experiments. Results of the analysis suggest that the Spherocarb-oxygen reaction is intrinsic and occurs fully within the micropores within the temperature range investigated here, up to at least 600 ^{o}C.

Another useful analysis uses the diffusivity obtained from application of the microporous grain model to sucrose reactivity data in order to assess the severity of diffusion limitations for Spherocarb. To do this, one needs to know the length scale for microporous diffusion in Spherocarb carbon. An estimate of this length scale is the characteristic radius of microporous grains, defined here as those regions containing no pores larger than 100 Å in diameter, and calculable from the measured surface area lying in pores with diameters greater than 100 Å. Microporous grains according to this definition have an external area of .092 m^2/gm and a radius of 24 μm for sucrose carbon, and an external area of 15 m^2/gm and a radius of .15 μm for

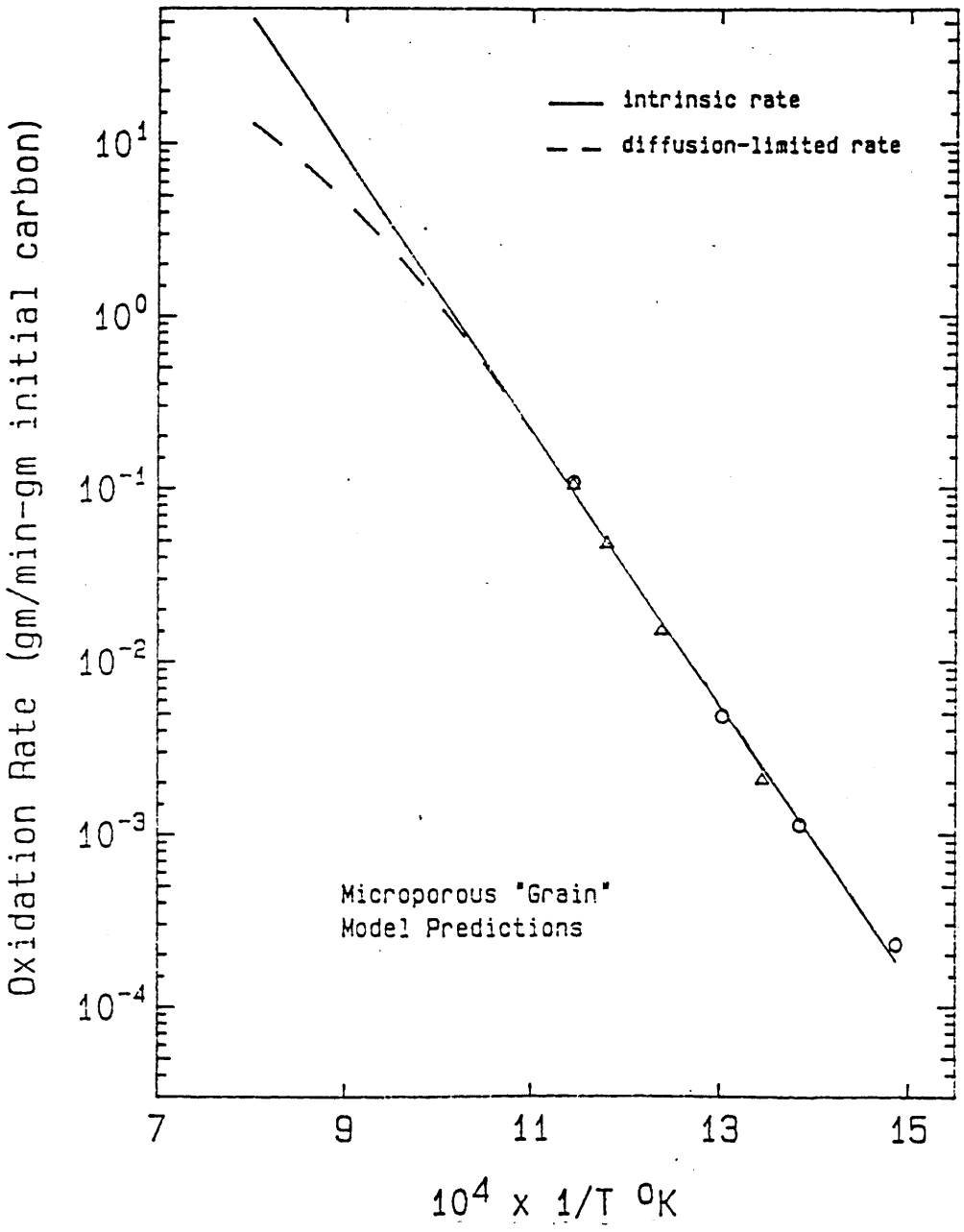

Figure 3.19
Spherocarb-Air Reaction

Spherocarb. The large difference reflects the limited macroporosity of sucrose carbon in contrast to the extensive macroporosity of Spherocarb. Effectiveness factors for Spherocarb oxidation, calculated using this length scale and the microporous diffusivity from the sucrose model, are unity for each of the measured reaction rates in figure 3.19 between 400 and 600 ^{o}C. The diffusion limited solution at higher temperatures can be generated by extrapolating the existing (kinetic) data and using, again, the estimated length scale and the sucrose diffusivity. This solution is shown in Figure 3.19, and suggests that microporous diffusion limitations may start to become important for Spherocarb at temperatures higher than those examined here.

These analyses strongly suggest that the measured Spherocarb oxidation rates are intrinsic, and that the accessible total surface area for Spherocarb is expected, then, to be the 636 m^2/gm measured by carbon dioxide adsorption, and the measured activation energy of 36 kcal/mol to be the intrinsic activation energy for oxidation of this carbon. This is a typical activation energy for a low temperature char or carbon, but is substantially lower than activation energies measured for oxidation of some graphites(D2), the difference presumably arising from the different degrees of purity and crystallinity(D15). This level of understanding of diffusional processes is necessary for the fundamental treatment of many aspects of carbon gasification, including, in fact, the pore structure modeling effort summarized in section D4.

The major difference between the two synthetic carbons in this

study is therefore thought to be related to a difference in the characteristic size of microporous grains in the two carbons. The severity of microporous diffusion limitations for most chars should lie between that for the highly macroporous Spherocarb and that for the essentially non-macroporous sucrose carbon. The carbon dioxide surface area should therefore be the appropriate total surface area for the gasification of many pure carbons, although restricted diffusion limitations may be important during low temperature gasification for chars with little macroporosity.

D3.26 The role of microporous surface area in the gasification of a subbituminous coal char. Chars from untreated and acid-washed P.S.O.G. 156 subbituminous coal behaved very differently during gasification than did the synthetic chars of the previous section. In contrast to the sucrose char, carbon dioxide gasification of the low temperature coal chars was accompanied by a relatively slow burnout of the char's molecular sieve properties as seen in figure 3.14. In addition, gasification was not accompanied by measurable micropore widening, as indicated by the constant Dubinin gradient in figure 3.11. These two results suggest that the contribution of microporous surface area to the gasification rate is small.

In order to further investigate the role of the micropores in the gasification of the subbituminous coal chars, the char from the acid washed coal, heat treated previously at 1000 ^{o}C for one hour, was subjected to an additional heat treatment at 1200 ^{o}C for one hour, in hopes of eliminating the microporous surface area and observing the subsequent effect on gasification behavior. The surface area, measured

by carbon dioxide adsorption did drop from 510 to 4 m^2/gm, while the initial gasification rate decreased by only about a factor of 4. Further, as shown in figure 3.16, the gasification rate of the higher temperature coal char was near its maximum at 0% conversion, and thereafter decreased monotonically, while the carbon dioxide surface area increased strikingly, from 4 to over 200 m^2/gm. The gasification rate of this char bears no apparent relation to its total surface area.

A possible interpretation is that inaccessibility of or slow reaction within the micropores confines the reaction front to the surfaces of larger pores. This interpretation can be ruled out however, because each of the coal chars has a higher reactivity at a given temperature than either sucrose or Spherocarb carbons, which have been shown to undergo gasification within their micropores.

We seek, therefore an alternative explanation. Marsh(D16) has microscopically observed pitting, channeling, and/or uneven gasification of the surface of many carbons doped with various inorganic impurities. Rarely, if ever, did gasification in the presence of catalytic agents take place uniformly over the carbon surface, in contrast to the gasification of his pure carbons.

In light of the high gasification reactivity, the apparent independence of reactivity on surface area, and uneven surface gasification, we offer the interpretation that catalysis by inorganic impurities is important to the gasification of the subbituminous coal chars. The significance of the result in figure 3.16 is, then, that the rate of catalyzed gasification can be apparently unrelated to microporous surface area, presumably depending instead on properties of

the catalyst. Since many chars from naturally occurring organic material may be expected to contain catalytically active inorganic impurities, it is not surprising that previous studies have found an inadequate correlation between gasification reactivity and internal surface area(D2,7,15,17).

D4. The Phenomenon of Gasification-Induced Carbon Particle Shrinkage and Its Influence on Pore Structure Evolution

Dave Dudek, in a parallel study at M.I.T., has observed significant diameter reduction during kinetically controlled air-oxidation of single electrostatically levitated Spherocarb carbon particles(D9), as seen in figure 4.2. Spherocarb particles did not shrink upon heating in nitrogen under otherwise identical conditions. Possible explanations for the diameter reduction phenomenon are perimeter fragmentation, the presence of a significant reaction component on the external surface of the particle, and reaction induced homogeneous particle shrinkage. It was undertaken in this study to investigate the diameter reduction phenomenon and its implications, especially those relating to carbon gasification reactivity.

D4.1 Results.

A technique was developed with which individual features on the external surface of individual particles can be observed by S.E.M. as a function of gasification conversion, in order to distinguish between the possible interpretations of the diameter reduction phenomenon.

In table 4.1 are presented particle diameters (d/d_o) for various chars at different stages of conversion, measured from photographs

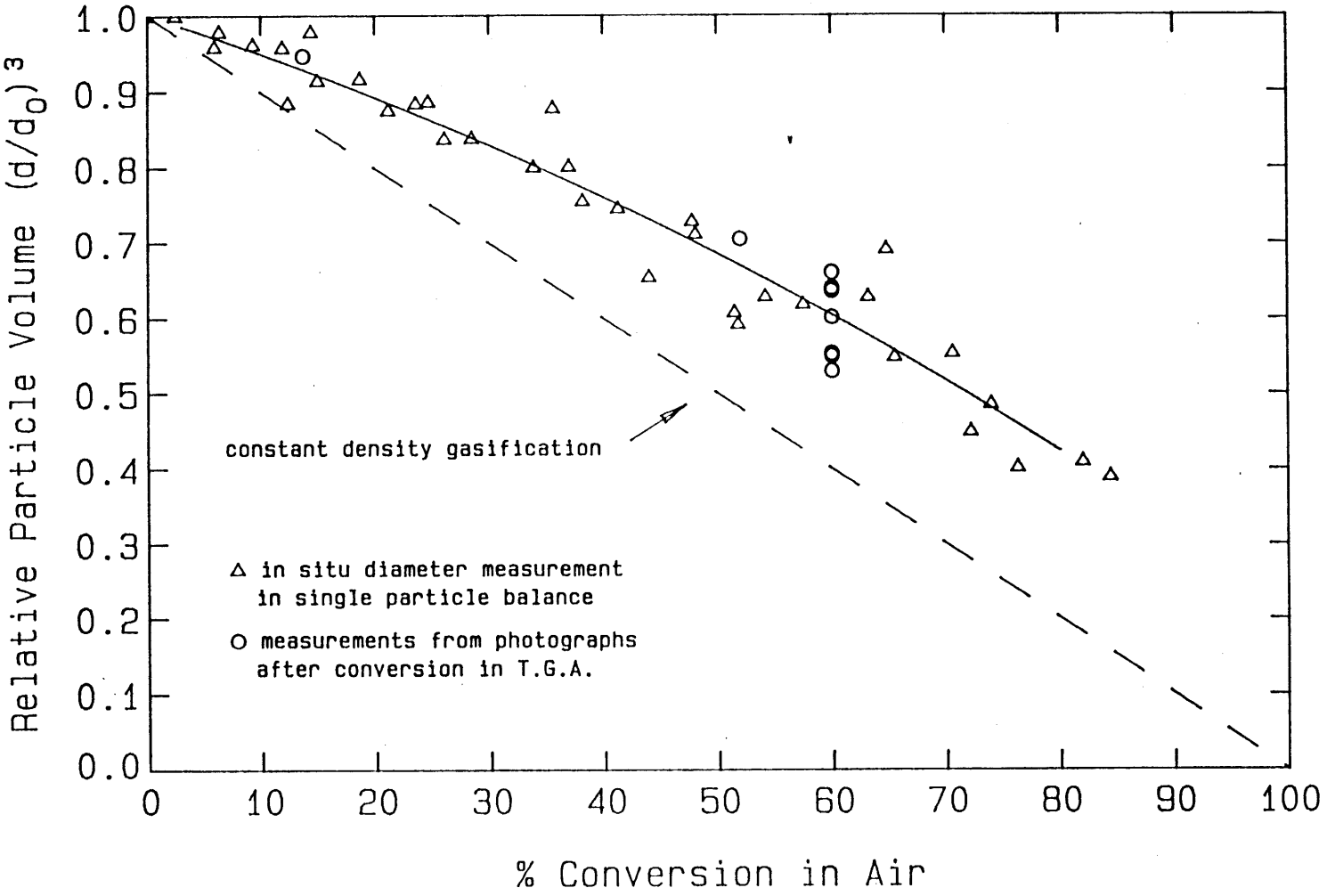

Figure 4.2 Spherocarb Particle Shrinkage

using either the captive-particle S.E.M. technique or optical microscopy on single particles partially gasified in a T.G.A..

Several sample photographs showing particle shrinkage are given in figure 4.1, while the preservation of even the finest visible surface features during gasification is apparent from the S.E.M. micrographs in figure 3.1.

Table 4.1
Extent of diameter reduction during gasification of various carbons and chars

Carbon	Reaction Conditions	Conversion	d/d_o
Spherocarb	.21 atm. O_2, 495 °C (163 min) . .	60%	.821
			.871
			.809
			.844
		52%	.890
		13.7%	.982
	.21 atm. O_2, 450 °C	60%	.860
	.21 atm. O_2, 600 °C	60%	.862
			.819
	.5 atm. CO/.5 atm. CO_2, 990 °C . .	60%	.862
	1 atm. N_2, 495°C, 163 min	0%	1.0
	1atm. N_2, 960 °C, 60 min	0%	.983
Sucrose char	.21 atm. O_2, 495 °C	60%	.882
			.863
			.921
		20%	.990
Sucrose with carbon black	. . . . .	.51.5%	.989
		71.2%	.886
Pitt. #8 char	. . . . .	.61%	1.0
			.98
			.94
Calcium-doped sucrose	.21 atm. O_2, 370 °C	70%	1.0
Montana lignite char	. . . . .	44%	1.0
			.971
		85%	.575
			.646

Most but not all of the carbons exhibited significant shrinkage, with Spherocarb carbon exhibiting the most pronounced shrinkage. Char

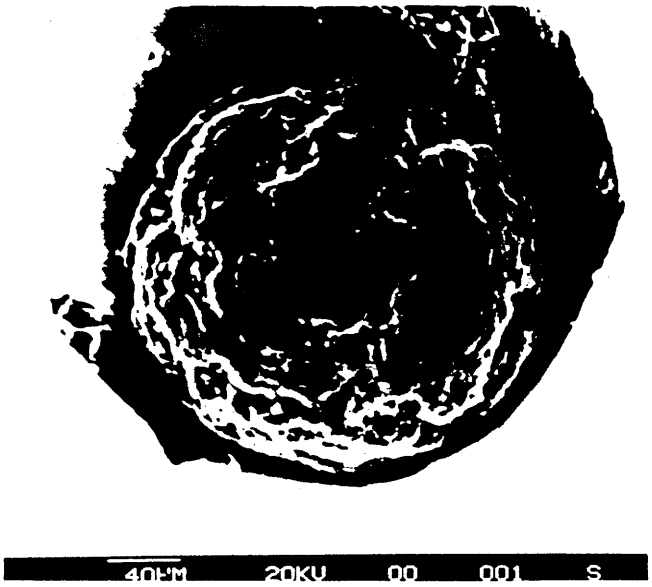

Unreacted

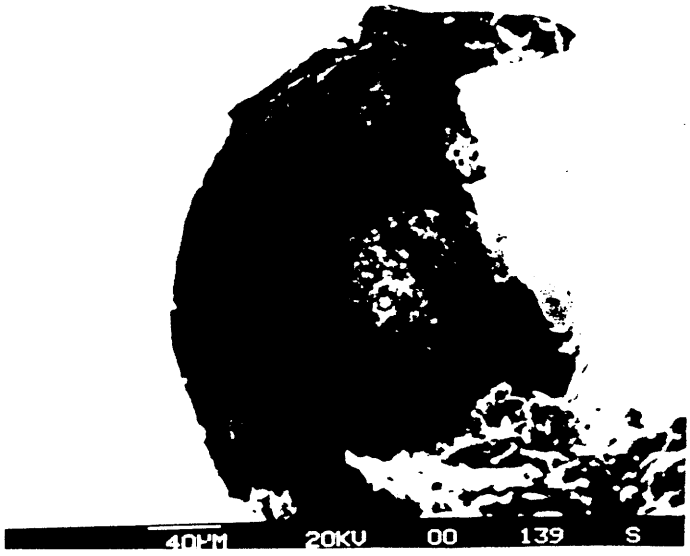

Partially
Reacted
(presumably high
conversion)

Spherocarb in .21 atm O_2, 495 ^{o}C

Figure 4.1 Photographs and S.E.M. Micrographs

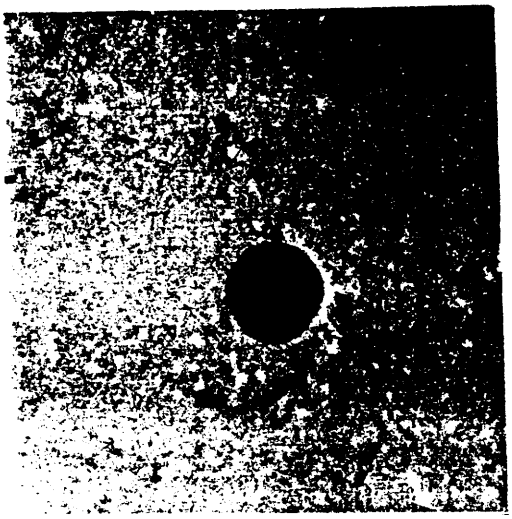

Unreacted
d = 198 μ

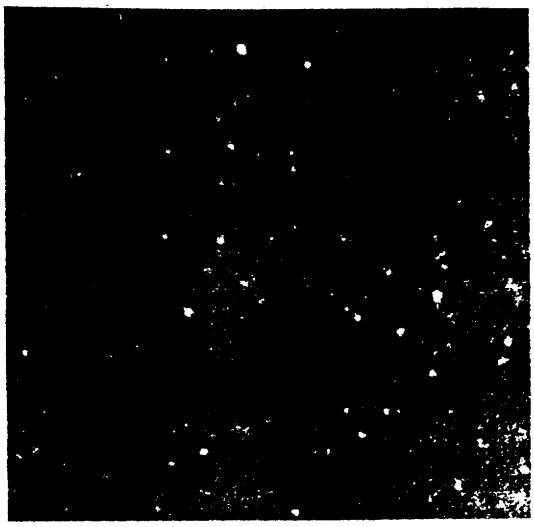

60% Conversion
d = 167 μ

Unreacted

60% Conversion

Spherocarb in .21 atm. O_2, 495 °C
Set of optical photographs at increasing magnification

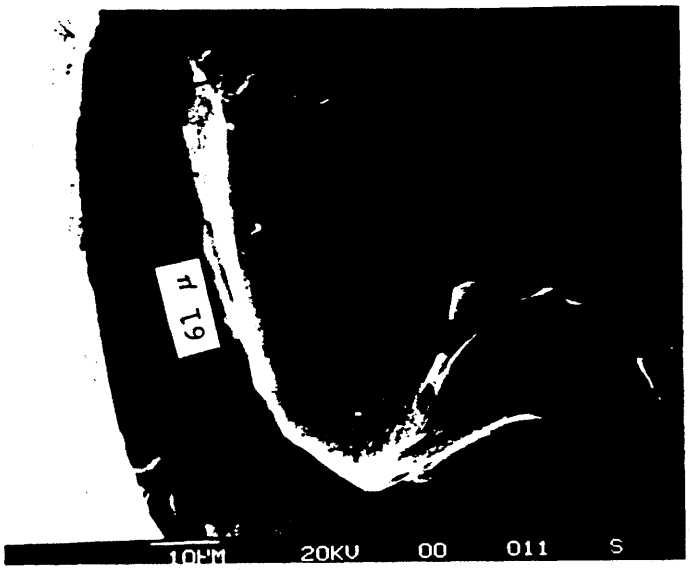

Unreacted

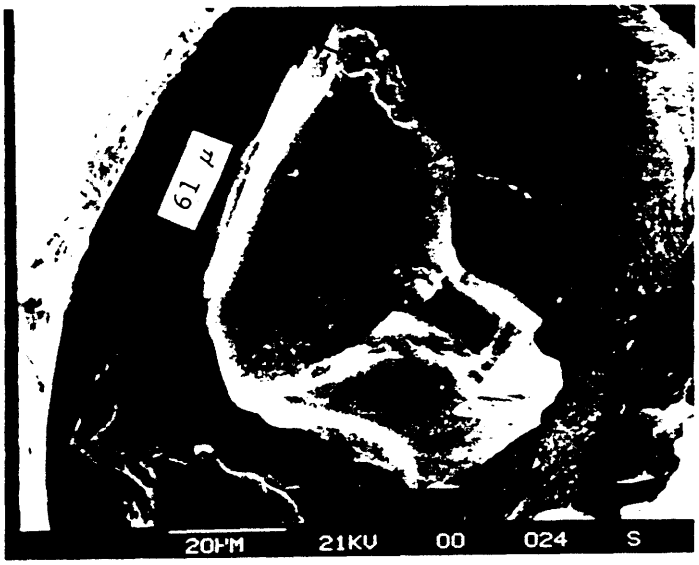

44%
Conversion

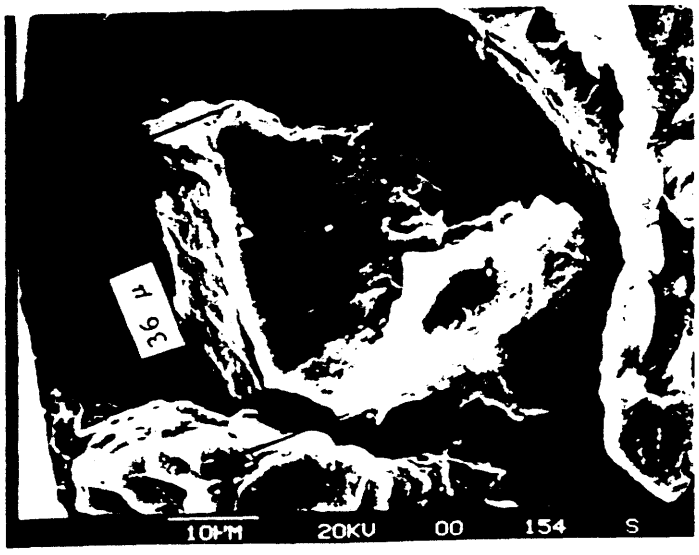

85%
Conversion

Montana
lignite
char

in air
370 °C

from a Montana lignite coal shrank very little if at all up to 44% conversion, but markedly at 85%.

Figure 4.2 is a compilation of d/d_o vs. conversion measurements for Spherocarb carbon from table 4.1 and from Dudek's single particle electrodynamic balance technique(D9). Diameter reduction becomes quite pronounced at high conversions, although always lying above the curve representing constant density gasification.

Measurements of the dimensions of various surface features of Spherocarb particles, which were, after 52% or 60% conversion, clearly identified as surface features originally photographed at 0%, were made from various photographs and S.E.M. micrographs. All surface features, both pores and solid regions, shrank, and in the same proportion as the particle diameter. These data form the basis for the information plotted in figure 4.3.

D4.2 Discussion.

D4.21 Homogeneous shrinkage. During the kinetically controlled gasification of high surface area carbons, an insignificant fraction of the gasification can be expected to occur on the external surface proper of the particle. This fact is illustrated for 200 μm diameter Spherocarb carbon particles by comparing the numerical values of the external, macropore (diameter > 200Å), and total surface areas:

External area, $4\pi R^2_{particle}$: .03 m^2/gm

Macropore area(D18): 5 m^2/gm

Total carbon dioxide surface area: 636 m^2/gm

Spherocarb gasification rates presented in chapter 3 were not a

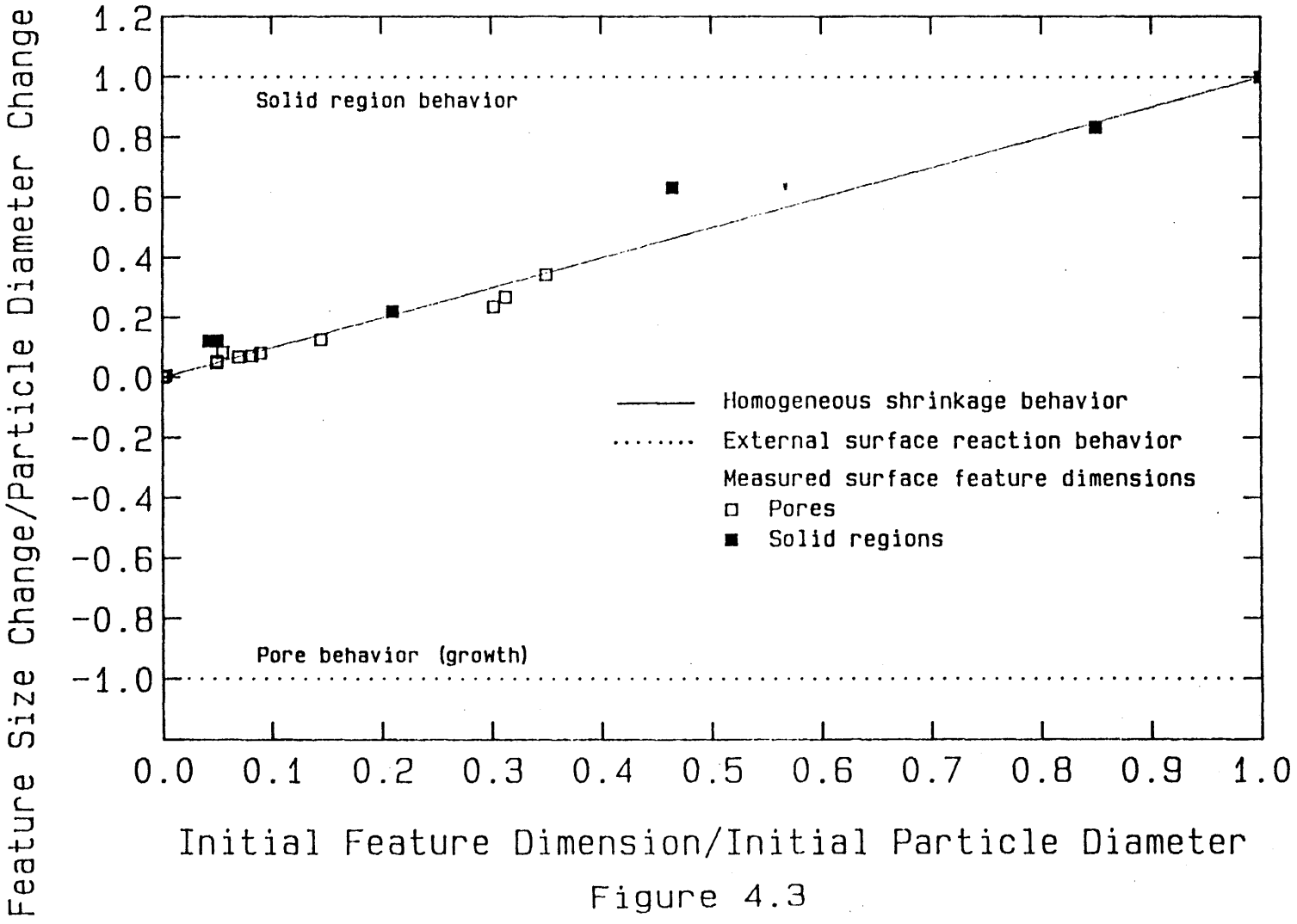

Figure 4.3

Shrinkage of Spherocarb Surface Features

function of particle size, which is a classical indication of complete reactant penetration and the absence of a significant reaction component on the particle's external surface. Further evidence that Spherocarb gasification at temperatures below 600 ^{o}C in air is, in fact, kineticaly controlled, and even occurs fully within the micropores is summarized in section 3. Indeed, the photographs and S.E.M. micrographs provide direct evidence that no significant gasification occurs on the external surface, but rather that surface features are preserved and undergo a homogeneous shrinkage during gasification.

The homogeneous shrinkage of topographic features is illustrated in figure 4.3, where measured surface feature dimensions are compared to the behavior expected during homogeneous shrinkage and to the behavior expected in the presence of a reaction component on the external surface proper.

D4.22 Gasification-induced carbon densification. The observation of pronounced particle diameter reduction during gasification in the intrinsic kinetic regime, with preservation yet homogeneous shrinkage of topographical features, indicates the presence of a gasification-induced solid phase densification phenomenon. Note that the carbon particles densify <u>with respect</u> to those participating in a hypothetical reaction at constant diameter. Density is simultaneously increased by densification and decreased by gasification of carbon atoms, the net effect on density being a function of the specific relationship between diameter and conversion.

It is believed that densification is the result of solid state

rearrangements producing loss of pore volume in fine pores. At the length scale of the larger pores in a carbon particle, then, the optically homogeneous "microporous solid" appears to undergo a densification/shrinkage, the larger pores shrinking also, acting as holes in a homogeneously shrinking matrix.

To understand the densification phenomenon, consider that carbons are composed of small and imperfect graphitic carbon layers, whose irregular packing arrangement is responsible for carbon micropores. Since the thermodynamically preferred form of carbon is crystalline graphite, which is non-microporous, it is only energy barriers associated with solid state rearrangements that trap the imperfect layer-packing and the resulting microporosity.

Atomic rearrangements that lead to surface area loss can occur in an inert environment at temperatures as low as 1000 ^{o}C(D19) and can be thought of as the initial stage of graphitization. The solid state rearrangements accompanying gasification of Spherocarb and other carbons in this study are reaction induced and occur at temperatures at least as low as 450 ^{o}C. It is believed that the gasification reaction, by breaking bonds, removing cross links, and removing carbon atoms, "loosens" entanglements, and increases the driving force for, and facilitates densification via rearrangements analogous to those occurring spontaneously at somewhat higher temperatures in the initial stages of graphitization.

Amorphous solid densification is also seen in germanium and glasses(D20), and it is especially noteworthy that Kaae(D21) has observed densification during neutron irradiation of a glassy carbon at

1100 ^{o}C, under conditions where no densification occurred during heating in the absence of the neutron beam.

D4.23 Implications. The phenomenon of gasification-induced carbon densification makes measurements of particle size or density unreliable tests for determining the fraction of the gasification occurring on the external surface of the particle. In addition, by reducing internal porosity during gasification, the phenomenon should be an important factor determining the fragmentation behavior of carbon particles, which is a topic of much current interest in gasification research. Finally, shrinkage is important in pore structure evolution and surface area evolution during gasification or activation and will affect gasification rates and activated carbon adsorptive properties. The reduction of surface area and reactivity would be most pronounced at high conversion, potentially contributing to the difficulty in achieving high carbon conversions in some gasification processes. This topic is explored at length in the following section.

D4.3 Modeling of surface area evolution

D4.31 The Gavalas Random Pore Model. Gavalas(D22) has derived an exact analytical solution with no empirical parameters for the evolution of the pore size distribution and total surface area during carbon gasification (without allowance for densification) for an arbitrary initial pore size distribution, assuming randomly distributed, infinite cylindrical pores, with no initial closed porosity. We undertook here to compare, for the first time, measured surface areas with the exact Gavalas solution requiring as input the complete measured pore size

distribution, available to us courtesy of Niksa(D18). The prediction of the Gavalas random pore model for Spherocarb surface area evolution is compared in figure 4.11 to measured surface areas calculated from carbon dioxide adsorption isotherms measured gravimetrically in Dudek's single particle electrodynamic balance. The discrepency between the data and the model without allowance for densification/shrinkage is striking. In fact, the measured areas decrease when normalized by the mass of carbon remaining, whereas both the Gavalas and the Simons random pore models, which do not consider reaction induced shrinkage, predict monotonically increasing areas per remaining mass for the kinetically limited gasification of all carbons (i.e. regardless of the initial pore structure of the carbon).

D4.32 Modeling of gasification with concurrent shrinkage. Surface area development during gasification with concurrent shrinkage can be treated as the sum of two terms as follows:

$$dA/dX = (\delta A/\delta X)_d + (\delta A/\delta d)_x(dd/dX)$$

The first term on the right-hand side represents the evolution of surface area during gasification at constant diameter and is dealt with by existing models. The second term contains the change in diameter with respect to conversion, which can be obtained directly from measurements, and the change in area with respect to diameter at constant mass, which requires the development described in the next paragraph.

D4.33 Reaction and densification: simple model. During shrinkage at constant mass, the total porosity is a unique function of the initial porosity and the extent of shrinkage. We postulated that there are

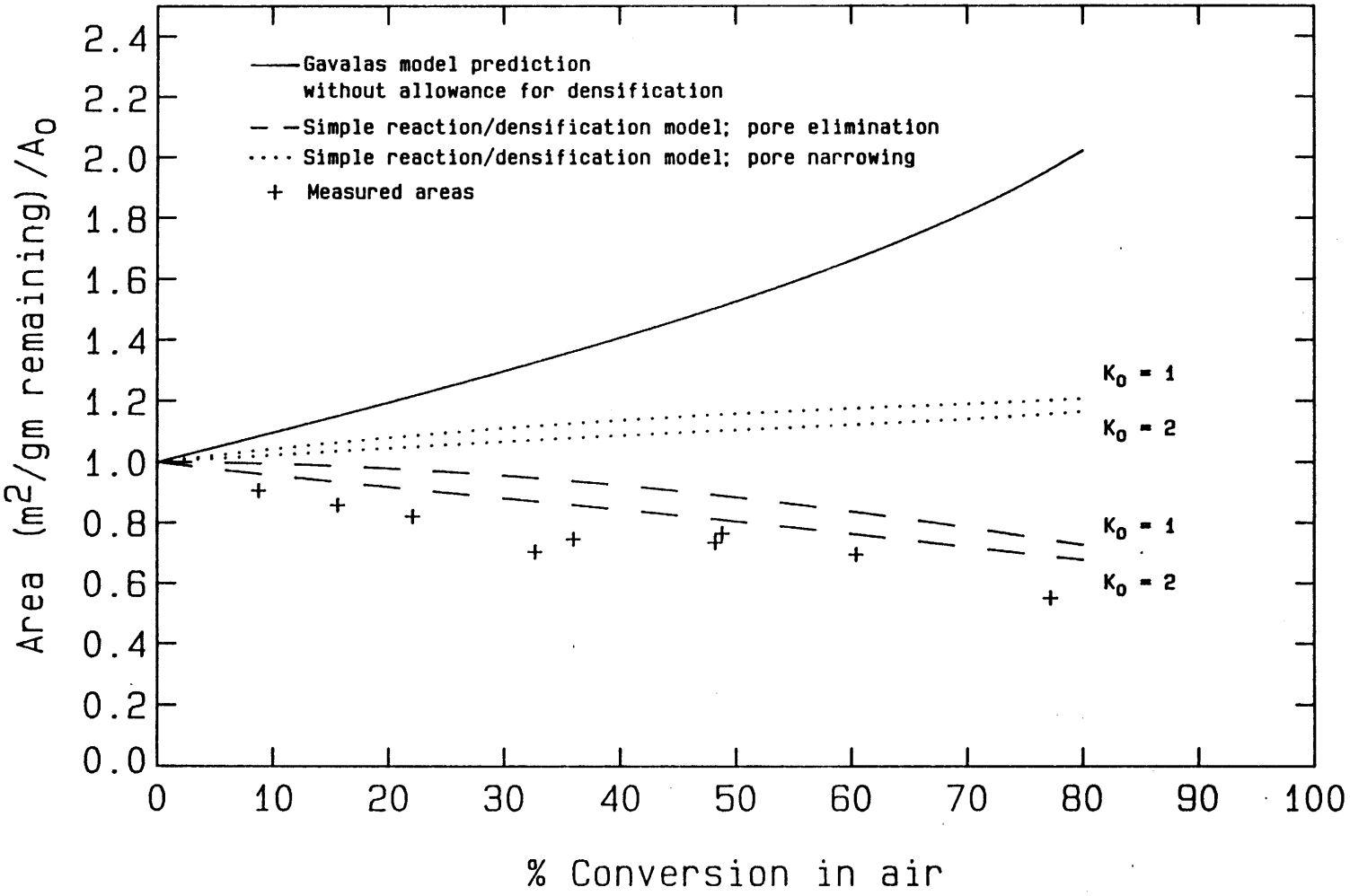

Figure 4.11 Spherocarb Surface Area Evolution

two distinct classes of pores, smaller pores in which the solid state rearrangements occur and larger pores which shrink homogeneously as holes in a shrinking microporous solid. The characteristic of homogeneous shrinkage is that the large pore diameters shrink in the same proportion as the particle diameter, from which it could be shown that the large pore porosity is constant during shrinkage at constant mass. The small pore porosity was obtained as the difference between the total and large pore porosities. The effect on surface area was modeled by considering the atomic rearangements to be a combination of elimination and narrowing of cylindrical pores.

The prediction of the constant volume Gavalas model was coupled to the results of the shrinkage at constant mass formulation above to generate a simple analytical model of gasification with concurrent shrinkage whose prediction can be seen in figure 4.11. The parameter K_o, which is a property of the initial pore structure of the carbon, has a rather weak influence on the predicted area development, whereas the chosen model of the rearrangement process (pore elimination vs. pore narrowing) is quite important. In all cases, however, the shrinkage term has an important influence on the predicted area development.

D4.34 Exact numerical solution of gasification with concurrent shrinkage. The approach was to treat both reaction and shrinkage by altering Gavalas' pore-axis probability density function throughout conversion and to use relations derived by Gavalas to compute the porosity and total surface area from the altered P.D.F. at any point.

The logic of the numerical solution scheme is represented in a flowchart, figure 4.12. The procedure constitutes a numerical solution of the 2 coupled integro-differential equations describing gasification with concurrent shrinkage. Results are presented in figure 4.14 of several solutions for pure pore elimination and various K_o values. Again K_o, within the range of possibility for Spherocarb, is not a very important parameter. Again, densification is in each case a major factor determining Spherocarb surface area development, although the numerical predictions are significantly different from those of the simple, analytical model. The numerical solution for $K_o = 2$ and pure pore elimination, shown in figure 4.14, is the best obtainable fit to the experimental curve.

The numerical solutions based on elements of the Gavalas formulation are the best representation of the physics of gasification with concurrent shrinkage, and can account for much, but not all of the discrepency between the data and the constant volume pore models. Other phenomena may also be contributing to the deviation of surface area evolution from the Gavalas model prediction, such as heterogeneity in carbon reactivity, gasification by pore production(D23), or pore coalescence or coarsening.

For example, in figure 4.15 appears the result of a numerical solution of gasification with concurrent shrinkage with allowance for an arbitrary extent of pore coalescence. This model is clearly capable of providing an adequate description of Spherocarb carbon surface area evolution, and the area developed at 80% conversion is more than a factor of three lower than that expected in the absence of

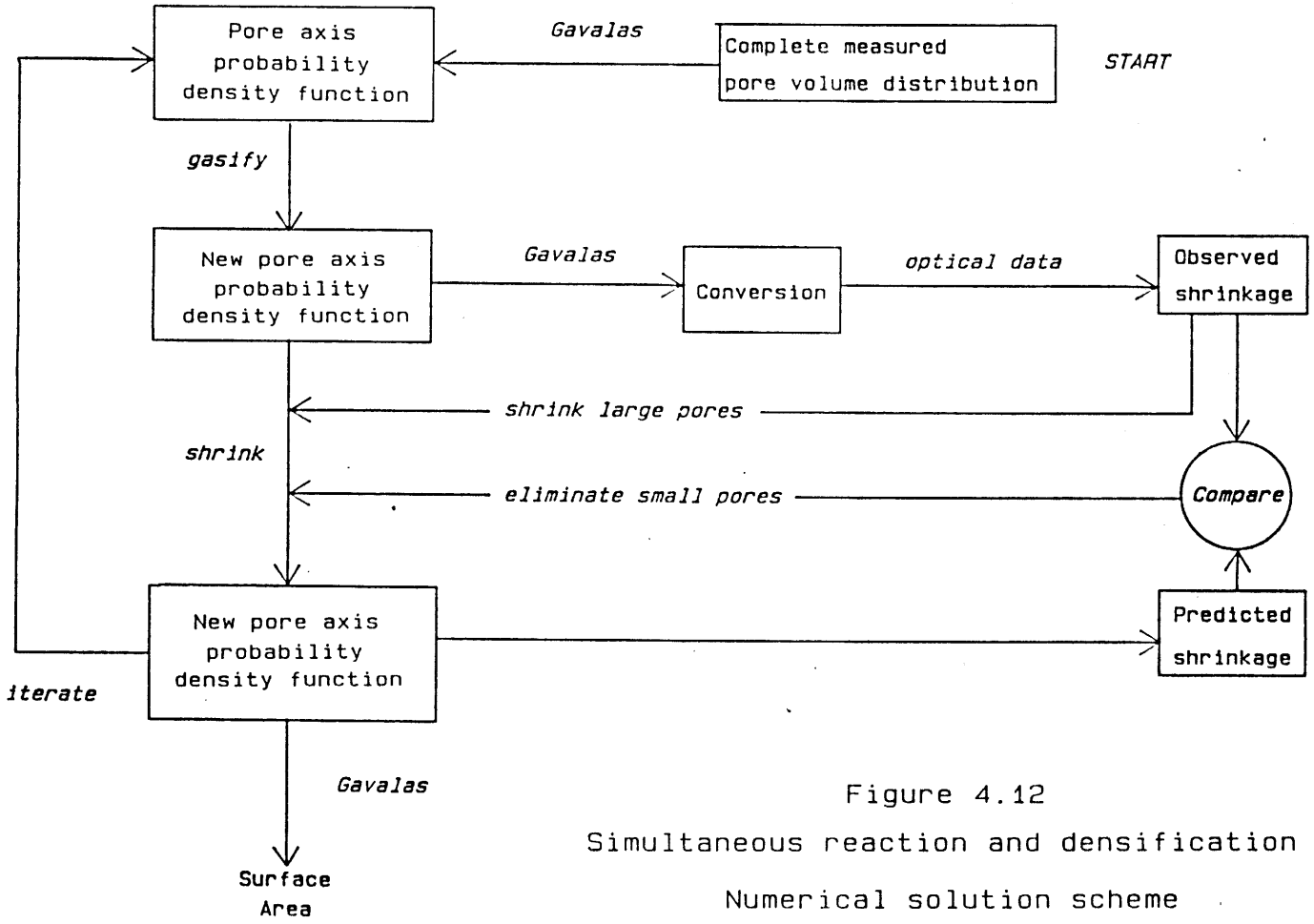

Figure 4.12

Simultaneous reaction and densification

Numerical solution scheme

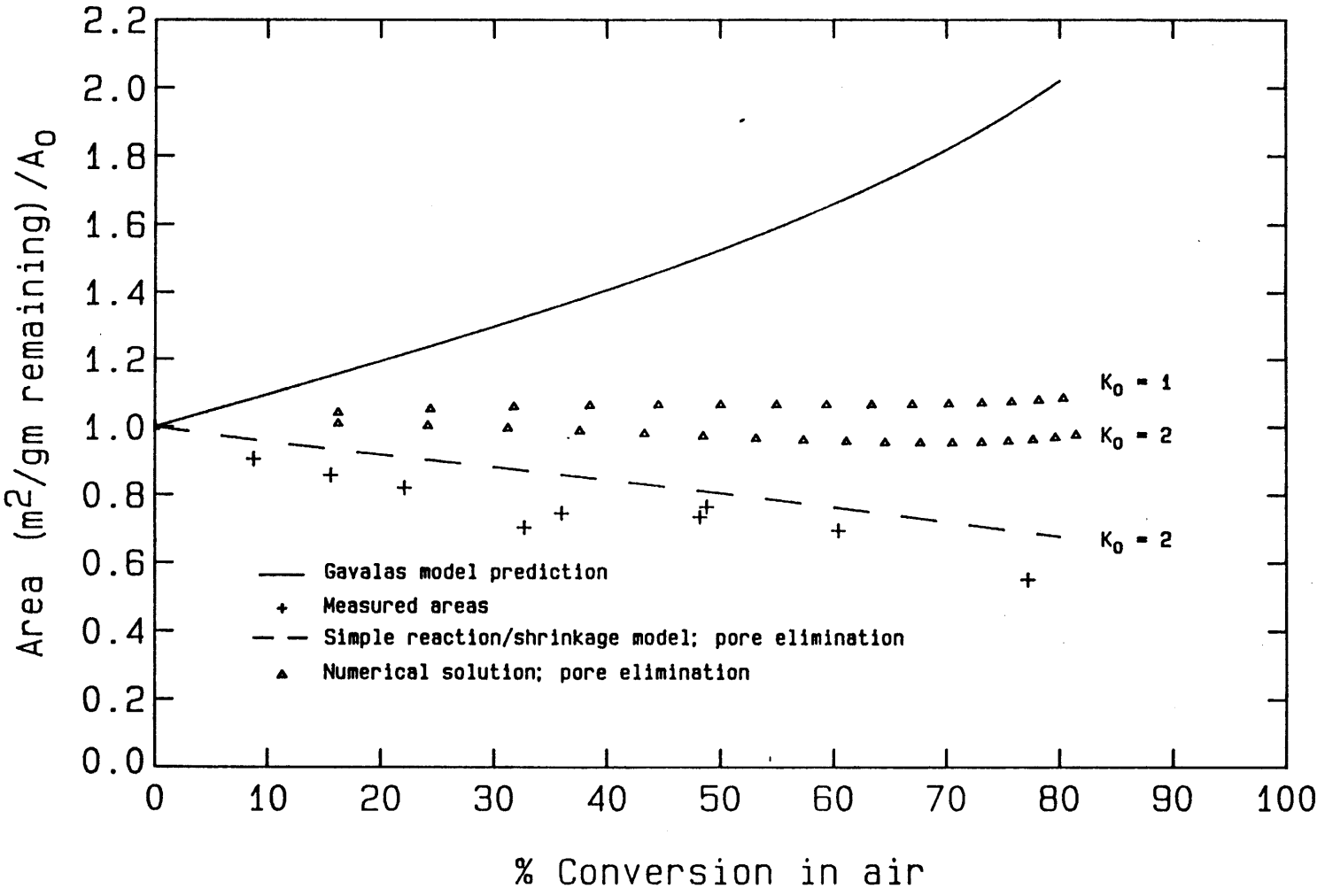

Figure 4.14 Spherocarb Surface Area Evolution

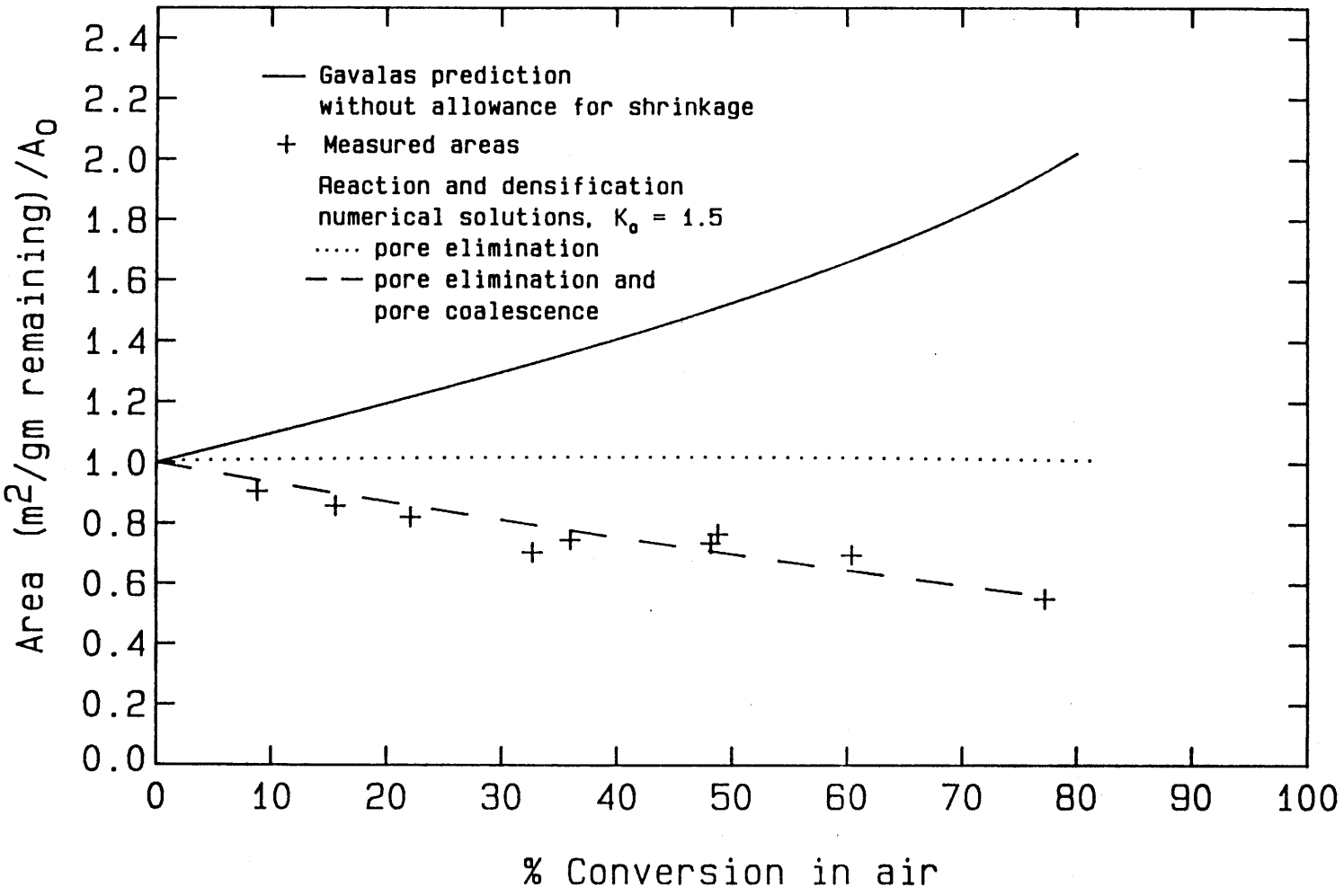

Figure 4.15 Spherocarb Surface Area Evolution

gasification-induced atomic rearrangements.

D5. The Effect of Coal Type or Maceral Content on Char Reactivity

Vitrain and fusain, the two most important macerals or type-determining coal components, were handpicked from blocks of PSOC 156 sub-bituminous coal, examined and purified under low magnification, and analyzed (along with the whole coal) for maceral composition under reflected light. The fusain fraction was 92% fusinite, and the vitrain fraction was 96% vitrinite, by volume.

The gasification reactivities of chars made at 1000 ^{o}C from the raw lithotypes and the whole coal are plotted in figure 5.1 as a function of conversion in one atmosphere carbon dioxide. The reactivity of fusain was lower that the reactivity of vitrain by a factor of about two at low conversion, while at high conversion the two curves diverged, reactivities differing by a factor of 15 at 90% conversion. Clearly the reactivity-conversion curves for the two lithotypes are qualitatively different, and figure 5.2 illustrates directly that a much longer time is required to gasify the fusain sample to high conversion. The whole coal reactivity curve in figure 5.1 lies between the lithotype curves, but does not closely approach the fusain curve at high conversion, indicating that, in terms of gasification behaviour, a whole coal with its complex petrography cannot be accurately modeled as a composite of the two lithotypes alone.

We attempted to relate the gasification behaviour of these lithotypes to their physical and chemical properties. Carbon dioxide

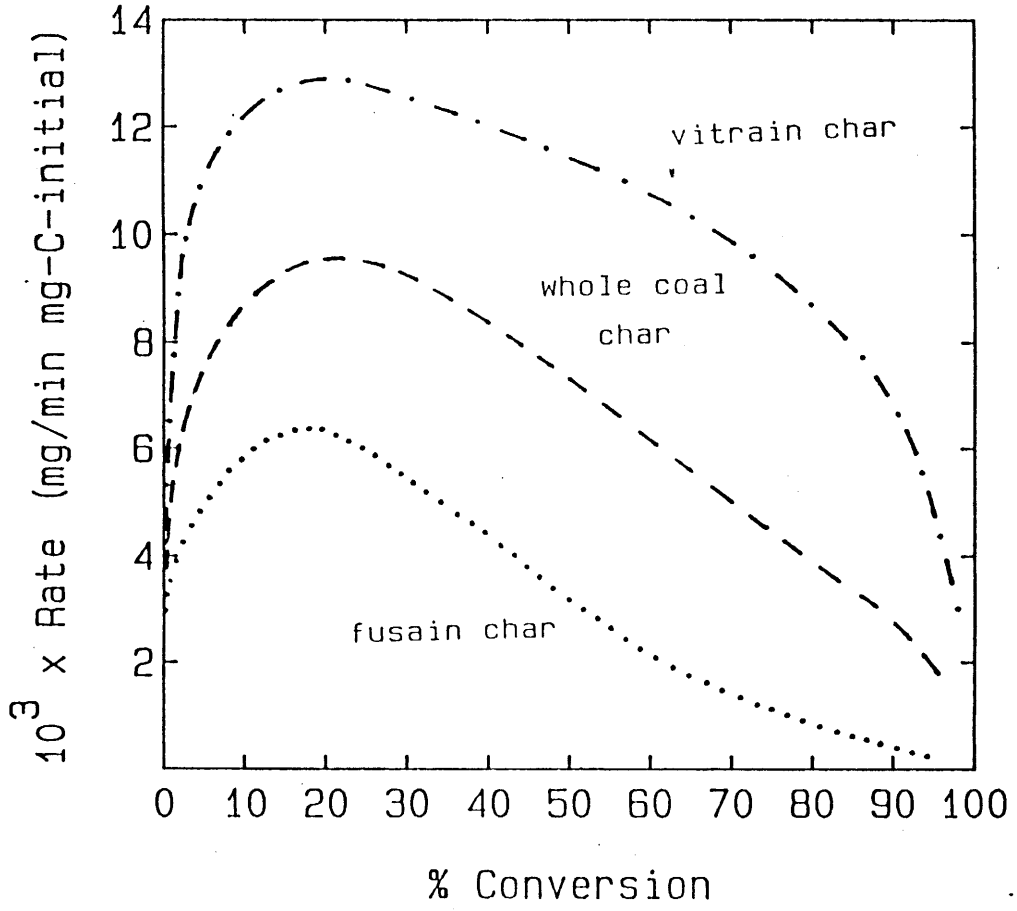

Figure 5.1

Gasification reactivity of lithotype and whole coal chars in 1 atm. carbon dioxide at 800 ^{o}C.

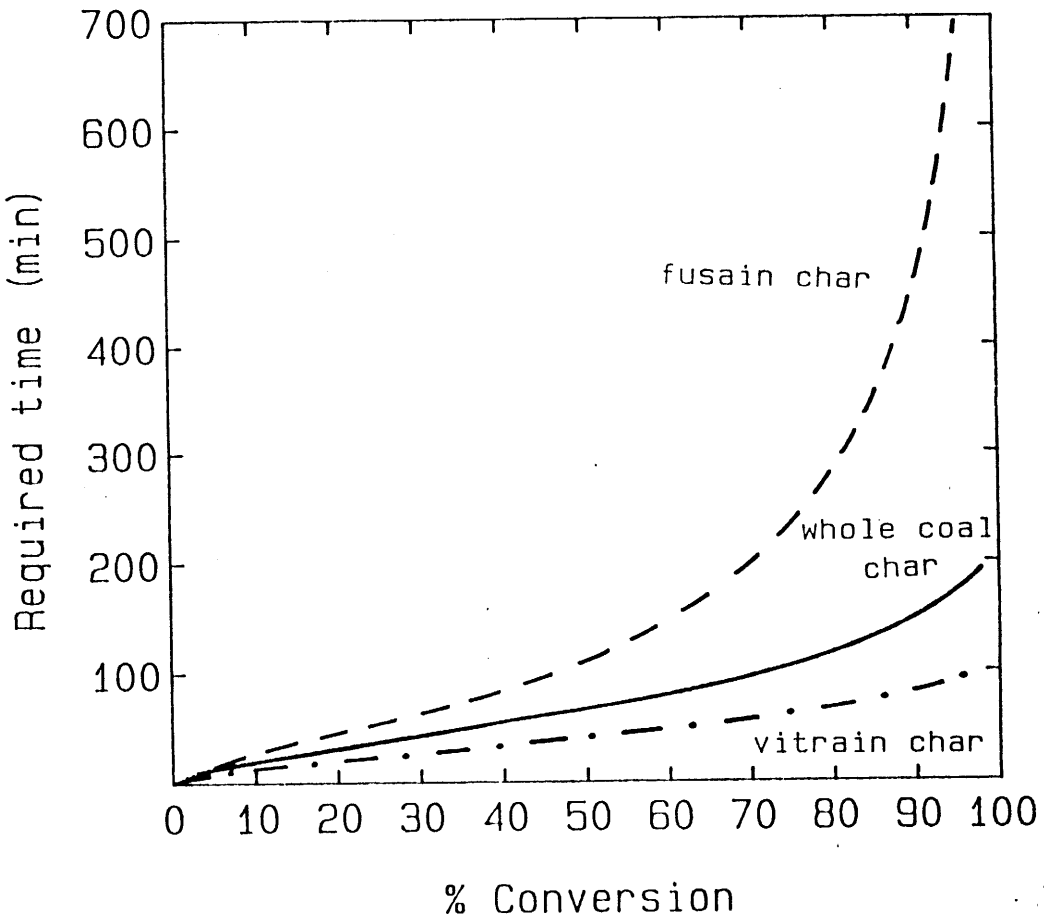

Figure 5.2

Gasification of lithotype and whole coal chars in 1 atm. carbon dioxide at 800^{o}C

surface areas of the lithotype chars (measured at approximately 50% conversion) were similar. Measurements of the gasification reactivity of demineralized chars, chars from coals whose naturally-occuring ion-exchanged cations had been removed, and untreated chars appear in table 5.1. Direct comparisons were made between pairs of chars at experimentally convenient temperatures and the results presented as ratios of reactivities.

Table 5.1. Comparison of carbon dioxide gasification reactivities of acid washed, ion-exchanged, and raw chars

Char	Temperature (°C)	% Conversion at which reactivity was measured	Ratio of reactivities
vit_{raw}/fus_{raw}	800	65	5.8
vit_{dem}/fus_{dem}	875	65	2.3
vit_{ion}/fus_{ion}	830	15	0.68
vit_{raw}/vit_{ion}	800	15	8.2
vit_{raw}/vit_{dem}	790	65	3.4
fus_{raw}/fus_{dem}	890	65	1.7

Demineralization lessened the difference between the reactivities of vitrain and fusain as shown by the first two entries in the table. Further, the divergence of the reactivity curves for the raw chars at high conversion in figures 5.1 and 5.2 was not seen for the two demineralized chars at high conversion.

Chars made from fusain and vitrain whose naturally occuring ion-exhanged cations had been removed had similar reactivities, indicating that differences in exchangeable cation content are responsible for the major differences between untreated lithotype chars. The ion-exchange results also suggest, by comparison, that demineralization had left appreciable amounts of residual catalytic inorganic matter.

The fourth entry in table 5.1 is a direct comparison of raw and

ion-exchanged vitrain which indicates that catalysis by ion-exchangable matter dominates the reactivity of raw vitrain char. The ion-exchange filtrates were analysed for calcium and magnesium using atomic absorption spectroscopy. Values of 0.13 wt% calcium and .03% magnesium were obtained for fusain, and the average cation loadings from two independent extractions on the vitrain sample (which were in close agreement) were 0.40% Ca and 0.13% Mg.

The higher cation content and higher reactivity of vitrain is consistent with the higher oxygen content of this vitrain sample and the higher oxygen content of vitrinites in general(D10).

It is concluded that individual macerals from a given coal can have significantly different gasification reactivities due to differences in the amount of naturally occurring, ion-exchanged metals. This effect should be most important in the gasification of low rank coals which have high carboxylic group contents and, therefore, high ion-exchange capacities.

D6. Conclusions

The gasification behavior of carbons from a number of natural and synthetic organic materials has been studied, in order to obtain a better understanding of the relationship between carbon properties and carbon gasification reactivity. Three aspects of this relationship were focused upon: the role of microporous surface area in gasification, the role of reaction-induced densification in gasification, and the effect of coal type on gasification reactivity.

D6.1 The role of microporous surface area in carbon gasification.

There is much evidence that non-catalyzed carbon gasification occurs on the large surface area lying within carbon micropores. Further, several quantitative analyses of reaction and diffusion during Spherocarb oxidation indicate that oxygen penetration at temperatures under 600 ^{0}C is complete, and that the reaction rate is strictly kinetically limited. The accessible total surface area for Spherocarb is expected, then, to be the 636 m^2/gm measured by carbon dioxide adsorption, and the measured activation energy of 36 kcal/mol to be the intrinsic activation energy for oxidation of this carbon.

The gasification rate of a sucrose char on the other hand, depends on particle size, evidence for some incomplete reactant penetration, under conditions where the assumptions of Knudsen diffusion and a tortuosity of five predict complete reactant penetration and hence no effect of particle size. The nature of the effect of particle size on sucrose char reactivity is consistent with a model in which restricted diffusion limitations exist in microporous grains with radii of 27 μm. There is the possibility that an effect of grinding contributes to the increase in reactivity with decreasing particle size effect, in light of which the fitted model parameters (grain size, intrinsic rate, and diffusivity) should be regarded as setting an upper limit on the severity of diffusion limitations for sucrose char.

The severity of diffusion limitations scales as L^2/D, and depends, therefore, on the local microporous diffusivity, a parameter determined by micropore size, and the characteristic size of the microporous regions, a parameter determined by macroporosity. The major difference

between the two synthetic carbons in this study is probably related to a difference in the characteristic size of microporous grains in the two carbons. The severity of microporous diffusion limitations for most chars should lie between that for the highly macroporous Spherocarb and that for the essentially non-macroporous sucrose carbon.

The gasification of the sub-bituminous coal chars in this study, in contrast, was not accompanied by micropore widening, and the rate of gasification bore no apparent relation to measured microporous surface areas. We believe that the gasification of these chars is dominated by catalysis, and that the rate of catalyzed gasification can be apparently unrelated to microporous surface area, presumably depending instead on properties of the catalyst. Since many chars from naturally occurring organic material may be expected to contain catalytically active inorganic impurities, it is now not surprising that previous studies have found an inadequate correlation between gasification reactivity and internal surface area.

D6.2 The phenomenon of reaction-induced carbon densification.

Kinetically limited carbon gasification does not occur at constant particle diameter as heretofore widely assumed. Gasification of various carbons at low temperatures in oxygen and carbon dioxide induces a homogeneous solid densification, which results in carbon particle shrinkage with the preservation of external surface features. Densification is the result of atomic rearrangements producing loss of pore volume in fine pores. At the length scale of the larger pores,

the optically homogeneous "microporous solid" appears to undergo a densification/shrinkage, with the larger pores shrinking also, acting as holes in a homogeneously shrinking matrix.

It is believed that the gasification reaction, by breaking bonds, removing cross links, and removing carbon atoms to reduce the density and "loosen" entanglements, increases the driving force for, and facilitates densification via rearrangements analogous to those occurring spontaneously at somewhat higher temperatures in the initial stages of graphitization.

Particle shrinkage is important in pore structure evolution during gasification or activation and therefore affects gasification rates, effective diffusivities, fragmentation behavior and activated carbon absorptive properties. For example, measured surface areas for Spherocarb as a function of conversion are in pronounced disagreement with the prediction of random pore models, which do not account for shrinkage. In addition, measurements of particle size or density are not reliable tests for determining the fraction of the reaction occurring on the external surface.

Models have been developed to predict pore structure evolution during gasification with concurrent shrinkage. The phenomenon of reaction-induced densification is an important factor determining surface area evolution during Spherocarb gasification, according to each of the models considered. Inclusion of the effect of densification/shrinkage on surface area can account for most of the large discrepancy between data and existing constant volume models.

One of several phenomena may be responsible for the remaining

discrepency between the measured surface area evolution and the numerical moswl solutions, such as heterogeneity in carbon reactivity, gasification by pore production, or pore coalescence or coarsening. A numerical solution with allowance for pore coalescence, as an illustration, provided a quite satisfactory description of Spherocarb area evolution.

D6.3 The effect of coal type on coal char gasification reactivity.

Chars from the lithotypes vitrain and fusain picked from a sub-bituminous coal had very different intrinsic gasification reactivities in carbon dioxide. The vitrain and fusain samples were almost pure concentrates of the macerals vitrinite and fusinite respectively. The vitrain char was significantly more reactive than the fusain char, especially at high conversions. This illustrates that chars from individual macerals from a given coal can have very different gasification reactivities, in which case the gasification behavior of a whole coal char must be understood in terms of the gasification behavior of its individual petrographic constituents.

The major differences between the gasification behavior of the two subbituminous lithotypes in this study were attributed to differing amounts of naturally occurring ion-exchanged metals. The higher cation content and higher reactivity of vitrain in this study is consistent with its higher oxygen content and the higher oxygen content of vitrinites in general. This effect is expected to be most important in the gasification of low rank coals, with their high oxygen contents and accompanying high ion-exchange capacities.

Digest References

D1. Von Fredersdorf C.G. and Elliott M.A. in "Chemistry of Coal Utilization" Supplemental Volume, (H.H. Lowry ed.) John Wiley and Sons Inc. N.Y. (1963) p. 969

D2. Smith I.W., Fuel Vol. 57, pp. 409-414 (1978)

D3. Nandi S.P. and P.L. Walker Jr., Fuel 43 385 (1964)

D4. Walker P.L.Jr., L.G. Austin, and S.P. Nandi in "Chemistry and Physics of Carbon, Vol. 2 pp.257-371 (P.L. Walker Jr. ed.) Marcel Dekker Inc. (1966)

D5. Johnson J.L., Am. Chem. Soc. Div. Fuel Chemistry Preprints 20 (4), 85 (1975)

D6. Rist L.P. and D.P. Harrison, Fuel 64 291 (1985)

D7. Dutta S., C.Y. Wen, and R.J. Belt, Ind. Eng. Chem. Proc Des. Dev. Vol. 16 1 (1977)

D8. Kawahata M. and P.L. Walker Jr., Proc. Fifth Carbon Conf. Vol 2 p.251, Pergamon Press, New York (1963)

D9. Dudek D., privat communication, Ph.D. Thesis in progress Department of Chemical Engineering, Massachusetts Institute of Technology

D10. Neavel R.C. in "Chemistry of Coal Utilization" Second Supp. Vol. (M.A. Elliott ed.) John Wiley and Sons Inc., p.91 (1981)

D11. Hippo E. and P.L. Walker Jr., Fuel 54 245 (1975)

D12. Floess J.K., Ph.D. Thesis, Dept. of Chemical Engineering, Massachusetts Inst. of Tech., Cambridge, Mass. (1986)

D13. Lamond T.G. and H. Marsh, Carbon Vol.1, pp.281-292 (1964)

D14. Satterfield C.N., "Heterogeneous Catalysis in Practice" Mcgraw-Hill, New York (1980) p.172

D15. Radovic L.R., Ph.D. Thesis, Department of Materials Science and Engineering, The Pennsylvania State University (1982)

D16. Adair R.R., E.H. Boult, E.M. Freeman, S. Jasienko, and H. Marsh Carbon, Vol. 9, pp.763-771 (1971)

D17. Kini K.A., Fuel 42 344 (1963)

D18. Niksa S., private communication, Measured pore size distribution for Spherocarb

D19. Chiche P., S. Durif, and S. Pregermain Fuel 44, 5 (1965)

D20. Bienenstock A., Proc. Int. Conf. 5th, 1 pp. 49-58 (1973)

D21. Kaae J.L., Carbon Vol. 23, No.1, pp.39-43 (1985)

D22. Gavalas G.R., AIChE Journal 26 4 577 (1980)

D23. Lamond T.G. and H. Marsh, Carbon 1 293 (1963)

Chapter 1. Introduction and Background

1.1 Introduction

Carbon, as the term will often be used in this thesis, refers not to an entry in the periodic table, but to a class of solid materials containing primarily carbon, with varying amounts of impurities including hydrogen, oxygen, nitrogen, sulfur, and inorganic material. Carbons can be found in nature, such as natural graphite, or can be made by heating almost any organic material in the absence of air. Much of the original organic material that is rich in hydrogen and oxygen is lost to the gaseous phase upon heating, leaving a porous solid residue, carbon or char, containing some hydrogen and oxygen in amounts that decrease with increasing charring temperature.

Carbons participate in high temperature reactions with a variety of gaseous species, in which the solid carbon is consumed and new gaseous species are produced. These are the so-called gas reactions of carbon, and the set of gaseous reactants includes oxygen, carbon dioxide, hydrogen, and water vapor.

The gas reactions of carbon are fundamental to many commercial endeavors, including coal gasification and combustion, the production of activated carbon, and those applications in which carbon is used as an engineering material. The gasification reactivity of carbons is especially important in many gasification processes, determining equipment size and/or carbon conversion efficiency(1).

The gasification of coal is important in much of the non-petroleum based energy technology. For instance, it is clear that at some time in the future, gasification of coal on a large scale will be needed to

meet the demand for natural gas. In addition, the production of low B.T.U. gas from coal appears attractive in conjunction with gas-steam turbine power cycles as a solution to the sulfur problem in power production(2). Also, the production of hydrogen through char gasification is important in coal liquifaction.

Many different gasification processes have been proposed, and for the optimal design and selection of processes, an understanding of gasification kinetics is important. Under most conditions, the total time required for the gasification of a coal particle is dominated by the burn-out of the residual char remaining after devolatilization. The design of many gasifiers is carbon reactivity limited and, in fact, many gasifiers operate with significantly less than 100% carbon conversion despite strong economic incentives to use coal efficiently. (The cost of coal has been estimated to be about 40% of the total cost of conversion to pipeline quality gas (3).) Carbon conversions for several industrial gasification systems are given in table 1.1.

Table 1.1: Carbon Conversions in Industrial Gasification Processes*

Gasifier	Koppers-Totzek	B+W du Pont	Winkler
Type	Entrained Flow	Entrained Flow	Fluid Bed
Fuel Carbon Conversion**	88.6%	84.1%	80%

* from (4)
** carbon in gases/carbon in input fuel

Note that carbon losses in fluidized bed systems are largely due to entrainment of dust and increase with the friability of the fuel(5).

Entrained flow gasifiers have difficulty achieving high carbon

conversions in part because they operate with cocurrent reactant flow in which both the temperature and the carbon concentration decrease from inlet to outlet, providing the lowest driving force for reaction in the high conversion region. Carbon conversion, then, becomes rather insensitive to increases in reactor size, and it becomes uneconomical to gasify more than 85-90% of the carbon in a single pass(1). Pulverized coal combustion, on the other hand, has been operated successfully for years with high carbon conversions. In one case, however, use of an unfamiliar coal in an existing pilot scale boiler resulted in unacceptable carbon conversions, apparently due to the low reactivity of the partially burned char residue(6).

Because of its importance there has accumulated a large body of research on coal char gasification kinetics, much of which is very empirical. Many recent studies are attempting to obtain more fundamental kinetic information which will hopefully be widely applicable. The common goal of the empirical and fundamental approaches is to predict the effect of reactant gas composition, pressure, temperature, coal type, char preparation and prior gasification history on the gasification rate and the product distribution.

1.2 Problem statement

This thesis concernsitself with the relationship between carbon properties and carbon gasification reactivity. The wide variation in gasification reactivity among different carbons in a given gaseous environment is evident from the reactivity data compiled and analyzed

by Smith(7). Reactivity in the carbon-oxygen system per unit internal surface area, corrected for external and pore diffusion limitations, and normalized to 101 kP oxygen partial pressure, varies by as much as four orders of magnitude at a given temperature.

There is, at present, an inadequate understanding of the phenomena that determine the rate at which a given carbon will gasify. It is anticipated that char reactivity is influenced by factors which include choice of the parent organic material, possible addition of catalyst, and the char's temperature-time and reaction history. Identification and fundamental understanding of the important phenomena could guide the design of gasification processes to enhance char reactivity, and thus improve performance. The Exxon catalytic coal gasification process(8) is an example of a design that relies on enhancement of char reactivity to improve performance. K_2CO_3 is added to coal to increase char reactivity, making possible a reduction in temperature to 700 ^oC, where significant direct methanation occurs, while maintaining acceptable carbon and steam conversion. A review of the current literature on carbon gasification, with an emphasis on phenomena that determine gasification reactivity is the subject of the next section.

1.3 Literature review

The literature on carbon is truly enormous, with the literature on the gas reactions of carbon being a substantial contributor. Fortunately, many good review articles are available on the topic of carbon gasification and combustion, each with a somewhat different emphasis(9,10,11,12), as are more comprehensive reviews on important

subtopics such as catalyzed gasification(13), and activated diffusion in carbons(14). These are the sources to which to turn for general information or as a starting point. Here I will discuss those aspects of carbon structure and carbon-gas reactions which are especially relevant to our research results.

1.31 Carbon structure

Crystalline graphite is composed of sheets of aromatically bonded carbon, stacked together with a uniform interlayer spacing, and aligned in such a way as to produce a regular three-dimensional crystal structure. Graphite is almost pure carbon, impurities residing only in defects, at crystallite boundaries, or as physically incorporated inclusions. Non-graphitized carbons are also composed of stacked sheets of aromatically bonded carbon, which, however, are small, often imperfect, often misaligned, and without three dimensional order. The lack of a three dimensional crystal structure, even among regular stacks of perfect graphitic layers, is the characteristic of the "turbostratic" structure of lower temperature carbons. Hydrogen, oxygen, and other heteroatoms are relatively common in low temperature carbons, existing at the edges of graphitic layers, as cross linkages between layers, or as defects within layers. For a variety of coal chars prepared at 700 ^{o}C the atomic ratio of carbon to hydrogen was about 5 to 1, and the atomic ratio of carbon to heteroatoms about 20 to 1(15). The hydrogen content in graphite is much lower(15).

X-ray diffraction is perhaps the most powerful tool for the investigation of carbon structure, yielding information on average

layer diameter, layer diameter distribution, interlayer spacing, average stacking depth, and fraction non-crystalline or X-ray amorphous material(16,17,18,19,20). A model of carbon structure, arising primarily from these X-ray studies, is depicted in Figure 1.1(21). The lines in the diagram are small, graphitic layers, viewed from the side, whose imperfect packing arrangement is responsible for carbon micropores. The circles in the diagram are not part of the structure, but rather indicate regions which would be identified as crystalline by X-ray diffraction. (Note that the crystallite size determined by X-ray diffraction is smaller than the true dimension of the continuous but kinked graphitic layers.) Not shown in the diagram are cross linkages between layers and some amorphous material, possible heteroatoms or tetrahedral carbon(16).

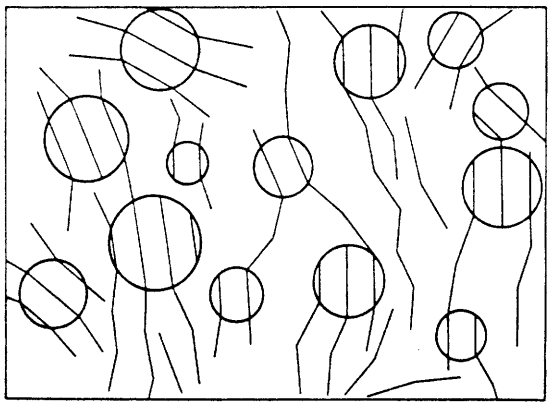

Figure 1.1 Amorphous carbon structure, taken from Marsh et al.(21)

Whereas the imperfect packing arrangement of graphitic layers is responsible for carbon microporosity, larger pores are physical rather than chemical cracks in the solid matrix. Carbon contains pores with diameters from several microns or larger to several angstroms, with many carbons having significant pore volume throughout the entire range of pore diameter(22). Carbon pore structure will be discussed in more detail in subsequent sections.

1.32 Studies of the gas-reactions of graphite and pure carbons

The current fundamental understanding of factors that determine carbon gasification reactivity comes primarily from the literature on graphite and pure carbons. Important factors include the following:

1.321 Crystallite orientation. Several researchers(23,24) have found large differences between the reactivities of the different crystalline faces of graphitized carbons. Walker et al.(23) have established a qualitative correlation between the reactivity of graphitized carbon plates and the proportion of the exposed surface composed of crystallite edges. Smith and Polley(24) have found a higher reactivity by a factor of about 200 for a carbon black surface containing many exposed edge sites compared to a graphitized sample composed entirely of crystallites with their basal planes oriented parallel to the surface. Attack can occur on basal planes if active sites are provided by surface imperfections such as dislocations. Reaction on such sites creates active surface area in the form of edge sites, and in the presence of a catalyst particle these sites of attack can grow into hexagonal pits which have been observed optically(25).

1.322 Crystallite size. It is generally difficult to distinguish between crystallite size and orientation effects because the two variables are often coupled in practice. Armington(26), however, has been able to change crystallite size independently by looking at the special system of graphitized carbon black, which forms non-porous polyhedral particles whose surfaces are composed almost entirely of carbon basal planes. He measured the reactivity of different sized particles (which are composed of different sized crystallites) and found that specific reactivity ($gm/min\text{-}m^2$) increased with increasing crystallite size. He theorizes that the larger the crystallite, the greater number of impurity atoms capable of affecting any given edge carbon via pi-electron transfer through the basal plane. This effect is probably less important than that of crystallite orientation.

1.323 Non-carbon sites. Carbons contain varying amounts of hydrogen, oxygen, nitrogen and sulfur, which are thought to occur in structures which are generally more reactive than the aromatic carbon systems. The importance of non-carbon sites to reactivity has been stressed in several studies(27,28,29,30). Snow et al.(27) have found that carbon black oxidation rate is generally proportional to the hydrogen content of the blacks although other factors are also important.

Blackwood et al.(29) have correlated the carbon dioxide reactivity of purified carbons with their oxygen contents and have observed the depletion of oxygen sites during reaction. In another paper(30), Blackwood correlated the hydrogen reactivity of various carbons to their oxygen content and has further postulated the existence of two types of oxygen containing active sites.

1.324 Catalysis. Inorganic impurities can profoundly affect the rate of carbon gasification. The addition, for example, of 100 ppm (atomic ratio) Fe to pure polyfurfural alcohol carbon increased the rate of gasification in carbon dioxide at 893 ^{o}K by a factor of 450(31)! With many carbons made from naturally occurring organic materials containing typically 10% ash, the potential for catalytic effects in the gasification of these carbons is clear.

A wide range of inorganic materials have been found to be active gasification catalysts, with the magnitude of the catalytic effect being a function of the metal, its dispersion, its chemical state, and the gaseous environment(13). Active catalysts for the reaction between carbon and molecular oxygen include alkali metal oxides and salts and the alkaline earth oxides and salts(13), with Amariglio and Duval(32) reporting catalytic efficacy in the order Na > Ba > Sr > Mg > Ca. Many transition metals and oxides are also active, with Ni > Co > Cu > Ag > Fe > Ca (inactive), at an impurity level of 400 ppm as reported by Marsh and Adair(31). Note that this group of transition metals is much more active than the alkaline earths, Ca being regarded as inactive at the 400 ppm level. Other active catalysts include compounds involving Ag, Pt, Ir, Rh, Ru, Pd, Au, Cu, Pb, Cd, As, Sb, and Bi(13). Certain additives have been observed to inhibit the oxygen reaction including phosphorus pentoxide and certain compounds containing halogens. A more detailed discussion and information on catalyzed gasification in other environments can be found in McKee(13).

Catalyst dispersion is critical to catalyst efficacy, as illustrated by the work of Floess(33). Addition of 3.6 wt% initially

atomically dispersed Ca to a sucrose carbon, increased the carbon's gasification reactivity in air by almost two orders of magnitude, while addition of 1 μ sized $CaCO_3$ inclusions by physical mixing increased reactivity by only a factor of two. In addition, Radovic(34), has related the gasification reactivity of a lignite char to the degree of CaO dispersion measured by X-ray diffraction line broadening.

Electron microscopy and, especially, controlled atmosphere electron microscopy have been very valuable in elucidating the nature of the catalytic action on carbon surfaces. Gasification is seen to occur directly at the carbon catalyst-particle interface, often producing channels or etch pits in the carbon substrate. Ir, for example, has been observed by C.A.E.M. to form channels in graphite upon heating in 5 torr O_2 at 1000 ^{o}C(13). In a study of gasification of polyfurfuryl alcohol carbon in CO_2, N_2O and O_2, with a variety of inorganic additives, rarely, if ever, was gasification seen to proceed evenly over the entire surface(35), in contrast to the gasification of the pure, undoped carbon. Other catalysts have been observed to wet and spread over graphite edge planes, causing gasification by uniform surface recession(13,36). Recent detailed C.A.E.M. studies have painted a complex picture, with the behavior of catalyst particles depending on many factors including particle size, oxygen partial pressure, and temperature(13,36). In some cases, channeling occurs in well-defined crystallographic directions and, in other cases, in random directions. Some catalyst particles have even been observed to produce channeling and etch pits simultaneously in different regions of the graphite surface(13).

1.33 Studies of low temperature chars from naturally occurring organic materials

Low temperature chars from naturally occurring organic materials are the chars of commercial importance in energy applications. These chars are more complex than graphite and pure, high temperature carbons, and have thus been the subject of fewer fundamental investigations. One factor that has been directly shown to be important to the gasification of many low rank coal chars is the presence of naturally occurring group I and II metals, ion-exchanged on carboxylic functionalities on the coal surface(37,38,34). Removal of the naturally occurring cations in lignites markedly decreases the gasification reactivity of lignite chars, and subsequent re-loading of the ion-exchange sites with calcium ions can essentially restore the initial reactivity(34).

The importance of catalysis in higher rank coals, in contrast, is unclear. Tomita et al.(39) have reported little or no catalytic effect in the carbon oxygen reaction upon physically mixing a pure carbon with many minerals commonly found in association with coal. In light of the results of Floess pertaining to Ca dispersion, this is not surprising. The pure carbon studies discussed above demonstrate that only a <u>very</u> small fraction of the mineral matter in coal chars would need to be well dispersed to produce a significant catalytic effect, such as the organically bound mineral matter. Nevertheless, demineralization of bituminous coals often <u>increases</u> the reactivity of their chars(40)! The increase in reactivity may be due to an increased accessibility of internal surface area following mineral matter removal(41). This

result does suggest, however, that catalysis by mineral matter is not playing a dominant role in the gasification of the high rank coal chars. There have also been many studies in the past several years of enhancement of char reactivity by addition of catalytic inorganic matter(42,43,44,45,).

Drawing again from the pure carbon studies, it is believed that char reactivity is determined primarily by total surface area and its accessibility, the presence of inorganic catalysts, and the concentration of carbon active sites, which are thought to involve heteroatoms, edge atoms, etc., and to be generally related to the degree of disorder in the carbon(40,10,11,38). It is known that char reactivity tends to decrease with increasing rank or increasing severity of heat treatment(46,47,34). This is reassuring, but fails to provide any further insight, as each of the variables surface area, accessibility, catalyst efficacy, and carbon disorder is expected to decrease with increasing rank or increasing severity of pyrolysis conditions.

In order to attack the posed problem of fundamentally relating carbon reactivity to carbon properties, we believe it is necessary to directly examine the underlying phenomena that are thought to be important to gasification reactivity. This fundamental approach should best start with phenomena determining the accessible surface area for gasification, from which a meaningful intrinsic rate can be calculated. This intrinsic rate would be a true property of the carbon surface, and could potentially be fundamentally related to (or at least correlated with) other properties of the carbon surface.

1.34 The appropriate total surface area for gasification

There is, at present, much uncertainty about the effective total surface area for gasification. It is well known that carbon surface areas measured by vapor adsorption techniques are often a strong function of the size of the adsorbate molecule(14). A striking example is the difference between the carbon dioxide surface area (510 m^2/gm) and the nitrogen area (1 m^2/gm) for the untreated subbituminous coal char in this study. Note that the nitrogen and carbon dioxide molecules are quite close in size, with kinetic diameters of 3.16 and 3.23 Å respectively(48). Such large discrepancies between areas measured by carbon dioxide and nitrogen are quite common, and Nandi et al.(49) have presented good evidence that they are associated with the occurrence of restricted diffusion in carbon micropores.

Restricted diffusion occurs when the size of the pore approximates the size of the diffusing molecules. The diffusing molecules, then, are at all times under the influence of the potential energy field associated with the adjacent pore walls, and the rate of diffusion is slow, activated, and very sensitive to the size of the pores and the size and shape of the diffusing species(14). Restricted diffusion is commonly observed for a variety of gases including nitrogen and carbon dioxide in both zeolites and coals or carbons, and is responsible for the long times often required to attain equilibrium in surface area measurements, as well as for the molecular sieve nature of coals and chars(14). Several reviews are available on the topic of diffusion in

fine pores(14,50). Nandi et al. have measured characteristic times for diffusion of nitrogen and carbon dioxide into carbon micropores at and above room temperature. Near room temperature, nitrogen diffused faster than carbon dioxide, but an extrapolation of measured nitrogen diffusion rates to the temperature of nitrogen adsorption experiments (77 ^{o}K) revealed that nitrogen diffusion would be very slow at that temperature, and that a negligible fraction of the total surface area would be accessed within the time alloted for adsorption equilibration(49).

The identification of the appropriate total surface area for gasification is equivalent to understanding the role of the microporous surface area. There is, at present, insufficient information on this topic, a fact that is apparent from the following summary of relevant information from existing studies. Several studies have demonstrated that carbon reactivity can not be adequately correlated with total surface area(7,51,52). Laurendeau questions the accessibility of the total surface area in his review of gasification kinetics(10), while restricted diffusion was expected to be important only during low conversion for the gasification of an anthracite char in oxygen(53). Johnson(46) cites evidence for micropore widening during gasification of coal chars, while Rist et al.(54) observed a characteristic micropore diameter of 20 Å, independent of conversion. Dutta observes that the rates of gasification of his chars are proportional to the surface area lying in pores with diameters larger than 30 Å(51), while there is evidence for micropore widening and thus microporous reaction during the gasification of an anthracite char(55).

Further, Gavalas expects that slow diffusion in micropores will confine the reaction front to a region in the vicinity of the large pores, and thus formulates his model explicitly considering only the larger pores, assuming that the micropores contribute to the reaction an amount that is proportional to the large pore surface(56). Simons, on the other hand, considers reaction in all of the pores measured by carbon dioxide adsorption(22). There is, clearly, much confusion in the literature surrounding this topic, as well as a lack of experimental information.

1.35 Surface area evolution

In addition to identifying the effective total area for gasification, predicting the evolution of that surface area during gasification is an important and interesting problem. Gasification widens carbon pores, usually causing an initial increase in surface area until a point is reached where the coalescence of pores or loss of surface area on walls between pores begins to dominate, and surface area per particle decreases. The area evolution is an interesting geometric problem which is dealt with by several existing models of carbon pore structure(56,57,58,59).

The model containing the most detailed and rigorous treatment of this problem is that devised by Gavalas(56), which presents an exact solution for the surface area development during uniform reaction of a porous solid, containing infinitely long cylindrical pores with no closed porosity and an arbitrary initial pore size distribution. The model has been successfully compared with reaction rate data, assuming

that the concentration of active sites on the total surface area is constant, and allowing the zeroth and first moments of the initial pore size distribution to be adjustable parameters. Calculation of the two moments from a measured pore size distribution would make possible the generation of the exact Gavalas solution and a more rigorous comparison with experimental data. The random pore model devised by Simons(22,57), offers an alternative picture of carbon pore structure, and, although not dealing with the pore growth and overlap problem in as much detail, does offer an alternative prediction for surface area evolution.

1.36 The phenomenon of gasification-induced carbon particle shrinkage

During the course of this thesis, Dudek(60), in a parallel study at M.I.T., observed significant diameter reduction during air-oxidation of Spherocarb carbon particles under conditions where no preferential gasification on the external surface is expected. Carbon particle diameter reduction has also been inferred from measurements of pore volumes or particle densities by Floess(33) and by Culver and Heath(61). Johnson(46) has observed diameter reduction during hydrogen gasification of coal chars, which he attributes to a homogeneous densification phenomenon. All fundamental treatments of kinetically-limited carbon gasification, on the other hand, consider reaction at essentially constant particle volume. Possible explanations for the diameter reduction phenomenon are perimeter fragmentation, the presence of a significant reaction component on the external surface of the particle, and reaction induced homogeneous particle shrinkage. The

origin of this phenomenon remains unknown, however, as do its implications regarding gasification behavior.

1.37 The effect of coal type or maceral composition

Another variable which may have an important influence on gasification reactivity is petrographic composition, or coal type. Type refers to the classification of a coal according to its vegetable matter composition at the start of coalification, in contrast to rank, which is a measure of the extent of coalification, or geologic age. All coals are composed of microscopic, optically homogeneous materials that have been called macerals (in an analogy to inorganic minerals). In addition, characteristic groupings of macerals occur, called lithotypes, which give coals their more or less pronounced macroscopic banding. It is the relative proportion and spatial arrangement of the different macerals and minerals which distinguishes coals by type(62).

Whereas a correlation between coal rank and char gasification reactivity has been noted(38), relatively little is known about the relationship between maceral composition (coal type) and reactivity. Variations in the reactivities of individual macerals may be especially important in determining reactivity as a function of conversion as some macerals may be attacked preferentially, others persisting and becoming concentrated in the highly converted char.

Many different macerals have been identified by geologists and paleobotanists, but for the purposes of this study it is most useful to classify material according to the three maceral groupings: vitrinite, exinite, and inertinite. Vitrinite, which constitutes typically 80% of

most coals, is derived from plant structural material (woody material) and is the plasticizing, coke-making component of coals. Among the three maceral groups it is intermediate in H/C ratio, aromaticity and volatile matter content. Although inertinite is also composed of lignocellulosic (woody) material, it has undergone more significant chemical changes in the biochemical stage, probably associated with high temperatures. Inertinite has the least hydrogen and volatile matter and has the highest fraction of aromatic carbons.

Exinite is composed on non-woody plant remains, is relatively rich in aliphatic structures, and has high hydrogen and volatile matter contents(63).

The differences between macerals are most pronounced in low rank coals; by the time coalification has proceeded to the anthracite stage these differences are much less important. The available information on chemistry and structure suggests that inert macerals should have lower intrinsic reactivities in combustion or gasification. Indeed, Nandi et al.(64) have observed the occurrence of very poor carbon conversion for coals of high inert maceral content tested in a pilot scale pulverized coal-fired boiler. Unburned residue from the poorly performing coal consisted of inert macerals and the carbon conversion was insensitive to changes in combustion conditions. It is interesting to note that the results of Nandi et al. do not necessarily imply that the macerals found in the unburned residue are intrinsically less reactive since pulverized bituminous coal particles can take on one of several different structures in a flame, which structure, depending in part on petrographic composition. In fact, there is some indication

that inert macerals indeed tend to form char particles with highly developed internal structures which might persist in flames.

On the other hand, Alpern and Chauvins as reported in Stach(65) found that fusite and semifusite were the most reactive microlithotypes in the combustion of anthracite briquettes. This could be a surface area or porosity or mineral matter effect, especially since the chemical differences between macerals in high rank coals are expected to be small. Measurements of surface areas of maceral concentrates are few(66,67,68), and no data exist to the author's knowledge on surface areas of chars made from maceral concentrates. Johnson(46) has measured reactivity in steam and hydrogen of chars made from whole coals and from hand picked vitrains and fusains. He correlated reactivity with the carbon content of the unpyrolyzed coals, independent of petrographic composition. Overall, the experimental information is somewhat ambiguous, although Johnson's work strongly suggests that coal type is less important than coal rank in determining reactivity.

1.4 Thesis objectives

This thesis addresses several aspects of the relationship between carbon reactivity and carbon properties. The first is the identification of the accessible total surface area for carbon gasification, an endeavor which is important in the successful development of correlations of carbon reactivity, and in the development of gasification or pore structure models. The lack of knowledge of the appropriate area is, in addition, a major stumbling

block to the measurement of meaningful intrinsic reactivities and thus the attainment of a more fundamental understanding of the factors determining carbon gasification reactivity. A properly calculated intrinsic rate would be a true property of the carbon surface and could potentially be fundamentally related to (or at least correlated with) other properties of the carbon surface. We hoped to identify the effective surface area for gasification of several carbons, and, further, to understand the factors that determine the effective area for carbons in general.

Secondly, it was undertaken in this thesis to investigate the phenomenon of gasification-induced carbon densification/shrinkage observed in this lab by Dudek(60). The first goal was to find an explanation for the observed diameter reduction during gasification, the second to measured diameter reduction during the gasification of other carbons, and the third to understand the influence of the phenomenon on surface area, and to develop models of surface area evolution during gasification with concurrent shrinkage.

Finally, we look at an important topic which has thus far received insufficient attention: the effect of coal type or maceral composition on coal char gasification reactivity. Our goal was to measure the reactivities of chars from maceral concentrates separated from one coal to directly assess the importance of type to its gasification behavior, and hopefully to gain some insight into the role of coal type for other coals.

Chapter 2. Materials and Experimental Procedures

2.1 Char preparation

This thesis presents experimental results obtained for Spherocarb carbon and chars from a Utah sub-bituminous coal, Pittsburgh #8 high-volatile bituminous coal, a Montana lignite, reagent grade sucrose, and a sucrose and carbon black composite.

The sub-bituminous coal is PSOC 156 from Alton Mine, Kane County, Utah, with an apparent and reflectance rank of sub-bituminous A. It was obtained from the Penn. State University Coal Bank in the form of approximately 4 inch pieces in which sizable pure lithotype inclusions could be identified. Vitrain and fusain were handpicked from this coal, examined and purified under low magnification, and analyzed (along with the whole coal) for maceral composition using a Leitz MM5 microscope and a Leitz 100X oil immersion objective. The coal was ground in a metal rod mill and then sieved to produce samples having relatively narrow particle size distributions in the pulverized range. A 45-53 μ fraction was used in this study. The maceral fractions were ground in a small mortar and pestle. Elemental analyses of the maceral fractions and the whole coal appear in table 2.1.

Experiments were also performed on chars from PSOC 156 sub-bituminous coal which had been washed with hydrochloric and hydrofluoric acids in an attempt to remove its mineral matter, according to a procedure taken from Radovic(52). The acid-washing removed much but not all of the mineral matter as seen in Table 2.2.

Table 2.1. Elemental analyses of PSOC 156 whole coal and lithotype samples

Elemental analysis (dry, ash-free)	Whole Coal*	Vitrain**	Fusain**
%C	76.5	70.6	79.7
%H	5.3	5.3	4.0
%O	16.7	21.8	14.8
%N	0.1	1.3	0.8
%S	1.4	1.1	0.7

* from Penn. State Coal Data Base (oxygen by difference)
** from Huffman Labs. Inc., Wheat Ridge, CO. (direct oxygen)

Table 2.2: Ash contents of various coals and chars

Sucrose carbon	370 ppm
Spherocarb	760 ppm(69)
Subbituminous coal	8.5%
Acid-washed subbituminous coal	.74%

Experiments were also performed on chars from PSOC 156 sub-bituminous lithotypes and whole coal whose naturally occurring cations had been extracted by ion-exchange with ammonium acetate, according to the procedure of Morgan et al.(37). The filtrate was analyzed for Ca^{2+} and Mg^{2+} by atomic absorption spectroscopy. Sucrose chars were prepared from a low temperature sucrose char (heat treatment at 900°K) provided by Joe Floess(33), with particle sizes of 150-212 μm or 90-106 μm. The calcium sucrose char used here is identical to Floess' 3.6 wt% Ca sucrose char. The Pittsburgh #8 high-volatile bituminous coal was obtained from M.J. Warnat(70), and the Montana lignite is that used by T. Hastings(71).

Chars were made from these parent materials by heat treatment in nitrogen in a small tube-furnace, in a reproducible manner, involving a slow temperature ramp followed by a one hour holding period at approximately 1000 °C. A higher temperature char from the acid-washed

sub-bituminous coal was made by heating the 1000 °C char further, at 1200 °C for one hour.

Two carbons which were studied without prior heat treatment were Spherocarb carbon, a pure, synthetic carbon consisting of spherical particles (60/80 mesh) sold by Analabs, and a sucrose char/carbon black composite supplied by J. Helble(69). The ash contents of some of the chars and coals appear in table 2.2.

Experiments were performed on smaller particle sizes of several of the chars. 60/80 mesh (177-250 μm) Spherocarb particles were crushed with a small mortar and pestle and sieved to <38 μm. The oversize material was reground until it also passed a 38 μm sieve. Small particle sizes of the sucrose char were obtained several ways. The small particle sample designated sample A was obtained by grinding the 90-106 μm particles, collecting the fraction that passed a 38 μm sieve, and then regrinding the oversize fraction until all of the material was <38 μm, as with Spherocarb. Sample B was treated in the same way, except that the <38 μm material was subsequently further ground. The three samples with mean particle sizes of 50, 20, and 5 μm, were obtained as follows. The 150-212 μm particles were ground and sieved and the 45-53 μm fraction collected and designated the 50 μm sample. The material <38 μm was collected in a test tube, then entrained in a flow of nitrogen gas which was fed through a hypodermic needle to a cascade centripeter (Bird and Tole, from B.G.I. Inc., Waltham MA). The particles collected on the second stage were determined to have a mean particle size of 20 μm by S.E.M., and became the 20 μm sample. A portion of the 20 μm sample was further ground, examined by S.E.M.,

determined to have a mean particle diameter of 5.3 μm, and designated the 5 μm sample. Diameters of 1281 particles were measured, and the mean particle size was calculated as $\Sigma d^3/\Sigma d^2$ so that the mean particles have the same external area per unit weight (or per unit volume) as the original sample. After measurement of the particle size distributions it was clear that the centripeter classification had been poor, giving fractions with quite broad particle size distributions. However, since the fractions collected were already characterized, contained sufficient material, and did have the desired mean particle sizes, it was decided not to try to identify the problem or to improve the centripeter separation. Size distributions of the four samples are presented in table 2.3.

Table 2.3. Particle size distributions of sucrose char samples

Diameter range (μm)	Number of particles 5 μm sample	20 μm sample
0 - 5	612	297
5 - 10	31	186
10 - 15	5	72
15 - 20	0	39
20 - 25	0	24
25 - 35	0	9
35 - 45	0	4
45 - 55	0	2
55 - 65	0	0

Chars at various stages of gasification conversion were produced by reaction in a thermo-gravimetric analyzer or, for larger samples, in a small-tube furnace. For the experiments in the tube furnace, carbon conversions were determined after the experiment by measuring either ash content or total sample weight. Uniform gasification could be

obtained for samples as large as 200 mg by dispersing the particles as a thin bed on a piece of platinum foil no more than 2 inches long. The sample density gm/cm^2-bed-area was approximately the same as during T.G.A. experiments while the volumetric flow rate of reacting gas was higher, 1 lit/min in comparison to 200 ml/min in the T.G.A.. Measurements of ash content at various positions in the bed confirmed that gasification under these conditions was uniform. Measured gasification rates in the T.G.A. using platinum and alumina pans were identical, demonstrating that platinum pans do not influence gasification.

2.2 Gasification rate measurements

Gasification rates were measured with the Cahn thermogravimetric analyzer (T.G.A.) described by Floess(33). Measurements of the gasification reactivities of the chars from the sub-bituminous lithotypes were made in the Dupont T.G.A. in 66-053. The configuration of the Cahn T.G.A. and the procedure for kinetic measurements was essentially the same as in Floess(33), with several exceptions. Rates were measured with the Cahn T.G.A. in both the up- and downflow configuration, and the vacuum pump and critical orifice system for reduction of noise due to room pressure fluctuations were not needed for the relatively large sample sizes used in these studies. The char samples were given their final heat treatment before the start of T.G.A. experiments and were therefore not heat treated in the T.G.A. before reaction. Carbon dioxide gasification rates were measured in the upflow configuration to minimize diffusion of atmospheric oxygen

into the reaction chamber from the large vacuum bottle housing the balance mechanism. Air gasification rates were measured in either the up- or down flow configuration. A total flow rate of 200 cc/min was used. The reaction gases were high purity air, nitrogen, and carbon monoxide from Matheson, as well as Matheson oxygen-free carbon dioxide.

The reaction rate was maintained below .2 mg/min to avoid the effects of external or intra-bed mass and heat transfer limitations(33). Gasification reactivities were, in fact, found to be independent of bed size for under several conditions tested here (each with a gasification rate <.2 mg/min).

2.3 Microscopy

Many carbon particles at various stages of conversion were examined in this study by S.E.M. and by optical microscopy. It was important in this investigation to be able to observe, at high resolution, the transformation of surface features of particles over the course of gasification conversion. We needed to examine a given particle in a given orientation at several stages of conversion. This requires that the particle be mounted in a holder that is stable and inert under gasification conditions, is preferably electrically conductive to improve the S.E.M. image, and can be mounted on an S.E.M. stub; and that the S.E.M. preparation does not destroy or contaminate the particle (such as occurs during coating with a conducting material). A first attempt to make a suitable holder resulted in a piece of thin platinum sheet, folded to hold on its

surface several stacked layers of 80 mesh platinum gauze. Upon distribution of a small sample of carbon on the gauze surface, the particles settled into more or less stable locations within the three-dimensional gridwork of the stacked layers. This mounting produced a satisfactory S.E.M. image and was inert under gasification conditions, but an insufficient number of particles retained their original orientation throughout the specimen handling that occurs during the preparation for both microscopy and gasification.

The final, successful particle mounting consisted of a 1 cm cube of graphite with conical pits indented in the surface with a sharp instrument, into which the carbon particles of interest were lightly pressed. The graphite was observed to undergo little gasification in the T.G.A. under the conditions used to partially gasify the carbon particles. (Significant graphite oxidation could raise the sample temperature, deplete the reactant gas, and/or eventually destroy the mounting.) The graphite mounting produced a good S.E.M. image with relatively little charging, and at least a complete hemisphere was visible for most particles. It was discovered that the extent of conversion was greater for Spherocarb particles on the graphite mounting, than that expected from T.G.A. rate measurements on a bed of particles under identical conditions. (The expected extent of conversion was compared to that estimated from the extent of particle shrinkage, the relationship between shrinkage and conversion having been independently established by experiments in the electrodynamic balance, in which single particle conversions are directly measured.) Covering the exposed graphite surfaces by enclosing the piece in folded

platinum foil before making the pits eliminated this problem, which was apparently due to an effect of the graphite piece with its high emissivity on the sample temperature in the T.G.A.. With the graphite mounting covered with platinum foil, enough of the particles (80% on average, although varying with particle type) were present and maintained their orientation after reaction and handling to make the technique useful.

Several of the sub-bituminous coal chars were examined by S.E.M. using conventional techniques. Small powder samples were dispersed on a S.E.M. stud covered with graphite paint, and coated with a thin layer of gold to improve conductivity and enhance the image. The microscope in both cases was a Cambridge Instruments Stereoscan 250 Mk3 with 35 Å resolution under optimal conditions. Surface features of some carbon particles were also examined by optical microscopy as a function of conversion. After photographing selected surface features of the unreacted particles, the particles were placed in a very small quartz dish, which had been made be sealing and then cutting off the end of a 4 mm I.D. quartz tube. This dish was placed in the T.G.A., on top of the platinum pan, and exposed to reaction conditions which had been chosen to produce the desired extent of conversion. The particles were then removed, placed in a shallow ceramic dish, and repeatedly disturbed, under the microscope, until the original particle orientation was obtained. This procedure was successful, although tedious, and was inferior to the captive-particle S.E.M. technique only with respect to the images obtained, that being

the case because of the limited resolution and very limited depth of focus of optical microscopy.

2.4 Adsorption isotherms, and adsorption equilibration times

Nitrogen and carbon dioxide adsorption isotherms and adsorption equilibration times were measured for many of the carbons in a volumetric adsorption apparatus. The apparatus and procedures are those described by Floess(33) with the following exceptions. The gas delivery system was expanded to handle carbon dioxide, using similar equipment to that installed for nitrogen and helium delivery. A 1000 torr pressure transducer was added to the two existing 10 psi units in order to allow measurement of pressures up to (and somewhat above) one atmosphere to provide the capability of measuring complete nitrogen isotherms. A second port for a pressure transducer was connected to the gas storage volume in order to store one of the transducers not in current use under vacuum, and to thus eliminate the lengthy evacuation/desorption procedure upon switching to a different transducer. This configuration also makes possible an easy independent check of the pressure reading from the installed transducer at any time by opening the three-way stopcock.

In order to protect the pressure transducers from contamination (which has occurred in the past!), O-ring valves were placed between both transducers and the vacuum system. The best procedure for evacuating a sample whose surface area is to be measured, while protecting the pressure transducers, is as follows. The O-ring valve should be closed, and the sample stopcock opened very, very slowly

until it is wide open. (Opening this stopcock quickly is very likely to cause part of the sample to be entrained in the gas flowing from the sample stopcock into the calibrated volume (the complex shape between the sample and the pressure transducer), and thus deposit the sample in the calibrated volume. This situation requires disassembly of the glassware and a difficult cleaning procedure.) Atmospheric gases have now filled the calibrated volume. The O-ring valve leading to the pressure transducer should now be opened very slowly, allowing gas into the transducer. The three-way stopcock should now be opened slowly while observing the pressure reading, until the pressure begins to drop slowly. After some period of time the three-way stopcock can be further opened to speed-up the evacuation at low pressures.

Note that the calibrated volume has to be determined again by experiment when a new transducer is installed in the top position, and that the position of the inner piece of the O-ring valve has some effect on this value. The calibrated volume must be determined by experiment from the only independently known volume in the apparatus, which is that of the pear shaped vessel connected to the calibrated volume through a stopcock. Its volume including the channel in the stopcock is 42.816 cm^3.

To facilitate the cleaning necessary if powder is carried into the sample volume, the glassware forming the calibrated volume, sample volume, and known volume was made removable, being connected to the vacuum system and gas delivery system by two Cajon O-ring fittings. These fittings are found inside the plywood box, near the top left, and connect the glassware in the box to the vacuum system via two legs

extending down into the box from above. After carefully removing this detachable section of glassware, it can be washed by immersion in a solvent.

There appears to be, at present, some material with finite adsorption capacity in the calibrated volume, as there is some carbon dioxide pressure loss with the sample stopcock closed. The material is probably carbon, existing as a film on the walls of the glassware or inside the transducer chamber. It is not a problem in the measurements of high surface areas, but is currently the factor that limits the accuracy of the measurement of low carbon dioxide areas. The effect on nitrogen measurements is negligible, as nitrogen adsorption at the temperature of the calibrated volume (room temperature) is quite small.

Adsorption isotherms of carbon dioxide were measured at 0 ^{o}C in an ice bath, and those of nitrogen at 77 ^{o}K in a liquid nitrogen bath. Surface areas were calculated from the carbon dioxide isotherms using the Dubinin-Polanyi equation, and from the nitrogen isotherms using the B.E.T. equation. The area of an adsorbed carbon dioxide molecule at 0 ^{o}C was taken to be 24.4 $Å^2$ from an interpolation of the data of Walker et al.(72), and the saturation pressure of carbon dioxide at 0 ^{o}C was 34.4 atm., taken from Lamond et al.(73). The B.E.T. equation was applied between the relative pressures of .05 and .2, and the area of an adsorbed nitrogen molecule was taken to be 16.2 $Å^2$(72).

The rate of carbon dioxide uptake into initially evacuated carbon samples at an initial carbon dioxide pressure of approximately 5 torr was measured for several carbons. Pressures were recorded by hand from the electric manometer if the rate of adsorption was slow, while some

of the faster rates were recorded with a Bascom-Turner data acquisition device.

The amount adsorbed was calculated from the measured pressures using the ideal gas law and software written for a programmable calculator. A Fortran program on the DEC Minc computer in 66-125, which calculates surface areas as well as moles of adsorbed gas from measured pressures, has recently been written by Z. Du(74).

Chapter 3. The Role of Microporous Surface Area in Carbon Gasification

As discussed in chapter 1, the role of the micropores, and thus the identification of the effective total area for the gasification of microporous carbons, is, at present, very much in question. In this chapter we are concerned with identifying the accessible total surface area for gasification, which is important as a guide to the development of a rational and accurate correlation of char reactivity, and as the logical starting point in the quest for an improved fundamental understanding of the factors that determine carbon gasification reactivity.

3.1 Approach

We attempted to determine the contribution of the microporous surface area to the gasification of various chars from a sub-bituminous coal, a char made from reagent-grade sucrose, and the commercially available carbon, Spherocarb. A number of experimental and analytical techniques were applied in this study which are capable of providing information on the role of microporosity in gasification. Micropore widening is one indication of gasification within micropores and was detected here by an increase in the value of the Dubinin gradient, derived from vapor adsorption isotherms(75). Micropore widening was also detected by the use of molecular probes, or the measurement of surface areas accessible to adsorbate molecules of varying size(14).

If gasification did not take place in the micropores, but rather were confined to macropore surfaces, macropore growth would ensue and

would be visible upon examination of particle surface features before and after gasification. Individual fine features on the surfaces of carbon particles were therefore examined as a function of gasification conversion by the captive-particle S.E.M. technique, in search of macropore widening or measurable recession of other surface features.

The quantitative determination of the accessible surface area for low-temperature gasification is equivalent to finding the effectiveness factor η for reaction within microporous grains lying between larger pores. The classical test for unity effectiveness factor, or complete reactant penetration, is the absence of an effect of particle size on reactivity, in light of which the effect of particle size on the reactivity of several carbons was measured in this study. The absence of a particle size effect is, however, a necessary but not sufficient condition for complete penetration, in cases where diffusion limitations are possible within microporous "grains" that are much smaller than the carbon particle(76).

It is possible to calculate the effectiveness factor corresponding to an observed reaction rate by the classical technique, knowing the appropriate diffusivity and the length scale over which the limiting diffusion occurs(77). The diffusivity and length scale appear in the effectiveness factor formulation in the combination L^2/D, which is the characteristic diffusion time in the system, and which can be inferred from transient uptake measurements. Measurements of L^2/D under adsorption conditions at low temperature were therfore used, after attempting an extrapolation to reaction temperature, to directly estimate η.

3.2 Results

3.21 Microscopy

Figure 3.1 consists of reproductions of photographs and S.E.M. micrographs of Spherocarb, sucrose char, and char from acid-washed subbituminous coal at various stages of conversion. It was not practical to reproduce all of the photographs and micrographs taken in this study, but many important ones are included in figure 3.1 as well as in figure 4.1. The first set of S.E.M. micrographs in figure 3.1 were taken using the captive particle technique discussed in chapter 2, and show the preservation of surface features during the oxidation of Spherocarb carbon. Surface features with dimensions as small as 100 nm are intact after 20% conversion, with no pore growth or surface recession detectable within the limits of S.E.M. resolution (about 50nm in these photos). The second set shows sucrose carbon surface features at various stages of conversion in air. Sucrose carbon contains few S.E.M. visible pores, but many fine irregular features, probably fracture surfaces, which are visible, and preserved during gasification. Figure 4.1 contains more photographic evidence for surface feature preservation during Spherocarb and sucrose carbon gasification.

S.E.M. micrographs of char from the acid-washed subbituminous coal char, on the other hand, show evidence of uneven gasification of the external surface, apparently in the form of production of approximately circular pits, as seen in figure 3.1. It was not possible here to examine the same particle in the same orientation during conversion, as

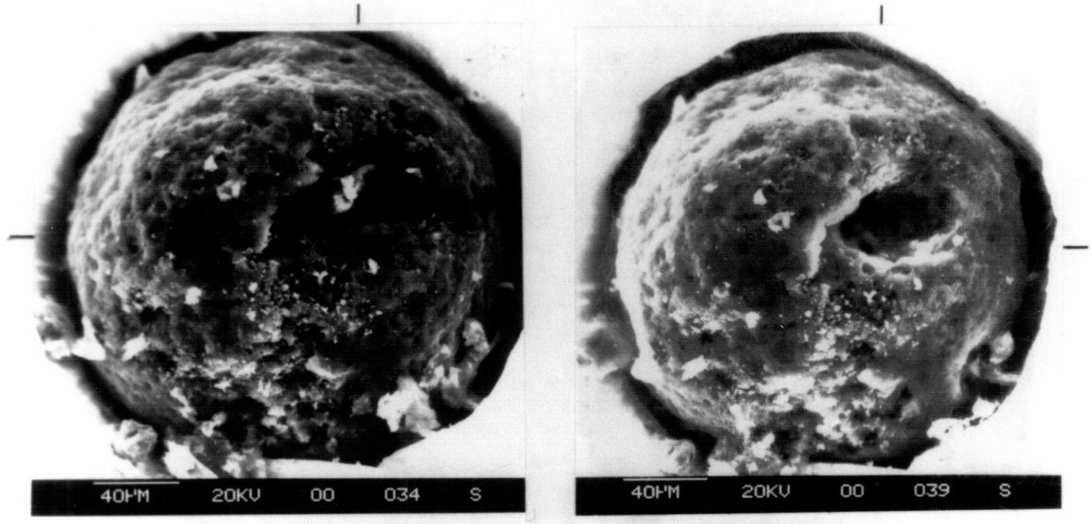

Unreacted

20% Conversion

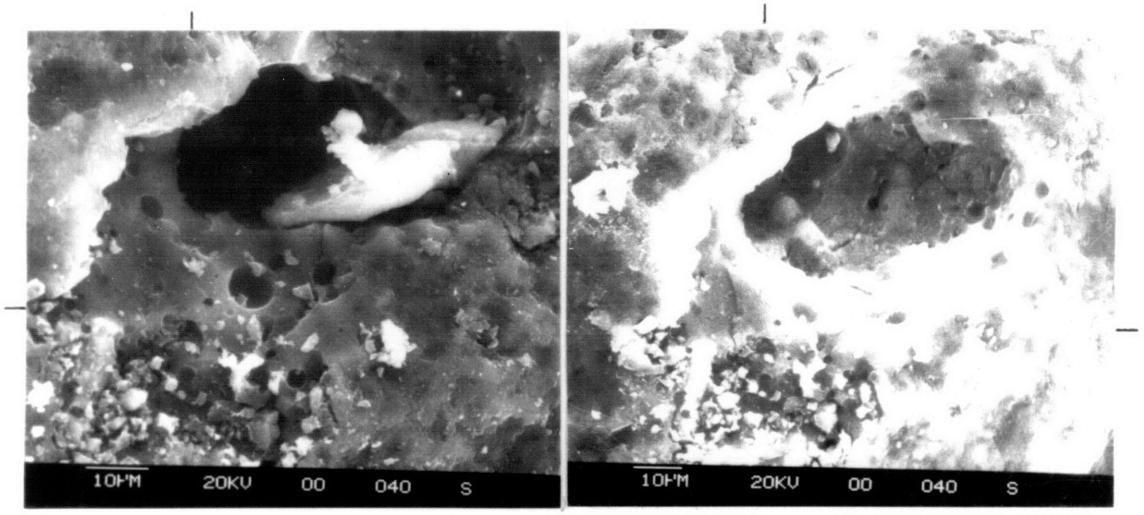

Unreacted

20%
Conversion

Spherocarb in .21 atm. O_2, 495 °C
Set of micrographs at increasing magnification

Figure 3.1 Photographs and S.E.M. Micrographs

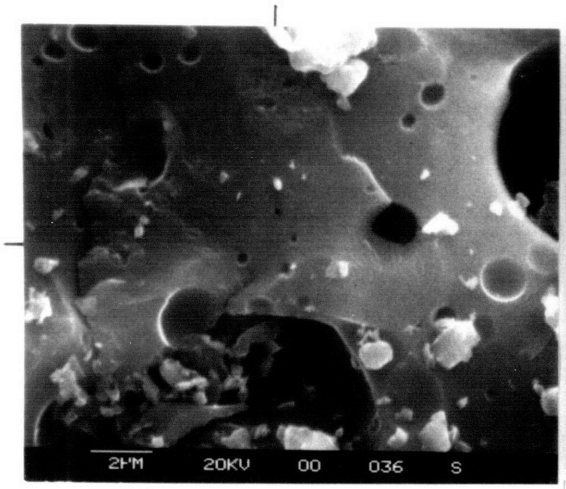

Unreacted

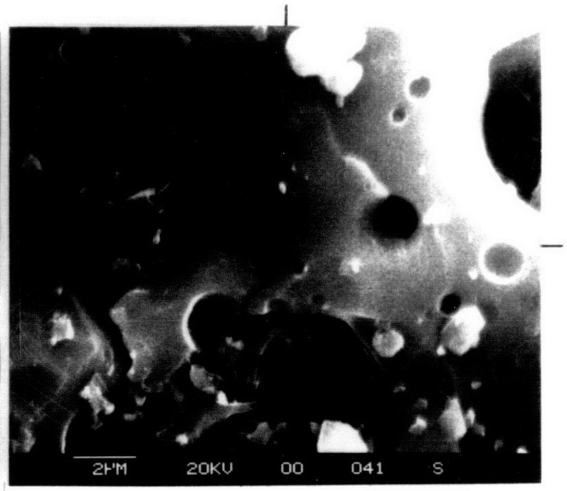

20%
Conversion

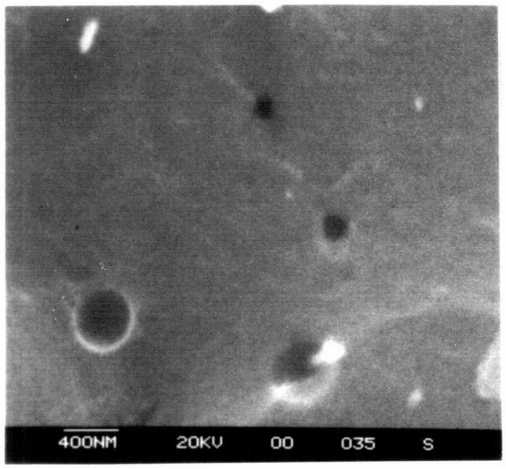

Unreacted

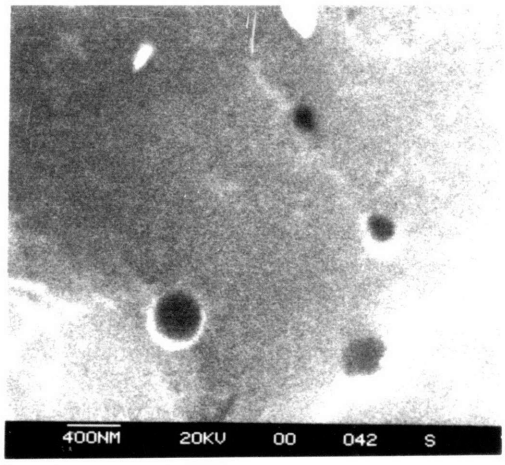

20% Conversion

Spherocarb in .21 atm. O_2, 495 °C
Set of micrographs at increasing
magnification, continued

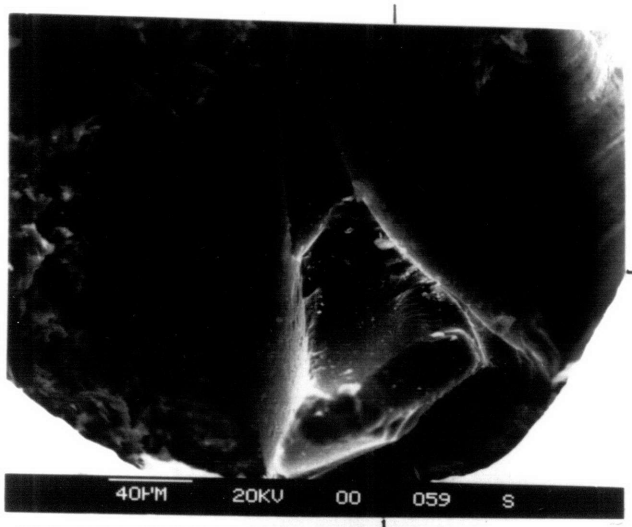

Unreacted

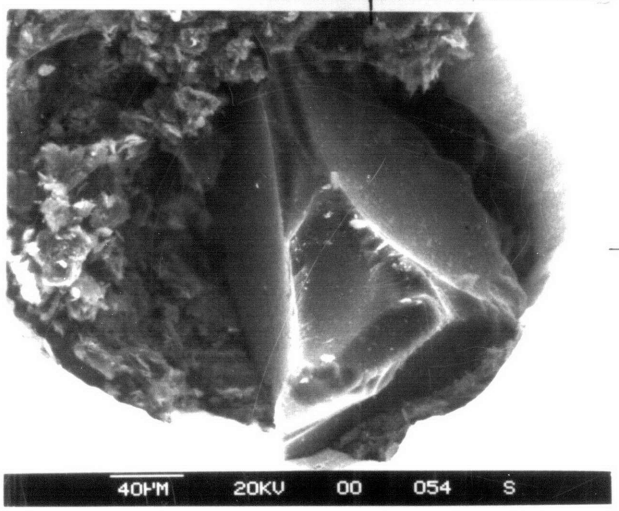

20%
Conversion

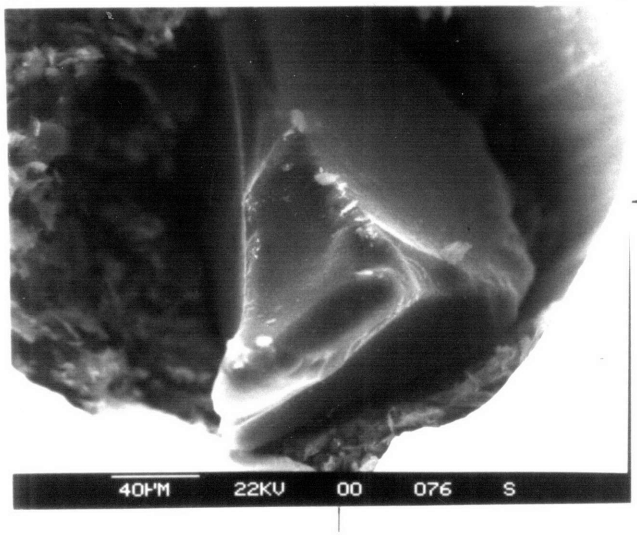

60%
Conversion

Sucrose carbon in .21 atm. O_2, 495 ^{o}C
Set of micrographs at increasing magnification

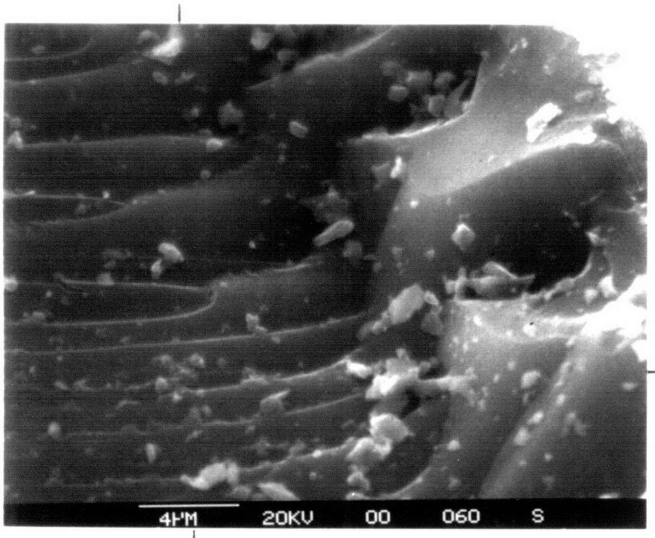

Unreacted

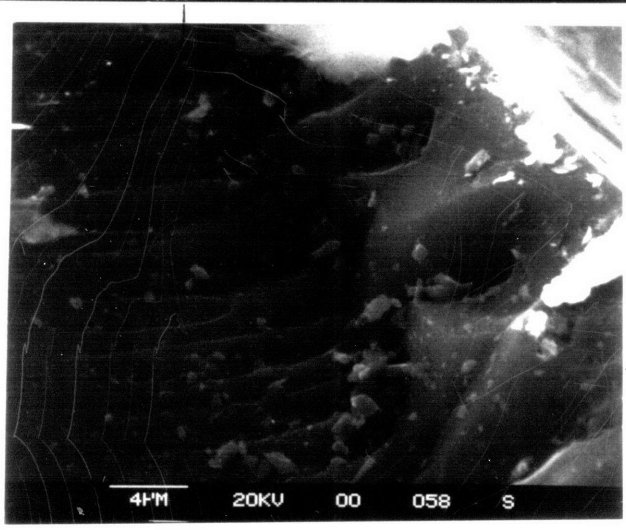

20%
Conversion

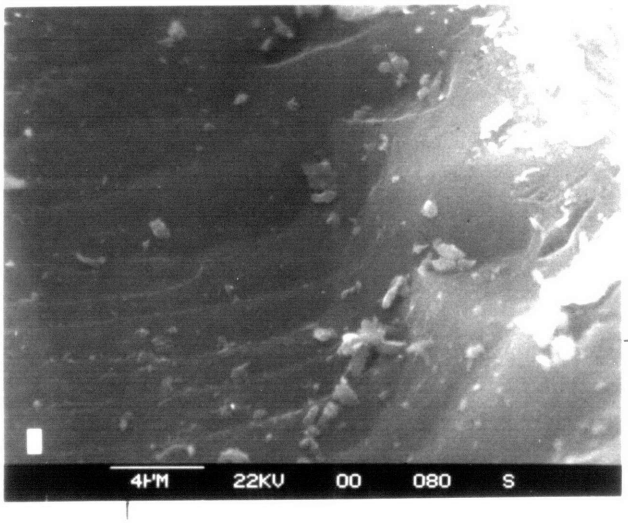

60%
Conversion

Sucrose carbon in .21 atm. O_2, 495 °C
Set of micrographs at increasing magnification, continued

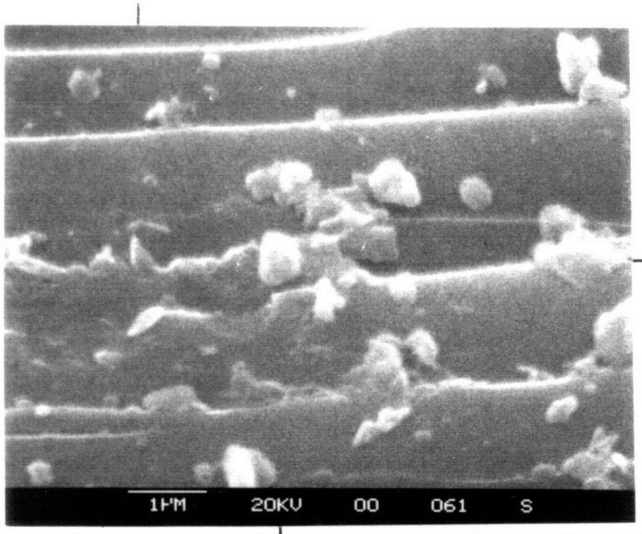

Unreacted

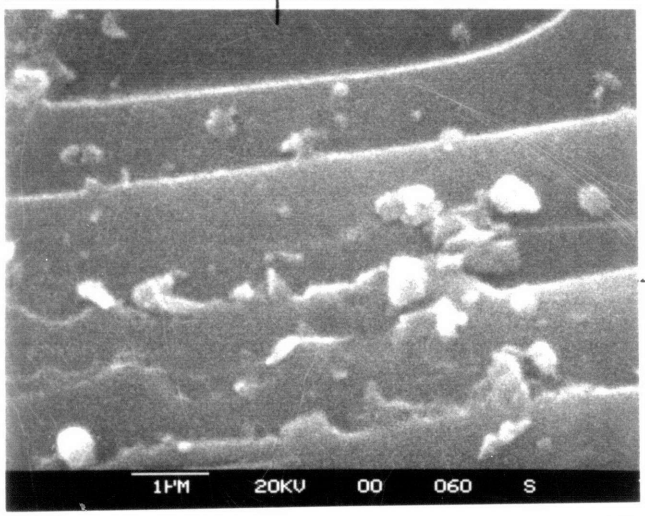

20%
Conversion

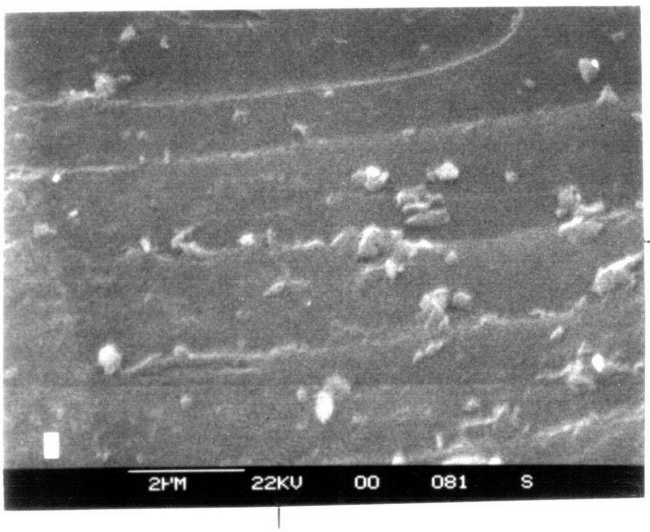

60%
Conversion

Sucrose carbon in .21 atm. O_2, 495 ^{o}C
Set of micrographs at increasing magnification, continued

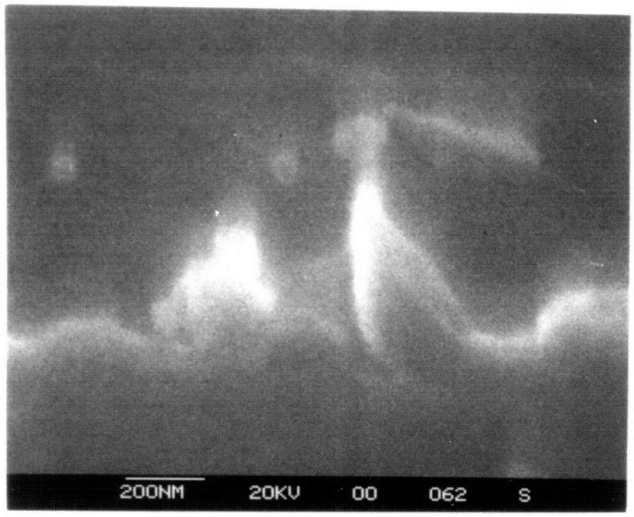

Unreacted

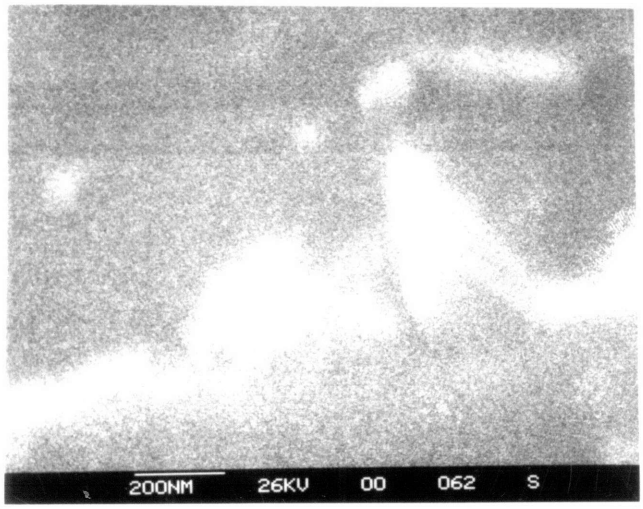

20%
Conversion

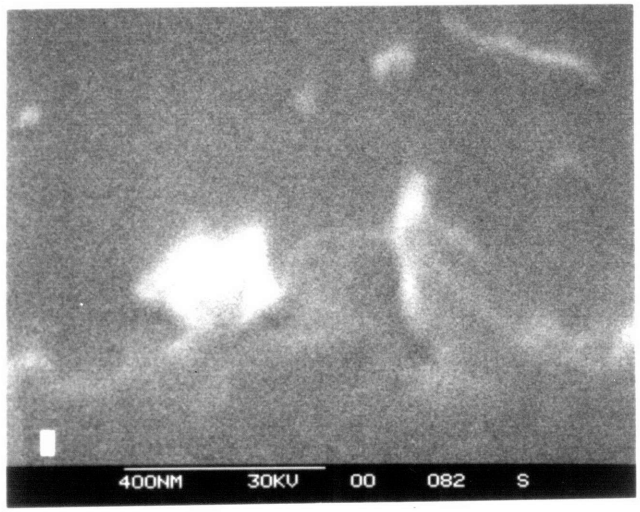

60%
Conversion

Sucrose carbon in .21 atm. O_2, 495 ^{o}C
Set of micrographs at increasing
magnification, continued

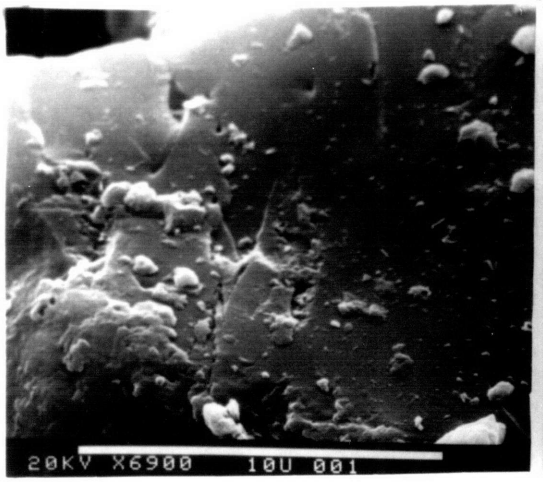

0% conversion

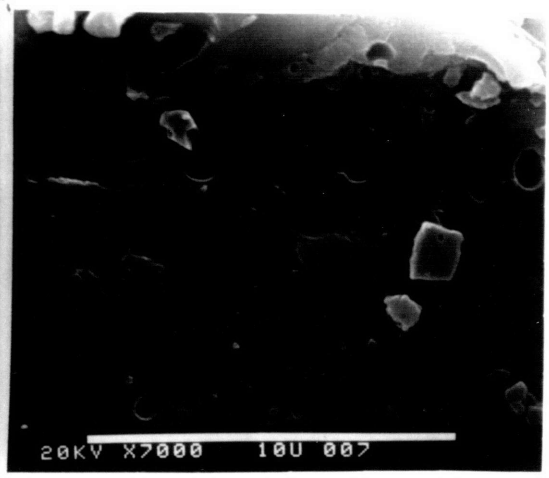

29% conversion

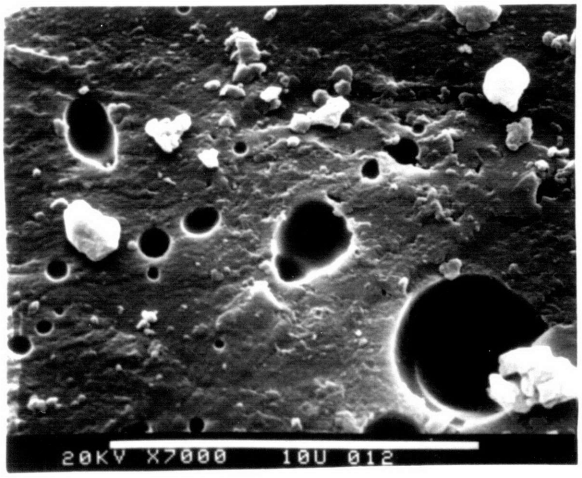

41% conversion

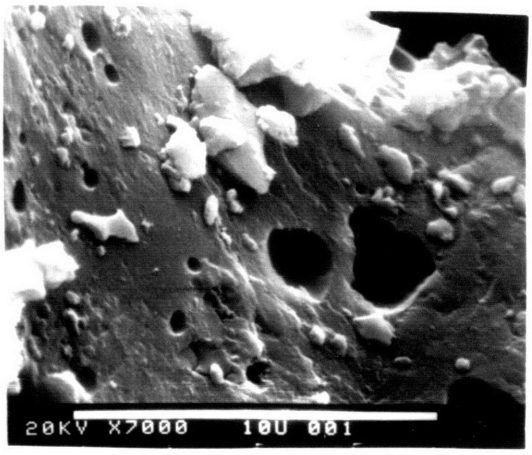

77% conversion

Acid-washed sub-bituminous coal char
in 1 atm. CO_2 at 860 ^{o}C

the captive particle technique was not used. The fields of view were chosen, however, with the intention of representing typical features.

3.22 Gasification rates

Reaction rates in air at 495 °C and 600 °C of two particle sizes of Spherocarb carbon are presented in figure 3.2. In addition, initial rates of gasification in a 50/50 by volume mixture of carbon dioxide/carbon monoxide at 990 °C were measured, and the average rates between 0 and 20% conversion were .0080 min^{-1} for the 214 μm particles and .0083 min^{-1} for the <38 μm particles. The rate of gasification is essentially independent of particle size under each set of reaction conditions. A comparison of the oxidation rate of Spherocarb before and after acid-washing appears in figure 3.3. The two curves are very similar, suggesting that the 760 ppm(72) of ash in Spherocarb do not exert a significant catalytic effect. The residual content of the acid-washed Spherocarb was 250 ppm by weight, however, which is enough to potentially catalyze Spherocarb gasification, depending on its elemental composition and dispersion, as discussed in chapter 1. Figure 3.4 is a compilation of Spherocarb oxidation rates at various temperatures and 40% conversion, measured here and by Floess(33).

Sucrose gasification rates in carbon dioxide were, in contrast, markedly dependent on particle size, as seen in figure 3.5. Note that the effect of particle size is rather small between particle diameters of 180 and 50 μ, but increases substantially with further diameter reduction. The particle size effect persists throughout most of conversion, although it is largest at low conversions. A decrease in

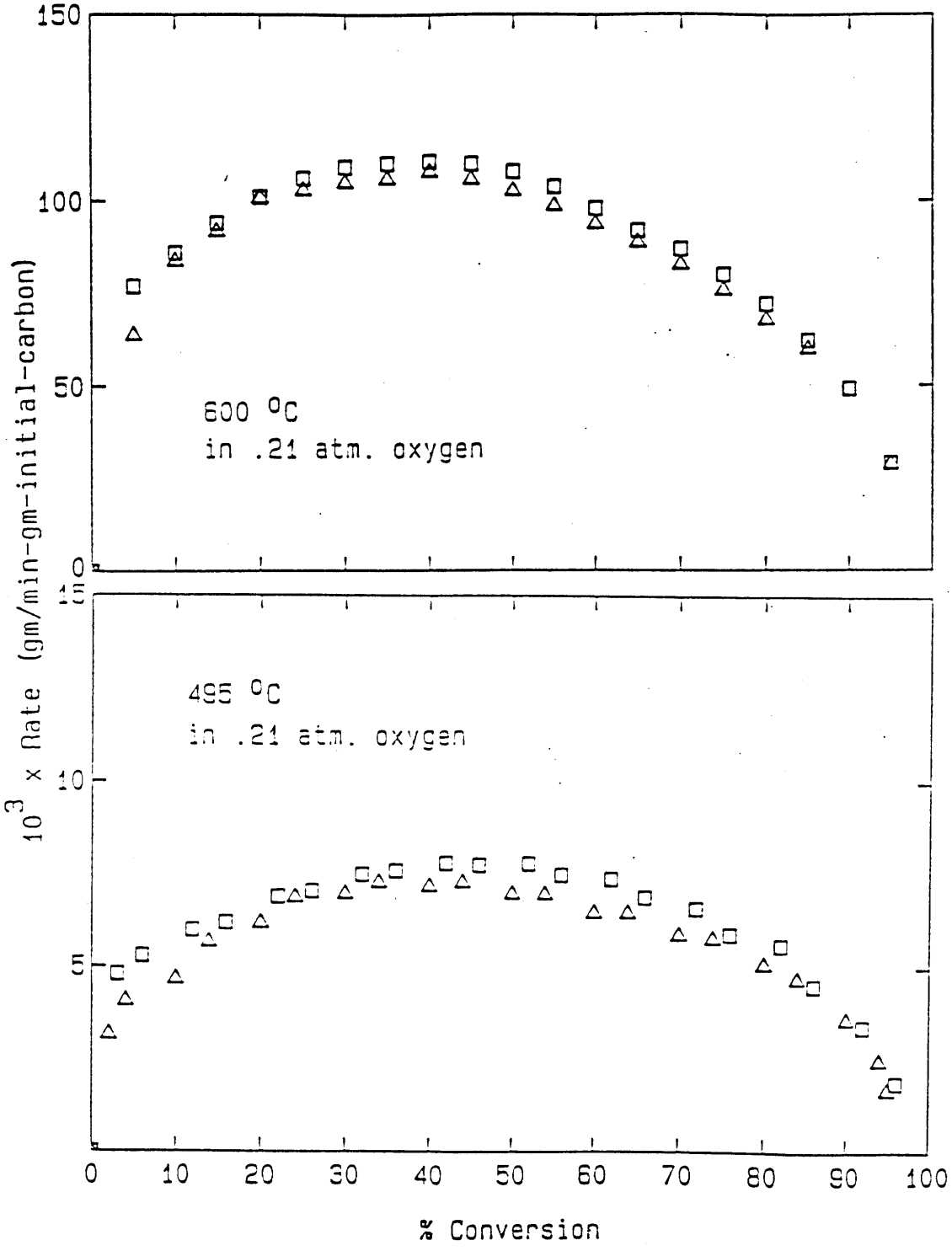

□ < 38 μm diameter particles

△ 214 μm diameter particles

Figure 3.2
Oxidation Reactivity of Spherocarb

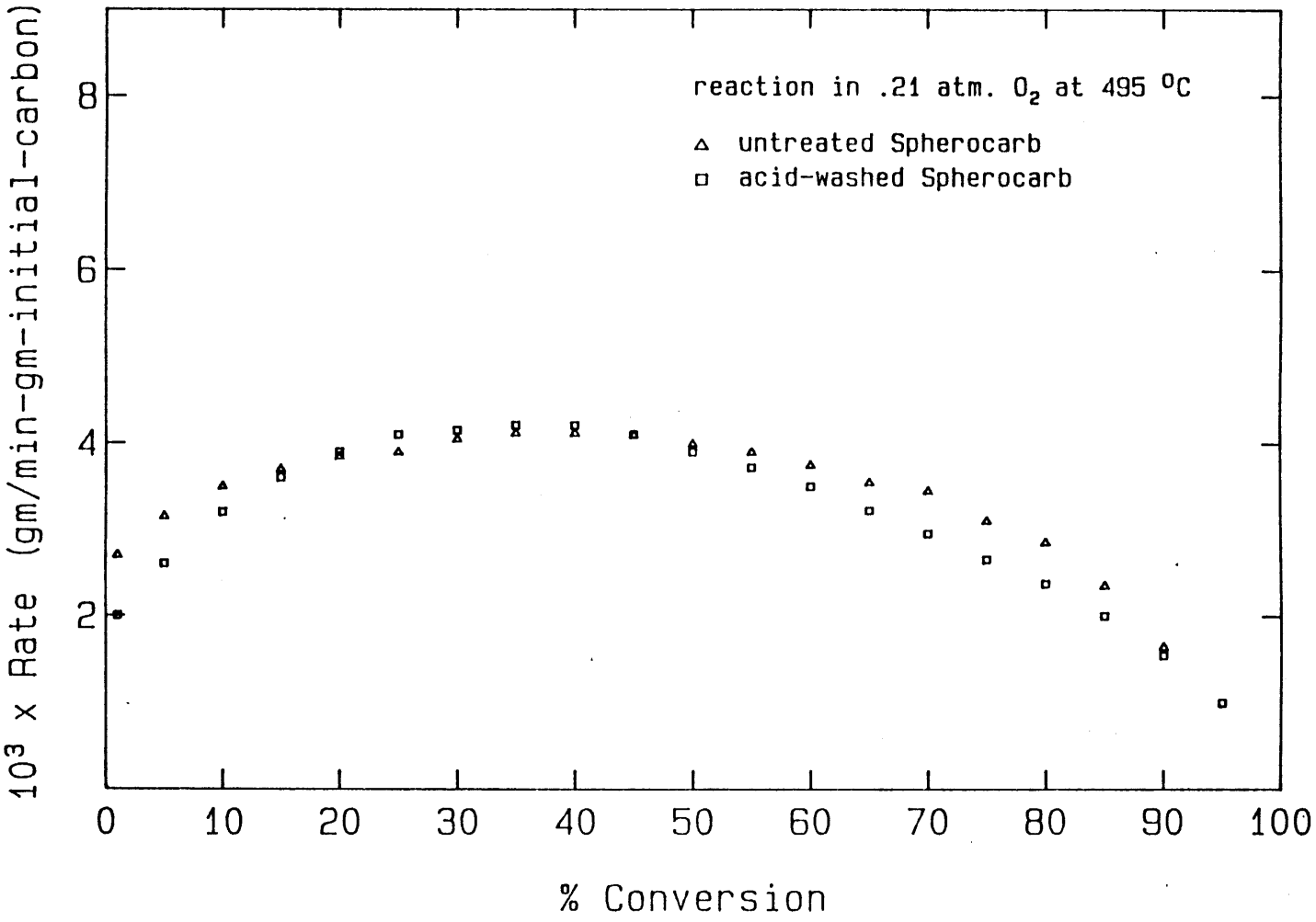

Figure 3.3

Untreated and Acid-Washed Spherocarb Oxidation Rates

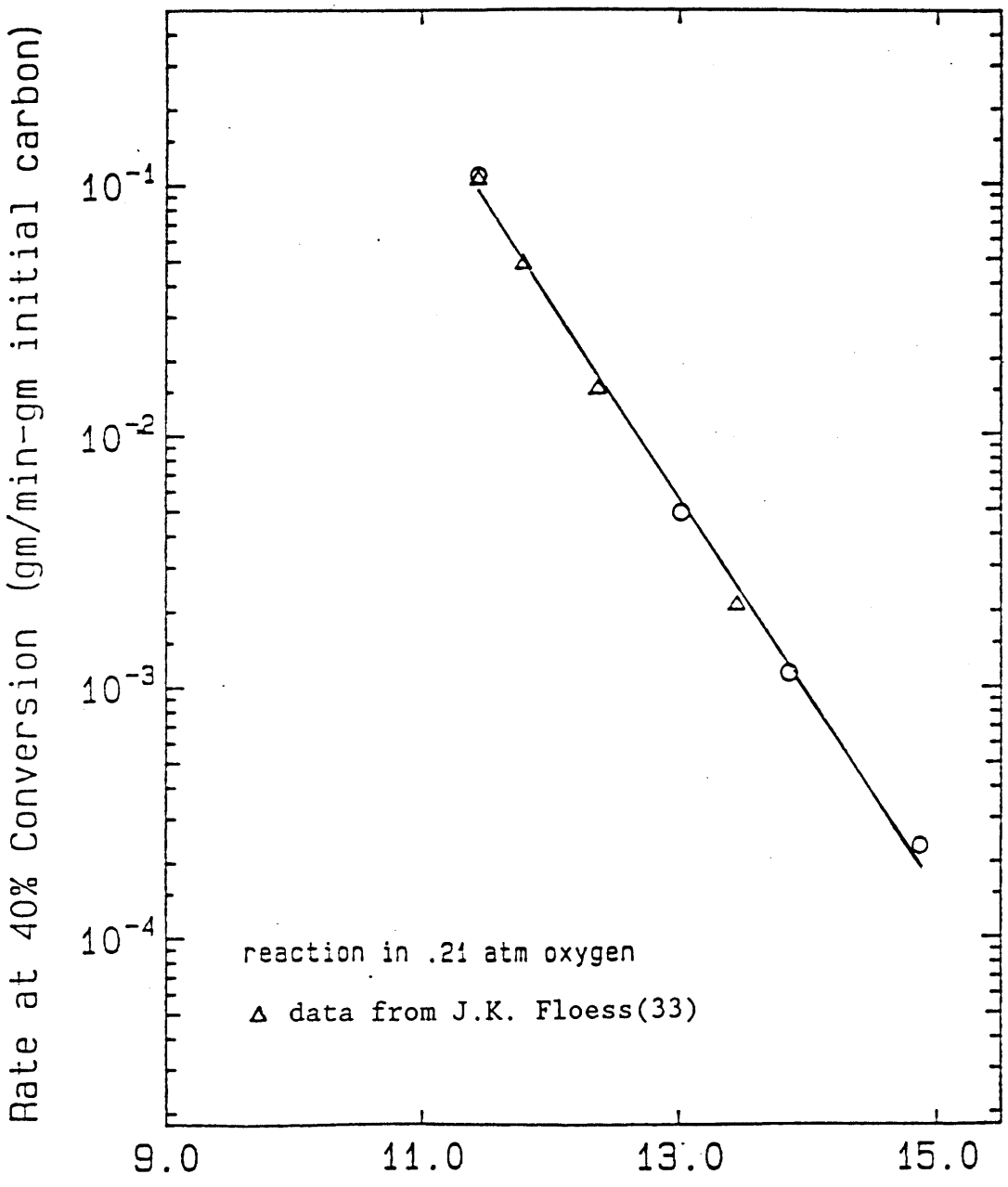

Figure 3.4
Spherocarb-Oxygen Reaction

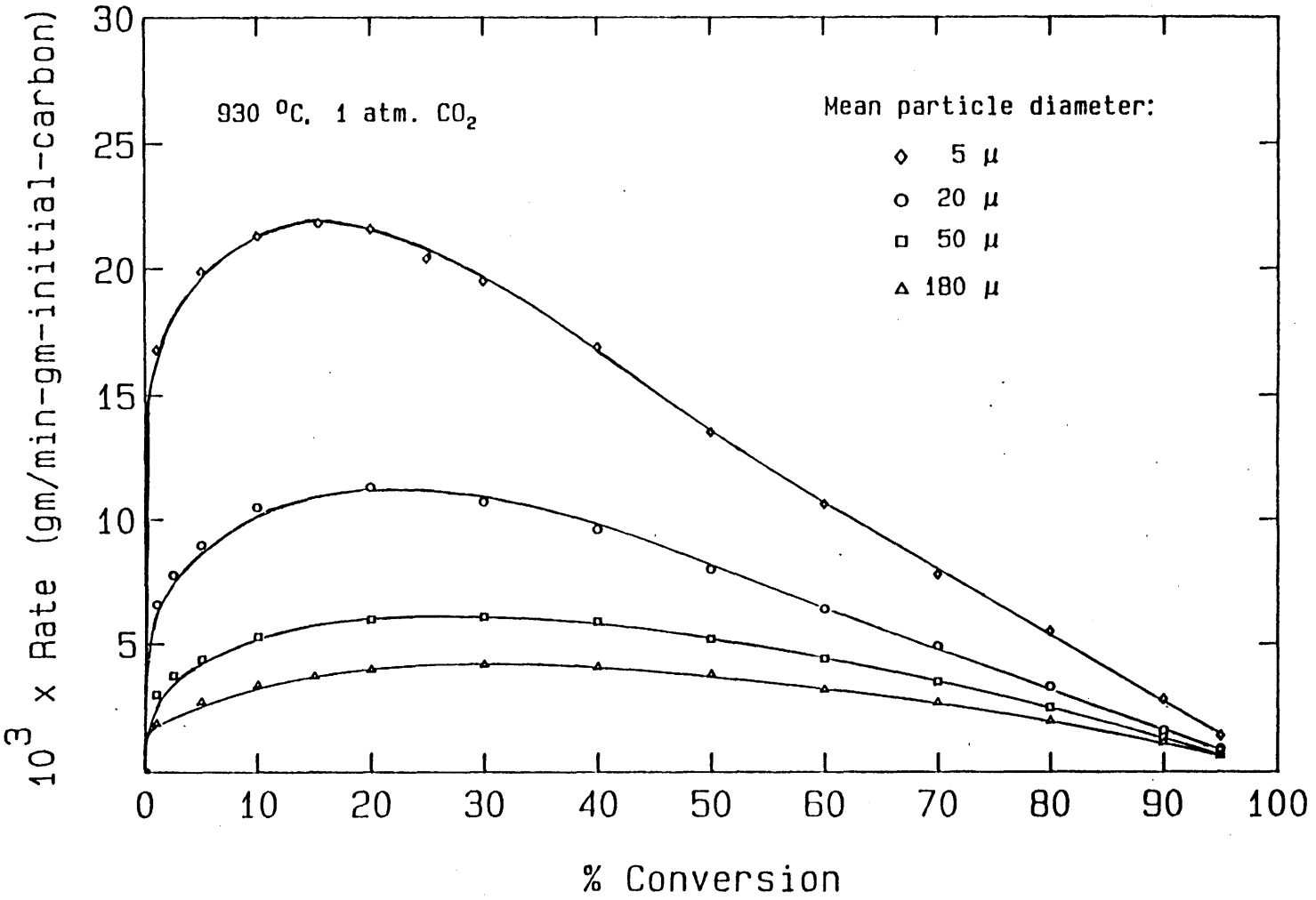

Figure 3.5

Gasification Reactivity of Sucrose Carbon

particle size also results in a shift in the location of the maximum rate toward lower conversions. In the center and bottom of figure 3.6 are presented the results from two additional particle size tests, in which the smaller particles were obtained by grinding the larger ones, sieving, and regrinding the oversize fraction until it passed a 38 μm sieve. (Sample B in figure 3.6 was ground further after passing the 38 μm sieve.) Thus, all of the original sample was retained, and possible segregation of char components having varying reactivities was avoided. The smaller particle sizes obtained in this way also had enhanced reactivities, indicating that the particle size effect was not due to segregation of char components having varying reactivities.

A comparison of the reactivities of the 150-212 μm fraction and the 20 μm mean diameter fraction was also made in a 50/50 by volume carbon dioxide/carbon monoxide mixture at 1005 ^{o}C. The reaction rate in the carbon dioxide/carbon monoxide mixture was lower by a factor of about 4 than the rate in 1 atm. pure carbon dioxide at the same temperature, but the effect of particle size was nearly the same, as can be seen at the top of figure 3.6.

Carbon dioxide gasification reactivities of untreated and acid-washed subbituminous coal char are presented in figure 3.7. Acid washing both reduced reactivity and changed the shape of the reactivity-conversion curve. (The ratio of untreated to acid-washed reactivities is estimated in the discussion section.) Gasification reactivities of the high temperature char from acid-washed subbituminous coal in both carbon dioxide and a carbon dioxide/carbon monoxide mixture are presented in figure 3.8. Heat treatment to 1200

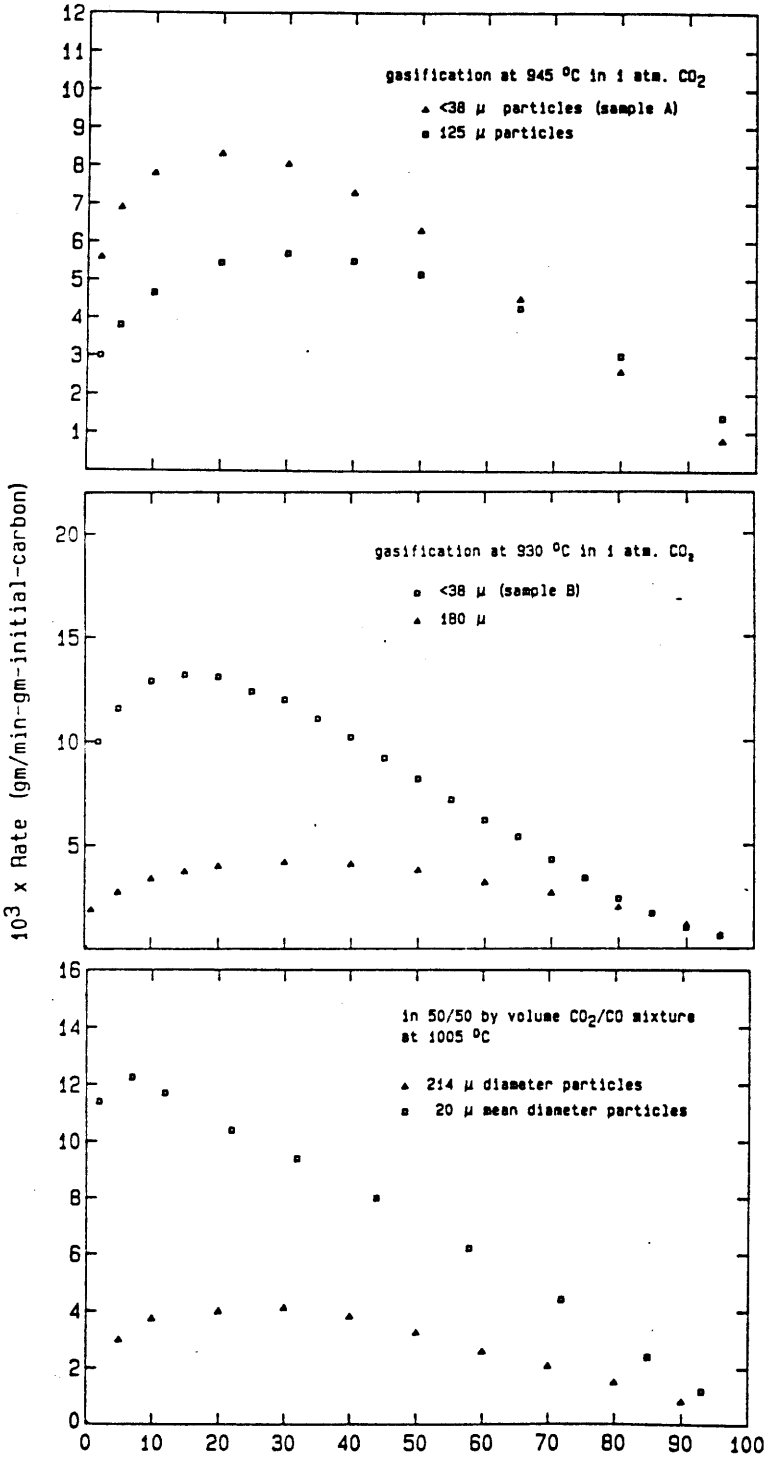

Figure 3.6
Gasification Reactivity of Sucrose Carbon

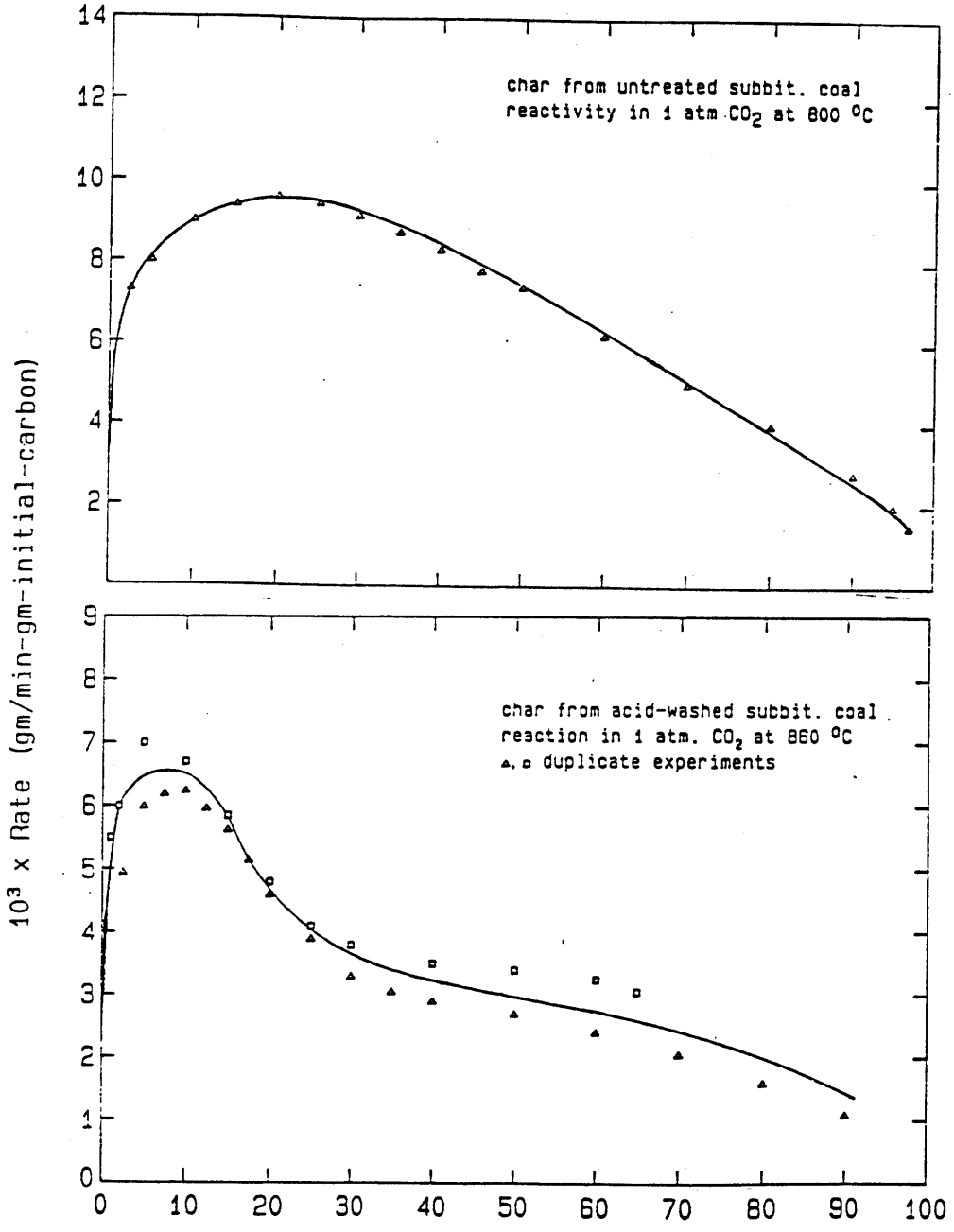

Figure 3.7
Coal Char Gasification Reactivity

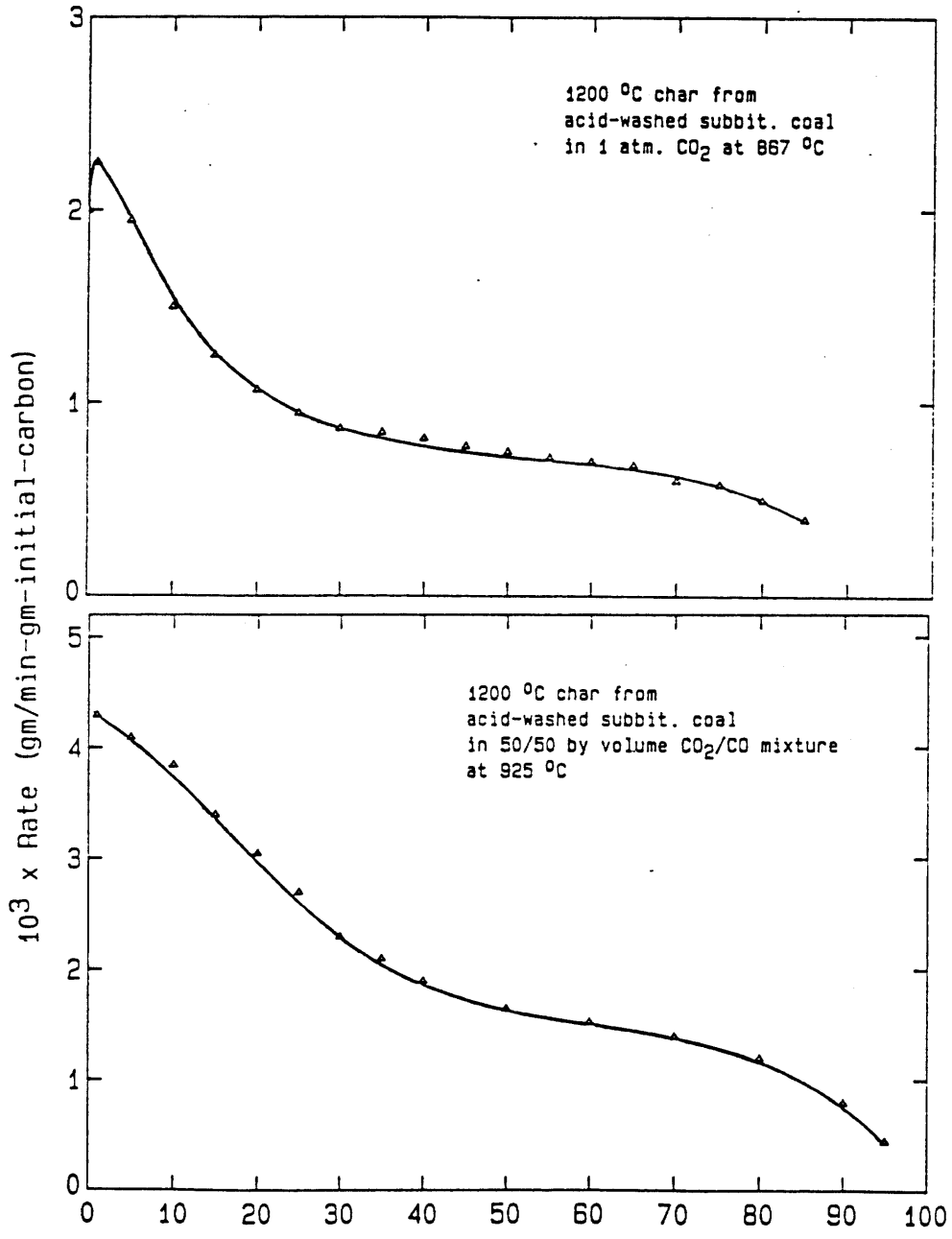

Figure 3.8
Gasification Reactivity of High Temp. Coal Char

^{o}C reduced the carbon dioxide gasification reactivity at 860 ^{o}C by a factor of about 4, while having relatively little effect on the shape of the rate-conversion curve.

3.23 Surface areas and adsorption equilibration times

Surface areas calculated from both nitrogen and carbon dioxide adsorption isotherms for both 180 (150-212) μm and <38 μm (sample A) sucrose carbon at several stages of conversion are presented in figures 3.9 and 3.10. The nitrogen area, initially, is very much lower than the carbon dioxide area in both cases, then rises over the course of conversion to meet the value of the carbon dioxide area, and finally, at high conversions, significantly exceedes the carbon dioxide area, reaching over 2500 m^2/gm. Dubinin-Polanyi gradients in log(gmol/gm-carbon) derived from this set of carbon dioxide isotherms rise over the course of conversion as seen in figure 3.11. Rates of carbon dioxide uptake observed during isotherm measurements for sucrose chars at several conversions are shown in figure 3.12. The adsorption equilibration time was on the order of 150 min. for unreacted sucrose carbon, while only several seconds for sucrose at 20% conversion. Carbon dioxide surface areas of the four particle sizes of sucrose char at 0% conversion appear in table 3.1.

Carbon dioxide surface areas for Spherocarb carbon at 0 and 65% conversion can be found in table 4.3. Rates of carbon dioxide uptake under adsorption conditions for Spherocarb at several conversions are

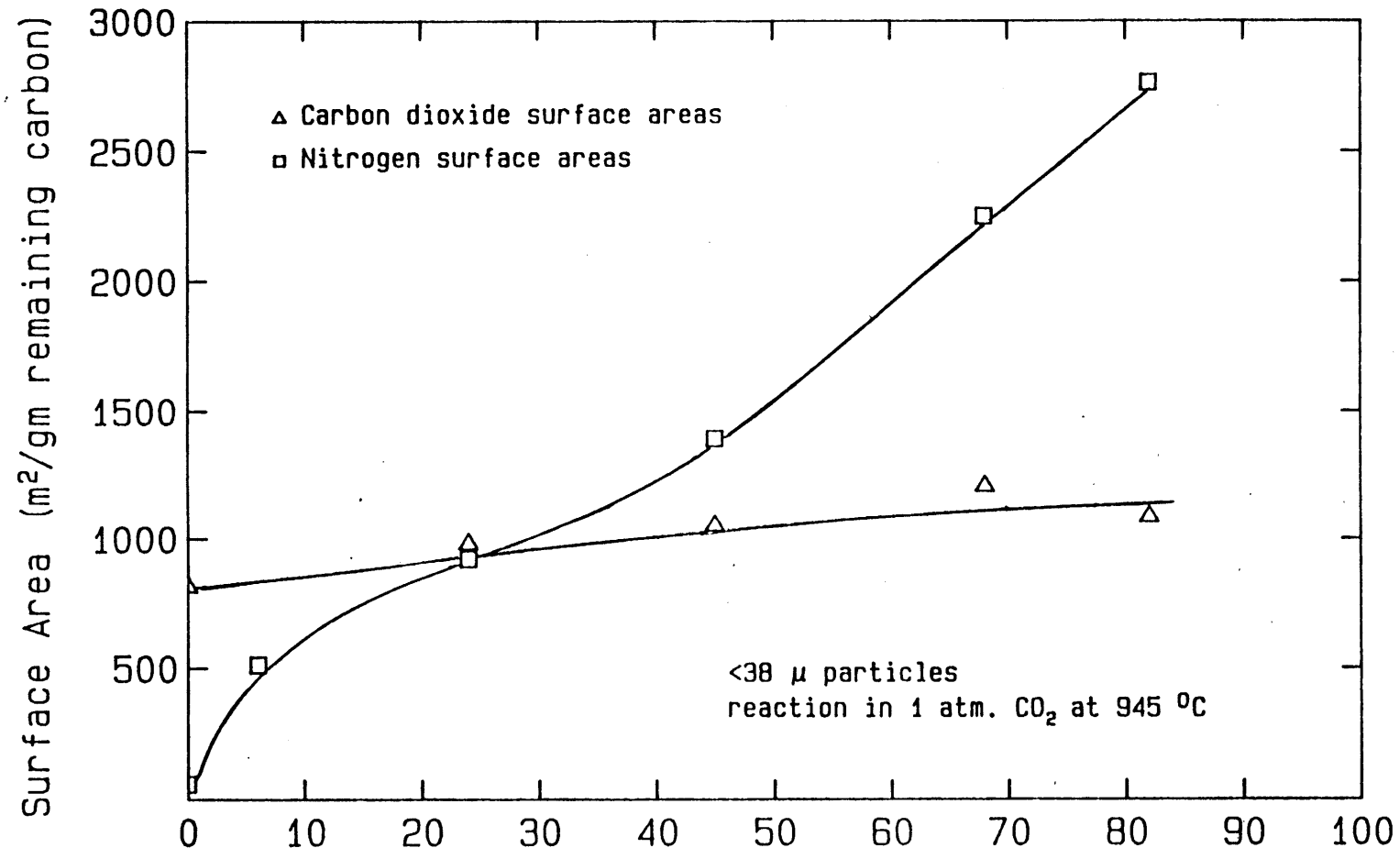

Figure 3.9

Sucrose Carbon Surface Area Evolution

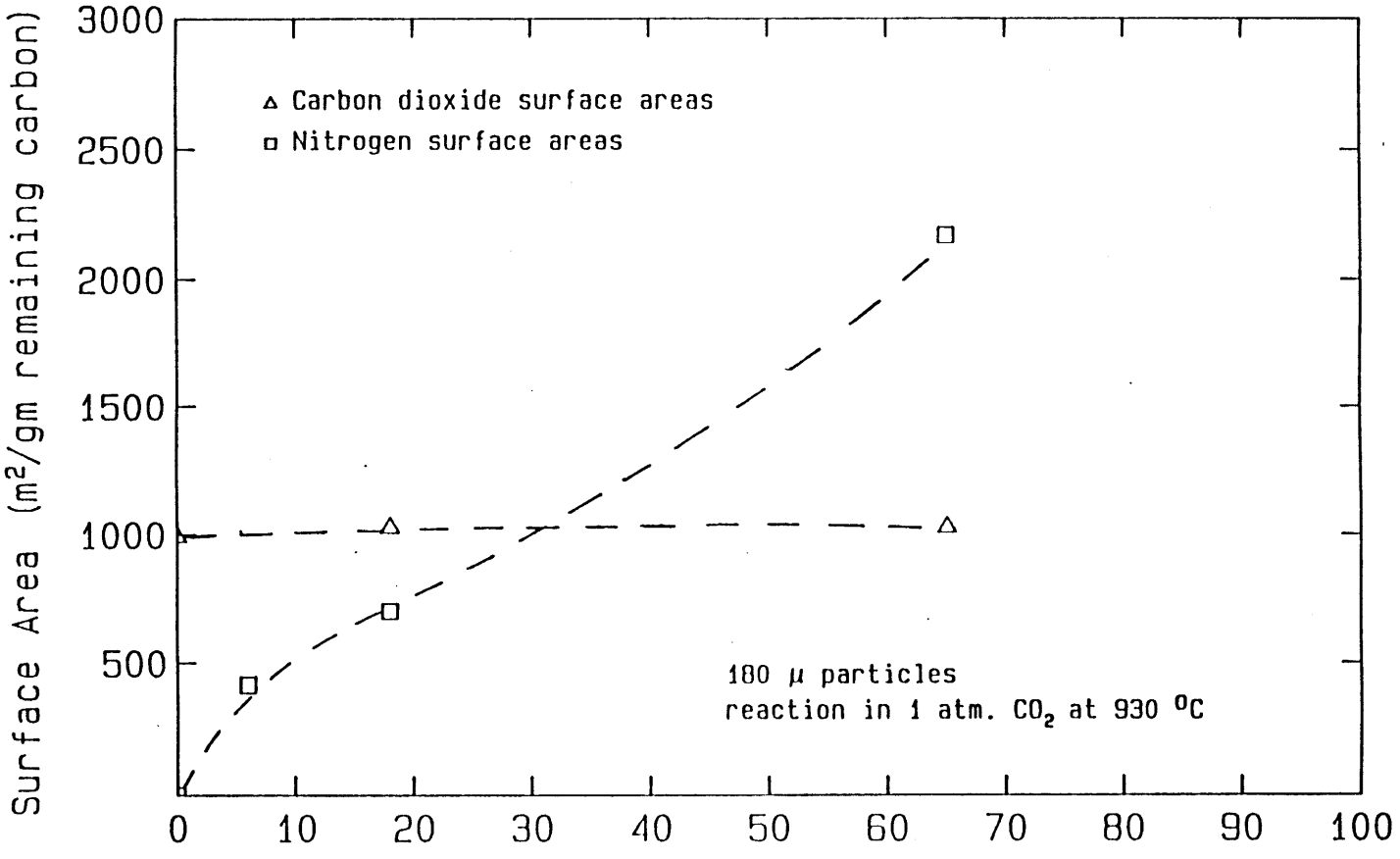

Figure 3.10

Sucrose Carbon Surface Area Evolution

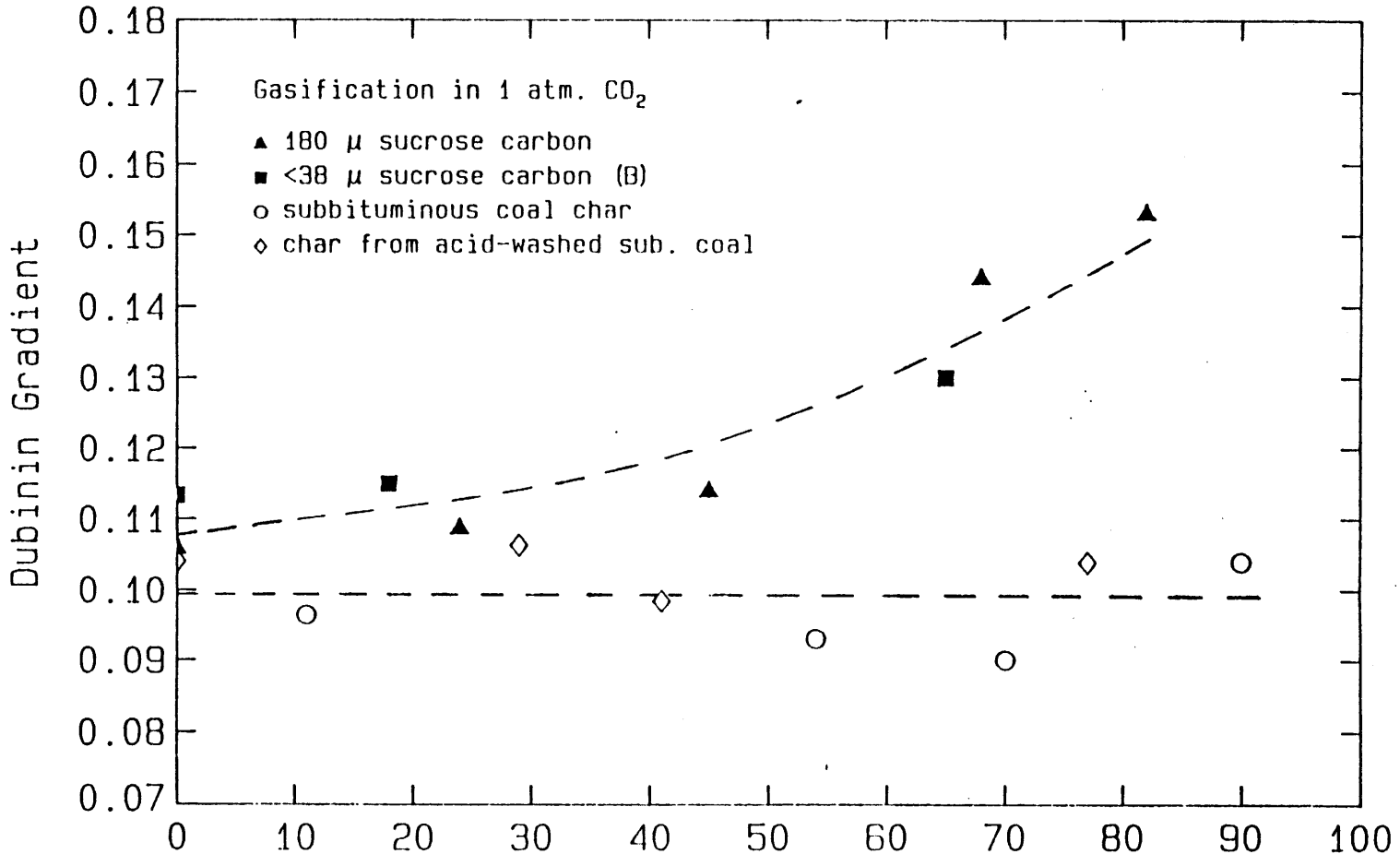

Figure 3.11

Effect of Conversion on the Dubinin Gradient

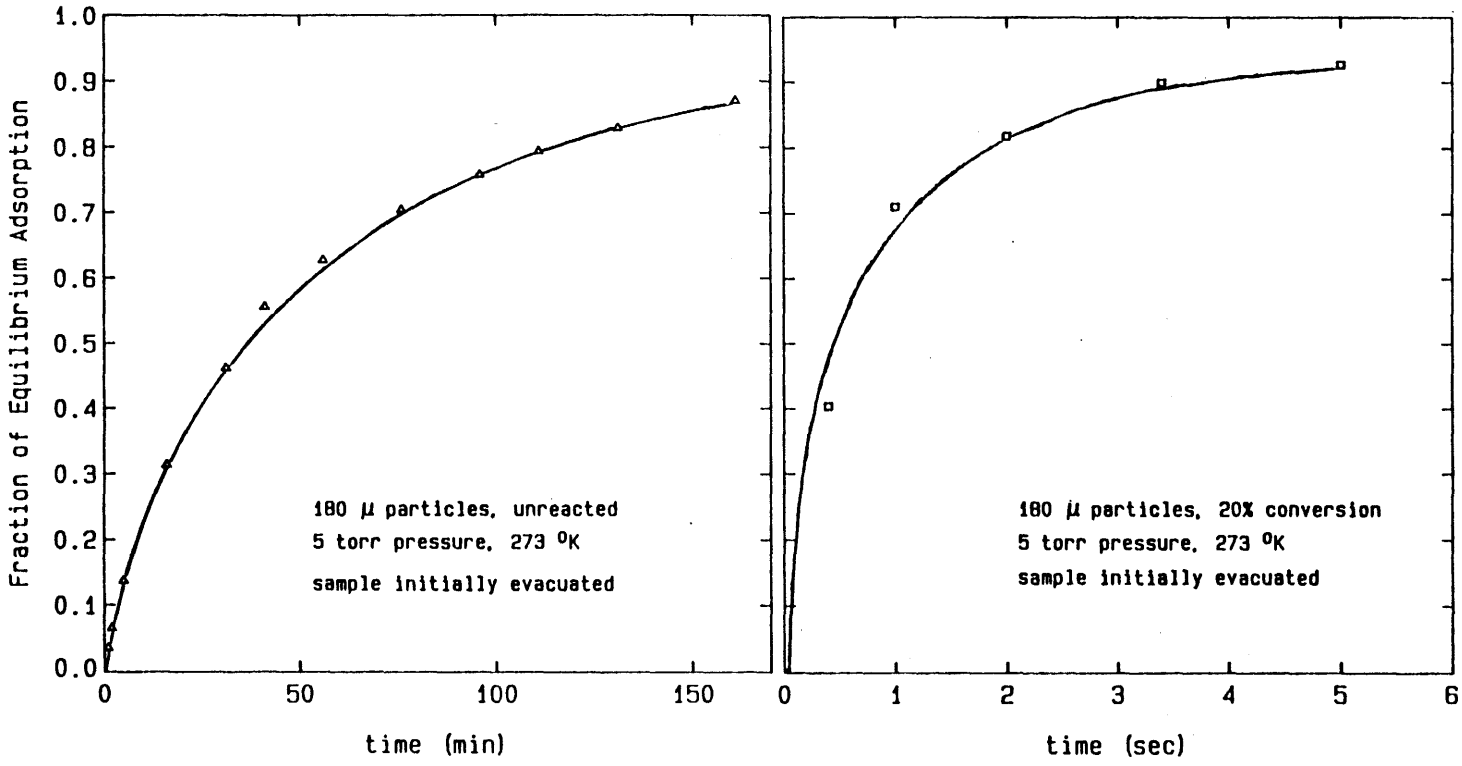

Rate of Carbon Dioxide Uptake into Sucrose Carbon

Figure 3.12

Table 3.1: Effect of Particle Size on Surface Area*

Mean particle diameter (μm)	Surface area (m^2/gm)
180	996
50	919
20	819
5	770

*areas from carbon dioxide adsorption isotherms

shown in figure 3.13. Adsorption equilibration times were on the order of one second for both unreacted and 45% converted Spherocarb.

Surface areas calculated from both nitrogen and carbon dioxide adsorption isotherms for chars from both the untreated and acid-washed subbituminous coal at various stages of conversion are presented in figure 3.14. The surface area evolution for these two chars is quite similar. The nitrogen areas initially are, again, very much lower than the carbon dioxide areas, but for the coal chars rise gradually over the course of conversion to approximate the value of the carbon dioxide areas only at high conversions. The Dubinin gradient was essentially constant for both chars over the course of conversion, unlike that for the sucrose carbon, as seen in figure 3.11. Rates of carbon dioxide uptake observed during isotherm measurements for the untreated sub-bituminous coal chars at several conversions are shown in figure 3.15. The adsorption equilibration time was on the order of 1000 min. for the unreacted char, and decreased steadily throughout conversion.

The evolution of the carbon dioxide surface area during carbon

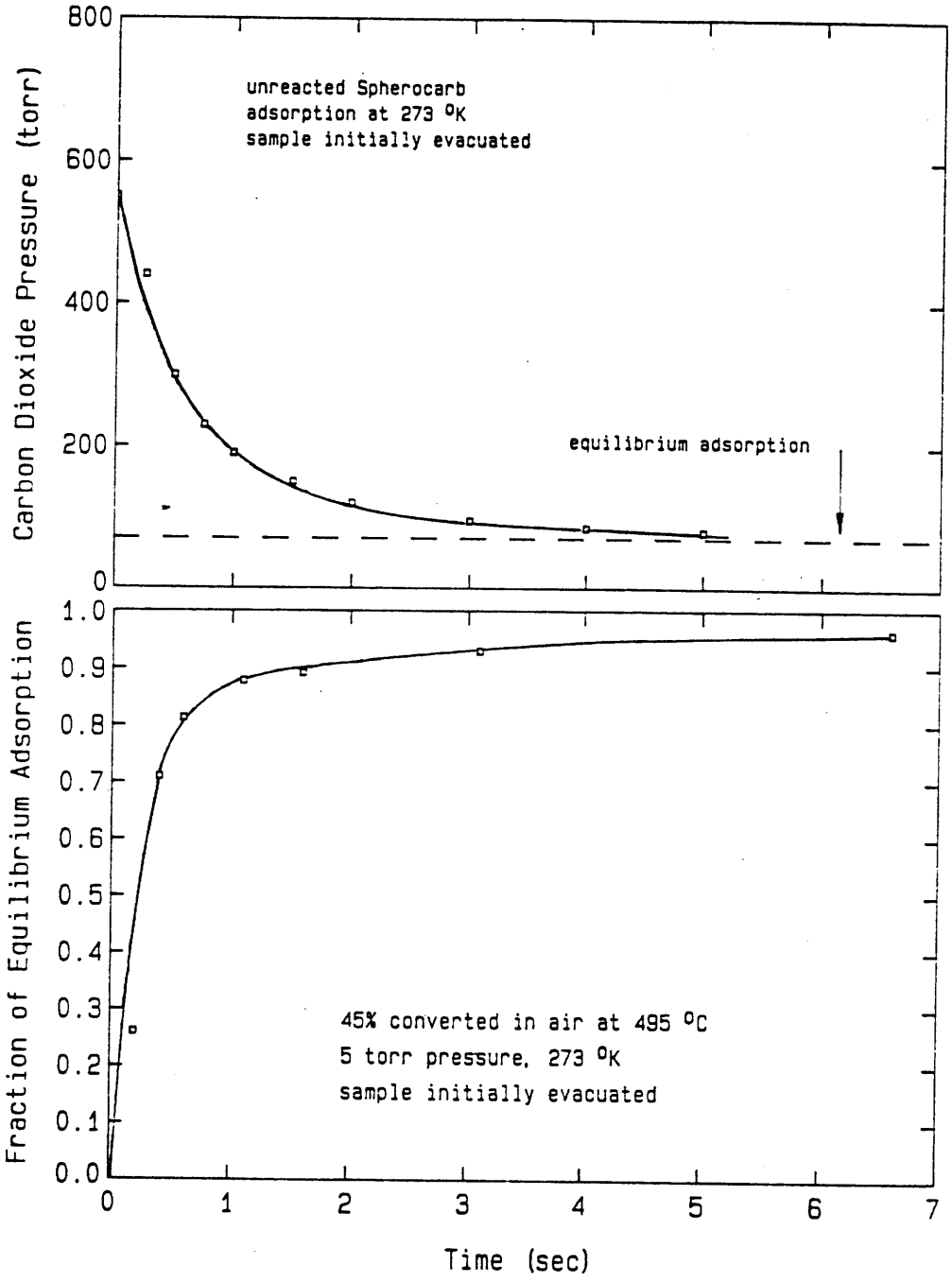

Rate of Carbon Dioxide Uptake into Spherocarb

Figure 3.13

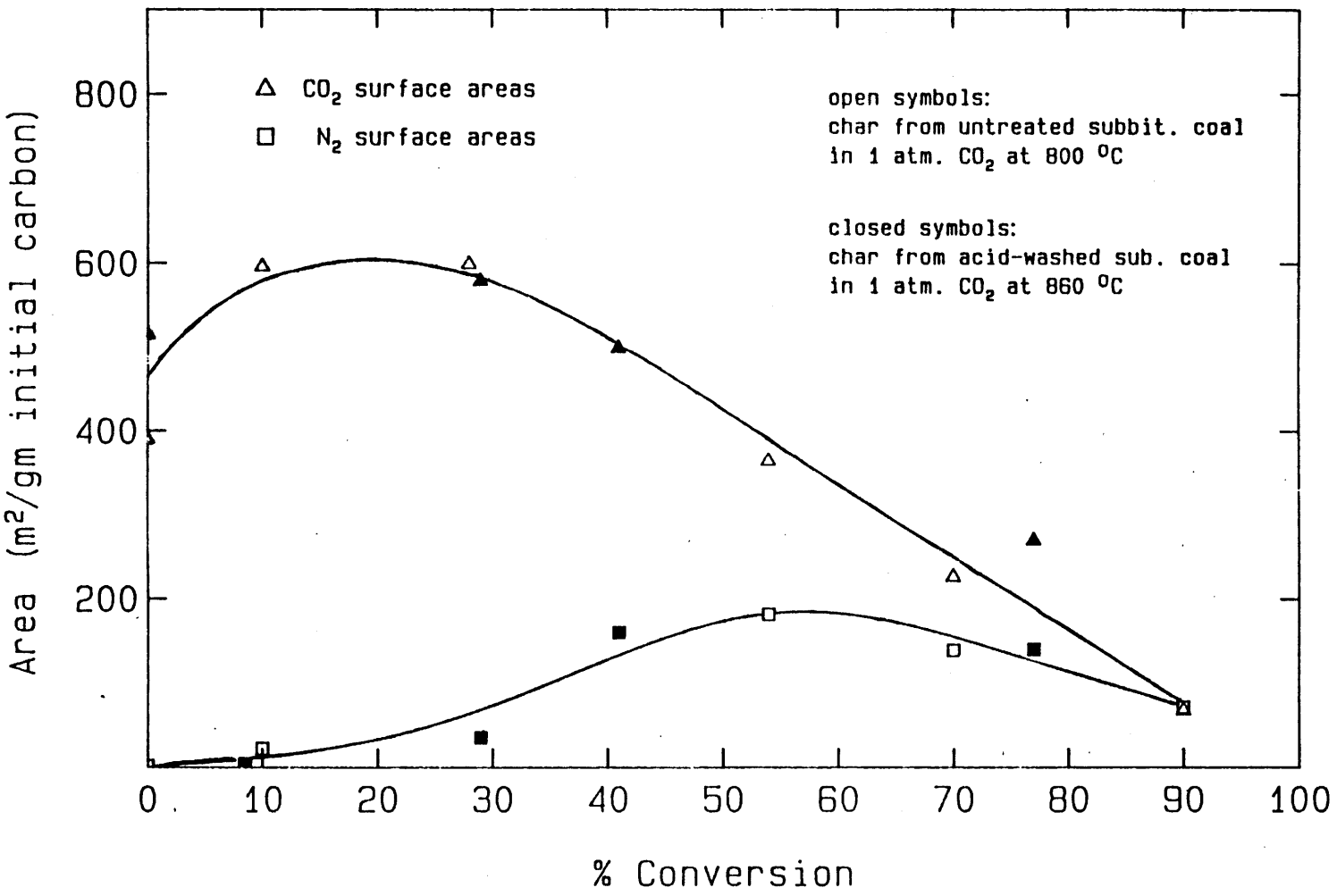

Figure 3.14
Coal Char Surface Area Development

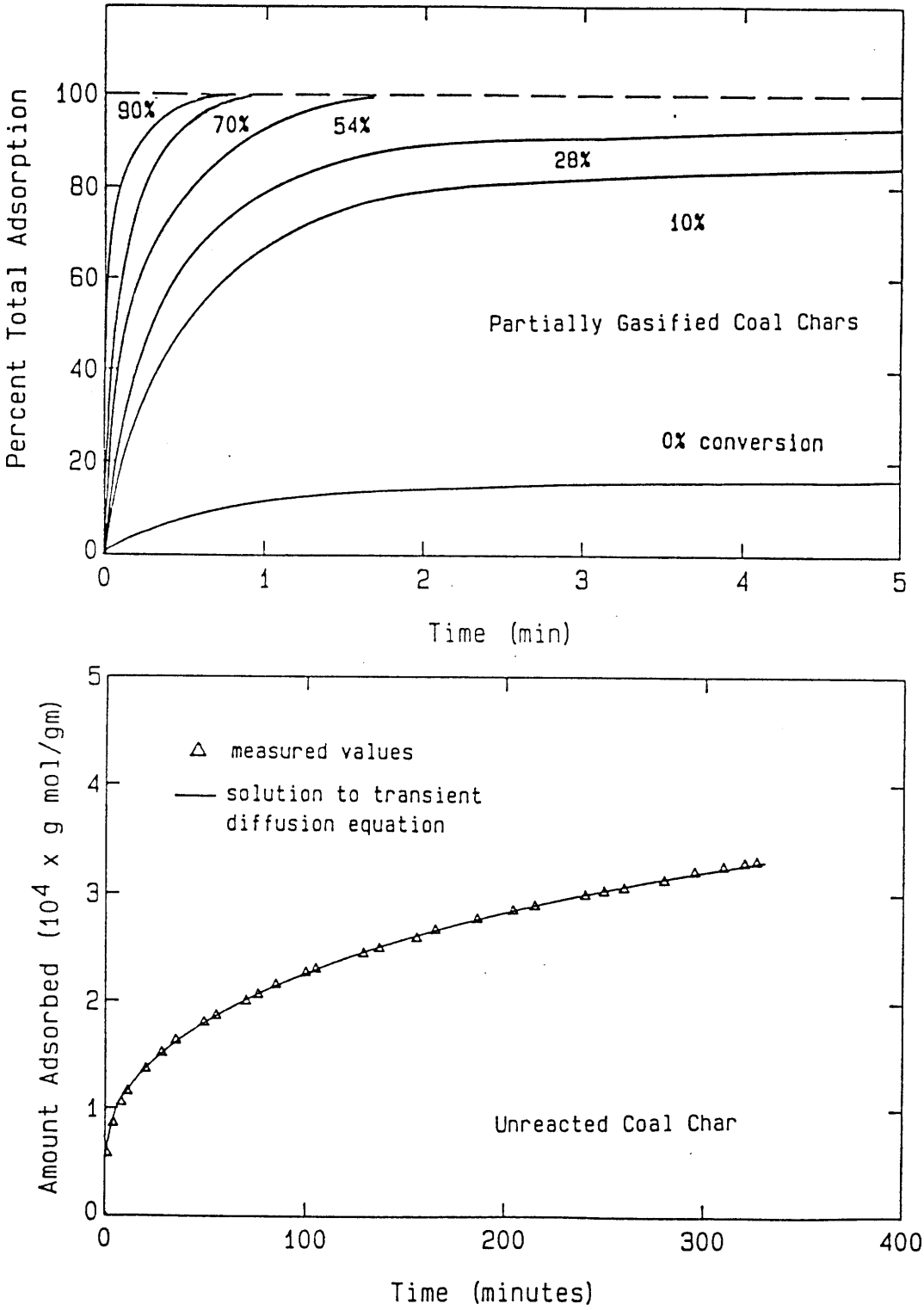

Figure 3.15
Rate of CO_2 Uptake into Untreated Coal Char

dioxide gasification of the high temperature char from the acid-washed coal appears in figure 3.16, along with that char's measured gasification reactivity-conversion curve. The initial carbon dioxide surface area of this char is only 4 m^2/gm, rising, however, by a factor of over 50, to over 200 m^2/gn, over the course of conversion. Gasification reactivity, in contrast, exhibits its maximum at essentially 0% conversion, bearing no apparent relationship to the measured surface areas.

All reaction rates referred to above were measured with the T.G.A. in the upflow configuration, except the Arrhenius plot of compiled data and the comparison of acid-washed and untreated Spherocarb carbon, which present rates measured in downflow. (Rates measured in upflow are about a factor of 1.5 higher than those measured in downflow.)

3.3 Discussion

3.31 Data summary

In order to understand the role the microporous surface area in the gasification of the various carbons in this study, we consider the following distinguishing features of the experimental results.

1) The gasification rate of sucrose carbon in figure 3.5 is a function of particle size, under conditions for which a consevative calculation of the effectiveness factor considering Knudsen diffusion in 10 Å diameter pores with a tortuosity factor of 5, and a porosity of 20% predicts essentially complete reactant penetration and thus no particle-size effect. (See table 3.2 for

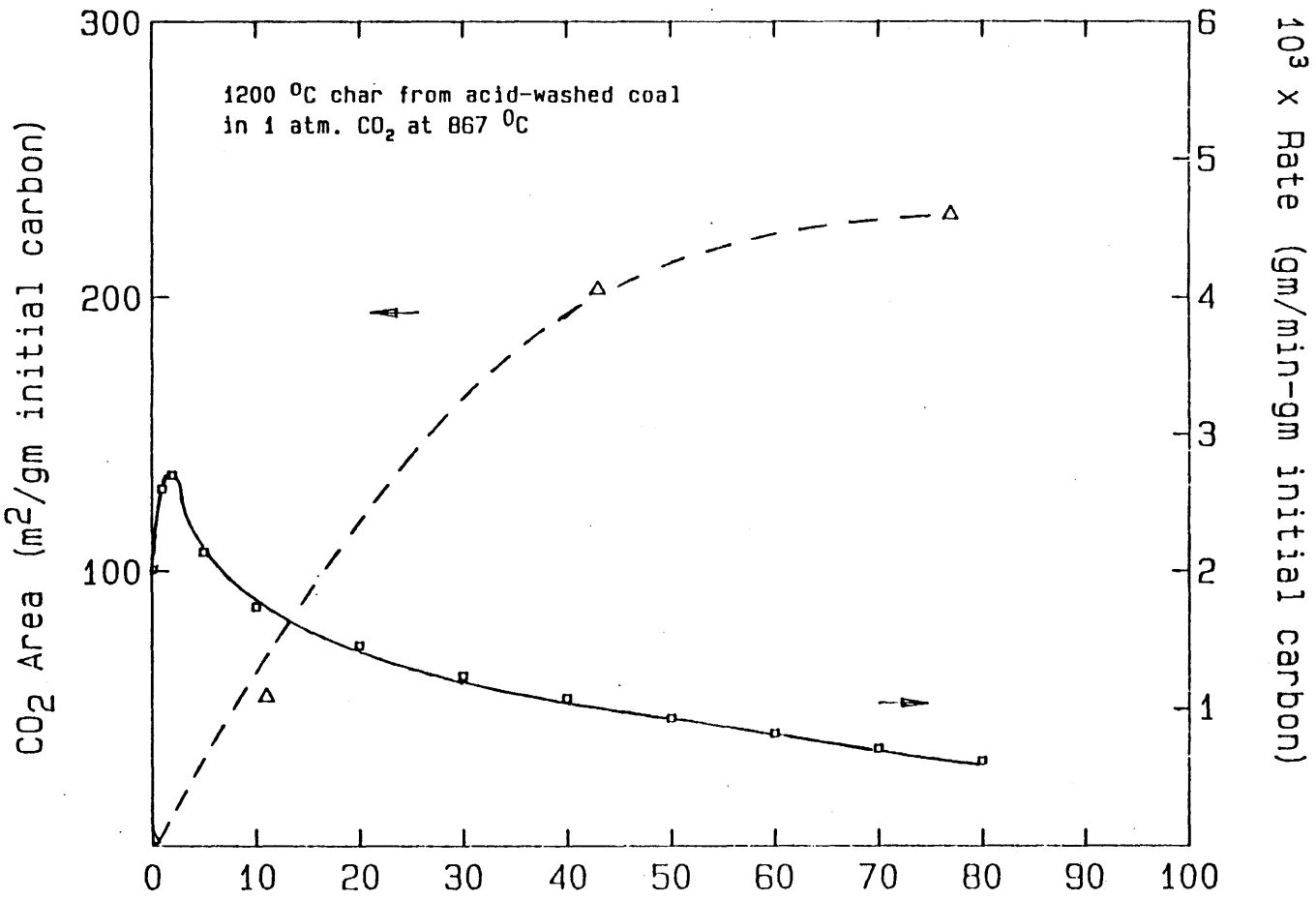

Figure 3.16

Reactivity and Area Evolution of High Temp. Coal Char

results of this calculation.) The experimental determination of the effect of particle size on reactivity is a classical test for the extent of reactant penetration, and the results in figure 3.5 suggest that only a portion of the total surface area is available, and that carbon dioxide diffusion in sucrose micropores is significantly slower than Knudsen diffusion with a tortuosity factor of 5.

Table 3.2: Calculated effectiveness factors for sucrose carbon gasification in the absence of restricted diffusion*

average pore radius	porosity**	effective diffusivity	effectiveness factor η zeroth order reaction	first order reaction
5 Å	.2	1.0×10^{-4}	1.0	.97
5 Å	.6	3.0×10^{-4}	1.0	.990
25 Å	.2	5.0×10^{-4}	1.0	.994
25 Å	.6	15.0×10^{-4}	1.0	.998

* for an intrinsic rate of 4.0×10^{-3} min^{-1} in 1 atm. CO_2 at 1203 °K., and Knudsen diffusion with a tortuousity factor of 5.
** Floess measures .25 for the porosity of unreacted sucrose carbon(33).

The gasification rate of Spherocarb carbon was, on the other hand, essentially independent of particle size.

2) The gasification reactivity of the 1200 °C char from the acid-washed subbituminous coal bears no apparent relation to the char's total surface area, as seen in figure 3.16.

3) All features > 100 nm on the surfaces of sucrose and Spherocarb carbon particles are preserved during gasification. There is evidence of uneven gasification of the external surface of the acid-washed sub-bituminous coal char, on the other hand, apparently in the form of production of approximately circular

pits, as seen in figure 3.1.

4) The Dubinin gradient increases with conversion for the sucrose carbon, but is constant throughout conversion for the sub-bituminous coal chars.

5) The molecular sieve nature of sucrose carbon, as evidenced by the large difference between its nitrogen and carbon dioxide surface areas, is destroyed rapidly by gasification. The sub-bituminous coal chars also exhibit a molecular sieve nature, which, however, is only gradually destroyed throughout conversion.

6) The carbon dioxide adsorption equilibration time is much longer for unreacted sucrose carbon than for unreacted or partially reacted Spherocarb or for partially reacted sucrose carbon.

In the following sections, we attempt to understand the role of microporous surface area for sucrose and Spherocarb carbons by considering possible diffusion limitations within microporous grains lying between larger pores. The coal chars, on the other hand, behave much differently from the two pure carbons, and the hypothesis is developed in the following sections that mineral matter catalysis determines the coal char behavior, including the role of the microporous surface area. In light of this, the coal chars and the pure carbons are discussed separately, after the following general discussions of the roles of catalysis and microporous diffusion limitations in gasification.

3.32 Microporous diffusion limitations

Since diffusion of gasification reagents in carbon micropores may be in the restricted diffusion range and thus very much slower than molecular or Knudsen diffusion, there exists the possibility of diffusion limitations within microporous regions or "grains" lying between larger pores, under conditions where there are no diffusion limitations in the larger pores themselves. In the absence of restricted diffusion, this is not the case(53,78). For a constant pore aspect ratio it can be shown that the onset of diffusion limitations is expected first in the larger pores which feed the center of the particle(53,78).

The severity of microporous diffusion limitations scales as L^2/D, where D is the local microporous diffusivity, a parameter which depends upon micropore size, and L is the characteristic size of the microporous regions, a parameter determined by the extent of carbon macroporosity.

Microporous diffusion limitations will give rise to an effect of particle size on reactivity, whose magnitude will depend upon the relative sizes of the microporous grains and the carbon particle. In the limit of very small microporous grains there will be no effect of particle size, as fracture of the particle may be expected to occur without significant fracture of the small microporous grains in which the diffusion limitations actually lie. The particle size effect will be larger, however, for systems with less macroporosity, and thus with a larger characteristic grain radius. The grain radius may even approach the particle radius for an exclusively microporous carbon.

It will be prove to be useful to derive an expression relating the extent of solid surface regression during gasification to the effective surface area for gasification as follows: The process of gasification to complete conversion consists of the removal of all of the carbon atoms in the solid regions lying between the smallest class of pores in which reaction occurs. The linear dimension of these solid regions is an estimate of the extent of surface recession occuring during gasification to complete conversion. The size of the solid grains, and thus the expected extent of surface recession can be estimated from the amount of surface area lying in the pores participating in gasification. Considering a carbon particle to be a collection of solid grains which we will assume are spherical, the external grain area represents the pore surface area and is related to the solid grain radius by

$$A_{g,ext}(m^2/gm) = 3/(\rho_g R_g)$$

where R_g is the grain radius and ρ_g is the grain density. For a microporous surface area of 500 m^2/gm, the grain size (or one half the characteristic distance between micropores) is 30 Å, and the microporous gasification of such a carbon would be complete after 30 Å of surface recession, having produced no microscopically observable changes in particle appearance.

On the other hand, in the presence of severe microporous diffusion limitations, reactant penetration into microporous regions would be very limited, and the reaction front would be essentially confined to the surfaces of larger pores. Gasification in this mode would be accompanied by macropore growth, which would be potentially observable

by microscopy. Examination of individual pores or features on the external surfaces of carbon particles can, therefore, provide an indication of the presence or absence of severe microporous diffusion limitations or provide information on the effective area for gasification.

3.33 Catalysis

The role of surface area in catalyzed carbon gasification can be expected to depend upon the the nature of the catalytic action. For example, if a given catalyst can influence gasification only in the immediate vicinity of catalyst particles, the reaction rate may be related to the number of accessible catalyst particles, and be independent of surface area. Alternatively, the catalyst in a given system may be active only in association with specific sites on the carbon surface, and these surface sites may become saturated at high catalyst loadings(43). In this surface-limited reaction regime, the reaction may depend upon or even be proportional to the total surface area.

The relationship between surface area and the rate of catalyzed gasification is clearly complicated, but may provide some insight into the nature of the catalysis.

3.34 Evidence of gasification <u>within</u> the micropores of pure carbons

The micrographs in figures 3.1 and 4.1 from the captive-particle S.E.M. technique show the preservation of all external surface features larger than the limit of S.E.M. resolution (about 50 nm) during

gasification of Spherocarb and sucrose carbon. A gasification mode in which the reaction front were confined to macropore surfaces would result in macropore widening for Spherocarb and observable motion of the fracture ridges and other surface features for sucrose carbon. This is clearly not the case, the reaction occurring instead uniformly througout the structure at this length scale, in pores invisible to S.E.M.

Evidence for micropore widening during gasification, and thus additional evidence for reaction in micropores comes from the measurement of vapor adsorption isotherms for a set of sucrose carbons at various stages of gasification conversion. The initially low N_2 surface area for sucrose carbon shown in figures 3.12 and 3.13 is the result of the presence of severe restricted diffusion during the adsorption of nitrogen at 77 ^{o}K, rendering most of the microporous surface area inaccessible to nitrogen during the time alloted for the experimental determination of the vapor adsorption isotherm(49). (This phenomenon is also discussed in Chapter 1.) The rapid rise in nitrogen surface area (at almost constant carbon dioxide area) during gasification indicates that the micropores are becoming accessible to nitrogen, and is one indication of micropore widening. A second indication is the behavior of the Dubinin gradient as a function of gasification conversion, seen in figure 3.14. The Dubinin gradient is derived from the slope of the adsorption isotherm, and is an indication of the average micropore size, within the Dubinin potential theory of vapor adsorption in microporous materials(75). Its increase over the course of conversion indicates an increase in the average micropore

size, and thus the presence of gasification within micropores.

Another interesting feature of the surface area evolution for sucrose carbon is evident in figures 3.12 and 3.13, namely the extraordinarily high nitrogen areas at high carbon conversion, which are in disagreement with the carbon dioxide surface areas. The nitrogen area per gram of remaining carbon reaches 2760 m^2/gm, which, indeed, slightly exceeds the theoretical surface area of 2680 m^2/gm for graphitic planes accessible on both sides to adsorbate molecules. Apparent surfaces areas above about 1300 m^2/gm are thought to be unrealistic(79), indicating, rather, the presence of pore volume filling(74). This discrepancy between nitrogen and carbon dioxide areas for highly converted chars has been observed elsewhere and played an important role in the original recommendation of carbon dioxide as an adsorbent for the measurement of coal and char micropore <u>area</u> as distinguished from micropore <u>volume</u>(74). The nitrogen area is, then, in certain situations, unsuitable for the normalization of gasification rates, but a comparison of its value to the value of the carbon dioxide area may provide some insight into the average micropore size at high conversion, as follows: Pore volume filling at low relative pressures is thought to be due to overlap, in very fine pores, of the potential energy fields associated with the adjacent pore surfaces(80). Enhanced adsorption can also be the result of a "cooperative effect" in larger micropores with diameters up to about 20 Å(80). This may provide an upper limit on a characteristic pore size present in sucrose carbon at high conversions. A lower limit may be identified by considering the values of the two apparent surface

areas at high conversion. The difference between the amount adsorbed corresponding to monolayer coverage ($n = A_{pores}/A_{adsorbate}$) and that corresponding to complete volume filling ($n = V_{pores}\rho_{adsorbate}$) is insignificant for pores with diameters below about 10 Å. (Monolayer coverage in these pores ($d_{pore} < 3d_{adsorbate}$) leaves no room for pore filling.) The factor of about two difference between the two areas measured here would not be expected to occur until the pore diameter was about 20 Å, which serves then as an estimate of the characteristic micropore size for highly reacted sucrose carbon. The appearance of this effect at high conversion is, again, suggestive of micropore widening and gasification within micropores for sucrose carbon.

Less evidence for microporous gasification in the case of Spherocarb has been presented in this section, but it is anticipated that the gasification of Spherocarb occurs to an even greater extent within its micropores, as its initially high nitrogen area suggests the presence of wider micropores, and its extensive macropore structure suggests very small micropores grains. Microporous diffusion during the gasification of Spherocarb will be thoroughly discussed in later sections.

We consider next whether reactant penetration is complete, and the gasification strictly kinetically limited, or if there are some finite microporous diffusion limitations. That is the topic addressed in the next sections, and pursuit of the answer to that question will also help to confirm the conclusions reached in this section.

3.35 Estimation of η for sucrose carbon

As discussed earlier, the observed effect of particle size on gasification reactivity of sucrose carbon in figure 3.5 is a classical indication of incomplete reactant penetration. The interesting feature of the data in figure 3.5 is that the effect of particle size is rather small between particle diameters of 180 and 50 μm, but increases substantially with further diameter reduction. This behavior is characteristic of the gasification of a carbon in which there are diffusion limitations within microporous grains that are significantly smaller than the particle itself. Grinding of such a particle would cause only modest increases in reactivity, until the point were reached where significant fracture of the microporous grains began to occur.

We undertook to formulate the simplest possible model that incorporates the feature of diffusion limited microporous grains, in order to illustrate and quantify this concept. A sucrose carbon particle is modeled as a collection of accessible but internally diffusion limited microporous grains which are spherical and have a monodisperse distribution of radii. Access to the microporous grains is provided by larger pores, which, in the case of sucrose carbon, may be the relatively few macropores(33) and/or some fraction of the wider micro- and mesoporosity. Note that the dependence of diffusivity on pore size in the restricted range is very strong and that only in the smaller micropores or "ultramicropores" is restricted diffusion thought to occur(14).

The observed gasification rate R_{obs} of such a particle of radius R_p is a function of the intrinsic reaction rate R_i, the effective microporous diffusivity D_m, and the grain radius R_g, which comprise the

three parameters in this model. The observed rate is given by $R_{obs} = \eta R_i$, where η is calculated from R_i, R_g, and D_m according to the classical formulation.

We need now to consider the effect of grinding on the grain size R_g. It is assumed that the particles fracture along random planes during grinding and not preferentially along grain boundaries or near the particle surface. After fracture there will be a distribution of both particle and grain sizes and shapes. The calculation of the exact particle and grain sizes and shapes, along with the solution to the reaction/diffusion problem for randomly fractured spheres is very difficult and not appropriate within the framework of this very simple model. The average grain size will of course be reduced by grinding, and the simplest model of this grinding effect can be formulated assuming that both the fractured particles and grains are spherical and monodisperse. The radii of the fractured grains can be calculated as follows: The external area of the initial grains is given by

$$A_{g,ext}(m^2/gm) = 3/(\rho_g R_g)$$

The external area of grains after fracture is

$$A_{g,ext} = A_{g,ext(before)} + \Delta A_{p,ext}$$

where $\Delta A_{p,ext}$ is the external particle area created during grinding and is given by

$$\Delta A_{p,ext} = (3/\rho_g)(1/R_p - 1/R_{p(before)})(1 - \theta_\lambda)$$

where θ_λ is the porosity in large pores, or between the grains. θ_λ is assumed to be small, which is probably quite a good assumption for sucrose carbon. This equation is an expression of the fact that all new external particle surface area generated by fracture is also new

grain external area (which is true, as mentioned, in the limit θ_λ = 0). The new grain radius can now be calculated from the first expression above.

Figure 3.17 is a plot of the gasification reactivity at 20% conversion taken from figure 3.5 for the four particle sizes, along with the predictions of the model generated using the optimum values of the parameters determined by non-linear least-squares regression. The particle size effect is quite consistent with the model of accessible but internally diffusion limited microporous grains. The least-squares parameters are given in table 3.3. This parameter set is unique and is not overly sensitive to the reactivity data.

Table 3.3 Microporous Grain Model: Optimum Parameters

$$D_m = 2.7 \times 10^{-7} \text{ cm}^2/\text{sec}$$

$$R_i = .02597 \text{ min}^{-1}$$

$$R_{g,o} = 27 \ \mu\text{m}$$

The corresponding grain area or large-pore area is .083 m^2/gm. This diffusivity is between two and three orders of magnitude lower than the effective Knudsen diffusivity in 10 Å pores with a tortuosity factor of 5, and a porosity of 0.2, which is 1.0×10^{-4} cm^2/sec. Tortuosity factors as high as 20 have been observed in carbons(81), which may account for some of the difference. Even if the tortuosity were 20, this diffusivity would be significantly lower than the Knudsen diffusivity and, therefore, in the restricted diffusion range.

Gasification, by widening pores and increasing diffusivities, would be expected to increase accessiblity and reduce or eliminate the particle size effect over the course of conversion. The particle size

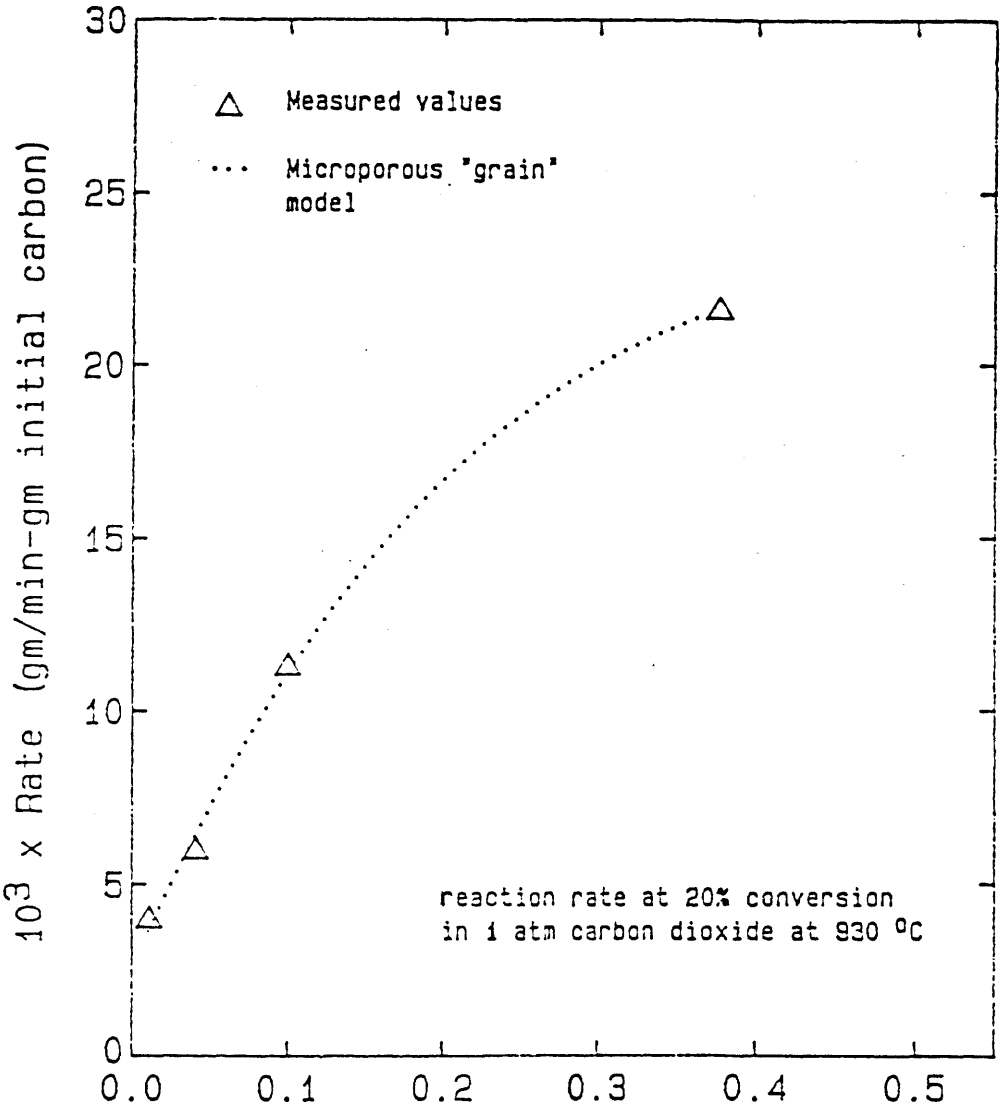

Figure 3.17

Effect of Particle Size on Sucrose Char Reactivity

effect is, indeed, largest at low conversions, but significant reactivity differences persist throughout conversion. The persistance may be a result of the phenomenon of gasification-induced carbon densification, which does occur during sucrose gasification (see chapter 4), and which would, to some extent, offset the pore widening accompanying gasification.

Alternative interpretations of the sucrose particle size effect have been considered. The increase in reactivity with decreasing particle size can not be attributed to an increase in carbon dioxide surface area upon grinding, as can be seen in table 3.1.

Pronounced inhibition of carbon dioxide gasification by carbon monoxide has been reported, and can cause a particle size effect if carbon monoxide produced during gasification accumulates in the particle interior(82). It can be difficult, because of this effect, to obtain uniform activation of carbons in carbon dioxide without the addition of carbon monoxide to the reactant gas to override the small CO buildup(83). For sake of argument we assume that carbon dioxide diffusion limitations are negligible, and that the particle size effect is caused by a buildup of carbon monoxide in the particle interior. Carbon dioxide, being a larger molecule than carbon monoxide(48), is expected to diffuse slower than carbon monoxide in carbon micropores. Therefore, in the absence of carbon dioxide diffusion limitations, when carbon dioxide gradients must be small, carbon monoxide gradients must be at least as small, or $P_{CO} = \epsilon \ll 1$ atm. Addition of .5 atm. carbon monoxide to the gas phase would reduce the ratio of carbon monoxide partial pressure in the particle center to that at the particle surface

to $(.5 + \epsilon)/.5 \simeq 1$, and thus should nearly eliminate the particle size effect. In fact, however, the particle size effect persists upon addition of .5 atm. carbon monoxide, indicating that the effect of particle size is not associated with product inhibition during otherwise kinetically limited gasification.

The effect of particle size on the pyrolysis process and thus on the resulting char is not a satisfactory explanation for the particles in this study were ground and classified after the completion of pyrolysis during heat treatment at 1000 ^{o}C for 1 hour.

Segregation of the carbon into fractions having different reactivities can also not be responsible for the effect, as the small particles in figure 3.8 were obtained from larger particles while retaining all of the material.

Contamination of the original sample is unlikely, as grinding of Spherocarb carbon in the same manner had essentially no effect on reactivity.

Tidjani et al. have observed structural changes in graphite using X-ray diffraction during intensive grinding in both a ceramic and a steel ball mill(84). Although the grinding of Tidjani's graphite was more severe than the grinding of the sucrose char in this study, it is not possible to rule out an effect of grinding on the reactivity of sucrose char. It is interesting that grinding of Spherocarb in the same manner resulted in essentially no change in reactivity, and the outstanding difference between the two carbons is pore structure. (The smaller Spherocarb fraction corresponds roughly to the 20 μ mean diameter sucrose fraction.) It is interesting that the particles were

heated to 930 °C during the carbon dioxide reaction, a temperature which is near the original heat treatment temperature of 1000 °C, and at which one might expect any structural changes introduced by grinding to be removed by annealing.

The possibility exists, however, that a grinding effect contributes to the increased reactivity of smaller particles, especially for the 5 μ fraction, which was intensively ground. The parameters in table 3.3 should therefore be considered to set an upper limit on the severity of diffusion limitations during sucrose gasification.

Floess has measured activation energies for the carbon dioxide gasification of a similar sucrose carbon, which also exhibited a particle size effect(33). His smaller particles exhibited a slightly (15%) higher activation energy than the larger particles, a trend which is consistent with diffusion limitations, and the reverse of that expected if the smaller particles were more reactive due to an effect of grinding on carbon chemistry. This result indicates that the reactant penetration is at least to some extent incomplete.

The temperature dependence of the rate of gasification of Floess' sucrose chars in both carbon dioxide and oxygen deviates, however, from that predicted by the classical theory of reaction and diffusion, as discussed by Floess(33). No final explanation for this phenomenon is offered in this thesis, but it is believed that the observed temperature dependence is still consistant with the hypothesis of incomplete penetration into microporous grains. Based on preliminarly modeling work, such a deviation from the classical prediction may be

expected for reaction in a medium with a widely varying diffusivity, in which much of the large-pore porosity is accessible from the surface only through microporous regimes.

3.36 Determination of η for Spherocarb carbon

As mentioned in the preceding section, the reactivity of Spherocarb carbon, unlike that of sucrose carbon, is essentially independent of particle size. This is a necessary but not sufficient condition for intrinsic gasification, due to the possibility of incomplete reactant penetration into microporous grains that are much smaller than the particle itself. Since the severity of diffusion limitations scales as L^2/D, however, it is unlikely that the gasification of a solid with very small microporous grains would be microporous-diffusion limited. It is, in fact, unlikely in the particular case of Spherocarb, in which the microporous grains must be small enough to ensure no particle size effect, and in which the local microporous diffusivity is expected to be as large or larger than that in sucrose carbon (Spherocarb's initially high nitrogen area suggests wider micropores). Nevertheless, the extent of reactant penetration into microporous regions in Spherocarb needs to be established, and in order to do so, we turn to measurements of diffusion times during vapor adsorption experiments.

The adsorption of carbon dioxide in Spherocarb at both 0 and 45% conversion was complete after several seconds, as can be seen in figure 3.13. Characteristic diffusion times calculated from the data in figure 3.13 can be used to estimate the effectiveness factor at

reaction conditions. (In addition to the following discussion there is some information in appendix A.) The measured amounts of carbon dioxide adsorbed as a function of time were fit to the solution of the transient diffusion equation in a sphere to obtain L^2/D. L_2/D was, in practice, calculated from the slope and intercept of a plot of $dN_{ads}/dt^{1/2}$ vs. $t^{1/2}$ as in Walker et al.(14) or, for short characteristic diffusion times, from the time required for 87% completion of adsorption(14). The adsorption into 45% converted Spherocarb was 87% complete at .95 seconds, yielding a characteristic diffusion time (L^2/D) of 5.9 sec. The solution used is for unsteady diffusion into a sphere at constant external pressure following an initial step change in pressure. The adsorption experiments were carried out at constant volume, instead of constant pressure, but changes in the external pressure during adsorption were relatively small for the small samples used, and were neglected. The Thiele modulus for first order reaction in a sphere is given by $\phi = [(R^2/D\theta)/(1/k_v)]^{1/2}$ where R_2/D has been extrapolated to reaction temperature, θ is the porosity, and $1/k_v$ is the intrinsic rate constant per unit volume. $1/k_v$ is given by $1/k_v = [C_r MW_c/\nu\rho_p]T$ where C_r is the concentration of the reacting gas, MW_c is the molecular weight of carbon, ν is the moles of reacting gas consumed per mole of carbon, ρ_p is the particle density, and T is the reciprocal of the intrinsic reaction rate with units of gm/sec-gm.

There is some uncertainty associated with the extrapolation of restricted diffusion coefficients to other conditions, and thus some uncertainty associated with this analysis, due to an incomplete understanding of the phenomenon of restricted diffusion(86). We

believe it to be a valuable analysis nevertheless, especially in connection with other analyses and experiments.

It is important, before discussing the results of the calculation, to note the following things concerning this technique of estimating the effectiveness factor. There are two ways of interpreting the diffusivity in the value of L^2/D obtained by fitting the uptake curve to the solution of the transient diffusion equation. If the appropriate driving force for fine pore diffusion in a given case is the total adsorbate concentration, then the diffusivity obtained is the true diffusivity. If, however, the appropriate driving force is the gas phase concentration only, with the adsorbed species not diffusing, the diffusivity obtained is less than, but related to the true diffusivity(86). One does not, in general, know what the appropriate driving force for diffusion in a given system is, and must, therefore, recognize the possibility that the true diffusivity is larger than the diffusivity obtained directly from the uptake curve. Secondly, a finite rate of dissipation of heat generated upon adsorption may often hinder further adsorption and lengthen the observed rate of uptake(87). Mass transfer limitations within the apparatus, and to and through the bed of particles can also limit the rate of uptake. The observed rate of uptake of carbon dioxide into Spherocarb is, in fact, quite comparable to the rate of helium flow through the sample stopcock and into the sample bottle. The equilibration times measured here may reflect to a large extent various mass transfer limitations external to the particle. Thirdly, some restricted diffusion coefficients have been observed to be pressure or concentration dependent(14), increasing

with decreasing pressure. Since the extrapolation from adsorption conditions to reaction conditions involves a large reduction in concentration in the pores, the measured and extrapolated diffusivity may be too low. Fourthly, the diffusivities were extrapolated using the temperature dependence of the Knudsen diffusion coefficient, which should represent a lower limit on the temperature sensitivity of the diffusivity. Finally, the microporous diffusivities used are those for carbon dioxide diffusion, and can be expected to be lower than those for oxygen, which has a smaller kinetic diameter(48). (Oxygen has, in fact, been observed to diffuse faster than nitrogen in 4 Å molecular sieve, while nitrogen diffuses faster than carbon dioxide above room temperature in carbons(49).) In each case the approximations involved are such, that the effectiveness factor calculated from the measured and extrapolated diffusivity should be regarded as a minimum effectiveness factor, defining an upper limit on the severity of diffusion limitations during Spherocarb gasification.

For the Spherocarb reaction rates on the upper portion of figure 3.4, use of the diffusion times from adsorption measurements predicts a minimum effectiveness factor significantly less than 1. Since this is a <u>minimum</u> effectiveness factor, the question of the existence of diffusion limitations is still open. It was clear from the analysis, however, that extension of the existing oxidation rate data for Spherocarb on the upper portion of figure 3.4 to lower temperatures would make possible an unambiguous evaluation of possible microporous diffusion limitations. In fact, at 400 ^{o}C the measured reaction rate was found to be 2.3×10^{-4} min^{-1}, as seen on figure 3.18, and the

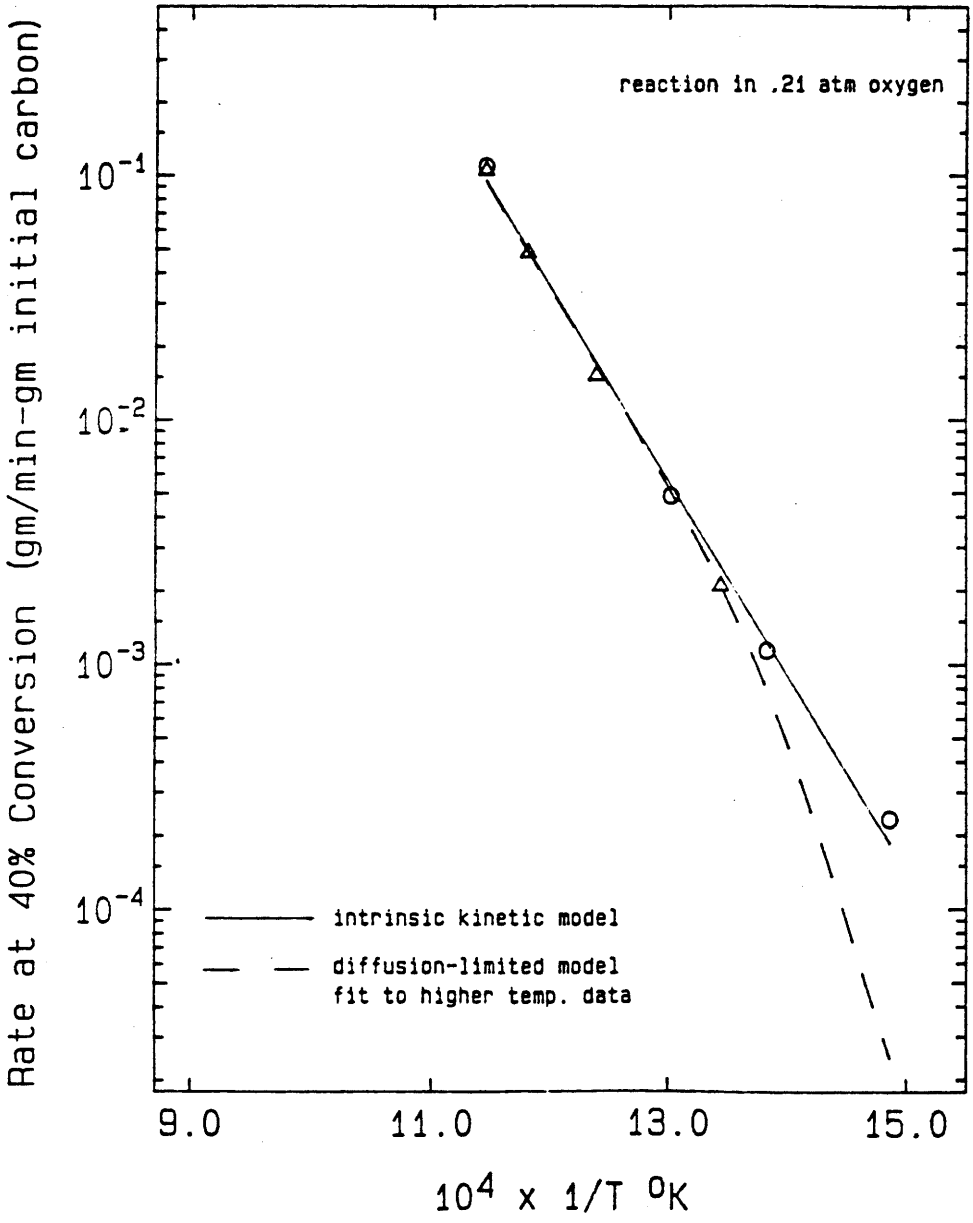

Figure 3.18
Spherocarb-Oxygen Reaction

minimum effectiveness factor was calculated to be .92. This rate is nearly intrinsic, and further, since all of the measured rates fall on a straight line on the Arrhenius plot in figure 3.18, the effectiveness factor for Spherocarb oxidation cannot deviate far from unity up to at least 600 ^{o}C. Alternatively, we assume for sake of argument that the true effectiveness factor is equal to the calculated minimum effectiveness factor, and that the rates at higher temperatures in figure 3.18 are diffusion limited. Use of the classical effectiveness factor analysis for extrapolation of the diffusion-limited solution to lower temperatures requires that the Arrhenius curve bend over, as the calculated effectiveness factor approaches unity. The measured points in figure 3.18 continue to lie on the same line, however, and are thus inconsistent with the diffusion limited assumption.

Another useful analysis uses the diffusivity obtained from application of the microporous grain model to sucrose reactivity data in order to assess the severity of diffusion limitations for Spherocarb. To do this, one needs to know the length scale for microporous diffusion in Spherocarb carbon. An estimate of this length scale is the characteristic radius of microporous grains, calculated as discussed in the section on sucrose char modeling. For this calculation, microporous grains were defined as those regions containing no pores larger than 100 Å in diameter. With this definition, the grain radius is calculated knowing the amount of surface area lying in pores larger than 100 Å, a quantity which is obtainable from mercury porosimetry for both Spherocarb(88) and sucrose carbon(33). Microporous grains according to this definition

have an external area of .092 m^2/gm and a radius of 24 μm for sucrose carbon, and an external area of 15 m^2/gm and a radius of .15 μm for Spherocarb. The large difference reflects the limited macroporosity of sucrose carbon in contrast to the extensive macroporosity of Spherocarb. Effectiveness factors for Spherocarb oxidation, calculated using this length scale and the microporous diffusivity from the sucrose model, are unity for each of the measured reaction rates in figure 3.4 between 400 and 600 ^oC. The diffusion limited solution at higher temperatures can be generated by extrapolating the existing (kinetic) data and using, again, the estimated length scale and the sucrose diffusivity. This solution is shown in Figure 3.19, and suggests that microporous diffusion limitations may start to become important for Spherocarb at temperatures higher than those examined here. Note that the diffusivity used in this analysis is for carbon dioxide in sucrose carbon micropores. Because of the difference between oxygen and carbon dioxide, the possible difference in width of sucrose and Spherocarb micropores, and the fact that the sucrose diffusivity itself is best regarded as a minimum possible diffusivity (discussed above), this analysis strongly suggests that the measured Spherocarb oxidation rates are intrinsic, and would continue to be intrinsic at least until the point of incipient diffusion limitations seen in figure 3.19, and perhaps beyond.

3.37 Summary of sucrose and Spherocarb analyses

There is much evidence of gasification <u>within</u> the micropores of both synthetic carbons. Further, several quantitative analyses of

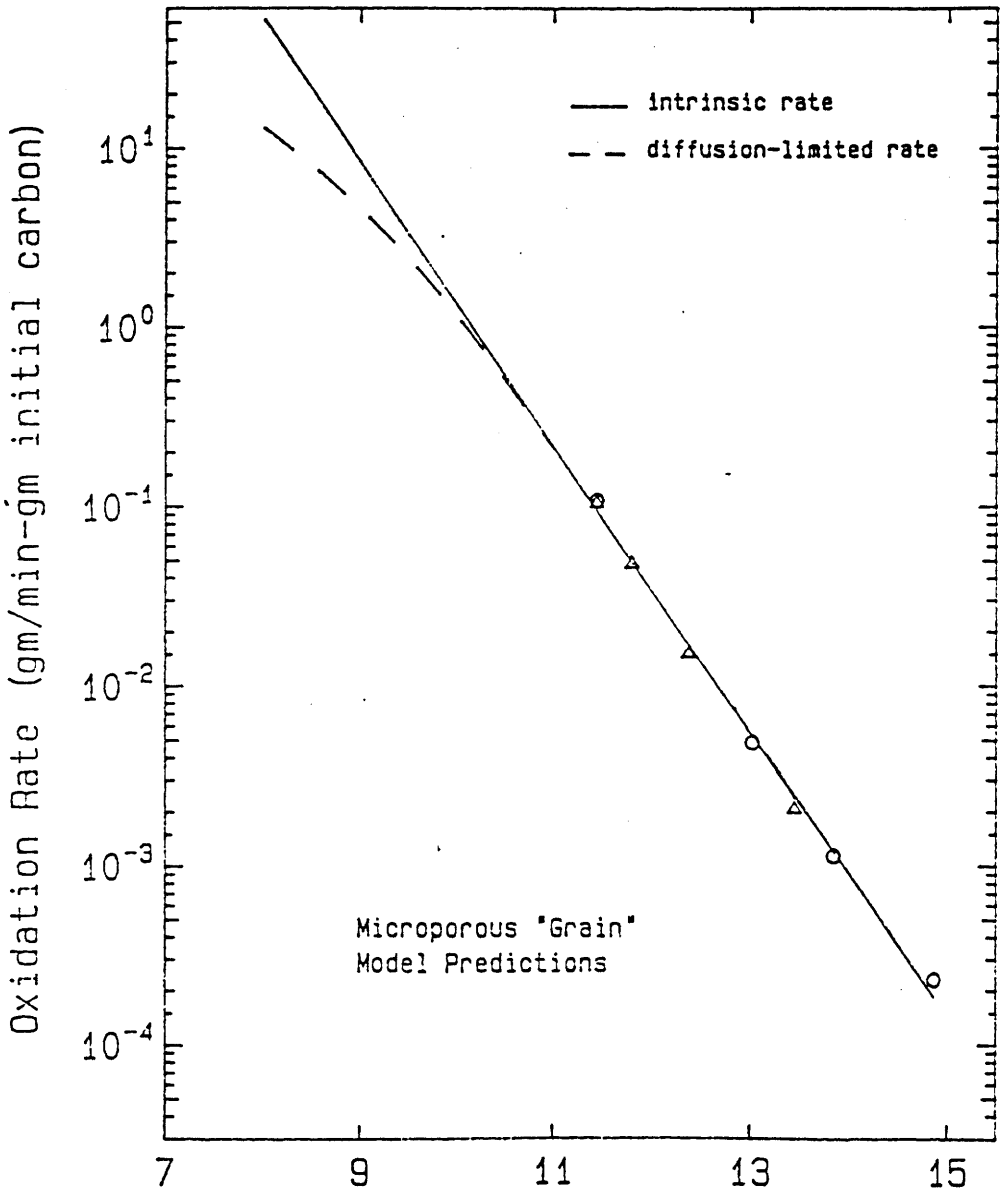

Figure 3.19
Spherocarb-Air Reaction

reaction and diffusion during Spherocarb oxidation indicate that oxygen penetration is complete, and that the reaction rate is strictly kinetically limited. The accessible total surface area for Spherocarb is expected, then, to be 636 m^2/gm, and the measured activation energy of 36 kcal/mol to be the intrinsic activation energy for oxidation of this carbon. This can be compared to about 250 kJ/mol (60 kcal/mol) typically measured for the oxygen gasification of graphite and pure carbons(7), the difference presumably arising from the different degrees of purity and crystallinity(76).

There is some evidence for sucrose carbon, on the other hand, that reactant penetration is incomplete. The nature of the effect of particle size on sucrose char reactivity is consistent with diffusion limitations in microporous grains with radii of 27 μm. There is the possibility that an effect of grinding contributes to the increase in reactivity with decreasing particle size effect, in light of which the fitted model parameters should be regarded as setting an upper limit on the severity of diffusion limitations for sucrose char. It is important to check whether or not the diffusion interpretation is consistent with the results of an effectiveness factor calculation based on measured adsorption equilibration times for sucrose char. The method of calculation has already been discussed earlier in this chapter. L^2/D for 180 μm sucrose carbon at 0% conversion was 6.1×10^4 sec (or 16.9 hrs), while at 20% conversion only 17.8 sec. The values of the effectiveness factor (which are intended as minimum values) assuming zeroth and first order reaction are 2.8×10^{-4} and 1×10^{-4} respectively, for unreacted sucrose, and .62 and .45 for 20%

converted sucrose. The very low initial effectiveness factor at 0% conversion reflects that carbon's very long adsorption equilibration time as seen in figure 3.12. Although the particle size effect is indeed the largest at low conversion, it does persist longer than would be expected from the diffusion analysis. This may support the notion that a chemical difference contributes to the particle size effect. On the other hand it is probable that one cannot expect the analysis based on diffusion times measured under adsorption conditions to precisely predict gasification effectiveness factors.

The severity of diffusion limitations scales as L^2/D, and depends, therefore, on the local microporous diffusivity, a parameter determined by micropore size, and the characteristic size of the microporous regions, a parameter determined by macroporosity. The major difference between the two synthetic carbons in this study is probably related to a difference in the characteristic size of microporous grains in the two carbons. The severity of diffusion limitations for most chars should lie between that for the highly macroporous Spherocarb and that for the essentially non-macroporous sucrose carbon. Hippo et al.[40] have also emphasized the importance of feeder pores in determining the likelihood or severity of microporous diffusion limitations.

3.38 The role of microporous surface area in the gasification of a subbituminous coal char

Chars from untreated and acid-washed P.S.O.C. 156 sub-bituminous coal behaved very differently during gasification than did the synthetic chars of the previous section. In contrast to the sucrose char, carbon dioxide gasification of the low temperature coal chars was accompanied by a relatively slow burnout of the char's molecular sieve properties as seen in figure 3.14. The nitrogen areas remain significantly lower than the carbon dioxide areas up to very high conversion. In addition, gasification was not accompanied by measurable micropore widening, as indicated by the constant Dubinin gradient in figure 3.11. These two results suggest that the contribution of microporous surface area to the gasification rate is small. (Here one must be careful, because one can expect micropore widening due to gasification and, possibly, simultaneous micropore narrowing due to the phenomenon of gasification-induced shrinkage, discussed in chapter 4. The observed change (or lack of change) in micropore dimensions during conversion reflects the competition between the two processes. Net micropore widening is certainly an indication of microporous reaction, but a constant micropore diameter is only a necessary (and not sufficient) condition for no microporous gasification.

Carbons can be expected to undergo a loss of surface area, presumably due to solid state rearrangements, upon high temperature heat treatment. Some carbons undergo catastrophic loss of carbon dioxide surface area during heat treatment at temperatures just above 1000 ^{o}C(90). In order to further investigate the role of the

micropores in the gasification of the subbituminous coal chars, the char from the acid washed coal, heat treated previously at 1000 °C for one hour, was subjected to an additional heat treatment at 1200 °C for one hour, in hopes of eliminating the microporous surface area and observing the subsequent effect on gasification behavior. The surface area, measured by carbon dioxide adsorption, did, indeed, drop from 510 to 4 m^2/gm, while the initial gasification rate decreased by about a factor of 4. Further, as shown in figure 3.16, the gasification rate of the higher temperature coal char was at its maximum at essentially 0% conversion and thereafter decreased monotonically, while the carbon dioxide surface area increased strikingly, from 4 to over 200 m^2/gm. The gasification rate of this char bears no apparent relation to its total surface area. Especially noteworthy is the maximum reaction rate at 0% conversion, associated with a char having almost no measurable internal surface.

A possible interpretation is that inaccessibility of or slow reaction within the micropores confines the reaction front to the surfaces of larger pores. A comparison of the magnitude of the carbon dioxide gasification rates of the various chars used in this study (see table 3.4) can be used to rule out this interpretation. Each of the coal chars has a higher reactivity at a given temperature than either sucrose or Spherocarb carbons, which have been shown to undergo gasification within their micropores. The comparison is between the coal chars and Spherocarb is especially interesting, for Spherocarb is believed to have an effective gasification area approximating the 636 m^2/gm measured total surface area. If micropore inaccessibility

Table 3.4: A Comparison of the carbon dioxide gasification rates of various chars

Char	Temperature (°C)	$R/R_{sucrose}$*
Spherocarb	977	1.38
Subbit. Coal Char	977	97.6
Acid-Washed Subbit. Coal Char	860	6.25
Acid-Washed 1200°C Subbit. Coal Char	860	1.63

* Gasification rate of 100 μm particles at various temperatures from Arhenius parameters measured by Floess(33). Sucrose rates at 800 and 860 °C obtained by extrapolation.

were confining the coal char gasification reaction to larger pores (having a surface area < 4 m^2/gm), this rate would be expected to be on the order of 4/636 of the Spherocarb rate on a weight basis, and not, in fact, greater than the Spherocarb rate. A second argument is as follows. The coal chars at high conversion have nitrogen areas which approximate their carbon dioxide area. In this respect the highly converted coal chars are similar to the two synthetic carbons, and should have micropores which are accessible during gasification. If gasification had originally been confined to larger pore surfaces, then conversion would have been accompanied by large increases in accessible area and thus large increases in reaction rate. This is clearly not the case and we therefore seek an alternative explanation for the coal char gasification behavior.

The S.E.M. micrographs in figure 3.1 indicate that gasification of this char, unlike gasification of the two synthetic chars, takes place unevenly over the external surface of the particle, apparently by the formation of approximately circular pits. Marsh(35) has

microscopically observed pitting, channeling, and/or uneven gasification of the surface of many carbons doped with various inorganic impurities. In contrast to his pure carbons, rarely, if ever, does catalytic gasification take place uniformly over the carbon surface.

In light of the high gasification reactivity, the apparent independence of reactivity on surface area, and uneven surface gasification, we offer the interpretation that catalysis by inorganic impurities is important to the gasification of the sub-bituminous coal chars. The untreated subbituminous coal contains 8.5% ash, and the acid-washed coal .79%. Both chars, therefore, contain enough potentially catalytic inorganic matter to dominate the gasification rate, which, as discussed in chapter 1, can be as little as 10 ppm of well dispersed transition metals. At least the untreated char is, indeed, expected to be catalytic based on a study of the gasification of its individual lithotypes, discussed in chapter 5. The significance of the result in figure 3.16 is, then, that the rate of catalyzed gasification can be apparently unrelated to microporous surface area, depending instead on properties of the catalyst. Normalization of the rate of catalyzed gasification with measured surface areas in such a case is inappropriate. The presence of catalyst here does not simply increase the intrinsic reactivity of the carbon surface, and the process of catalyzed gasification can not be treated as a total surface area evolution problem with an altered or adjustable intrinsic surface reactivity.

Several studies have shown that the gasification rates of coal

chars can not be adequately correlated with surface area alone(7,51,52) indicating at least that other variables are also important. Since many naturally occurring organic materials are rich in potentially catalytically active inorganic impurities, this is perhaps not surprising. The results of the present study suggest, further, that use of microporous surface area for the normalization of the gasification rate of many coal chars will be of limited use.

3.39 Possible nature of catalytic action during gasification of the coal chars

It is worthwhile to speculate on what the result of figure 3.16 further reveals about the nature of catalysis during gasification of the coal chars in this study. We first consider the model of carbon structure arising primarily from X-ray studies, depicted in figure 1.1(21). The lines in the diagram are small, graphitic layers, viewed from the side, whose imperfect packing arrangement is responsible for carbon micropores. (The circles in the diagram are not part of the structure, but rather indicate regions which would be identified as crystalline by X-ray diffraction.) Heat treatment of such a char can initiate solid state rearrangements resulting in improved packing and drastic loss of microporosity. An inorganic impurity, if dispersed uniformly over the initial total carbon surface, would be located, after heat treatment, <u>within</u> the structure of the high temperature char. The observation that heat treatment of the coal chars did not have a large effect on gasification reactivity suggests that either the catalyst trapped in the char structure is able to affect gasification at a distance, or that the catalyst was lying in larger pores, thus

remaining accessible to the gasification reactants. Further, the existence of catalyst particles initially in the micropores of the low temperature char, and thus trapped within the structure of the higher temperature char, would cause large increases in gasification rate with conversion as they were uncovered during the subsequent gasification of the high temperature char. This is not the behavior seen in figure 3.16. The catalyzed gasification rate of a carbon in which the catalyst particles were lying on large pores would, on the other hand, be insensitive to changes occurring in the underlying microporosity during both heat treatment and gasification. Inorganic material may be located preferentially on large pores, if it were deposited there preferentially in the parent organic material, or if it had migrated out of the micropores during heat treatment by a process of random motion and coalescence, as has been observed by several researchers(91,92).

The connection between surface area and reaction rate for catalyzed systems clearly depends on the nature of the catalytic action and can be expected therefore to vary between catalyzed systems. We present the hypothesis of uneven catalyst distribution as a possible, plausible explanation for the very interesting gasification behavior of the subbituminous coal chars in this study.

3.4 Summary

There is much evidence for gasification within the micropores of the synthetic carbons. Further, there is evidence that reactant penetration during Spherocarb oxidation is complete, and that the reaction rate is strictly kinetically limited. The accessible total surface area for Spherocarb is expected, then, to be the 636 m^2/gm measured by carbon dioxide adsorption, and the measured activation energy of 36 kcal/mol to be the intrinsic activation energy for oxidation of this carbon. This is a typical activation energy for a low temperature char or carbon, but is substantially lower than activation energies measured for oxidation of some graphites and pure carbons(7), the difference presumably arising from the different degrees of purity and crystallinity(76). This level of understanding of diffusional processes is necessary for the fundamental treatment of many aspects of carbon gasification, including, in fact, the pore structure modeling effort undertaken in chapter 4.

There is some evidence for sucrose carbon, on the other hand, that reactant penetration is incomplete. The nature of the effect of particle size on sucrose char reactivity is consistent with restricted diffusion limitations in microporous grains with radii of 27 μm. There is the possibility that an effect of grinding contributes to the increase in reactivity with decreasing particle size effect, in light of which the fitted model parameters (grain size, intrinsic rate, and diffusivity) should be regarded as setting an upper limit on the severity of diffusion limitations for sucrose char.

The severity of diffusion limitations scales as L^2/D, and depends,

therefore, on the local microporous diffusivity, a parameter determined by micropore size, and the characteristic size of the microporous regions, a parameter determined by macroporosity. The major difference between the two synthetic carbons in this study is probably related to a difference in the characteristic size of microporous grains in the two carbons. The severity of microporous diffusion limitations for most chars should lie between that for the highly macroporous Spherocarb and that for the essentially non-macroporous sucrose carbon. The carbon dioxide surface area should therefore be the appropriate total surface area for the gasification of many pure carbons, although restricted diffusion limitations may be important during the gasification of some exclusively microporous materials.

The rate of catalyzed gasification can, on the other hand, be apparently unrelated to microporous surface area. The behavior of the sub-bituminous coal chars in this study is consistent with the hypothesis that gasification is catalyzed, with the catalyst particles lying preferentially in larger pores.

The experiments in the present study provide kinetic data which demonstrate that the rate of catalyzed gasification can be independent of total surface area. Normalization of the rate of catalyzed gasification with measured surface areas in such a case is inappropriate. The presence of catalyst here does not simply increase the intrinsic reactivity of the carbon surface, and the process of catalyzed gasification can not be treated as a total surface area evolution problem with an altered or adjustable intrinsic surface reactivity.

Several studies have shown that the gasification rates of coal chars can not be adequately correlated with surface area alone, indicating at least that other variables are also important. Since many naturally occurring organic materials are rich in potentially catalytically active inorganic impurities, this is perhaps not surprising. The results of the present study suggest, further, that use of microporous surface area for the normalization of the gasification rate of many coal chars will be of limited use.

Catastrophic surface area loss can accompany heat treatment of chars, depending upon temperature-time history, char properties, and the presence or absence of gasification (see chapter 4). Based on the results of this chapter, choosing process conditions to maintain or enhance char microporous surface area should be important in the efficient gasification of some chars, and not in that of some others.

Chapter 4: The Phenomenon of Gasification Induced Carbon Particle Shrinkage and its Influence on Pore Structure Evolution

During the low-temperature gasification of high surface area carbons, the reaction is generally expected to occur uniformly throughout the particle and not preferentially on or near the particle's external surface. Dudek, however, during single particle gasification experiments in an electrodynamic balance, has observed significant diameter reduction during air-oxidation of Spherocarb carbon particles at low temperatures(60), as seen in figure 4.2. Spherocarb particles do not shrink upon heating in nitrogen under otherwise identical conditions. Possible explanations for the diameter reduction phenomenon are perimeter fragmentation, the presence of a significant reaction component on the external surface of the particle, and reaction induced homogeneous particle shrinkage. It was undertaken in this study to investigate the diameter reduction phenomenon and its implications, especially those relating to carbon gasification reactivity.

4.1 Results

A technique was developed with which individual features on the external surface of individual particles can be observed by S.E.M. as a function of gasification conversion, in order to distinguish between the possible interpretations of the diameter reduction phenomenon. The technique is described in detail in chaper 2. In table 4.1 are presented particle diameters (d/d_o) for various chars at different stages of conversion, measured from photographs using either the

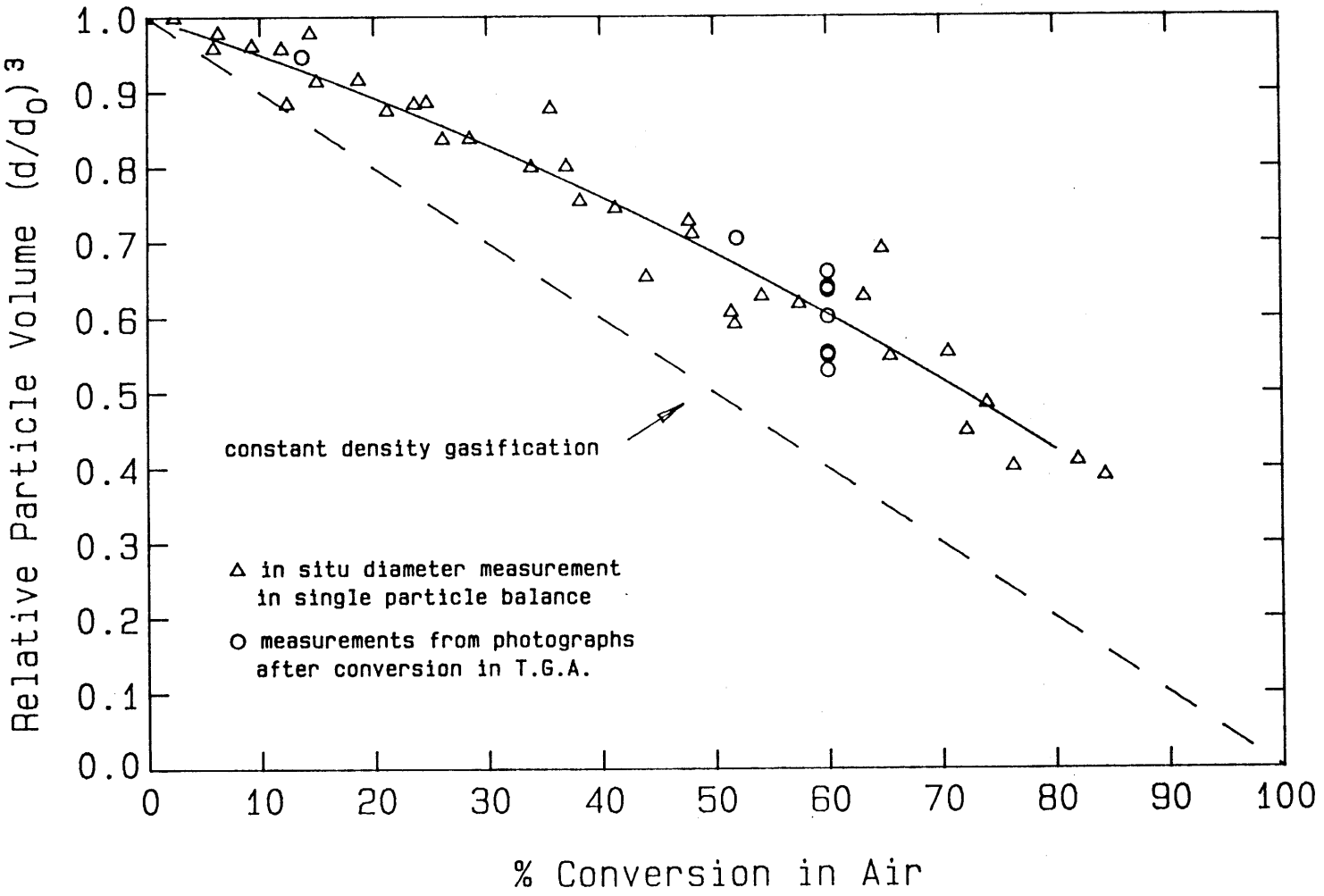

Figure 4.2 Spherocarb Particle Shrinkage

captive-particle S.E.M. technique or optical microscopy on single particles partially converted in a conventional T.G.A., as discussed in chapter 2. It would not be practical to reproduce all of the

Table 4.1
Extent of diameter reduction during gasification of various carbons and chars

Carbon	Reaction Conditions	Conversion	d/d_o
Spherocarb	.21 atm. O_2, 495 °C (163 min) . . .	60%	.821
			.871
			.809
			.844
		52%	.890
		13.7%	.982
	.21 atm. O_2, 450 °C	60%	.860
	.21 atm. O_2, 600 °C	60%	.862
			.819
	.5 atm. CO/.5 atm. CO_2, 990 °C . .	60%	.862
	1 atm. N_2, 495°C, 163 min	0%	1.0
	1atm. N_2, 960 °C, 60 min	0%	.983
Sucrose char	.21 atm. O_2, 495 °C	60%	.882
			.863
			.921
		20%	.990
Sucrose with carbon black	. . . . .	51.5%	.989
		71.2%	.886
Pitt. #8 char	. . . . .	61%	1.0
			.98
			.94
Calcium-doped sucrose	.21 atm. O_2, 370 °C	70%	1.0
Montana lignite char	. . . . .	44%	1.0
			.971
		85%	.575
			.646

photographs taken in this study, but many important ones appear in figure 4.1 and in figure 3.1. (Note that the magnification varies from photograph to photograph, and that the diameter reduction, which is easily measurable and presented in Table 4.1, is in some cases not

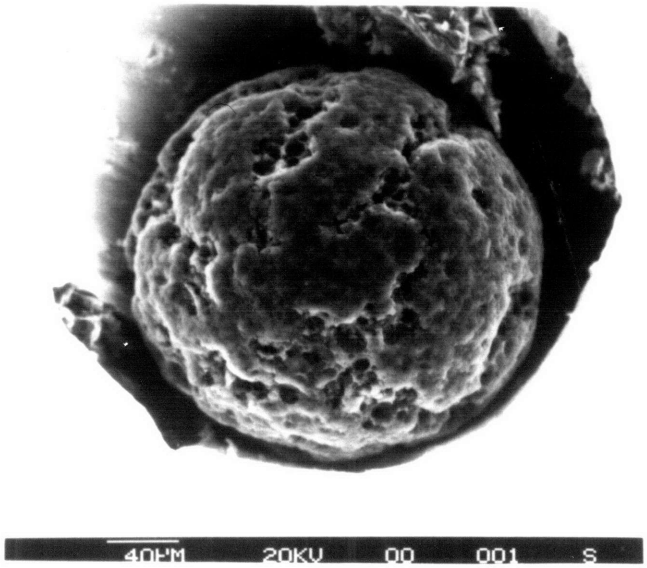

Unreacted

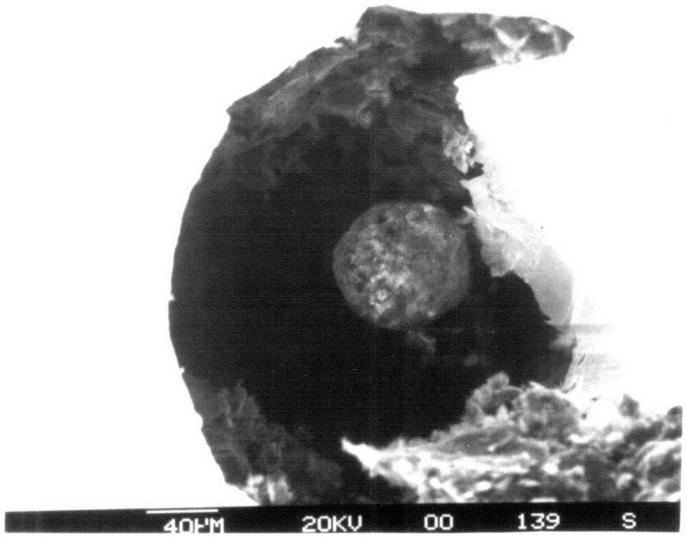

Partially
Reacted
(presumably high
conversion)

Spherocarb in .21 atm O_2, 495 ^{o}C

Figure 4.1 Photographs and S.E.M. Micrographs

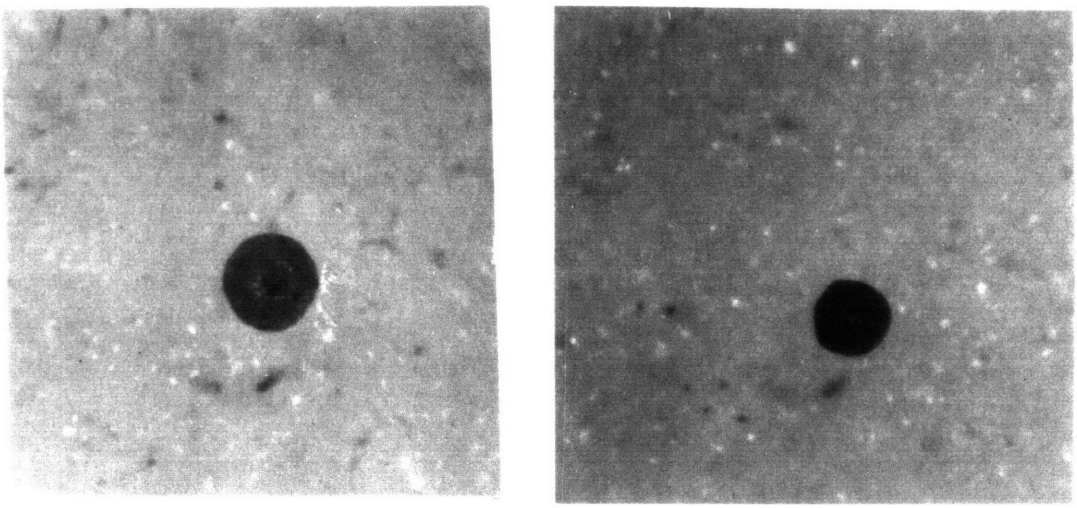

Unreacted
d = 198 μ

60% Conversion
d = 167 μ

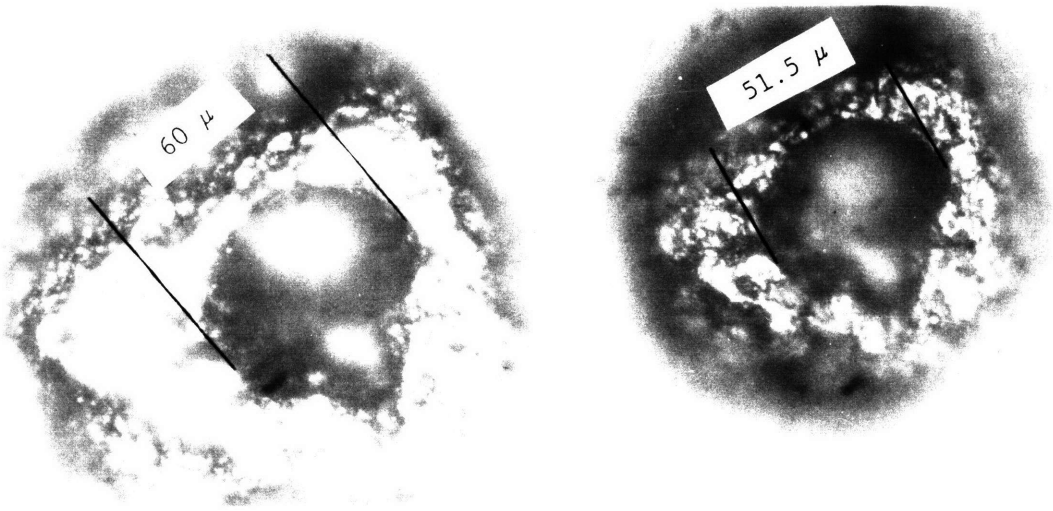

Unreacted

60% Conversion

Spherocarb in .21 atm. O_2, 495 ^{o}C
Set of optical photographs at increasing magnification

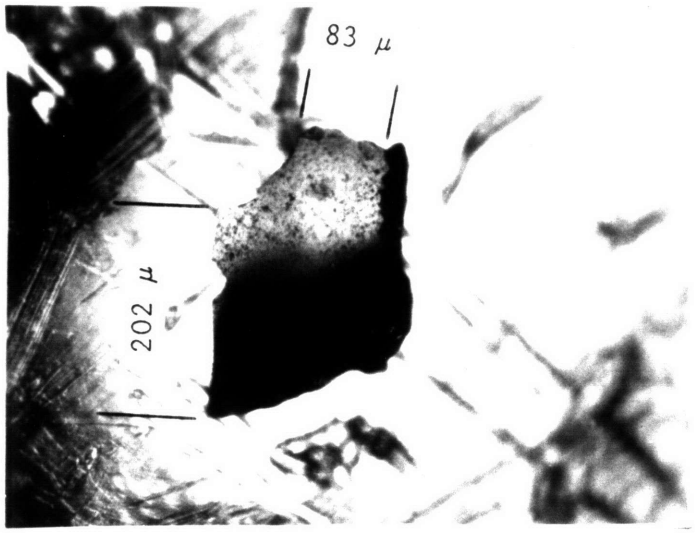

Unreacted

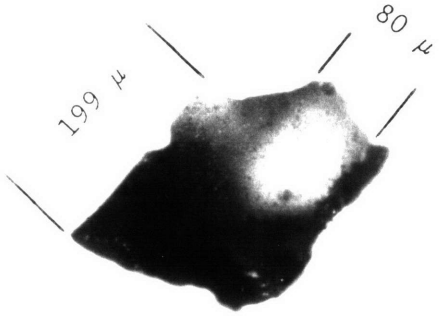

20%
Conversion

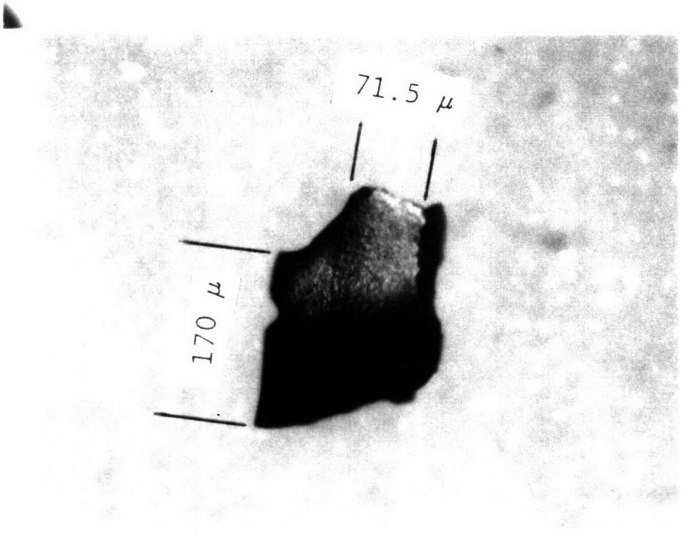

60%
Conversion

Sucrose carbon in .21 atm. O_2, 495 °C
Optical photographs

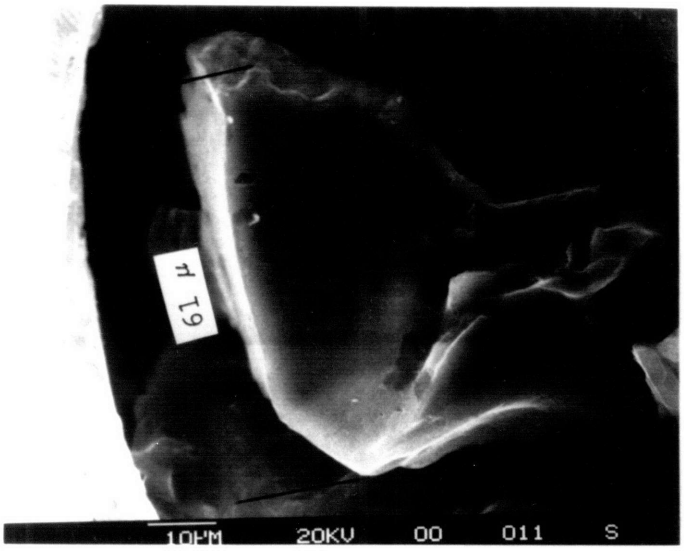

Unreacted

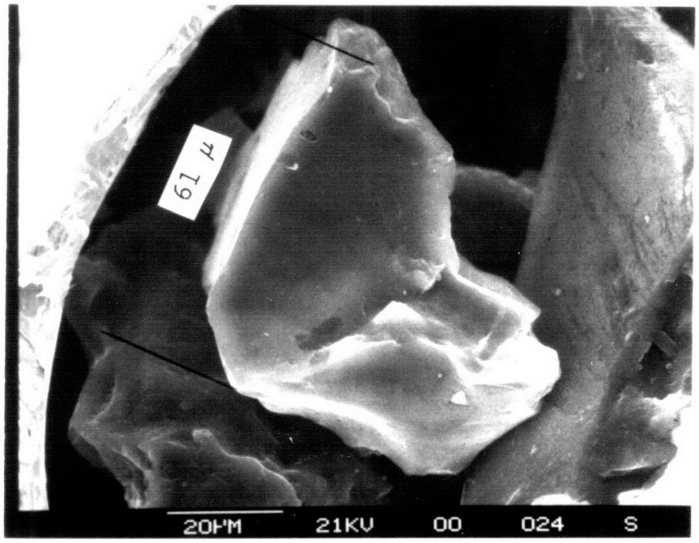

44%
Conversion

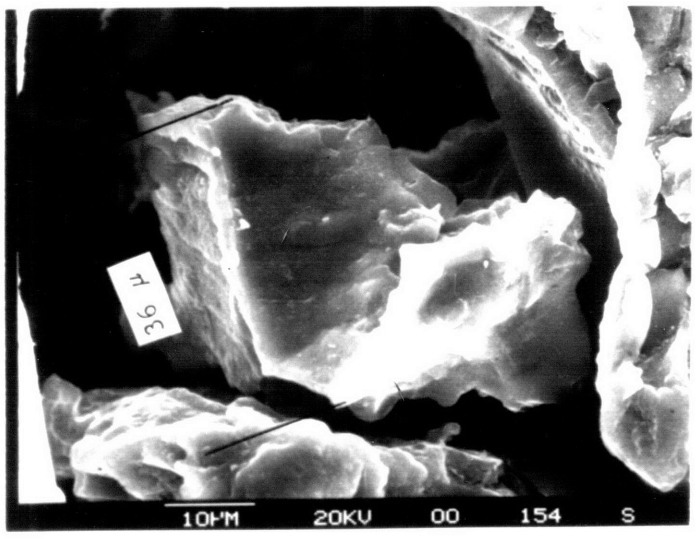

85%
Conversion

Montana
lignite
char

in air
370 °C

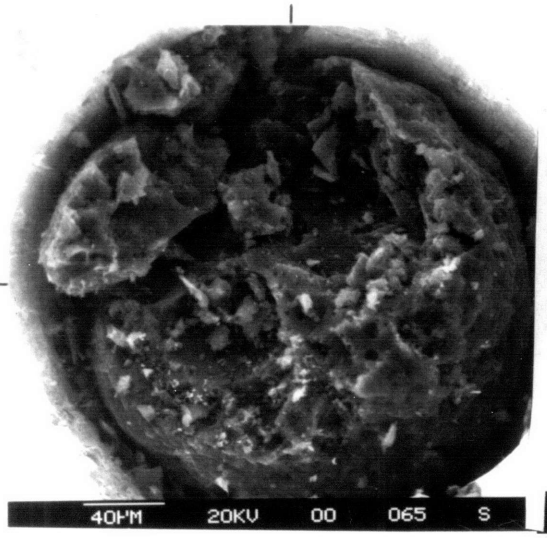

Unreacted

(diameter = 227 μ)

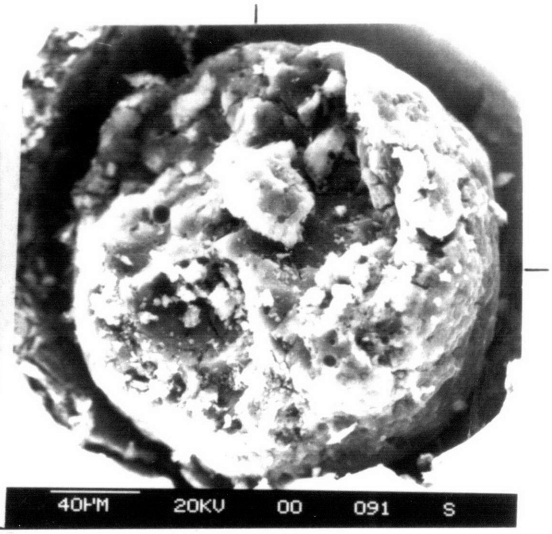

52% Conversion

(diameter = 199 μ)

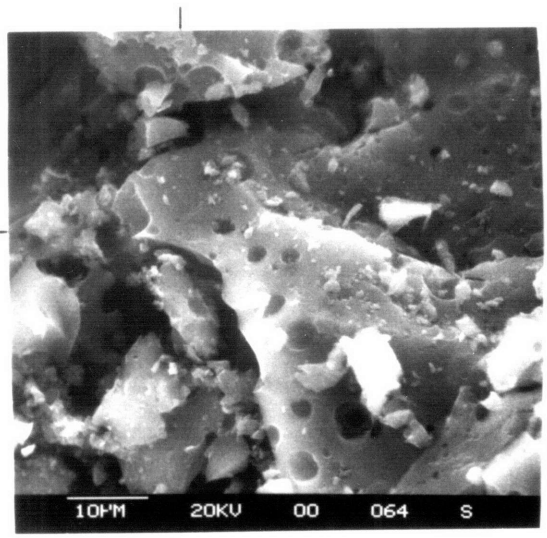

Unreacted

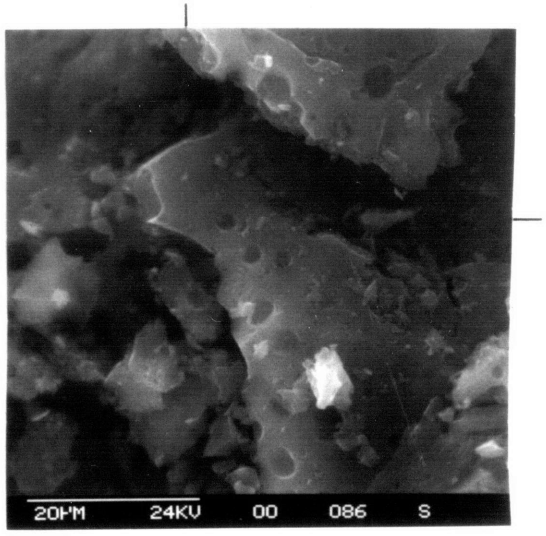

52% Conversion

Spherocarb in .21 atm. O_2, 495 °C
Set of micrographs at increasing magnification

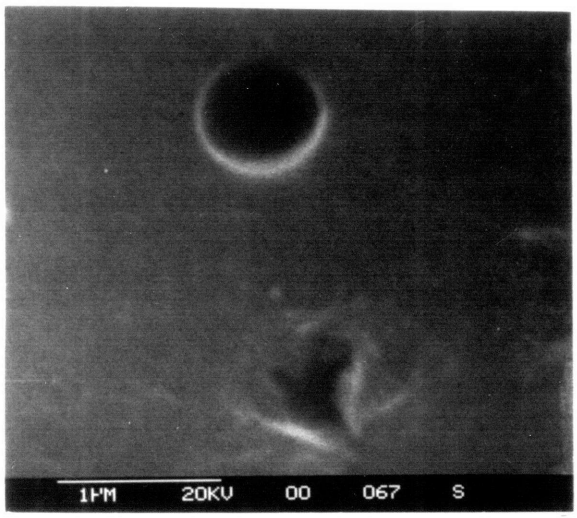

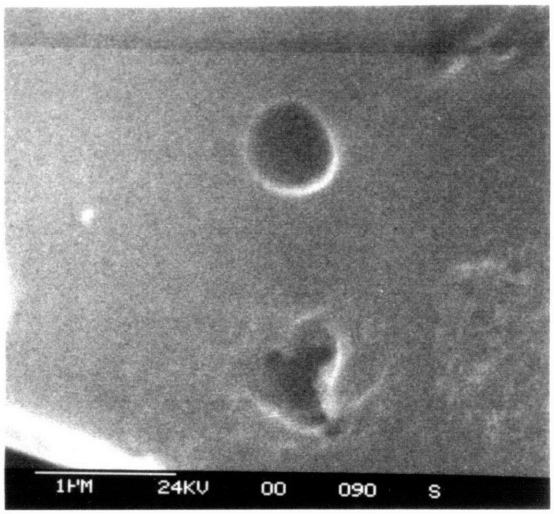

Unreacted

52% Conversion

(continued from previous page)

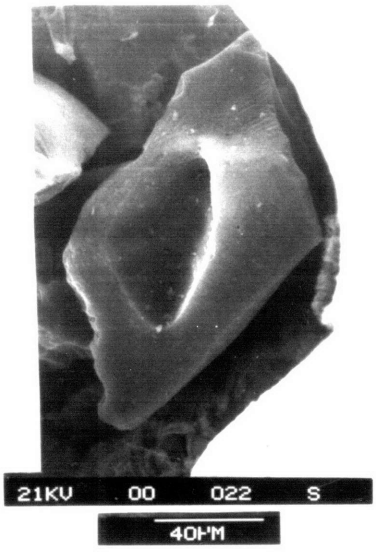

Unreacted

70% Conversion

approx. 95% Conversion

Ca-doped sucrose carbon
in .21 atm O_2, 370 ^{o}C

obvious from a casual examination of the photographs.) The photographs and S.E.M. micrographs in both figures 4.1 and 3.1 show the preservation of even the finest visible surface features during gasification. Examples of the measurement of the dimensions of surface features are shown on several of the photographs in figure 4.1.

Most of the carbons exhibited significant shrinkage, with Spherocarb carbon exhibiting the most pronounced shrinkage. Spherocarb heated in nitrogen at identical temperatures and for identical times did not show any diameter reduction. Char from a Montana lignite coal shrank very little if at all up to 44% conversion, but markedly at 85%. Calcium-doped sucrose char and char from Pittsburgh #8 bituminous coal did not shrink under the experimental conditions studied. It is possible that they shrink at higher conversions, based on the behavior of the Montana lignite char.

It is not clear for calcium-doped sucrose carbon at 95% whether true shrinkage has occurred, whether the particle is an intact ash residue, or whether some perimeter fragmentation has occurred (as there appear to be some shape changes). From the measurements in table 4.1 of diameter reduction for Spherocarb after 60% conversion at various temperatures in air and in carbon dioxide/carbon monoxide mixtures, it appears that the extent of Spherocarb shrinkage is dependent upon conversion alone, independent of reactant, reaction rate, or reaction temperature. The gasification rate of Spherocarb in a mixture of carbon dioxide and carbon monoxide was not a function of particle size, as was the case for the oxygen reaction, as discussed in Chapter 3.

No particles in this study were observed to undergo disinigration,

including particles of calcium-doped sucrose char up to 95% conversion, pure sucrose char up to 60% conversion, Montana lignite char up to 85% conversion, and Spherocarb up to over 90% conversion.

Figure 4.2 is a compilation of d/d_o vs. conversion measurements for Spherocarb carbon from table 4.1 and from Dudek's single particle electrodynamic balance technique(60). Diameter reduction becomes quite pronounced at high conversions, although always lying above the theoretical curve representing constant density gasification.

Measurements of the dimensions of various surface features of Spherocarb particles, which were, after 52% or 60% conversion, clearly identified as surface features originally photographed at 0%, were made from various photographs and S.E.M. micrographs. All surface features, both pores and solid regions, shrank, and in the same proportion as the particle diameter. These measurements are the basis of the results presented in figure 4.3, which is discussed in the next section.

Finally, table 4.2 contains several Spherocarb surface areas, calculated from carbon dioxide isotherms measured in a conventional volumetric adsorption apparatus, in order to provide validation for the single particle surface area measurement technique being developed by Dudek(60).

Table 4.2
Spherocarb surface areas
from isotherms measured in the volumetric adsorption apparatus

% Conversion	Surface Area (m^2/gm) from CO_2 isotherm at 273 ^oK
0%	636 m^2/gm
65%	450 m^2/gm

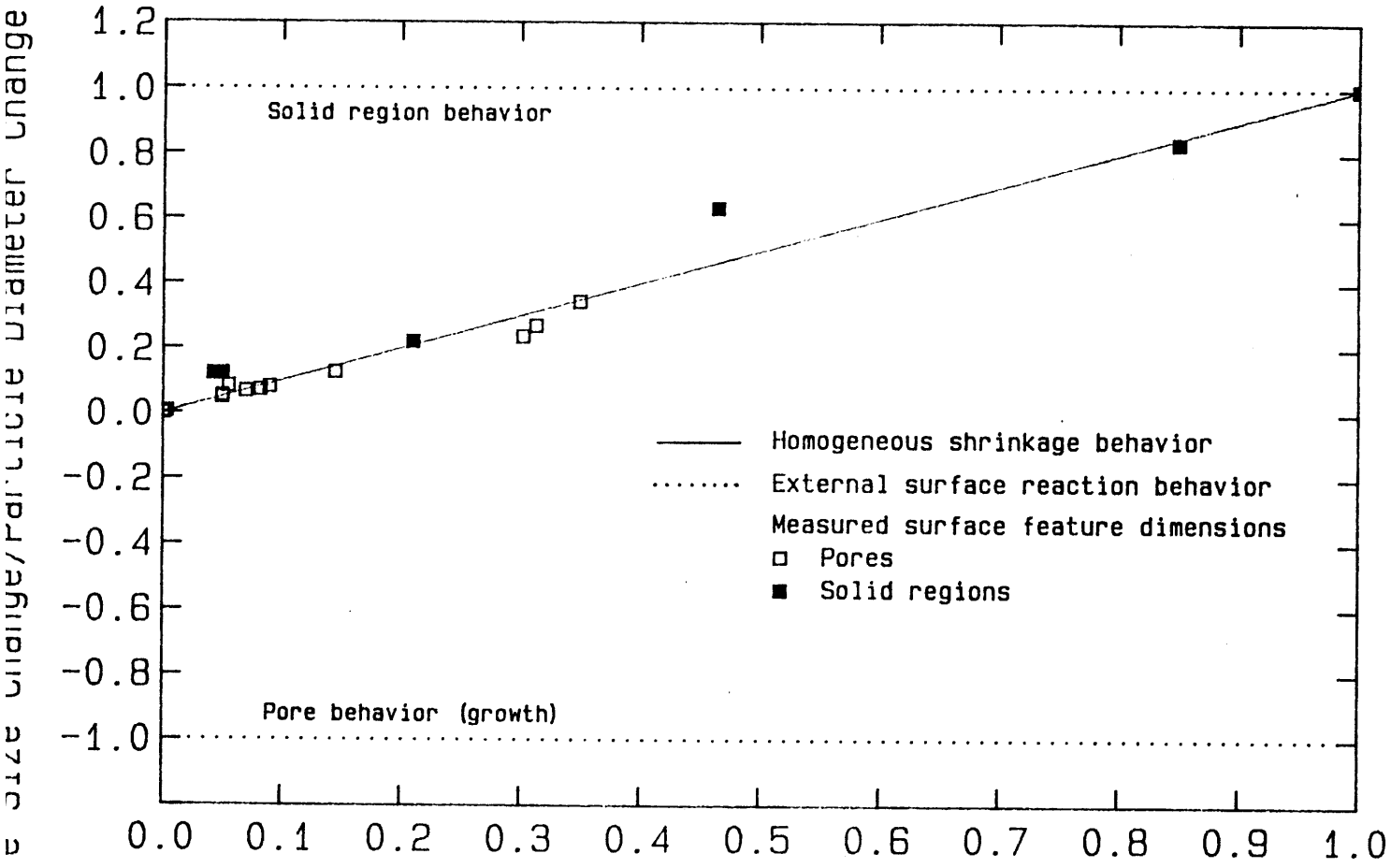

Figure 4.3

Shrinkage of Spherocarb Surface Features

4.2 Discussion

4.21 Homogeneous shrinkage

During the kinetically controlled gasification of high surface area carbons, an insignificant fraction of the gasification can be expected to occur on the external surface proper of the particle. This fact is illustrated for 200 μm diameter Spherocarb carbon particles by comparing the numerical values of the external, macropore (diameter > 200Å), and total surface areas:

External area, $4\pi R^2_{particle}$: .03 m^2/gm

Macropore area(88): 5 m^2/gm

Total carbon dioxide surface area: 636 m^2/gm

The ratio of the external surface area to the macropore area is 1:167 and to the total area is 1:21,200, indicating that the mass fraction of gasification occurring on the external surface would be insignificant if the reaction occurred within the micropores as well as if the reaction were confined to macropore surfaces. Alternatively, the area information can be used to estimate the extent of surface regression during conversion as discussed in chapter 3. The expected external surface recession at 100% conversion is .6 μm for an effective gasification area of 5 m^2/gm and 47 Å for an effective gasification area of 636 m^2/gm, in both cases insignificant in comparison to the 100 μm particle radius.

Spherocarb gasification rates presented in chapter 3 were not a function of particle size, which is a classical indication of complete reactant penetration and the absence of a significant reaction component on the particle's external surface. Further evidence that

Spherocarb gasification at temperatures below 600 ^{o}C in air is, in fact, kineticaly controlled, and even occurs fully within the micropores is presented and discussed at length in chaper 3. Indeed, the photographs and S.E.M. micrographs provide direct evidence that no significant gasification occurs on the external surface, but rather that surface features are preserved and undergo a homogeneous shrinkage during gasification.

The homogeneous shrinkage of topographic features is illustrated in figure 4.3, where measured surface feature dimensions are compared to the behavior expected during homogeneous shrinkage and to the behavior expected in the presence of a reaction component on the external surface proper. The theoretical curves for these two cases were derived as follows. Reaction on the external surface proper would cause a recession of the faces of all surface features by an amount that is equal to the recession of the external particle surface. Pores would then grow and solid regions would shrink, their dimensions changing by an amount $\pm \Delta d_s$ that is equal to the change in particle diameter Δd_p. $\Delta d_p = \pm \Delta d_s$ or $\Delta d_s/\Delta d_p = +1$ for solid regions or -1 for pores, which is the two branched curve plotted in figure 4.3. During homogeneous shrinkage both pores and solid regions would shrink, and to an extent that is proportional to their initial dimensions, or $\Delta d_s/d_s =$ constant $= \Delta d_p/d_p$. Rearranging, $\Delta d_s/\Delta d_p = d_s/d_p$ as plotted in figure 4.3. In fact, both pores and solid regions shrink, and to an extent that is proportional to the change in particle diameter, indicating homogeneous shrinkage.

4.22 Gasification-induced carbon densification

The observation of pronounced particle diameter reduction during gasification in the intrinsic kinetic regime, with preservation yet homogeneous shrinkage of topographical features, indicates the presence of a gasification-induced solid phase densification phenomenon. Note that the carbon particles densify with respect to those participating in a hypothetical reaction at constant diameter. Density is simultaneously increased by densification and decreased by gasification of carbon atoms, the net effect on density being a function of the specific relationship between diameter and conversion. Gasification of Spherocarb indeed produces a net density decrease, as the measured diameters always lie above those for the constant density (unreacted shrinking core) case indicated in figure 4.2.

It is believed that densification is the result of solid state rearrangements producing loss of pore volume in fine pores. At the length scale of the larger pores in a carbon particle, then, the optically homogeneous "microporous solid" appears to undergo a densification/shrinkage, the larger pores shrinking also, acting as holes in a homogeneously shrinking matrix.

In order to understand the nature of the gasification-induced atomic rearrangements responsible for densification, we need to consider again the model of the so-called "ultrafine structure" of carbons presented in figure 1.1(21). The lines in the diagram are small, graphitic layers, viewed from the side, whose imperfect packing arrangement is responsible for carbon micropores. The circles in the diagram are not part of the structure, but rather indicate regions

which would be identified as crystalline by X-ray diffraction. (Note that the crystallite size determined by X-ray diffraction is smaller than the true dimension of the continuous but kinked graphitic layers.) Not shown in the diagram are cross linkages between layers and some amorphous material, possibly heteroatoms or tetrahedral carbon(16). Since the thermodynamically preferred form of carbon is crystalline graphite, which is non-microporous, it is only energy barriers associated with solid state rearrangements that trap the imperfect layer-packing and the resulting microporosity.

The ability of a carbon to form graphite is a property of only some carbons and is recognized to be a function of the extent of cross linking and the initial degree of layer orientation in the low temperature char or pitch(16). One researcher's representation of glassy carbon structure is shown in figure 4.4(93). In this carbon the depicted layer entanglements hinder solid-state rearrangement and are responsible for this carbon's resistance to graphitization and crystallite growth during annealing.

Graphitization is a complex process comprising many elementary steps having a distribution of activation energies(94,95). Low energy rearrangement processes resulting in surface area loss occur at temperatures as low as 1000 ^{o}C(90) and can be thought of as the initial stage of graphitization. The final stage of graphitization, which may involve diffusion of crystalline defects, occurs above 2000 ^{o}C with an activation energy of approximately 250 kcal.mol(96).

The solid state rearrangements accompanying gasification of Spherocarb and other carbons in this study are reaction induced and

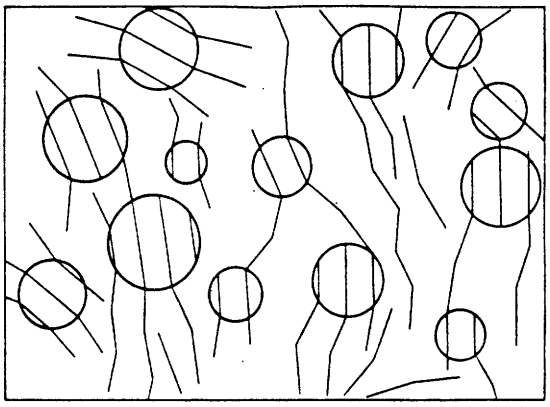

Figure 1.1
Structure of Low-Temperature Carbons(21)

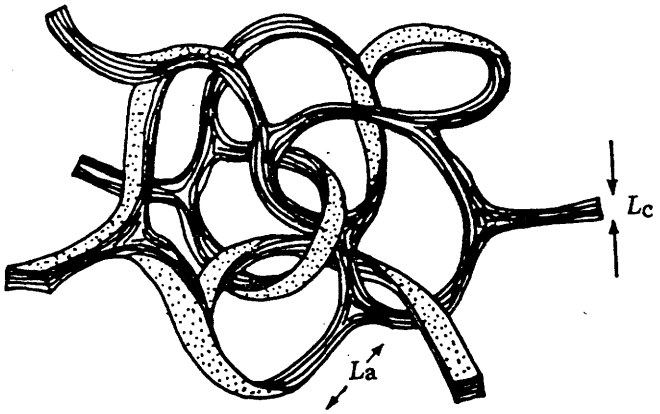

Figure 4.4
The Jenkins Model of Glassy Carbon Structure(93)

occur at temperatures at least as low as 450 °C. It is believed that the gasification reaction, by breaking bonds, removing cross links,and removing carbon atoms, "loosens" entanglements, and increases the driving force for, and facilitates densification via rearrangements analogous to those occurring spontaneously at somewhat higher temperatures in the initial stages of graphitization. Diameter reduction with the preservation of surface features has been observed and briefly discussed previously by Johnson in a study of the hydrogen gasification of coal char(46), and there, also, attributed to a reorientation of crystallites.

Amorphous solid densification is also seen in germanium and glasses(97), and it is especially noteworthy that Kaae(98) has observed densification during neutron irradiation of a glassy carbon at 1100 °C, under conditions where no densification occurred during heating in the absence of the neutron beam. Neutron bombardment is thought to facilitate densification by initially displacing carbon atoms from their equilibrium lattice positions.

The extent of shrinkage/densification appears to be a strong function of carbon type. At present there is an inadequate understanding of the factors that determine the propensity of a given carbon under given reaction conditions to undergo gasification-induced shrinkage. We believe, however, that one prerequisite for shrinkage is that gasification occur well within the ultrafine carbon structure, where it can exert an influence on the layer packing and hence the microporosity. We therefore anticipate little or no shrinkage for low surface area carbons or for those carbons which gasify via production

of relatively large channels or pits, a characteristic of some catalyzed systems.

4.23 Densification kinetics.

As the solid state rearrangements responsible for densification are expected to be activated, it was interesting to see if global kinetic parameters for densification could be measured. From table 4.1 it appears that the extent of Spherocarb shrinkage is a function of conversion only, independent of reactant, reaction temperature, or reaction rate. If one considers the process of gasification with concurrent shrinkage to consist of the two steps: (1) gasification at constant diameter, and (2) shrinkage at constant mass, it can be said that the kinetics of the second step were fast (not limiting) during these experiments and that the particle reached a pseudo-equilibrium size in a time << the characteristic reaction time. Having only the oxygen data would leave open the possibility that shrinkage rates <u>were</u> slow enough to measure, but had an activation energy comparable to that of the gasification reaction itself. This could result in the observed, apparent independence of extent of shrinkage on reaction conditions. The measurement of shrinkage during carbon dioxide gasification is particularly valuable, providing both a high temperature and a long reaction time, (i.e. destroying the unwanted correlation between the independent variables reaction temperature and reaction time). It is hoped that continuing experiments under the parallel study by Dudek(60) will provide more information on densification kinetics.

4.24 Implications

The phenomenon of gasification-induced carbon densification makes measurements of particle size or density unreliable tests for determining the fraction of the gasification occurring on the external surface of the particle. In addition, by reducing internal porosity during gasification, the phenomenon should be an important factor determining the fragmentation behavior of carbon particles, which is a topic of much current interest in gasification research.

Kerstein et al. have observed abrupt particle disintegration for a variety of carbons and graphites at a critical porosity which is reproducible for a given carbon, but is a complex function of material properties(99). One carbon in the Kerstein study did not disintegrate, while the critical porosity for disintigration varied from .5 to .85 among the others. Spherocarb has an initial porosity of .675, and, in this study, did not disintegrate at conversions at least up to 80%, at which point the porosity had increased to .85. The porosity developed at 80% conversion during a hypothetical reaction at constant diameter would be .935, which may be above the critical porosity for this carbon. If so, gasification-induced densification is preventing fragmentation of Spherocarb under our experimental conditions. Gasification-induced densification, in the general case, can be expected to postpone, to higher conversions, the occurrence of fragmentation.

Finally, shrinkage is important in pore structure evolution and surface area evolution during gasification or activation and should affect gasification rates and activated carbon adsorptive properties.

The reduction of surface area and reactivity would be most pronounced at high conversion, potentially contributing to the difficulty in achieving high carbon conversions in some gasification processes. This topic is explored at length in the following section.

4.3 Modeling of Gasification with Concurrent Shrinkage

Since carbon particle shrinkage during gasification is the direct result of loss of volume in small pores, shrinkage will certainly reduce porosity development during conversion and is expected to also reduce surface area, keeping in mind that almost all of the internal surface of high area carbon resides in small pores.

Presented in figure 4.5 is the prediction of Spherocarb surface area evolution from the random pore model devised by Gavalas(56), along with measured surface areas calculated from carbon dioxide adsorption isotherms measured gravimetrically in Dudek's single particle electrodynamic balance. (A description of the single particle surface area technique can be found elsewhere(60). Note that the surface areas calculated from isotherms measured in a conventional volumetric apparatus and presented in table 4.2 show the same trend as those in figure 4.5) The discrepency between the model and the data is striking, as the measured areas decrease when normalized by the mass of carbon remaining, whereas the Gavalas random pore model, which does not consider reaction induced shrinkage, predicts monotonically increasing areas per remaining mass. In fact, both the Gavalas and the Simons random pore models predict monotonically increasing areas per

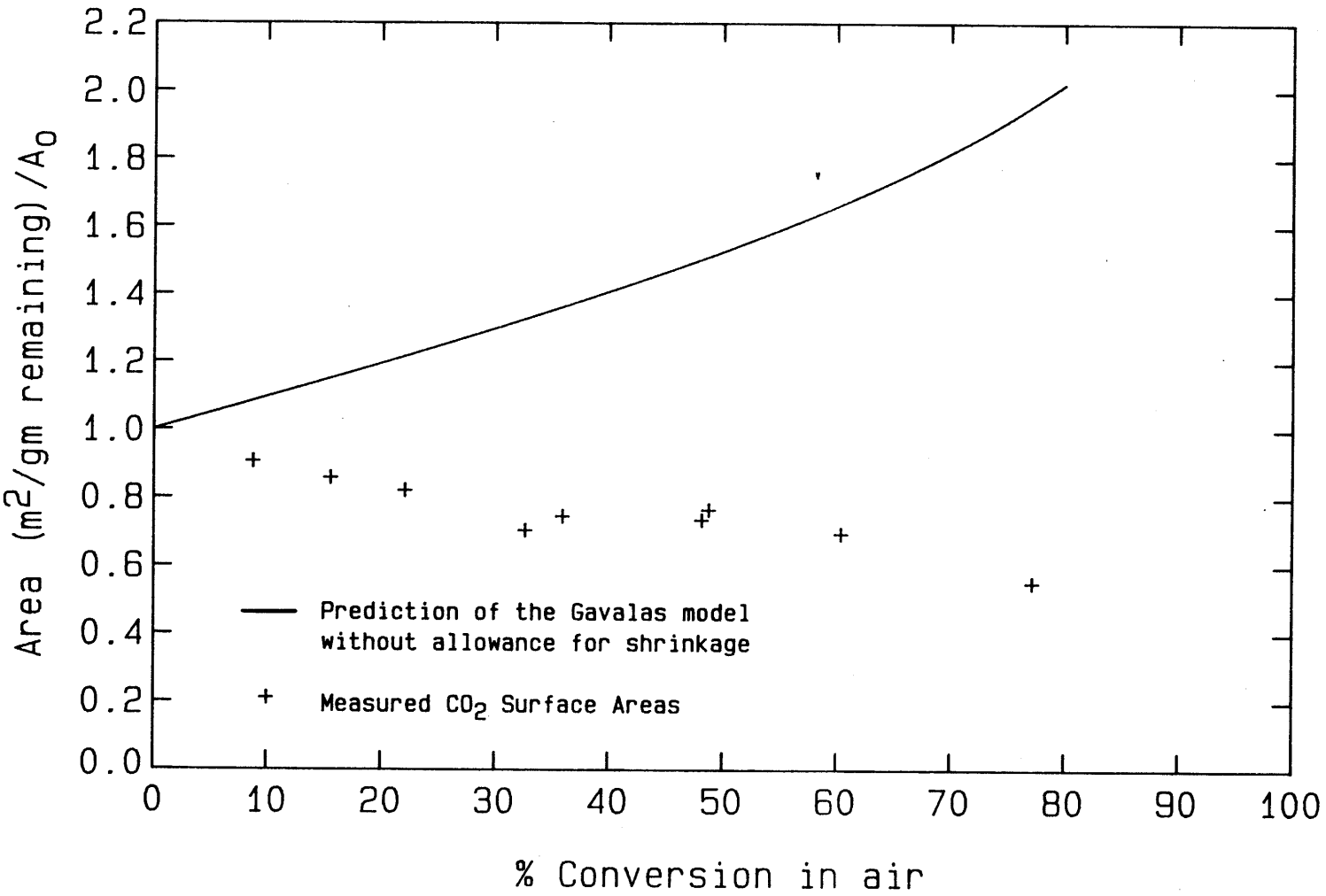

Figure 4.5 Spherocarb Surface Area Evolution

remaining mass for the kinetically limited gasification of all carbons (i.e. regardless of the initial pore structure of the carbon).

4.31 The Gavalas random pore model

Gavalas(56) has derived an exact analytical solution with no empirical parameters for the evolution of the pore size distribution and total surface area during carbon gasification for an arbitrary initial pore size distribution, assuming randomly distributed, infinite cylindrical pores, with no initial closed porosity. The model is based upon a probability-density function for pore axes, which contains all of the information about the pore structure, and is obtainable from measured pore volume distributions. The solution for the surface area (or reaction rate) per gram of remaining carbon, divided by the initial area, is

$$A/A_o = \{1 + [B_o/(2\pi B_1^2)]\ln(1/(1-X_c))\}^{\frac{1}{2}} \qquad (4\text{-}1)$$

where B_o and B_1 are the zeroth and first moments of the pore-axis probability density function. Because of the form of this expression, surface area per gram of remaining carbon always increases monotonically with conversion.

The model has, in the past, been successfully related to measured rate vs. conversion curves, assuming that the concentration of active sites is constant throughout conversion, and using the zeroth and first moments of the initial pore-axis probability density function as adjustable parameters(56). We undertook here to compare measured surface areas for Spherocarb with the exact Gavalas solution requiring as input the complete measured pore size distribution, available to us courtesy of Niksa(88).

The model was originally applied by Gavalas(56) to the case in which slow microporous diffusion causes the reaction to take place only on or near the surfaces of large pores. The reaction rate in that study was related to the amount of large-pore surface, treating the micropores as surface roughness, assuming that they contribute to the reaction an amount that is proportional to the large pore surface area. The model treated, then, the widening and coalescence of larger pores existing in a uniform microporous solid. Based on the conclusions reached in Chapter 3, the Gavalas model was applied to the Spherocarb-oxygen reaction assuming strict kinetic control with gasification occurring in all pores. The model here, then, treats the widening and coalescence of pores of all sizes, existing in a non-porous solid carbon matrix. The Gavalas formulation may be validly applied to either case.

The complete pore size distribution for Spherocarb carbon was compiled from mercury porosimetry and nitrogen adsorption data available to us courtesy of Niksa(88), and the total surface area for Shperocarb derived from carbon dioxide adsorption isotherms measured by Dudek(60). Details are given in appendix B. This measured pore size distribution was converted to the Gavalas pore axis probability density fuction by numerical integration of the following equation from Gavalas(56).

$$\lambda(R) = (1/2\pi R^2)[O(R)/\{1 - \int O(R')dR'\}] \qquad (4\text{-}2)$$

B_o and B_1 were obtained from $\lambda(R)$ for the unreacted carbon as

$$B_o = \int \lambda(R)dR \qquad (4\text{-}3)$$

$$B_1 = \int R\lambda(R)dR \qquad (4\text{-}4)$$

from which the exact Gavalas solution, as it appears in figure 4.5, was generated, according to equation 4-1. For Spherocarb carbon, Gavalas' B_o was found to be 425000 μm^{-2} and B_1 188 μm^{-1}.

4.32 Modeling approach

Surface area development during gasification with concurrent shrinkage can be treated as the sum of two terms as follows:

$$dA/dX = (\delta A/\delta X)_d + (\delta A/\delta d)_x(dd/dX) \qquad (4\text{-}5)$$

The first term on the right-hand side represents the evolution of surface area during gasification at constant diameter and is dealt with by existing models. The second term contains the change in diameter with respect to conversion, which can be obtained directly from measurements, and the change in area with respect to diameter at constant mass, which is the subject of the development in the next section.

The shrinkage at constant mass development will then be incorporated with reaction into a simple, approximate model of gasification with concurrent densification. An exact numerical treatment of gasification with concurrent densification is discussed in a later section.* The simple approximate model will be developed here first, as it is useful for investigating the importance of model

---

*No attempt was made to model or interpret the change in measured gasification rates with conversion in figure 4.5. There is evidence that these gravimetrically measured rates differ from the rate of carbon weight loss, due to simultaneous weight increases associated with transient oxygen chemisorption(33).

parameters, for easy extension to other carbons, and as an illustration of the general concepts.

4.33 Shrinkage at constant mass*

The total porosity is a unique function of the initial porosity and λ, the ratio of the particle diameter after shrinkage to the diameter before, provided that the true solid density is constant, which is assumed throughout. This relationship is shown in figure 4.6 and comes directly from a volume balance within the particle as follows:

$$V_t = V_p + V_c \tag{4-6}$$

$$V_t/V_{to} = \lambda^3 \tag{4-7}$$

$$V_p/V_{po} = (\lambda^3 V_{to} - V_c)/(V_{to} - V_c) = ((\lambda^3 - 1)/\theta_o) + 1 \tag{4-8}$$

$$\theta/\theta_o = (V_p/V_t)/(V_{po}/V_{to}) = (\lambda^3 - 1)/\lambda^3\theta_o + 1/\lambda^3 \tag{4-9}$$

where V_p is the pore volume, V_c is the carbon volume, and V_t is the total volume per particle. λ is the diameter ratio before and after shrinkage, θ is the porosity, and a subscript o indicates the value before shrinkage.

We now postulate that there are two distinct classes of pores, smaller pores in which the solid state rearrangements occur and larger pores which shrink homogeneously as holes in a shrinking microporous solid. The characteristic of homogeneous shrinkage is that the ratio of large pore diameters after shrinkage to those before is also λ. Therefore $V_l = \lambda^3 V_{lo}$, where V_{lo} and V_l are the large-pore volumes per

---

* Additional information regarding the development appears in Appendix B.

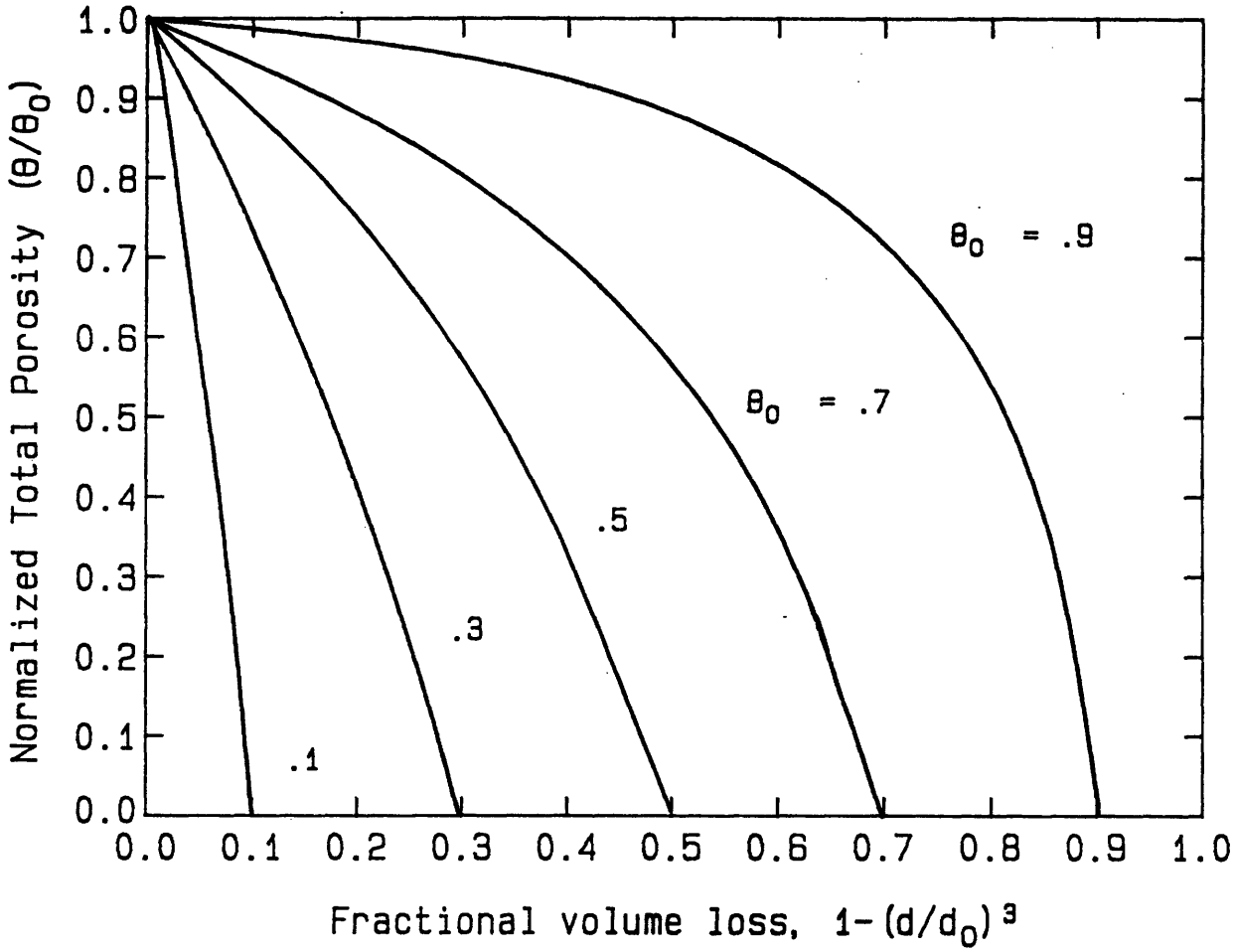

Figure 4.6

Shrinkage at Constant Mass

particle before and after shrinkage. The large-pore porosity θ_l, defined as the volume in large pores divided by the particle volume, is then constant during shrinkage at constant mass.

If the large-pore porosity is constant, and the total porosity changes according to figure 4.6, the small pore porosity can be obtained by difference, as shown below. A volume balance yields

$$V_s + V_l + V_c = \lambda^3(V_{so} + V_{lo} + V_c) \tag{4-10}$$

$$V_l = \lambda^3 V_{lo} \tag{4-11}$$

from which it can be shown that

$$V_s/V_{so} = \lambda^3 + (1-\theta_o)(\lambda^3 - 1)/\theta_{so} \tag{4-12}$$

or $$V_s/V_{so} = \lambda^3 + K(\lambda^3 - 1) \tag{4-13}$$

or $$\theta_s/\theta_{so} = 1 + K(1 - 1/\lambda^3) \tag{4-14}$$

where $K = (1-\theta_o)/\theta_{so}$

The small-pore porosity is plotted in figure 4.7 as a function of the parameter K, which is determined by the initial pore structure, and is a function of the radius chosen as the cutoff between the large and small pore classes.

An approximate expression for the effect of shrinkage on area can be derived by assuming

- cylindrical pores
- a monodisperse small pore size distribution
- that all the internal surface area resides in the small pores

We need, in addition, a physical model of the rearrangement events in small pores. Consider a single rearrangement event involving the motion of graphitic layers toward each other to produce a loss of

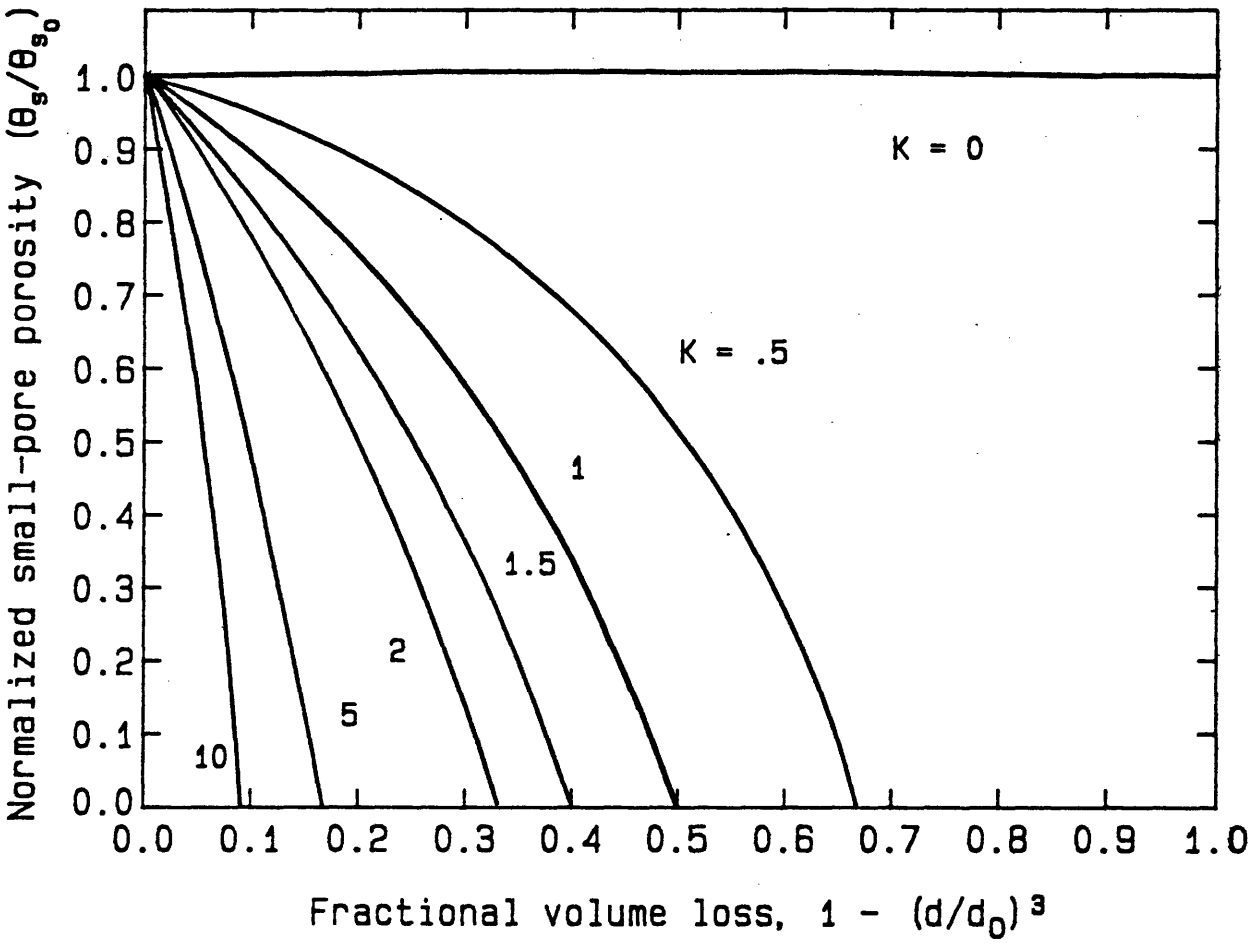

Figure 4.7 Shrinkage at Constant Mass

small-pore volume. If the layers come together completely, the event is a pore elimination, if the packing remains imperfect, the event can be considered a pore narrowing. Many such individual events comprise the overall densification process, whose effect on surface area can be modeled, we believe, by considering two limiting cases: pure pore elimination, and pure pore narrowing. For each case we need a relationship between the area loss in small pores and the known volume loss in small pores. For uniform pore narrowing:

$$V_{so} = N_{so}\pi R_{so}^2 L_{so} \qquad (4\text{-}15)$$

$$V_s = N_{so}\pi R_s^2 L_{so} \qquad (4\text{-}16)$$

$$V_s/V_{so} = R_s^2/R_{so}^2 \qquad (4\text{-}17)$$

It can then be shown that

$$A_s/A_{so} = A/A_o = R_s/_{so} = (V_s/V_{so})^{\frac{1}{2}} \qquad (4\text{-}18)$$

where V_s/V_{so} can be obtained from equation 4-13.

Similarly, it can be shown for pore elimination that $A/A_o = V_s/V_{so}$. These relationships are shown in figures 4.8 and 4.9.

4.34 Reaction and shrinkage of Spherocarb: simple model

In this section we to use the general results of the previous section to develop a simple model of gasification with concurrent shrinkage for Spherocarb. An input to the modeling is the observed extent of shrinkage as a function of conversion, for which the parameters of the empirical regression shown on figure 4.2 were used. (The fitting function is the least-squares second order polynomial constrained to pass through the point (0,1), of the form $(d/d_o)^3 = 1 + aX + bX^2$, where a= -.47575 and b= -.30314). The porosity evolution can

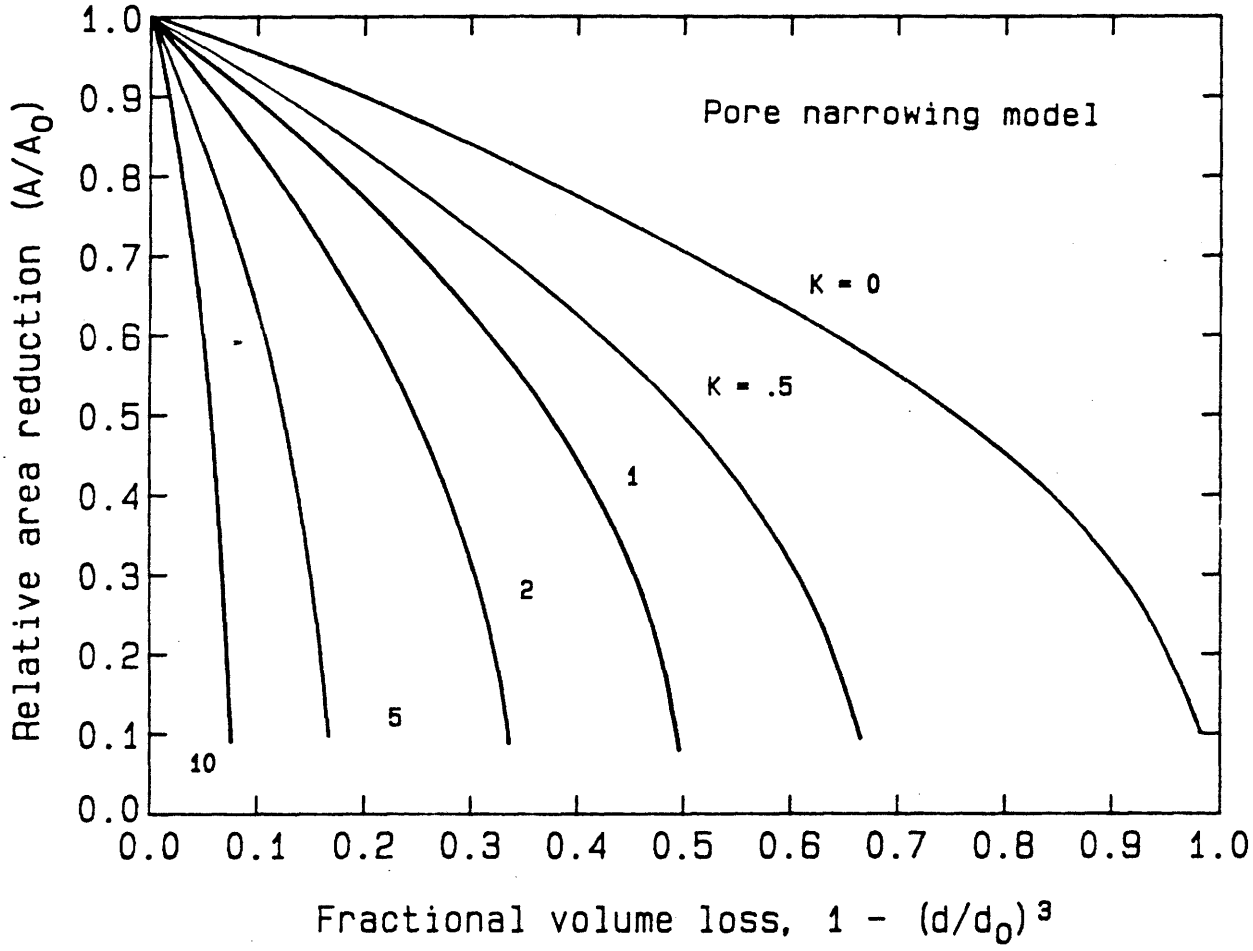

Figure 4.8 Shrinkage at Constant Mass

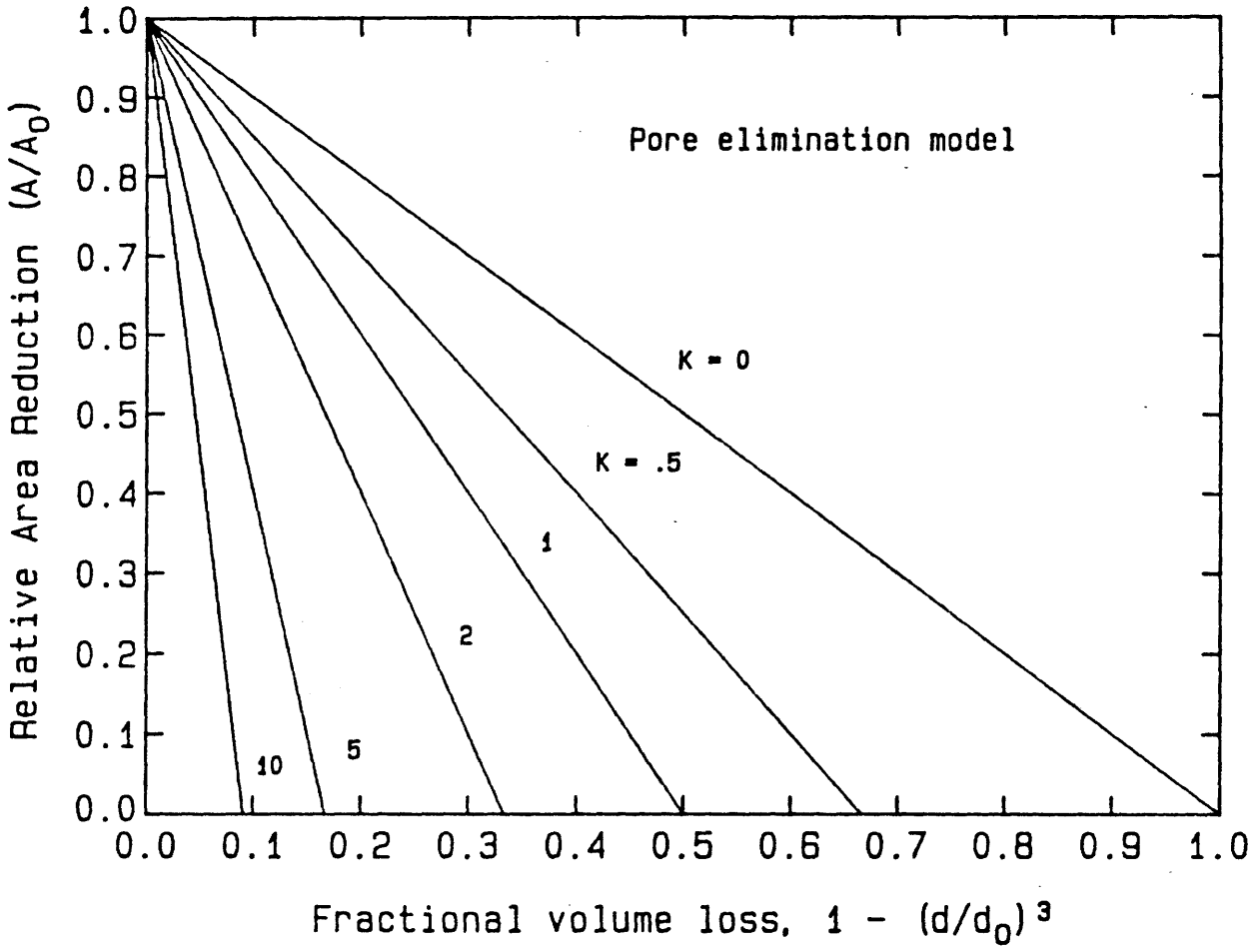

Figure 4.9 Shrinkage at Constant Mass

be calculated by assuming that all the gasification occurs in the small pores and that pores retain their initial membership in the small or large pore class during conversion (i.e. no pore graduation). The convenient assumption of no pore graduation is an arbitrary one, but does not introduce serious error because the extent of surface recession and thus the extent of pore growth is, according to the Gavalas model, only about 8 Å throughout conversion.

The change in pore volume is the sum of the increase in pore volume due to gasification $V_{co}X$, where V_{co} is the initial volume of carbon per particle, and the decrease in pore volume due to shrinkage $(1 - \lambda^3)V_{to}$, where V_{to} is the total volume, and o denotes the value for the unreacted particle. It follows that

$$\theta = V_p/V_t = [V_{po} + V_{co}X - (V_{to} - \lambda^3 V_{to})]/\lambda^3 V_{to} \qquad (4\text{-}19)$$

from which it can be shown that

$$\theta/\theta_o = (1/\theta_o\lambda^3)[\theta_o + (1 - \theta_o)X + \lambda^3 - 1] \qquad (4\text{-}20)$$

The large pore porosity is unchanged during conversion, and the behavior of the small pore porosity is obtained by difference, and can be shown to be

$$\theta_s/\theta_{so} = (1/\theta_{so}\lambda^3)[\theta_o + (1 - \theta_o)X + \lambda^3 - 1] - (\theta_o/\theta_{so}) + 1 \qquad (4\text{-}21)$$

The results are presented in Figure 4.10.

An solution for Spherocarb surface area evolution during gasification with concurrent shrinkage can be generated by modeling the pore structure at a given conversion as the result of reaction to that conversion at constant diameter followed by shrinkage at constant mass. The Gavalas model provides the intermediate result after the reaction step and the shrinkage at constant mass formulation provides the adjustment factor. This is an approximation which is tantamount to

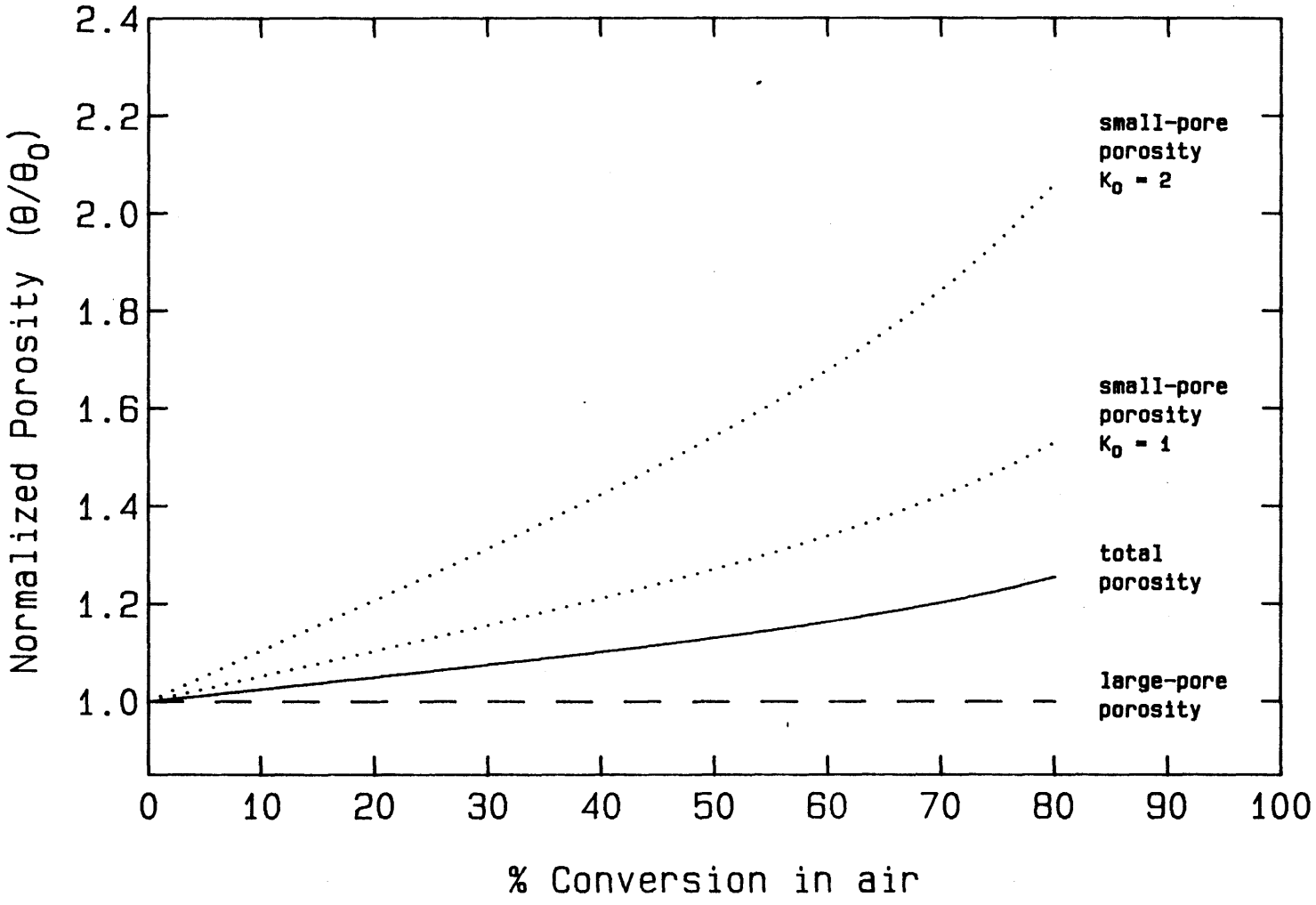

Figure 4.10 Spherocarb Pore Structure Development

a one step integration of the coupled equations governing reaction and shrinkage. The result is given in Figure 4.11.

The parameter K_o has a rather weak influence on the predicted area development*, whereas the chosen model of the rearrangement process is quite important. In all cases, however, the shrinkage term has an important influence on the predicted area development. For K_o =2 and pure pore elimination the effect of the observed shrinkage on surface area evolution can adequately account for the large discrepancy between the measured areas and the Gavalas prediction.

4.35 Exact numerical treatment of gasification with densification**

The approach is to treat both reaction and shrinkage by altering the pore-axis P.D.F. itself throughout conversion and to use relations derived by Gavalas to compute the porosity and total surface area from the altered P.D.F. at any point. This approach gives the modeler the flexibility to change the pore structure in any conceivable way (such as according to the rules of homogeneous shrinkage at constant mass!) and to rigorously calculate the effect of the changes on surface area evolution.

The logic of the numerical solution scheme is represented in a

---

* K_o = 1 and 2 are <u>strict</u> lower and upper bounds on K_o for Spherocarb, arising from strict lower and upper bounds on the cutoff radius separating the small and large pore classes. The large pore class must include pores of diameters > 100nm, which were microscopically observed to remain intact during conversion and thus not to have participated in rearrangements. The other bound corresponds to the small pore class consisting of only the smallest pores in the carbon, which are not further subclassified by standard pore characterization techniques.

** Additional information in Appendix B.

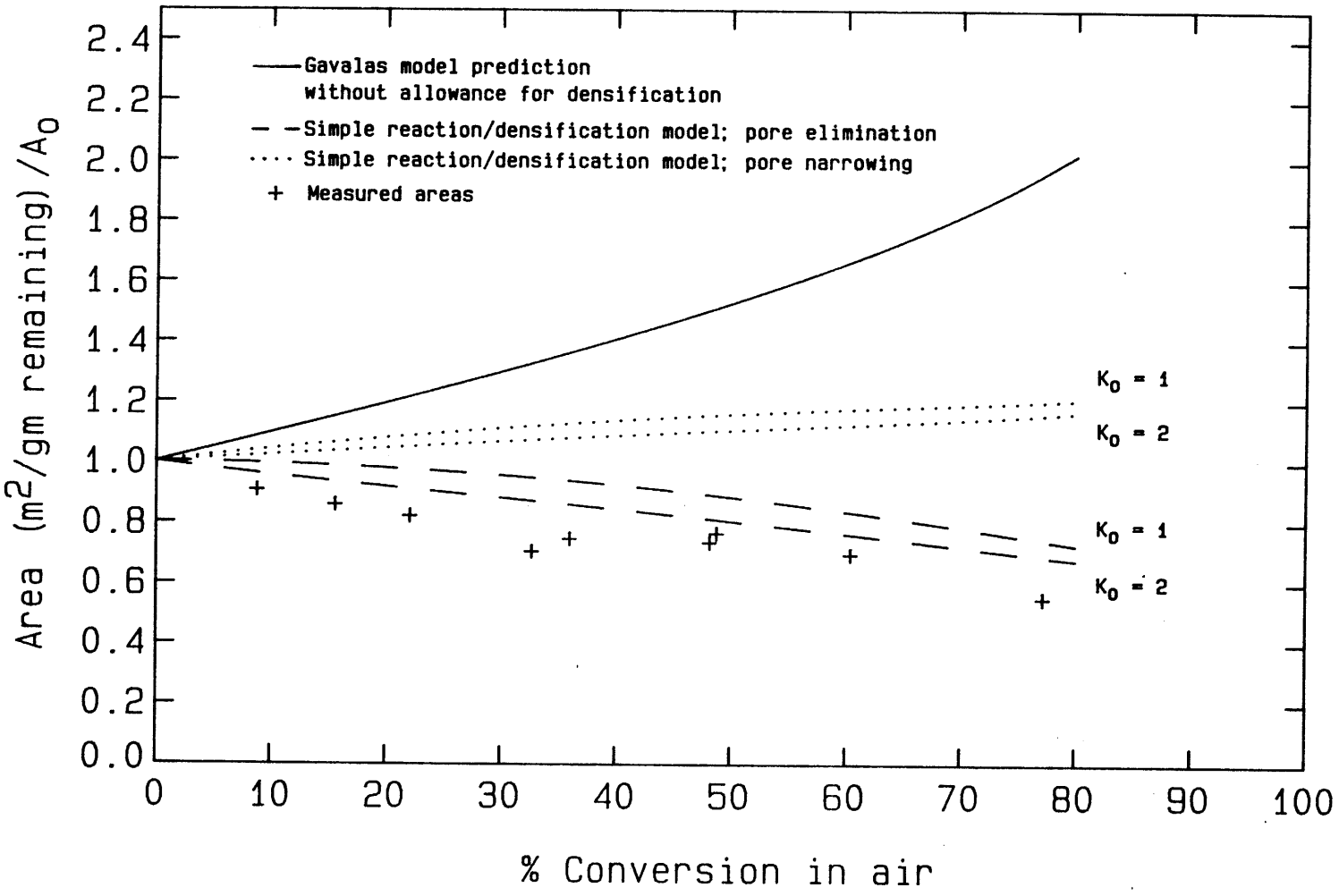

Figure 4.11 Spherocarb Surface Area Evolution

flowchart, figure 4.12. The initial pore size distribution for Spherocarb has already been converted to the Gavalas form, having been needed for the generation of the Gavalas solution without allowance for shrinkage. Gasification is achieved by increasing the radius of all pores by an increment q at constant pore-axis probability density. A new θ is calculated from the Gavalas expression

$$\theta_t = 1 - \exp[-2\pi\int R^2\lambda(R)dR] \qquad (4\text{-}22)$$

and, from it, the new, incrementally larger value of conversion, calculated from:

$$\Delta X = (R_p/R_{po})^3(\Delta\theta/(1 - \theta_o)) \qquad (4\text{-}23)$$

Shrinkage at constant mass is then accomplished by reducing the radius of large pores by the factor $d\lambda$, where $d\lambda = d_{pi+1}/d_{pi}$ and represents the shrinkage occuring during one conversion interval, and increasing the pore axis probability density for large pores by the factor $(d\lambda)^2$. In addition, to accomplish pore elimination, the pore axis probability density for small pores is reduced by a factor chosen to make the final porosity match the porosity required by the observed extent of shrinkage, which is given by

$$\theta_{i+1} = [(d\lambda)^3 - 1]/(d\lambda)^3 + \theta_i/(d\lambda)^3 \qquad (4\text{-}24)$$

which is equivalent to equation 4-9. This last step involves iteration. Finally, the Gavalas formulation is used to compute the surface area from the new P.D.F. according to

$$A\ (m^2/m^3) = 4\pi(1 - \theta)\int R\lambda(R)dR \qquad (4\text{-}25)$$

or $$A\ (m^2/gm) = [1/\rho_{He}(1 - \theta)]4\pi(1 - \theta)\int R\lambda(R)dR \qquad (4\text{-}26)$$

and the new P.D.F. becomes the input for a new reaction step at constant diameter. This procedure constitutes a numerical solution of

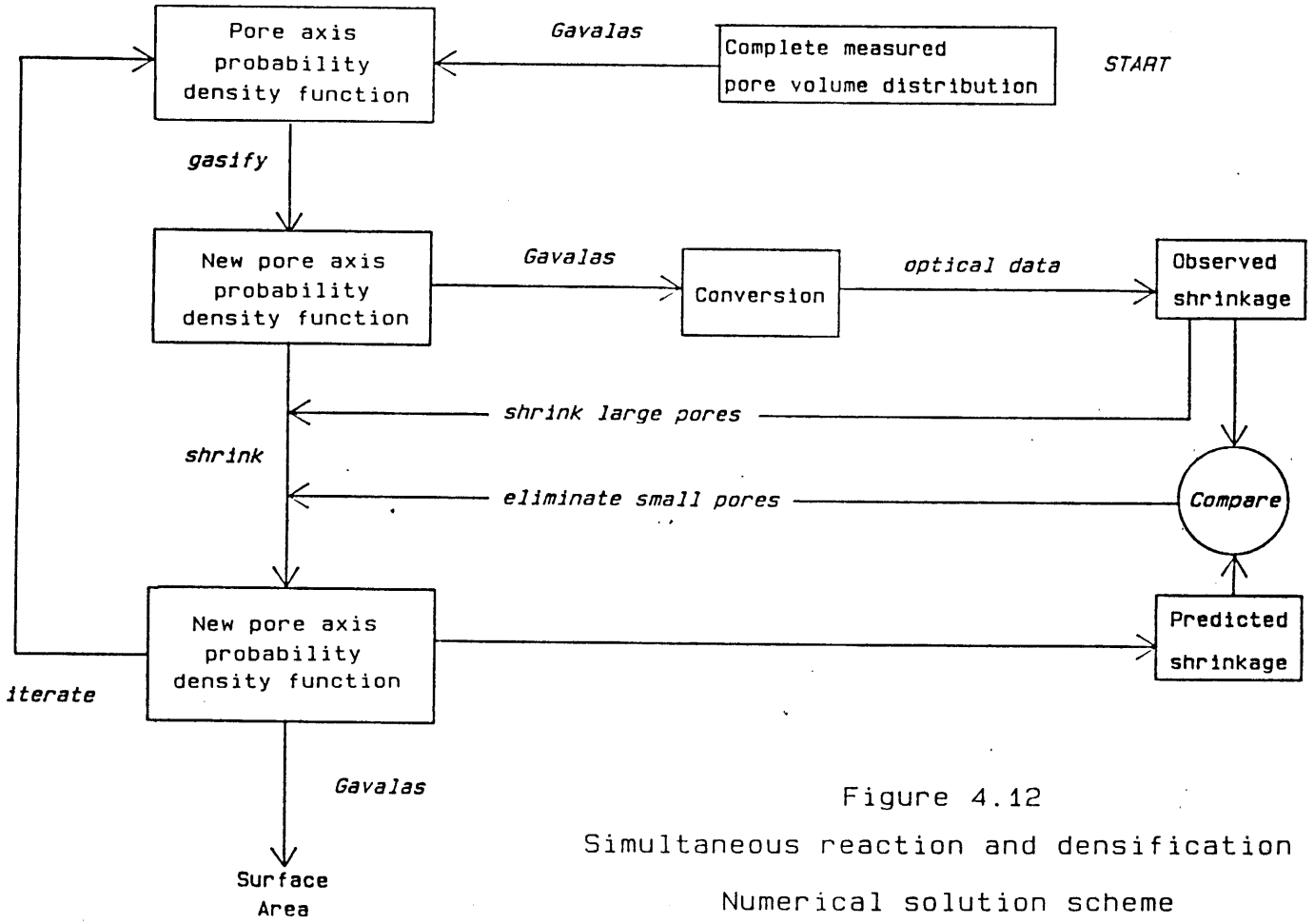

Figure 4.12

Simultaneous reaction and densification

Numerical solution scheme

the 2 coupled integro-differential equations describing gasification with concurrent shrinkage (via pore elimination with a given K_o), the only assumption being that the two pore classes are distinct. The numerical solutions were generated using Lotus 1-2-3 worksheet macros. A typical 40 step numerical solution required about two hours of processing time on an I.B.M. Personal Computer AT with an 8087 math coprocessor.

The effect of step size on the numerical results is illustrated in figure 4.13. Since the differences between the curves generated using 10 steps and 40 steps have become small, the remainder of the numerical solutions were generated using 40 steps. In figure 4.14 the results are presented of several solutions for pure pore elimination and various K_o values. Again K_o, within the range of possibility for Spherocarb, is not a very important parameter. The numerical predictions are significantly different from those of the simple, analytical model, primarily, it is believed, due to the distribution of small pore sizes and the provision for gasification in larger pores in the numerical treatment. The numerical solution for $K_o = 2$ and pure pore elimination, shown in figure 4.14, is the best obtainable fit to the experimental curve. The numerical solutions based on elements of the Gavalas formulation are the best representation of the physics of gasification with concurrent shrinkage, but cannot yet fully account for the discrepency between the data and the constant volume pore models. Other phenomena may also be contributing to the deviation of surface area evolution from the Gavalas model prediction, such as heterogeneity in carbon reactivity, gasification by pore

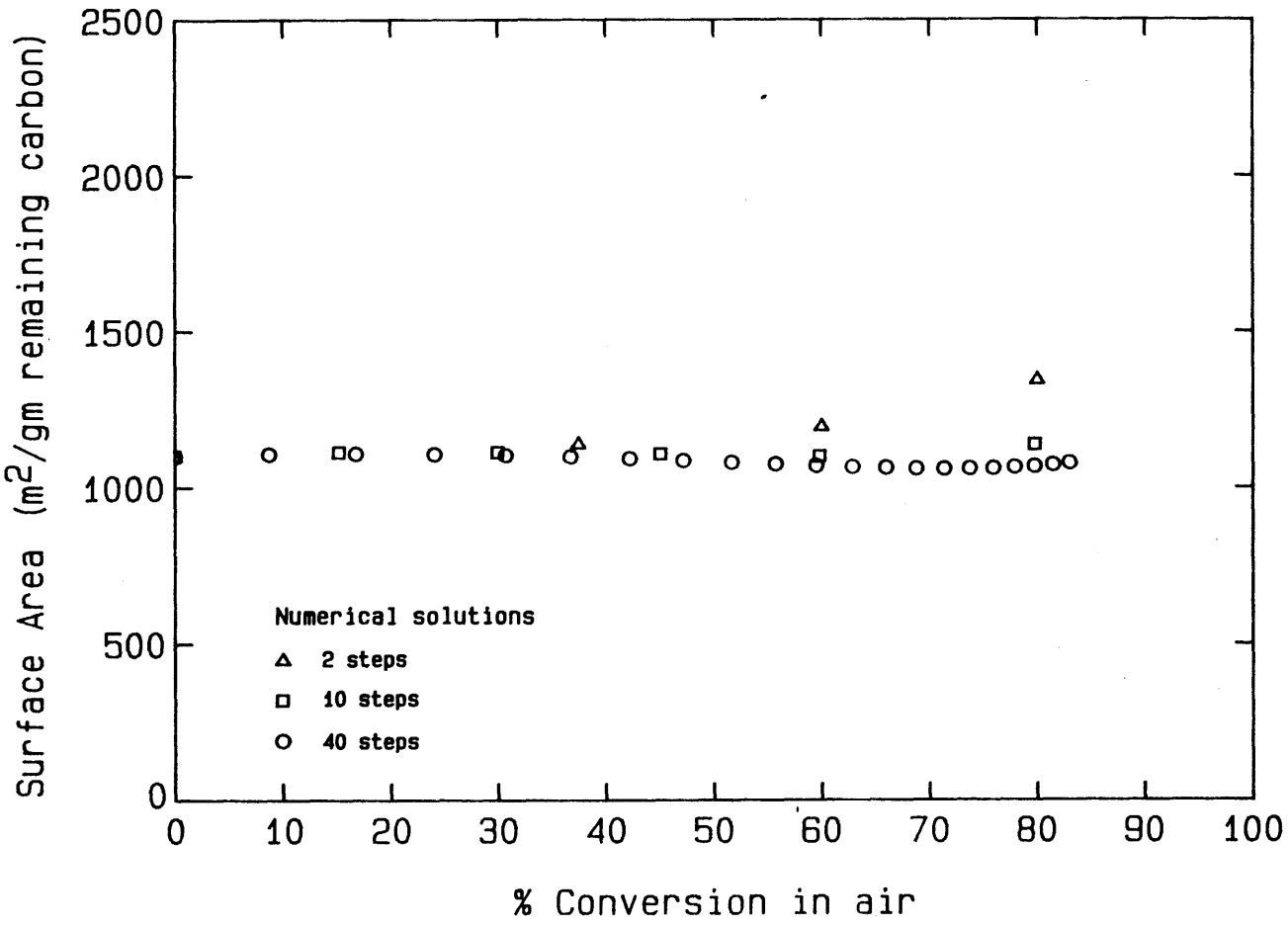

Figure 4.13 Spherocarb Surface Area Developement:
Effect of Step Size on Numerical Solution

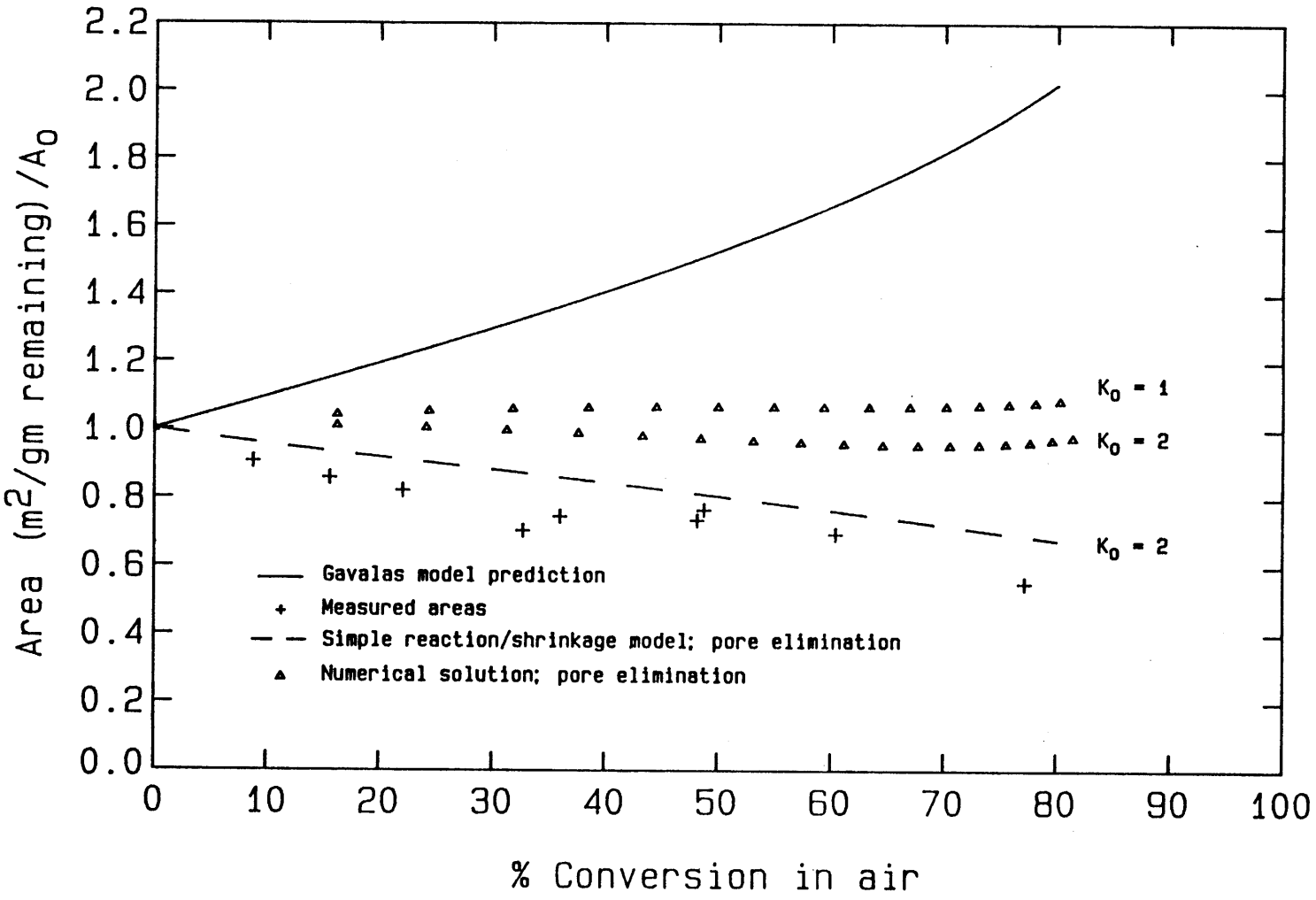

Figure 4.14 Spherocarb Surface Area Evolution

production(102), or pore coalescence or coarsening. In the limiting case of severe solid heterogeneity, the various heterogeneous carbon components would gasify sequentially, and the surface area per remaining gram of carbon would remain constant. Clearly, then, the presence of finite heterogeneity would cause the area evolution to be less than that predicted by Gavalas.

Similarly, if gasification were to proceed by pore production rather than uniform pore widening, and, in the limiting case, if the new pores were very large, the "microporous solid" would remain unchanged, as would the value of the total surface area per remaining gram. (It is unclear how area evolution during gasification via production of small pores would compare to the Gavalas prediction, but it would not be identical.)

It should be possible with the numerical approach to include either of these factors influencing area development. Because of the presence of atomic rearrangements, it is possible that the phenomenon of pore coalescence or pore coarsening is important to surface area evolution. Pore coarsening has been observed by several researchers during the heat treatment of glassy carbons(100,101). Since pore coalescence or coarsening leads to surface area loss at constant pore volume, it is, itself, not responsible for particle shrinkage, nor is the extent to which pore coalescence occurs limited by the extent of particle shrinkage. Pore coalescence is, therefore, capable of arbitrarily large reductions in surface area, and inclusion of pore coalescence in the numerical solutions to the model equations can freely account for the remaining discrepency between the model and the

measured areas. This is illustrated in figure 4.15 which displays the results of a numerical solution of gasification with concurrent shrinkage with allowance for pore coalescence. Following each pair of gasification and shrinkage steps, coalescense of 2n pores in the smallest pore class fo form n larger pores at constant volume was invoked until the model prediction matched the measured area curve. The model of gasification with concurrent shrinkage with allowance for pore coalescence is clearly capable of providing an adequate description of Spherocarb carbon surface area evolution, and the amount of porosity in pores which must have participated in coalescence events in each conversion range is given in table 4.3.

Table 4.3. Porosity in pores participating in coalescence

Conversion Range	Porosity
0 - 25%	5.4%
25 - 37%	1.2%
37 - 46%	2.7%
46 - 53%	2.8%
58 - 69%	3.1%
69 - 77%	4.2%

4.36 Area evolution according to the Simons pore tree model

The Simons model(57) offers an alternative representation of carbon pore structure, and, therefore, of surface area evolution during gasification. It is a random pore model based on finite-length pores, and, although it doesn't treat the area evolution problem in as much detail as the Gavalas model, it does include an expression for surface area as a function of porosity which is worthy of our attention. Simons prediction is that A/A_o (per remaining gram) is proportional to

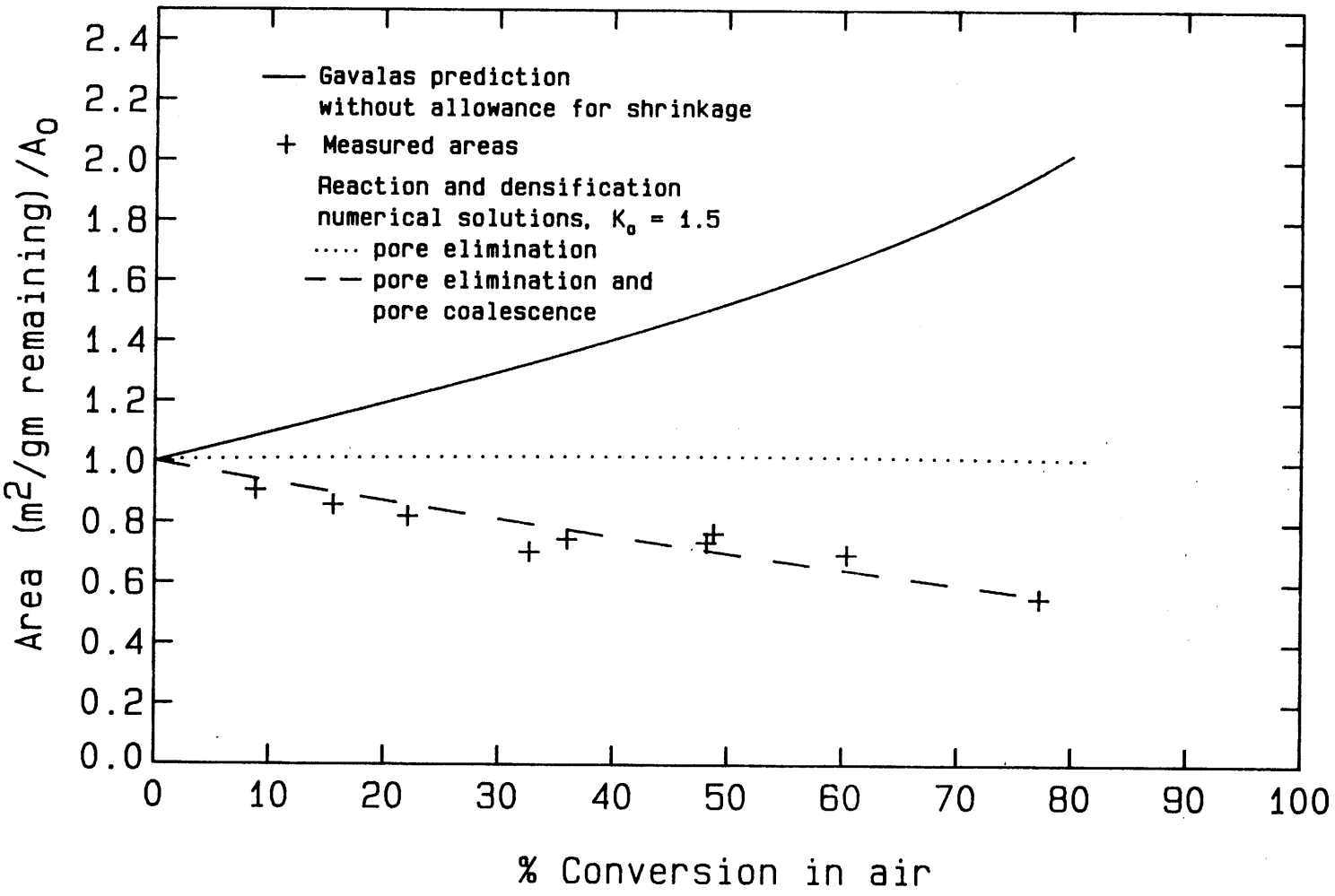

Figure 4.15 Spherocarb Surface Area Evolution

$(\theta)^{2/3}$. Unlike the Gavalas model prediction, the area per remaining gram remains finite as conversion approaches 1.

The prediction of the Simons model without allowance for shrinkage is presented in figure 4.16, along with the constant-volume Gavalas prediction and the measured areas. The Simons prediction is significantly lower than the Gavalas prediction, although the discrepancy between the Simons prediction and the data is still quite pronounced. The source of the difference between the Simons and Gavalas prediction is an interesting topic. The two formulations differ from the very beginning, and even incorporate somewhat different physics, in that the Simons model allows for finite length pores. The Simons model employs several approximations including the assumption of a $1/r^3$ pore size distribution at all porosities. Gasification in the kinetic regime is expected to alter the initial pore size distribution, and may be responsible for some of the discrepancy between the two models. Simons, in fact, treats the effect of kinetic gasification on the $1/r^3$ distribution and presents an asymptotic long-time solution for the internal area. The solution for the surface area following kinetic gasification at long times lies above the solution which assumes preservation of the $1/r^3$ distribution, but is, interestingly, still finite as θ approaches 1, unlike the Gavalas model.

The shrinkage at constant mass adjustment factors can be applied to the Simons expression to generate a simple model of gasification with concurrent densification, analogous to the simple model based on the Gavalas prediction. These results are presented in figure 4.17, in which it can be seen that the data are bracketed by the model

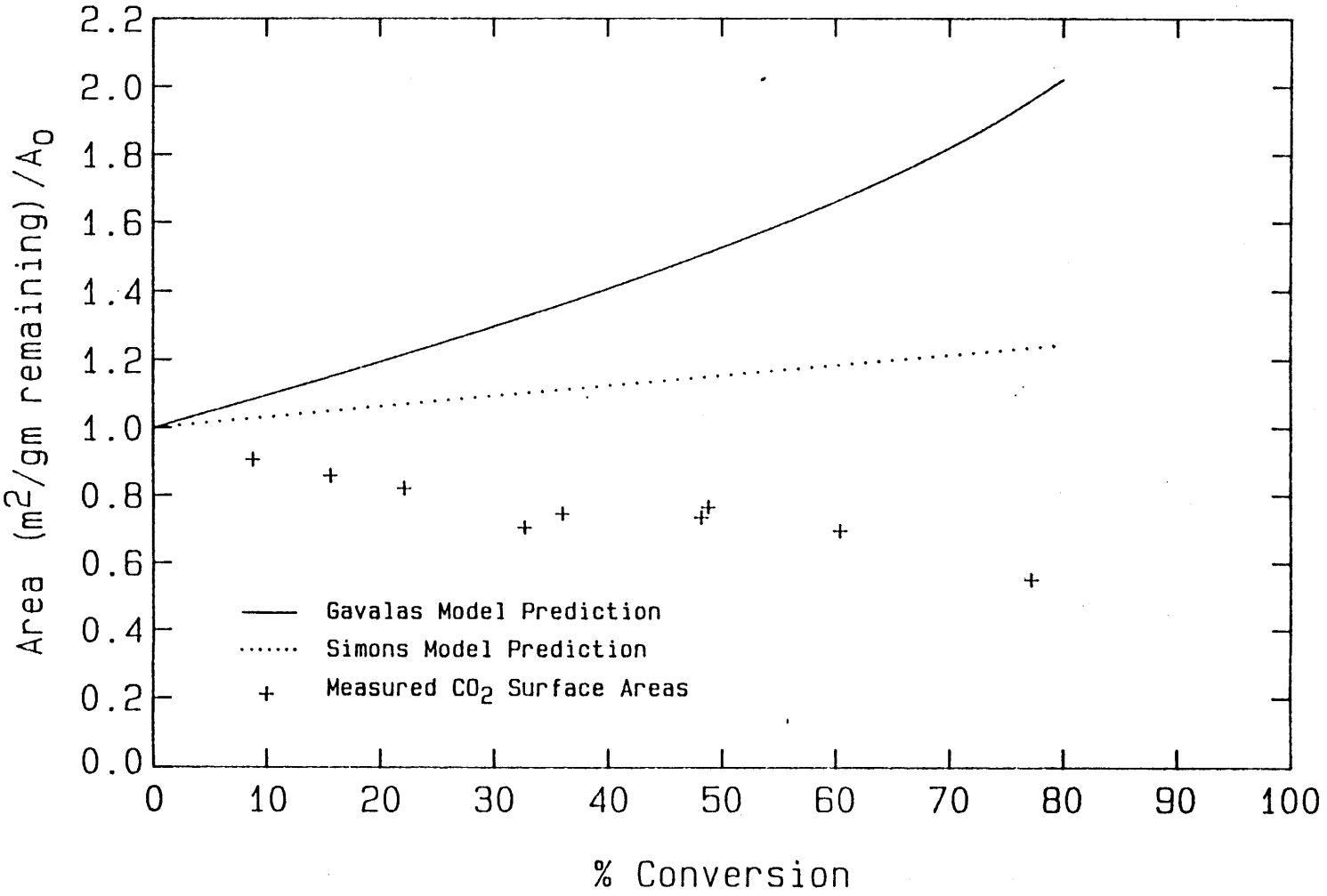

Figure 4.16

Spherocarb Surface Area Evolution

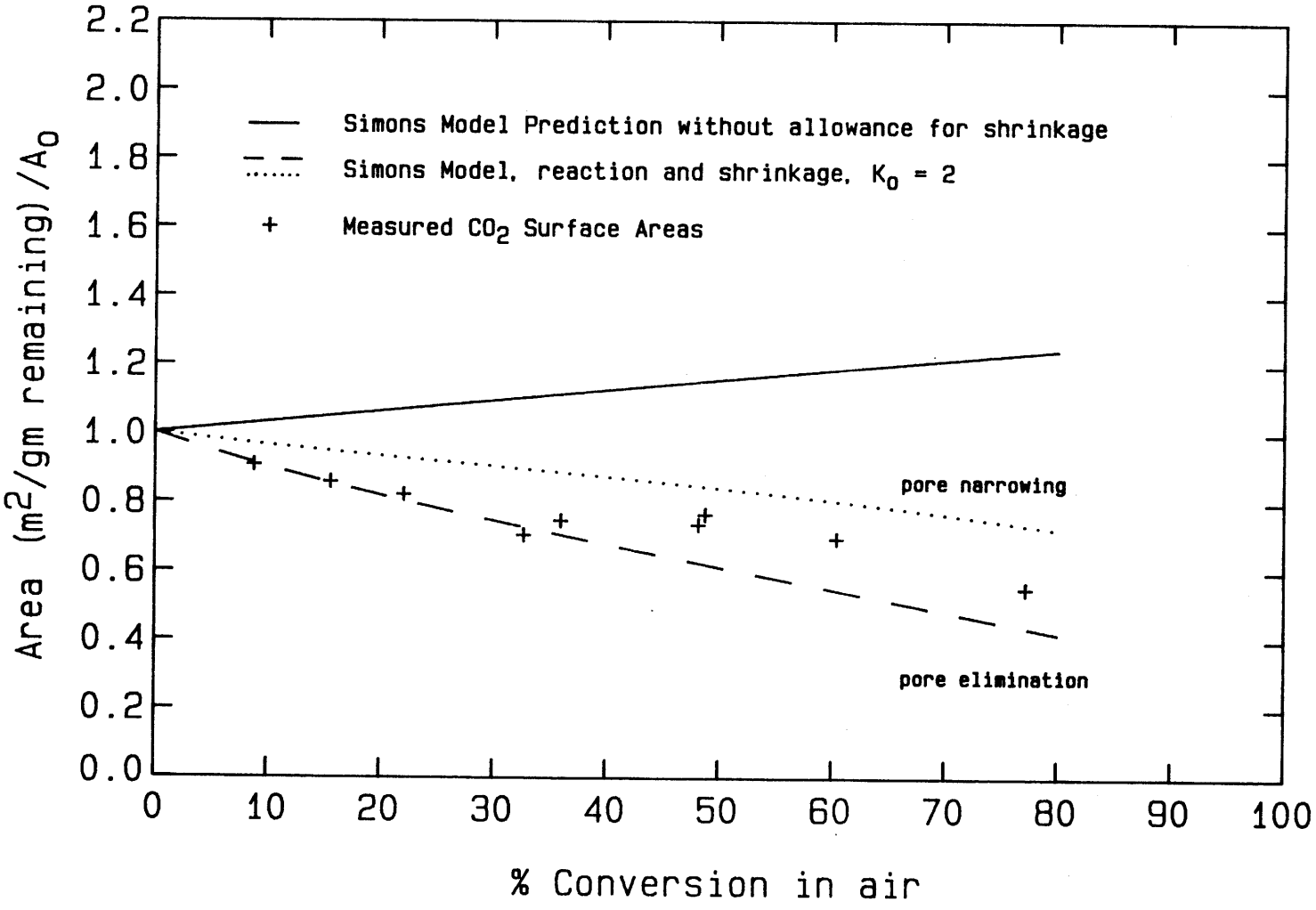

Figure 4.17 Spherocarb Surface Area Evolution

prediction for the two limiting cases: pure pore elimination, and uniform pore narrowing. A quite satisfactory fit can be obtained for the data by considering a shrinkage mode involving a combination of pore elimination events and pore narrowing events. The intermediate model prediction shown in figure 4.18 is the least-squares fit with adjustable parameter f (=.65), defined as the fraction of the total small-pore volume loss attributed to pore elimination.

4.37 Modeling summary

There is a large discrepancy between measurements and random pore model predictions of internal surface area evolution for Spherocarb carbon. The phenomenon of reaction-induced densification is an important factor determining surface area evolution during Spherocarb gasification according to each of the models considered. Inclusion of the effect on surface area of densification/shrinkage can, in fact, account for most of the discrepancy between data and existing models. The numerical solutions based on elements of the Gavalas formulation are the best representation of the physics of gasification with concurrent shrinkage, and yet cannot, without allowance for pore coalescence, fully account for the discrepency between the measured areas and the constant-volume random pore models. Other phenomena may also be contributing to the deviation of surface area evolution from the Gavalas model prediction, such as heterogeneity in carbon reactivity, gasification by pore production, or pore coalescence or coarsening. For example, a model of gasification with concurrent

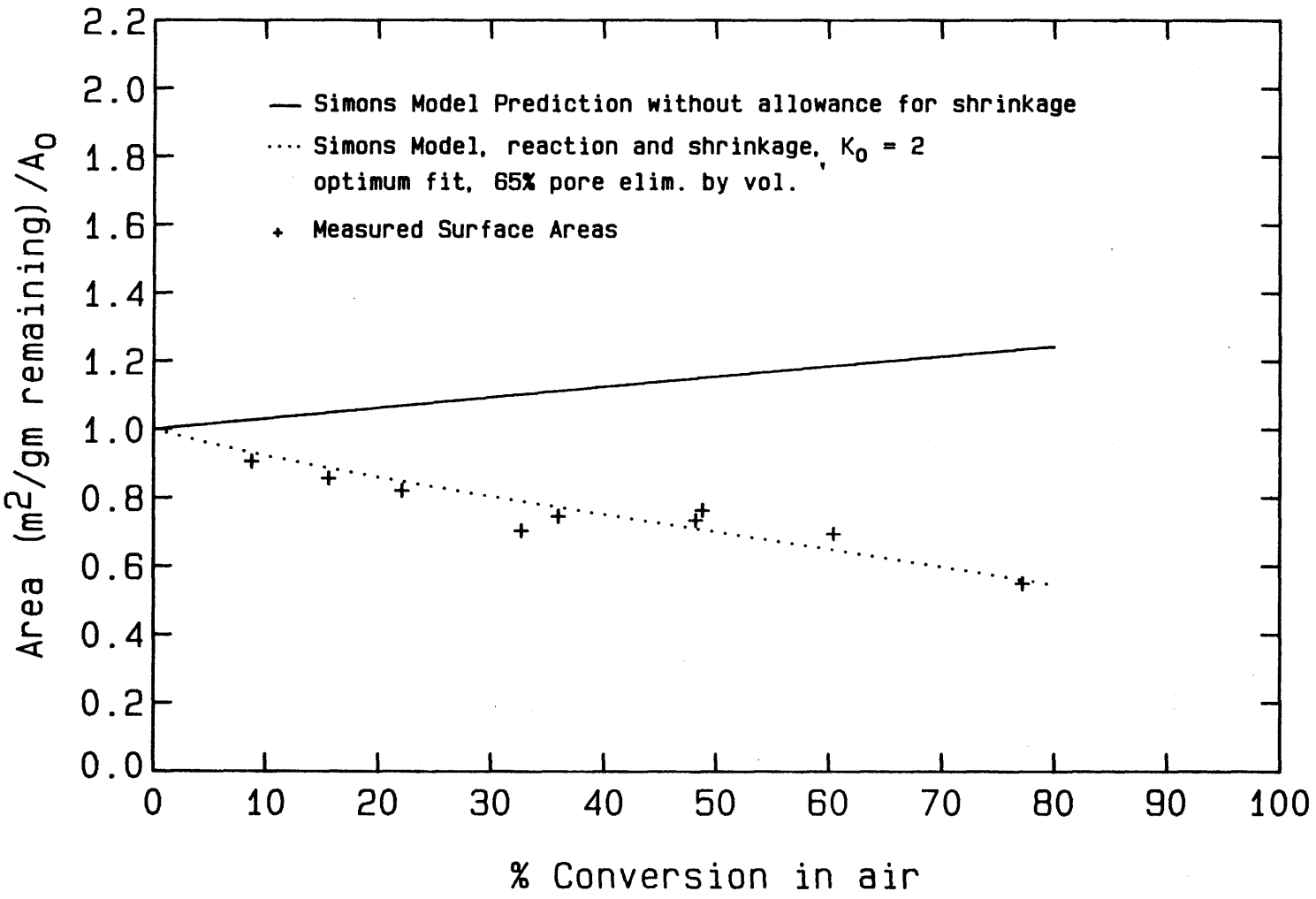

Figure 4.18 Spherocarb Surface Area Evolution

shrinkage with allowance for pore coalescence provides an adequate description of Spherocarb surface area evolution.

Glossary of Terms*

d_p particle diameter

d_s surface feature dimension

A surface area (m^2/gm)

B_o, B_1 zeroth and first moments of Gavalas' pore axis probability density function (μm^{-2}), (μm^{-1})

K pore structure parameter, defined in equation 14

N number of pores

R_s small pore radius

V_p pore volume

V_c carbon skeletal volume

V_t total particle volume

V_1 volume in large-pore class

V_s volume in small-pore class

X conversion

$\lambda(R)dR$ Gavalas' pore axis probability density function (μm^{-2})

l particle diameter ratio, d/d_o, where d_o is the diameter before shrinkage, or at 0% conversion

h ratio of particle diameters before and after a single conversion step in the numerical solution

θ, θ_s, θ_1 porosity, (pore volume/particle volume); total, small-pore, large-pore

ρ_{He} helium, or true carbon density

---

*subscript o denotes initial value, except for B_c

Chapter 5. The Effect of Coal Type or Petrographic Composition on Coal Char Gasification Reactivity

Vitrinite and fusinite are the two most important macerals or type-determining coal components, examples of which are sometimes found in rather high purity in the easily identified, macroscopic "lithotypes" vitrain and fusain. Vitrain and fusain were handpicked from blocks of PSOC 156 subbituminous coal, examined and purified under low magnification, and analysed (along with the whole coal) for maceral composition under reflected light. The fusain fraction was 92% fusinite, and the vitrain fraction was 96% vitrinite, by volume. The predominant constituents of the whole coal were vitrinite and inertinite, present in the ratio 1.9 vitrinite/1.0 fusinite on a weight of char basis. Some information on the whole coal and lithotypes, including ultimate analyses, was presented in chapter 2.

The gasification reactivities of chars from the raw lithotypes and the whole coal are plotted in figure 5.1 as a function of conversion in one atmosphere carbon dioxide. These reaction rates were insensitive to changes in sample bed size, indicating freedom from external or within-bed mass transfer limitations. The reactivity of fusain was lower that the reactivity of vitrain by a factor of about two at low conversion, while at high conversion the two curves diverged, reactivities differing by a factor of 15 at 90% conversion. Clearly the reactivity-conversion curves for the two lithotypes are qualitatively different, and figure 5.2 illustrates directly that a much longer time is required to gasify the fusain sample to high conversion. The whole coal reactivity curve in figure 5.1 lies between

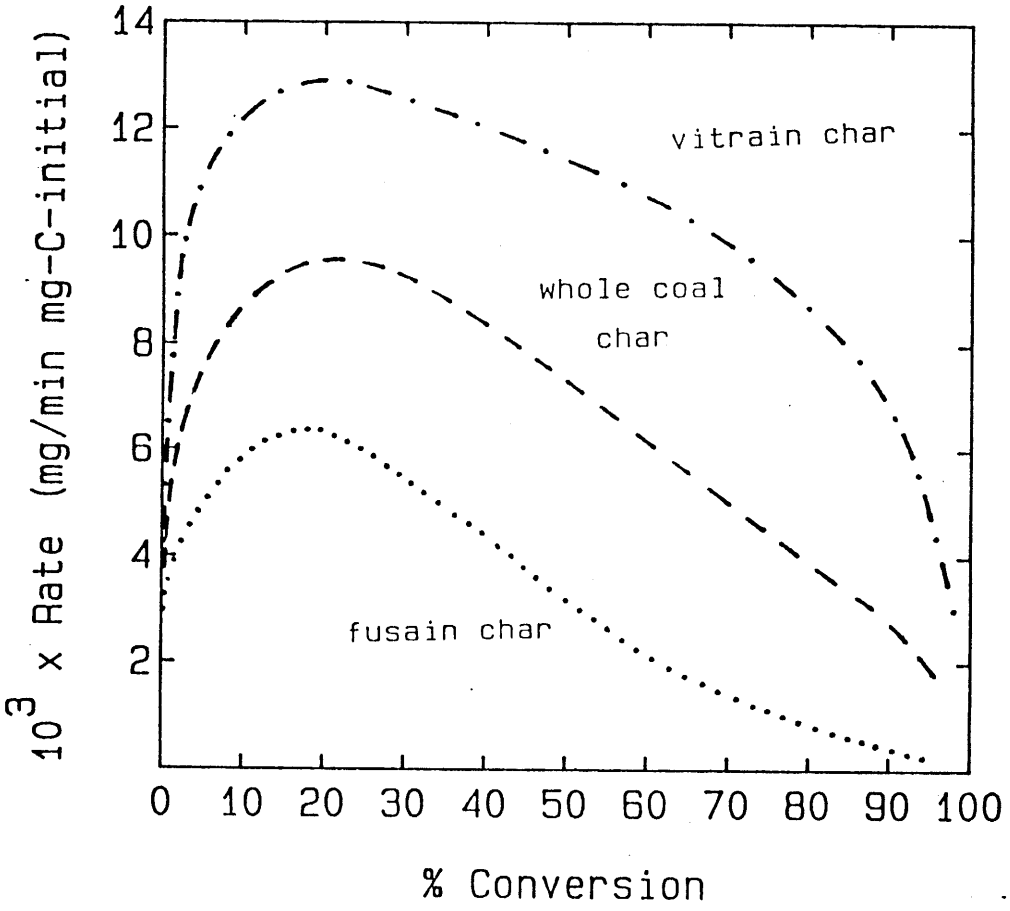

Figure 5.1

Gasification reactivity of lithotype and whole coal chars in 1 atm. carbon dioxide at 800 ^{o}C.

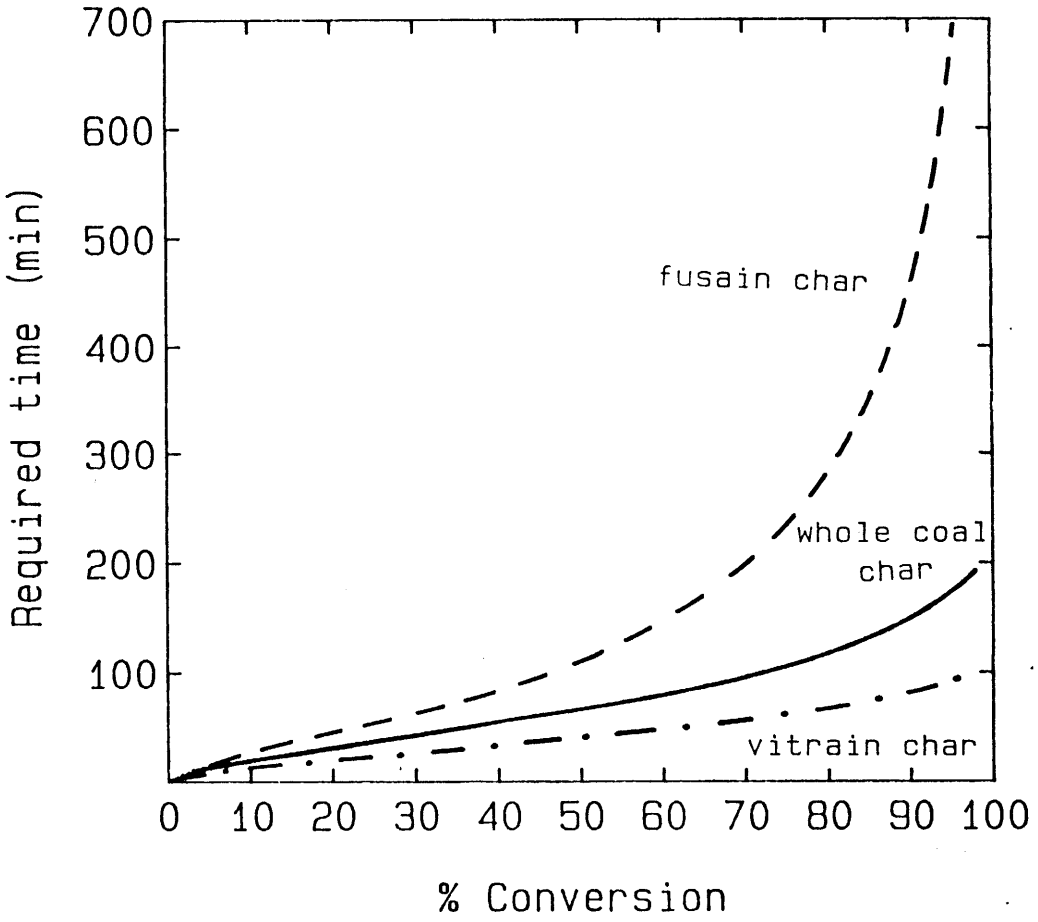

Figure 5.2

Gasification of lithotype and whole coal chars in 1 atm. carbon dioxide at 800^{o}C

the lithotype curves, but does not closely approach the fusain curve at high conversion, indicating that, in terms of gasification behaviour, a whole coal with its complex petrography cannot be accurately modeled as a composite of the two handpicked fractions alone.

The authors have attempted to relate the gasification behaviour of these lithotypes to their physical and chemical properties. Carbon dioxide surface areas of the lithotype chars (measured at approximately 50% conversion) were similar: 1005 m^2/gm-converted-ash-free-char for fusain and 860 m^2/gm-converted-ash-free-char for vitrain. Reactivity results for demineralized chars, chars from ion-exchanged coals, and untreated chars appear in 5.1.

Table 5.1. Comparison of carbon dioxide gasification reactivities of acid washed, ion-exchanged, and raw chars

Char	Temperature (°C)	% Conversion at which reactivity was measured	Ratio of reactivities
vit_{raw}/fus_{raw}	800	65	5.8
vit_{dem}/fus_{dem}	875	65	2.3
vit_{ion}/fus_{ion}	830	15	0.68
vit_{raw}/vit_{ion}	800	15	8.2
vit_{raw}/vit_{dem}	790	65	3.4
fus_{raw}/fus_{dem}	890	65	1.7

Direct comparisons were made between pairs of chars at experimentally convenient temperatures and the results presented as ratios of reactivities. The conversions at which the rate comparisons were made were chosen to give about the maximum rate for each char. (Note that all the comparisons involving a demineralized char had started with 50% converted material.) The demineralization procedure was performed on coal chars at about 50% conversion with the hope that the porosity

developed during gasification would facilitate the extraction of a larger fraction of the catalytic mineral matter.

Demineralization lessened the difference between the reactivities of vitrain and fusain as shown by the first two entries in the table. Further, the divergence of the reactivity curves for the raw chars at high conversion in figures 5.1 and 5.2 was not seen for the two demineralized chars at high conversion. Although the demineralization procedure can change coal or char surface areas substantially(41), the carbon dioxide areas for both fusain and vitrain (at 50% conversion) changed relativily little upon demineralization in this study, yielding 830 m^2/gm-converted-ash-free-char for demineralized fusain and 740 m^2/gm-converted-ash-free-char for demineralized vitrain.

Chars made from ion-exchanged fusain and vitrain had similar reactivities, indicating that differences in exchangeable cation content are responsible for the major differencs between untreated lithotype chars. The ion-exchange results also suggest, by comparison, that demineralization had left appreciable amounts of residual catalytic inorganic matter. The residual ash content was measured for the demineralized whole coal char and was 1 wt%, greater than a typical residual ash content following demineralization of a coal. In fact, Linares-Solano et al.(103) have previously observed significant residual catalytic effect in demineralized chars when compared with chars from demineralized coals, and the results obtained here suggest that prior gasification will not improve demineralization efficiency.

The fourth entry in table 5.1 is a direct comparison of raw and ion-exchanged vitrain which indicates that catalysis by ion-

exchangable matter dominates the reactivity of raw vitrain char. Demineralization was less effective than ion-exchange in reducing the reactivity of vitrain char as shown in the fifth table entry, again indicating significant residual catalytic inorganic matter in the demineralized char. Although the ratio of the reactivities of raw and ion-exchanged fusain was not measured, it can be calculated from the existing data as the product of the third and fourth table entries and the ratio fus_{raw}/vit_{raw} at 15% conversion, which can be taken from Figure 5.1. This ratio (fus_{raw}/fus_{ion}) is about 2.7 (again higher than the raw/demineralized fusain ratio, given as the last table entry) and suggests that the catalytic effect is less pronounced than in the vitrain char, but probably still important.

Because the most important naturally occurring exchanged cations found in low rank coals are Ca^{2+} and to a lesser extent Mg^{2+}, the ion-exchange filtrates were analysed for these two elements using atomic absorption spectroscopy. Calcium (0.13 wt%) and magnesium (0.03 wt%) were exchanged from the fusain, and the average cation loadings from two independent extractions on the vitrain sample (which were in close agreement) were 0.40% Ca and 0.13% Mg. Morgan et al. have discussed sources of interferences with the exchangeable cation determination(37), the most important being the solubilization of gypsum, which may provide as much as 0.1 or 0.2 wt% Ca. No statement, therefore, can safely be made about the cation content of the fusain sample in this study. Vitrain, on the other hand, had significant and unambiguously measurable cation contents, high enough to cause an important catalytic effect, but somewhat lower than has been reported

for lignite coals(37). The higher cation content and higher reactivity of vitrain is consistent with the higher oxygen content of the vitrain sample in table 2.1 and the higher oxygen content of vitrinites in general(104).

It is concluded that fusain can have a significantly lower gasification reactivity than vitrain from a given coal due to differences in the amount of naturally occurring, ion-exchanged metals, probably predominantly Ca. This effect should be most important in the gasification of low rank coals which have high carboxylic group contents and, therefore, high ion-exchange capacities. These results are consistent with and supplement the results of Johnson(46), which suggest that, in higher rank coals and in demineralized low rank coals, the chemical differences between associated macerals have relatively little effect on low temperature gasification reactivity.

Chapter 6. Conclusions and Recommendations

6.1 Conclusions

The gasification behavior of carbons from a number of natural and synthetic organic materials has been studied in order to obtain a better understanding of the relationship between carbon properties and carbon gasification reactivity. Three aspects of this relationship were focused upon: the role of microporous surface area in gasification, the role of reaction-induced densification in gasification, and the effect of coal type or maceral content on gasification reactivity.

6.11 The role of microporous surface area in carbon gasification

Here we have attempted to identify the accessible total surface area for gasification, which is important as a guide to the development of a rational and accurate correlation of char reactivity, and as the logical starting point in the quest for an improved fundamental understanding of the factors that determine carbon gasification reactivity.

There is much evidence that non-catalyzed carbon gasification occurs on the large surface area lying within carbon micropores. Further, several quantitative analyses of reaction and diffusion during Spherocarb oxidation indicate that oxygen penetration at temperatures under 600 ^{0}C is complete, and that the reaction rate is strictly kinetically limited. The accessible total surface area for Spherocarb is expected, then, to be the 636 m^2/gm measured by carbon dioxide

adsorption, and the measured activation energy of 36 kcal/mol to be the intrinsic activation energy for oxidation of this carbon. This can be compared to about 60 kcal/mol typically measured for the oxygen gasification of graphite, the difference presumably arising from the different degrees of purity and crystallinity. This level of understanding of diffusional processes is necessary for the fundamental treatment of many aspects of carbon gasification, including, in fact, the development of models of gasification with concurrent shrinkage, also undertaken as a part of this thesis.

The gasification rate of a sucrose char on the other hand, depends on particle size, evidence for some incomplete reactant penetration, under conditions where the assumptions of Knudsen diffusion and a tortuosity of five predict complete reactant penetration and hence no effect of particle size. The nature of the effect of particle size on sucrose char reactivity is consistent with a model in which restricted diffusion limitations exist in microporous grains with radii of 27 μ. There is the possibility that an effect of grinding contributes to the increase in reactivity with decreasing particle size effect, in light of which the fitted model parameters (grain size, intrinsic rate, and diffusivity) should be regarded as setting an upper limit on the severity of diffusion limitations for sucrose char.

The severity of diffusion limitations scales as L^2/D, and depends, therefore, on the local microporous diffusivity, a parameter determined by micropore size, and the characteristic size of the microporous regions, a parameter determined by macroporosity. The major difference between the two synthetic carbons in this study is probably related to

a difference in the characteristic size of microporous grains in the two carbons. The severity of microporous diffusion limitations for most chars should lie between that for the highly macroporous Spherocarb and that for the essentially non-macroporous sucrose carbon.

Adsorption of nitrogen fails to provide an accurate measure of the total microporous surface area under certain conditions, due to a propensity of the nitrogen molecule to fill pore volumes at low relative pressures, leading to anomalously high apparent surface areas. Surface areas determined from carbon dioxide adsorption isotherms at low pressures do not suffer from this effect, and should thus provide a better measure of the total surface area for kinetically limited noncatalyzed carbon gasification.

The carbon dioxide gasification of chars from a sub-bituminous coal, which is believed to be catalysis-dominated, was not accompanied by micropore widening, and the rate of gasification was apparently unrelated to total surface area. These kinetic data demonstrate that the rate of catalyzed gasification can be independent of total surface area. Normalization of the rate of catalyzed gasification with measured surface areas in this case is inappropriate. The presence of catalyst does not simply increase the intrinsic reactivity of the carbon surface, and the process of catalyzed gasification can not be treated as a total surface area evolution problem with an altered or adjustable intrinsic surface reactivity.

The gasification behavior of the coal chars is consistent with the occurance of reaction in the immediate vicinity of catalyst

particles which lie preferentially on the surfaces of large pores.

Since many naturally occurring organic materials are rich in potentially catalytically active inorganic impurities, the normalization of the gasification rates of many coal chars with microporous surface area may be of limited use.

6.12 The phenomenon of gasification-induced carbon densification

Kinetically limited carbon gasification does not occur at constant particle diameter as heretofore widely assumed. Gasification of various carbons at low temperatures in oxygen and carbon dioxide induces a homogeneous solid densification, which results in carbon particle shrinkage with the preservation of external surface features. It is believed that densification is the result of atomic rearrangements producing loss of pore volume in fine pores. At the length scale of the larger pores, the optically homogeneous "microporous solid" appears to undergo a densification/shrinkage, with the larger pores shrinking also, acting as holes in a homogeneously shrinking matrix.

It is believed that the gasification reaction, by breaking bonds, removing cross links, and removing carbon atoms to reduce the density and "loosen" entanglements, increases the driving force for, and facilitates densification via rearrangements analogous to those occurring spontaneously at somewhat higher temperatures in the initial stages of graphitization.

We believe that one prerequisite for shrinkage is that gasification occur well within the ultrafine carbon structure, where it

can exert an influence on the layer packing and hence the microporosity. We therefore anticipate little or no shrinkage for low surface area carbons or for those carbons which gasify via production of relatively large channels or pits, a characteristic of some catalyzed systems.

Particle shrinkage is important in pore structure evolution during gasification or activation and therefore affects gasification rates, effective diffusivities, fragmentation behavior and activated carbon absorptive properties. For example, measured surface areas for Spherocarb as a function of conversion are in pronounced disagreement with the prediction of random pore models, which do not account for shrinkage. In addition, measurements of particle size or density are not reliable tests for determining the fraction of the reaction occurring on the external surface.

Models have been developed to predict pore structure evolution during gasification with concurrent shrinkage. The phenomenon of reaction-induced densification is an important factor determining surface area evolution during Spherocarb gasification, according to each of the models considered. Inclusion of the effect of densification/shrinkage on surface area can, in fact, account for most of the large discrepancy between data and existing constant volume models.

Numerical solutions based on elements of the Gavalas random pore model formulation are the best representation of the physics of gasification with concurrent shrinkage, but cannot fully account for the discrepency between the data and the constant volume pore models.

One of several phenomena may be responsible for the remaining discrepency between the measured surface areas and the numerical predictions, such as heterogeneity in carbon reactivity, gasification by pore production, or pore coalescence or coarsening. A numerical solution with allowance for pore coalescence, as an illustration, provided a quite satisfactory description of Spherocarb area evolution.

6.13 The effect of coal type or maceral composition on char reactivity

Chars from the lithotypes vitrain and fusain picked from a sub-bituminous coal had very different intrinsic gasification reactivities in carbon dioxide. The vitrain and fusain samples were almost pure concentrates of the macerals vitrinite and fusinite respectively. The vitrain char was significantly more reactive than the fusain char, especially at high conversions. This illustrates that chars from individual macerals from a given coal can have very different gasification reactivities, in which case the gasification behavior of a whole coal char must be understood in terms of the gasification behavior of its individual petrographic constituents.

The major differences between the gasification behavior of the two subbituminous lithotypes in this study are attributed to differing amounts of naturally occurring ion-exchanged metals. The higher cation content and higher reactivity of vitrain in this study is consistent with its higher oxygen content and the higher oxygen content of vitrinites in general. This effect is expected to be most pronounced in low rank coals, with their high oxygen contents and accompanying high ion-exchange capacities.

6.2 Recommendations

The results obtained in this thesis suggest continuing investigations in several areas, including the following.

6.21 The accessible total surface area for carbon gasification

The role of microporous surface area and the importance of restricted diffusion should be determined for other chars, at higher temperatures, and using other experimental and analytical techniques.

In addition, our present, improved understanding of the role of micropores should be used to identify conditions under which the accessible total surface area for gasification is known, and meaningful intrinsic reactivities can be measured. This intrinsic rate would be a true property of the carbon surface, and could potentially be fundamentally related to (or at least correlated with) other properties of the carbon surface.

The measurement of intrinsic reactivities would be especially important in the development of a correlation of the rates of non-catalytic carbon gasification, which might proceed as follows: Intrinsic non-catalytic carbon reactivity may be expected to be dependent on heat treatment temperature, and, to some extent, on the parent organic material. A set of low temperature synthetic carbons should be made, which should be of high purity to ensure non-catalyzed gasification, and which should be macroporous to minimize the effects of microporous diffusion limitations, according to the results of this thesis. The chars should vary in carbon structure and in heteroatom

content, the variation arising from different parent materials, or from incorporation of heteroatoms before or during pyrolysis. Measurements of surface areas and low temperature gasification reactivities for the set of carbons as a function of heat treatment temperature would then provide, for the first time, direct information on the effect of heat treatment and carbon type on intrinsic non-catalyzed reactivity, and perhaps then the basis for a predictive correlation.

Surface areas and gasification rates could also be measured as a function of conversion, in order to understand the effect of partial reaction on carbon surface chemistry and thus intrinsic reactivity.

The surface area approach is expected to be less useful for catalyzed gasification, but the importance of catalysis to the gasification of a given carbon could be inferred from a comparison of its reactivity to that of the uncatalyzed carbons with the same heat treatment temperature, allowing for the possible variations at a given heat treatment temperature associated with heteroatom content or different carbon structures.

The conversion dependence of catalyzed gasification rates must probably be understood through models treating, for example, the accessibility, chemical deactivation, and coalescence of catalyst particles on carbon surfaces.

6.22 Gasification-induced carbon densification/shrinkage

To understand the importance of homogeneous shrinkage during fast reactions, measurements of diameter reduction during Spherocarb oxidation should be extended to higher temperatures, through the regime

in which the transition to diameter reduction by external reaction occurs. This data may, in addition, yield kinetic parameters for Spherocarb densification, which would enhance our understanding of the nature of the densification phenomenon.

There is, at present, an inadequate understanding of the factors that determine the extent to which a given carbon will undergo gasification induced shrinkage. It is expected that the propensity to densify will increase with increasing surface area, and will decrease with the extent to which a carbon gasifies by a mode involving the production of relatively large pits or channels, as is seen in some catalytic systems. A larger data base would be useful in the confirmation of these ideas and in the possible identification of other important factors.

The mechanism of gasification induced densification is another potentially interesting topic. A more detailed description of the atomic rearrangements causing densification might be possible following, for example, the measurement of densification kinetic parameters and/or the calculation of crystallite dimensions and amorphous material fraction from X-ray diffraction spectra.

Finally, the role of densification in determining particle fragmentation behavior is a fertile area which should receive more attention.

6.23 Surface area evolution during gasification

Because this is essentially a geometric problem, it is quite amenable to analysis, as is perhaps clear from the number of existing

models of pore structure and gasification. The manner in which the pore structure develops is important in determining gasification reactivity as a function of conversion, and possibly as a tool to provide insights into the chemistry of gasification.

Existing models consider gasification by uniform recession of the surfaces of all pores. This may not be the case, especially for high area carbons for which the appropriate length scale is the dimension of carbon micropores. The importance of the phenomena of pore production and carbon heterogeneity (deviations from uniform surface recession) on surface area evolution should be ascertained. Surface area measurements on a non-shrinking carbon (again, in the absence of catalysis and microporous diffusion limitations) would be very helpful here.

Pore production and carbon heterogeneity as well as pore coalescence can be rigorously added to the numerical solutions of area evolution based on the Gavalas model. Surface area and pore structure evolution should then be measured for other carbons, and all of the results understood in terms of the various phenomena known to affect pore structure evolution: pore widening, pore production, and pore overlap due to reaction; preferential gasification of certain carbon components; and pore elimination, narrowing, and coalescence due to atomic rearrangements.

Appendix A. Spherocarb Diffusion Analysis

The reaction effectiveness factor is defined as

$$\eta = \text{Rate}_{obs}/\text{Rate}_{int} \quad (1)$$

the ratio of the observed mass transfer limited rate to the intrinsic rate, and is related to the dimensionless Thiele modulus for a first order reaction in a sphere ϕ by

$$\eta = (3/\phi)(1/\tanh(\phi) - 1/\phi) \quad (2)$$

The Thiele modulus for first order reaction in a sphere is given by

$$\phi = [(R^2/D\theta)/(1/k_v)]^{1/2} \quad (3)$$

where R_2/D has been extrapolated to reaction temperature, θ is the porosity, and $1/k_v$ is the intrinsic rate constant per unit volume. $1/k_v$ is given by $1/k_v = [C_r MW_c/\nu\rho_p]T$ where C_r is the concentration of the reacting gas, MW_c is the molecular weight of carbon, ν is the moles of reacting gas consumed per mole of carbon, ρ_p is the particle (or grain) density, and T is the reciprocal of the intrinsic reaction rate with units of gm/sec-gm.

-- Time for 87% completion of adsorption = .95 sec = $.16(R^2/D)$
(from figure for 45% gasified Spherocarb); R^2/D under reaction conditions taken as $(273/T_{rxn})^{1/2}(R^2/D)_{meas}$ (Knudsen diffusion temperature dependence)

-- $C_R = (2.558 \times 10^{-3}/T_{rxn})$ in mol/cm^3

-- $MW_c = 12$ gm/mol

-- $\nu = 1$ (O_2 + C CO_2)

-- ρ_m and θ_m can be estimated reasonable closely from the measured CO_2 surface area as follows:

$V_{ms} = V_{sol} + V_s$ where V_{ms} is the specific volume cc/gm of microporous solid, V_{sol} that of the true solid, and V_s that of the micropores.

$1/\rho_m = 1/\rho_{He} + V_m$; ρ_m is quite close to 2.0 gm/cc and treating the 800 m^2/gm CO_2 area as a micropore volume yields .244 cc/gm for V_m.

ρ_m is, then, 1.34 gm/cc and $\theta_m = V_m/V_{ms} = .328$

Table Appl.1 contains the results of the Spherocarb diffusion analysis.

Table Appl.1. Spherocarb Diffusion Analysis**

Temp. °C	Measured Rate at 40% conversion (gm/min)/gm_i	η_{min}	$Rate_{reg}$	$Rate_{int}$	Predicted $Rate_o$
400	14.9	.92	1.86×10^{-4}	2.47×10^{-5}	2.45×10^{-5}
450	13.8	.65	1.22×10^{-3}	1.06×10^{-3}	7.81×10^{-4}
471	13.4*		2.49×10^{-3}	4.41×10^{-3}	2.08×10^{-3}
495	13.0		5.36×10^{-3}	.0205	5.04×10^{-3}
534	12.4*		1.70×10^{-2}	.2049	1.68×10^{-2}
574	11.8*		.0490	1.66	.0480
600	11.4		.0946	6.30	.0938
600	11.4*		.0946	6.30	.0938

* from J.K. Floess, Ph.D. Thesis
** all rates in gm/min-gm_i

η_{min} is calculated iteratively from equations 1 and 2, and is near 1 at the lowest temperatures. Since all of the measured rates extend upward along the straight Arrhenius plot from these rates, the rates cannot deviate far from intrinsic at least up to 600 °C.

The rightmost three columns represent the second Spherocarb analysis discussed in chapter 3, where diffusion limitations in the data are assumed for sake of argument. $Rate_{reg}$ is the value of the (log) linear regression of the measured rates at the given temperature, $Rate_{int}$ is the intrinsic rate calculated iteratively from equations 1 and 2 assuming that η_{min} calculated from the measured diffusion times is not a lower limit, but rather is identical to the true effectiveness factor. Predicted $Rate_o$ is the predicted diffusion limited (subscript o for "observed") rate, which was set equal to the data at the higher temperatures. This allowed the calculation of the intrinsic rate and its activation energy. Extrapolating the calculated values of $Rate_{int}$ down to lower temperatures, and calculating the Predicted $Rate_o$ results in the bending curve shown in figure 3.18. This curve does not fit the data, and we can throw out the premise on which this analysis was based, namely that the reactions rates in the higher temperature portion of the plot were diffusion limited.

Appendix B. Additional Information Pertaining to Modeling

The complete pore size distribution for use in the Gavalas model and in the models of reaction with concurrent densification was compiled from the Spherocarb pore structure characterization data of Niksa (see following pages) and carbon dioxide surface areas measured by D. Dudek, as follows.

The mesopore volume distribution (142.8 Å > d > 14.2 Å) was taken directly from the pore size distribution of Niksa obtained by application of the Kelvin equation to the N_2 adsorption isotherm, and totaled .1754 cc/gm. The micropore volume was obtained as follows, by assuming that nitrogen adsorbs in micropores by volume filling.

$$V_t = V_{mes} + V_{mic}$$

where V_t is the total volume of nitrogen adsorbed (= 275.1 standard cc/gm = .4255 cc/gm) and where V_{mes} is the volume found by the Kelvin analysis in pores with diameters larger than 14.2 Å (.1861 cc/gm), and V_{mic}, the micropore volume was obtained by difference and equals .2394 cc/gm.

The macropore volume distribution was obtained from the Hg porosimetry data after the pore radius defining the cutoff between pore volumes and interparticle voids was chosen. This cutoff was chosen using Spherocarb densities measured by Dudek and D'Amore as follows.

$$V_p + V_c = V_T = 1/\rho_p$$

where V_p is the pore volume in cc/gm, V_c is the carbon specific volume in cc/gm, V_T is the total particle volume, and ρ_p is the particle density of .65 from Dudek and D'Amore. For a true carbon density of 2.0, the total pore volume was 1.038 cc/gm and the volume in pores with

MICROMERITICS INSTRUMENT CORPORATION

DIGISORB 2600 V2.02 PAGE 2
101

DIA, 91105AW, MAL# 980-69 NITROGEN
TION 5 STARTED 4/19/84 11:48 COMPLETED 4/20/84 9:30

ADSORPTION ISOTHERM

PLE WEIGHT: 0.1520 G EQUILIBRATION INTERVAL: 20 SECS
E SPACE: 85.4236 CC MAX VOL INCREMENT: 100.000 CC/G STP

P/PO	VOL ADSORBED (CC/G AT STP)
0.0000	97.3295
0.0062	193.9901
0.0547	229.9966
0.0787	235.5328
0.1241	241.1421
0.1680	244.3220
0.2097	246.3628
0.8954	275.1337

MICROMERITICS INSTRUMENT CORPORATION

DIGISORB 2600 V2.02 PAGE 3
101

DIA, 91105AW, MAL# 980-69 NITROGEN
TION 5 STARTED 4/19/84 11:49 COMPLETED 4/20/84 9:30

SPECIFIC SURFACE AREA

BET SURFACE AREA:	828.2291	+/-	22.6326 SQ M/G
SLOPE:	0.005309	+/-	0.000142
INTERCEPT:	-0.000053	+/-	0.000020
C:	-98.3625		
VM:	190.2576 CC		

LANGMUIR SURFACE AREA:	1100.2694	+/-	2.4321 SQ M/G
SLOPE:	0.003956	+/-	0.000009
INTERCEPT:	0.000022	+/-	0.000001
A*PO:	176.2548		
VM:	252.7496 CC		

RELATIVE PRESSURE RANGE: 0.0500 TO 0.2100

MICROMERITICS INSTRUMENT CORPORATION

DIGISORB 2600 V2.02 PAGE 4
101

NDIA, 91105AW, MAL# 980-69 NITROGEN
ATION 5 STARTED 4/19/84 11:49 COMPLETED 4/20/84 9:30

DESORPTION ISOTHERM

MPLE WEIGHT: 0.1520 G EQUILIBRATION INTERVAL: 20 SECS
EE SPACE: 85.4236 CC MAX VOL INCREMENT: 100.000 CC/G STP

	P/PO	VOL ADSORBED (CC/G AT STP)
	0.9954	275.1337
	0.9851	274.5840
	0.9808	273.8284
	0.9748	273.7628
	0.9705	272.3120
	0.9608	271.9164
*	0.9491	272.7012
*	0.9388	271.9776
	0.9244	270.7366
	0.9025	270.6385
	0.8797	269.5884
	0.8518	269.0682
	0.8115	268.1942
	0.7648	267.3200
	0.7028	265.9844
	0.6326	264.2990
	0.5512	263.1208
	0.4531	253.3670
	0.3493	250.0758
	0.2001	245.2011
	0.1600	243.3006
	0.1196	240.3235
	0.0803	235.5281
	0.0563	230.3844
	0.0501	228.4806
	0.0448	226.6221
	0.0399	224.6282
	0.0307	220.1814

MICROMERITICS INSTRUMENT CORPORATION

DIGISORB 2600 V2.02 PAGE 5
101

IA, 91105AW, MAL# 980-69 NITROGEN
ION 5 STARTED 4/19/84 11:49 COMPLETED 4/20/84 9:30

DESORPTION PORE VOLUME AND PORE AREA DISTRIBUTIONS

PORE DIA. RANGE, A	AVERAGE DIA.,A	PORE VOLUME (CC/G)	CUMULATIVE PORE VOLUME	PORE AREA (SQ M/G)	CUMULATIVE PORE AREA
93.3-1322.5	1570.0	0.000882	0.000882	0.022	0.022
22.5-1030.2	1139.1	0.001266	0.002148	0.044	0.067
30.2- 790.4	876.7	0.000098	0.002246	0.004	0.071
90.4- 676.7	723.0	0.002505	0.004751	0.139	0.210
76.7- 515.2	572.5	0.000658	0.005409	0.046	0.256
15.2- 277.8	325.9	0.002108	0.007517	0.259	0.515
77.8- 214.0	234.9	0.000119	0.007636	0.020	0.535
14.0- 174.6	189.0	0.002089	0.009725	0.442	0.977
74.6- 142.8	154.5	0.001004	0.010729	0.260	1.237
42.8- 113.5	123.8	0.001813	0.012542	0.586	1.823
13.5- 91.5	99.1	0.001886	0.014428	0.761	2.584
91.5- 72.8	79.1	0.003128	0.017557	1.582	4.167
72.8- 58.8	63.4	0.004259	0.021816	2.688	6.854
58.8- 47.7	51.3	0.002881	0.024697	2.248	9.102
47.7- 38.5	41.3	0.032416	0.057113	31.374	40.476
38.5- 31.2	33.4	0.008452	0.065565	10.133	50.609
31.2- 23.8	25.6	0.013827	0.079392	21.579	72.188
23.8- 20.7	21.4	0.006486	0.085877	12.145	84.333
20.7- 18.9	19.5	0.012513	0.098390	25.699	110.032
18.9- 17.0	17.6	0.023672	0.122062	53.912	163.944
17.0- 15.5	15.9	0.028963	0.151026	72.750	236.694
15.5- 14.9	15.0	0.011311	0.162337	30.157	266.851
14.9- 14.5	14.6	0.011358	0.173695	31.019	297.870
14.5- 14.2	14.3	0.012402	0.186097	34.638	332.508

ALABS
105AW---980-1-CC10
TR NUMBER +746

LP 1:29:57 4/4/38
HP 2:40:27 4/4/38

LP EQUILIBRATION =	+10.0000 SEC	PNTR CONSTANT =	+10.7900 MICRO-L/PF
HP EQUILIBRATION =	+10.0000 SEC	THETA =	+130.0000
SAMPLE WEIGHT =	+0.1704 G	GAMMA =	+485.0000 DYNES/CM
PNTR WEIGHT =	+70.6266 G	INITIAL PRESSURE =	+1.3773 PSIA
NTR+SAMPLE WEIGHT =	+70.7970 G	STEM VOLUME =	+0.3840 CC
TR+SAMPLE+MERCURY =	+110.4990 G	MERCURY DENSITY =	+13.5335 G/CC
PNTR VOLUME =	+3.2159 CC		

TRUSION (PRESSURIZATION) DATA SUMMARY

TOTAL INTRUSION VOLUME =	+0.9174	CC/G
TOTAL PORE AREA =	+108.3760	SQ-M/G
DIAN PORE DIAMETER (VOLUME) =	+46.6054	MICROMETERS
DIAN PORE DIAMETER (AREA) =	+0.0045	MICROMETERS
AVERAGE PORE DIAMETER (4V/A) =	+0.0339	MICROMETERS
BULK DENSITY =	+0.6036	G/CC
APPARENT (SKELETAL) DENSITY =	+1.3526	G/CC

CAPILLARY = +40.7076

ABS
05AW---980-1-CC10
R NUMBER +746

LP 1:29:57 4/4/38
HP 2:40:27 4/4/38

PRESSURE PSIA	PORE DIAMETER MICRO-M	INTRUSION VOLUME CC/G	PORE SURFACE SQ-M/G	MEAN DIAMETER MICRO-M	DV
+1.4	+131.3150	+0.0000	+0.0000	+131.3150	+0.0000
+2.0	+89.1239	+0.0402	+0.0015	+110.2200	+0.0402
+3.0	+60.9564	+0.2196	+0.0110	+75.0401	+0.1794
+4.0	+45.5486	+0.4763	+0.0303	+53.2524	+0.2567
+5.5	+32.9604	+0.5490	+0.0377	+39.2544	+0.0727
+7.0	+25.9321	+0.5706	+0.0407	+29.4462	+0.0217
+8.4	+21.4300	+0.5784	+0.0420	+23.6810	+0.0077
+13.0	+13.9476	+0.5892	+0.0444	+17.6888	+0.0108
+16.0	+11.3245	+0.5939	+0.0459	+12.6360	+0.0047
+20.0	+9.0596	+0.5970	+0.0471	+10.1920	+0.0031
+22.9	+7.8823	+0.5985	+0.0478	+8.4709	+0.0016
+24.0	+7.5353	+0.5985	+0.0478	+7.7088	+0.0000
+29.1	+6.2244	+0.5985	+0.0478	+6.8798	+0.0000
+38.7	+4.6705	+0.5994	+0.0485	+5.4474	+0.0008
+49.3	+3.6706	+0.5994	+0.0485	+4.1705	+0.0000
+58.5	+3.0914	+0.5995	+0.0486	+3.3610	+0.0000
+73.6	+2.4575	+0.5995	+0.0487	+2.7744	+0.0001
+88.5	+2.0444	+0.6012	+0.0515	+2.2510	+0.0016
+113.9	+1.5681	+0.6028	+0.0552	+1.8163	+0.0017
+138.4	+1.3066	+0.6045	+0.0597	+1.4474	+0.0017
+173.4	+1.0432	+0.6062	+0.0655	+1.1749	+0.0017
+217.9	+0.8301	+0.6125	+0.0927	+0.9367	+0.0064
+267.0	+0.6773	+0.6236	+0.1512	+0.7537	+0.0110
+327.6	+0.5521	+0.6315	+0.2031	+0.6147	+0.0080
+417.4	+0.4333	+0.6535	+0.3816	+0.4927	+0.0220
+517.0	+0.3498	+0.6786	+0.6379	+0.3916	+0.0251
+636.1	+0.2843	+0.6960	+0.8575	+0.3171	+0.0174
+797.3	+0.2269	+0.7073	+1.0346	+0.2556	+0.0113
+983.8	+0.1838	+0.7156	+1.1954	+0.2053	+0.0083
+1197.7	+0.1510	+0.7223	+1.3561	+0.1674	+0.0067
+1394.0	+0.1297	+0.7259	+1.4571	+0.1404	+0.0035
+1590.4	+0.1137	+0.7294	+1.5723	+0.1217	+0.0035
+1890.3	+0.0957	+0.7330	+1.7119	+0.1047	+0.0037
+2289.8	+0.0790	+0.7383	+1.9542	+0.0873	+0.0053
+2624.7	+0.0689	+0.7403	+2.0534	+0.0738	+0.0020
+3017.2	+0.0599	+0.7439	+2.2856	+0.0644	+0.0036
+3481.6	+0.0519	+0.7475	+2.5422	+0.0559	+0.0036
+4011.7	+0.0451	+0.7511	+2.8372	+0.0485	+0.0036
+4622.7	+0.0391	+0.7562	+3.3228	+0.0421	+0.0051
+5412.5	+0.0334	+0.7582	+3.5491	+0.0363	+0.0021
+6172.5	+0.0293	+0.7617	+3.9548	+0.0314	+0.0035
+7096.4	+0.0255	+0.7668	+4.7309	+0.0274	+0.0050
+8169.3	+0.0221	+0.7702	+5.3139	+0.0238	+0.0035
+9495.6	+0.0190	+0.7752	+6.2971	+0.0206	+0.0050
+10866.6	+0.0166	+0.7817	+7.7414	+0.0178	+0.0065
+12535.6	+0.0144	+0.7862	+9.4078	+0.0155	+0.0045
+14413.2	+0.0125	+0.7962	+11.7740	+0.0135	+0.0100
+16797.6	+0.0108	+0.8057	+15.0376	+0.0117	+0.0095

LP 1:29:57 4/4/38
HP 2:40:27 4/4/38

AW---980-1-CC10
NUMBER +746

RESSURE PSIA	PORE DIAMETER MICRO-M	INTRUSION VOLUME CC/G	PORE SURFACE SQ-M/G	MEAN DIAMETER MICRO-M	DV
9122.3	+0.0095	+0.8120	+17.5497	+0.0101	+0.0064
2207.0	+0.0081	+0.8215	+21.8371	+0.0088	+0.0094
5187.4	+0.0072	+0.8293	+25.9257	+0.0077	+0.0078
9866.6	+0.0061	+0.8402	+32.5241	+0.0066	+0.0109
4918.4	+0.0052	+0.8557	+43.5633	+0.0056	+0.0155
9895.6	+0.0045	+0.8666	+52.4782	+0.0049	+0.0108
4813.3	+0.0040	+0.6789	+64.0017	+0.0043	+0.0123
9745.9	+0.0036	+0.8912	+76.8544	+0.0038	+0.0123
47E2.7	+0.0033	+0.9051	+92.8329	+0.0035	+0.0139
9715.3	+0.0030	+0.9174	+108.3760	+0.0032	+0.0123

3C4 -- 108 Å = 0.9174 - 0.8057 = 0.1117

diameters bigger than 144 Å = .624 cc/gm. This large pore volume corresponds to a cutoff radius of 44.6 μ.

Finally, the average diameter of the smallest pores (d < 14.2 Å) was chosen to match the carbon dioxide surface area for unreacted Spherocarb measured by D. Dudek of 1,118 m^2/gm. The complete pore size distribution for unreacted Spherocarb carbon appears on the following page.

Shrinkage at constant mass

Bounds on K_o for Spherocarb. $K_o = (1-\theta_o)/\theta_{so}$ as in the text or

$= V_c/V_s$ where V_c is .5 cc/gm and V_s is the small pore volume in cc/gm.

lower bound: pores are intact down to at least d = 100 nm which is the S.E.M. resolution limit under our conditions.

$V_s = .2394 + .1754 + (.7882 - .7294) = .4736$ cc/gm

$K_{min} = .5/.4736 = 1.056$

upper bound: rearrangements occur only in the smallest class of pores (d < 14.2 Å).

$V_s = .2394$ cc/gm

$K = .5/.2394 = 2.09$

Shrinkage via both pore elimination and pore narrowing

The expression for the effect of shrinkage at constant mass on area for the intermediate case where both pore elimination and pore narrowing are important was used in the section on the Simon's model but not given in the text. If f is the fraction of small pore volume loss occurring by pore elimination and (1-f) the fraction occurring by pore narrowing, then it can be shown by considering a two step

Complete Spherocarb Pore Size Distribution

Mean Radi (nm)	Incremental pore volume cc/gm
37520.07	0.0554
26626.25	0.2567
19627.25	0.0727
14723.12	0.0217
11840.52	0.0077
8844.4	0.0108
6318.025	0.0047
5096.025	0.0031
4235.475	0.0016
3854.4	0
3439.925	0
2723.725	0.0008
2085.275	0
1690.5	0
1387.225	0.0001
1125.475	0.0016
906.125	0.0017
723.675	0.0017
587.45	0.0017
468.325	0.0064
376.85	0.011
307.35	0.008
246.35	0.022
195.775	0.0251
158.525	0.0174
127.8	0.0113
102.675	0.0083
83.7	0.0067
70.175	0.0035
60.85	0.0035
52.35	0.0037
43.675	0.0053
36.975	0.002
32.2	0.0036
27.95	0.0036
24.25	0.0036
21.05	0.0051
18.125	0.0021
15.675	0.0035
13.7	0.005
11.9	0.0035
10.275	0.005
8.9	0.0065
7.75	0.0065
7.17	0
6.4075	0.001813

5.125	0.001886
4.1075	0.003128
3.29	0.004259
2.6625	0.002881
2.155	0.032416
1.7425	0.008452
1.375	0.013827
1.1125	0.006486
0.99	0.012513
0.8975	0.023672
0.8125	0.028963
0.76	0.011311
0.735	0.011358
0.7175	0.012402
0.397	0.2394

1.038967
total pore
volume cc/g

shrinkage process that

$$A_s/A_{so} = [V_s/V_{so} - f(V_s/V_{so})(1 - V_s/V_{so})]^{\frac{1}{2}}$$

Reaction and shrinkage: simple model

The effect of shrinkage at constant mass on surface area (A/A_o) is a function of the extent of shrinkage λ and the parameter K. In the simple model of reaction with concurrent shrinkage, the adjustment to the constant volume model area prediction due to shrinkage is a function of the extent of shrinkage λ and the value of the parameter K for the partially reacted carbon. This K can be related to K_o, the value of K for the unreacted material as follows.

$$K_o = V_{co}/V_{so}$$

for a constant volume reaction

$$V_s = V_{so} + V_{co}X, \text{ and } V_c = V_{co}(1-X)$$

and $$K = V_c/V_s = V_{co}(1-X)/(V_{so} + V_{co}X) = K_o(1-X)/(1 + K_oX)$$

Numerical solutions

The following expression

$$\Delta X = (R_p/R_{po})^3(\Delta\theta/(1 - \theta_o))$$

presented in the text for the incremental conversion as a function of the change in porosity during a constant volume reaction step was arrived at as follows.

$$\Delta X = X_2 - X_1 = (1 - m_2/m_o) - (1 - m_1/m_o) = (m_1 - m_2)/m_o$$

in each case $m = (4/3)\pi R^3\rho_{He}(1 - \theta)$

substitution yields, then, the final result above.

References

1. Von Fredersdorf C.G. and M.A. Elliott in "Chemistry of Coal Utilization" Supplemental Volume, (H.H. Lowry ed.) John Wiley and Sons Inc. N.Y. p. 969 (1963)

2. Hottel H.C. and Howard J.B., "New Energy Technology," MIT Press, Cambridge, MA pp.18-21 (1971)

3. Hottel and Howard, p.125

4. Von Fredersdorf, p.993

5. Von Fredersdorf, p.966

6. Nandi B.N., T.P. Brown, and G.K. Lee, Fuel 56 123 (1977)

7. Smith I.W., Fuel 57 409 (1978)

8. Nahas N.C., Fuel 62 239 (1983)

9. Essenhigh R.H., Chapter 19 in "Chemistry of Coal Utilization" Second Supp. Vol. (M.A. Elliott, ed.) John Wiley and Sons Inc. (1981)

10. Laurendeau N.M., Progress in Energy and Combustion Science 4 221 (1978)

11. Walker P.L.Jr., F. Rusinko Jr., and L.G. Austin, "Advances in Catalysis," Academic Press, New York 11 133-221 (1959)

12. Johnson J.L., Chapter 23 in "Chemistry of Coal Utilization" Second Supp. Vol. (M.A. Elliot, ed.) John Wiley and Sons Inc. (1981)

13. Mckee D.W. in "Chemistry and Physics of Carbon" (P.L. Walker Jr. ed.) Marcel Dekker, New York Vol 16 pp.1-118 (1981)

14. Walker P.L.Jr., L.G. Austin, and S.P. Nandi in "Chemistry and Physics of Carbon, (P.L. Walker Jr. ed.) Marcel Dekker Inc. Vol. 2 pp.257-371 (1966)

15. Spiro, C.L., D.W. McKee, P.G. Kosky, and E.J. Lamby Fuel 62 180 (1983)

16. Franklin R.E., Roy. Soc. of London Proc. Ser. A, 209 196 (1951)

17. Warren B.E., Phys. Review 59 9 693 (1941)

18. Franklin R.E., Acta Cryst. 3 107 (1950)

19. Cartz L. and P.B. Hirsch, Phil. Transactions 252 68 (1959)

20. Short M.A. and P.L. Walker Jr., Carbon 1 3 (1963)

21. Marsh H. and H.P. Stadler, Fuel 46 351 (1967)

22. Simons G.A. and M.L. Finson, Comb. Sci. and Tech. 19 217 (1979)

23. Walker P.L.Jr., F. Rusinko Jr., F. Rakszawski, and L.M. Liggett "Proceedings of the Third Conference on Carbon" Pergamon Press N.Y. p. 643 (1958)

24. Smith W.R. and M.H. Polley, J. Phys. Chem. 60 689 (1956)

25. Essenhigh R.H., p.1175

26. Walker P.L.Jr., F. Rusinko Jr., and L.G. Austin, in "Advances in Catalysis" Academic Press Inc., New York 11 p.205 (1959)

27. Snow C.W., D.R. Wallace, L.L. Lyon, and G.R. Crocker "Proceedings of the Fourth Conference on Carbon", Pergamon Press Ltd., N.Y. p. 79 (1960)

28. Blackwood J.D. and McGrory F., Aust. J. Chem. 11 16 (1958)

29. Blackwood J.D. and A.F. Ingeme, Aust. J. Chem. 13 194 (1960)

30. Blackwood J.D., Aust. J. Chem. 12 14 (1959)

31. Marsh H., and R.R. Adair, Carbon 13 327 (1975)

32. Amariglio H. and X. Duval, Carbon 4 323 (1966)

33. Floess J.K., Ph.D. Dissertation, Department of Chemical Engineering, Massachusetts Institute of Technology, Cambridge, MA (1986)

34. Radovic L.R., P.L. Walker Jr., and R.G. Jenkins, Fuel 62 209 (1983)

35. Adair R.R., E.H. Boult, E.M. Freeman, S. Jasienko, and H. Marsh Carbon 9 763 (1971)

36. Baker R.T.K. and J.J. Chludzinski Jr., Carbon 23 6 635 (1985)

37. Morgan M.E., R.G. Jenkins, and P.L. Walker Jr., Fuel 60 189 (1981)

38. Hippo E. and P.L. Walker Jr., Fuel 54 245 (1975)

39. Tomita A., O.P. Mahajan, and P.L. Walker Jr., ACS Div. Fuel Chem. Preprints 22 1 4 (1977)

40. Hippo E. and P.L. Walker Jr., Fuel 54 245 (1975)

41. Mahajan O.P. and P.L. Walker Jr., Fuel 58 333 (1979)

42. Yuh S.J. and E.E. Wolf, Fuel 62 253 (1983)

43. Mims C.A. and J.K. Pabst, Fuel 62 176 (1983)

44. Kapteijn F., J. Jurriaans, and J.A. Moulijn, Fuel 62 249 (1983)

45. Kapteijn F., O. Peer, and J.A. Moulijn, Fuel 65 1371 (1986)

46. Johnson J.L., Am. Chem. Soc. Div. Fuel Chemistry Preprints 20 (4) 85 (1975)

47. Radovic L.R., P.L. Walker Jr., and R.G. Jenkins Fuel 62 849 (1983)

48. Sevenster P.G., Fuel 38 403 (1959)

49. Nandi S.P. and P.L. Walker Jr., Fuel 43 385 (1964)

50. Ruthven D.M., Chapter 5 in "Principles of Adsorption and Adsorption Processes" John Wiley and Sons, p. 124 (1958)

51. Dutta S., C.Y. Wen, and R.J. Belt, Ind. Eng. Chem. Process Des. Dev. Vol. 16 1 (1977)

52. Radovic L.R., Ph.D. Thesis, Department of Materials Science and Engineering, The Pennsylvania State University (1982)

53. Walker P.L.Jr., Fuel 59 809 (1980)

54. Rist L.P. and D.P. Harrison, Fuel 64 291 (1985)

55. Kawahata M. and P.L. Walker Jr., Proc. Fifth Carbon Conf. Pergamon Press, New York Vol 2 p.251 (1963)

56. Gavalas G.R., AIChE Journal 26 4 577 (1980)

57. Simons G.A., Combustion. Sci. Tech. 19 227 (1979)

58. Hashimoto K. and P.L. Silveston, AIChE Journal 19 2 259 (1973)

59. Zygourakis K., L. Arrl, and N.R. Amundson, Ind. Eng. Chem. Fundam. 21 1 (1982)

60. Dudek D., Ph.D. Thesis in progress, Department of Chemical Engineering, Massachusetts Institute of Technology, Cambridge, MA

61. Culver R.V. and N.S. Heath, Faraday Soc. Trans. 51 1569 (1955)

62. Neavel R.C. in "Chemistry of Coal Utilization" Second Supp. Vol. (M.A. Elliott, ed.) John Wiley and Sons Inc., p.91 (1981)

63. Neavel. pp.113-121

64. Nandi B.N., T.P. Brown, and G.K. Lee, Fuel 56 125 (1977)

65. Stach E. ed., "Textbook of Coal Petrology" Third Edition Gebruder Borntraeger, Berlin pp.464-6 (1982)

66. Walker P.L. Jr., O. Cariaso, and R.L. Patel, Fuel 47 331 (1968)

67. Harris L.A. and C.S. Yust, Fuel 55 233 (1976)

68. Ergun S. and M. Mentser, Econ. Goel. 54 1068 (1959)

69. Helble J., Ph.D. Thesis, Department of Chemical Engineering, Massachusetts Institute of Technology, Cambridge, MA (1987)

70. Warnat M.J., Ph.D. Thesis in progress, Department of Chemical Engineering, Massachusetts Institute of Technology, Cambridge, MA

71. Hastings T., Ph.D. Thesis, Department of Chemical Engineering, Massachusetts Institute of Technology, Cambridge MA (1984)

72. Walker P.L.Jr. and K.A. Kini, Fuel 44 453 (1965)

73. Lamond T.G. and H. Marsh, Carbon 1 281 (1963)

74. Du Z., Ph.D. Thesis in progress, Department of Chemical Engineering, Massachusetts Institute of Technology, Cambridge MA (1984)

75. Dubinin M.M. in "Chemistry and Physics of Carbon" (P.L. Walker Jr. ed.) Marcel Dekker Inc., N.Y. pp.51-120 (1966)

76. Radovic, Dissertation, p.162

77. Satterfield C.N., "Mass Transfer in Heterogeneous Catalysis" Robert E. Krieger, Huntington, N.Y. p.140 (1970)

78. Simons G.A., Combustion and Flame 50, 275 (1983)

79. Pierce C., J.W. Wiley, and R. Nelson Smith, J. Phys. Chem. 53, 669 (1949)

80. Gregg S.J. and K.S.W. Sing, "Adsorption, Surface Area and Porosity" Second Edition, Academic Press, London (1982)

81. Hutcheon J.M. and B. Longstaff, Industrial Carbon and Graphite Conference, London p. 259 (1958)

82. Rand B. and H. Marsh, Carbon 9 79 (1971)

83. Austin J.G. and P.L. Walker Jr., AIChE Journal 9 303 (1963)

84. Tidjani M., J. Lachter, T.S. Kabre, and R.H. Bragg, Carbon 24 4 447 (1986)

85. Satterfield C.N., "Heterogeneous Catalysis in Practice" Mcgraw-Hill, New York, p.172 (1980)

86. Walker et al. in "Chemistry and Physics of Carbon" Vol.2 p.292

87. Sircar S., Carbon 19 153 (1981)

88. Niksa S., private communication, Spherocarb pore size distribution

89. Hippo E. and P.L. Walker Jr., Fuel 54 245 (1975)

90. Chiche P., S. Durif, and S. Pregermain, Fuel 44 5 (1965)

91. Wigmans T., K. Auwerda, J.W. Geus, and J.A. Moulijn, 15th Biennial Conference on Carbon, Extented Abstracts, Philadelphia p.441 (1981)

92. Radovic, Dissertation p.188

93. Jenkins, G.M., K. Kawamura, and L.L. Ban, Proc. Roy. Soc. A327, 501 (1972)

94. Oberlin A., Carbon 22 No.6 521-541 (1984)

95. Kawamura K. and R.H. Bragg, Carbon Vol. 24, No. 3 pp. 301-309 (1986)

96. Fishbach, D.B. in "Chemistry and Physics of Carbon" (P.L. Walker Jr. Ed.) Marcel Dekker, New York Vol. 7, pp. 1-70 (1971)

97. Bienenstock A., Proc. Int. Conf. 5th, 1, pp. 49-58 (1973)

98. Kaae J.L., Carbon Vol. 23, No.1, pp.39-43 1985

99. Kerstein A.R. and S. Niksa, 20th Symposium on Combustion p. 941 (1984)

100. Lachter J., L.G. Henry, and R.H. Bragg, J. Materials Research 1 6 832 (1986)

101. Bose S. and R.H. Bragg, Carbon 19 289 (1981)

102. Lamond T.G. and H. Marsh, Carbon 1 293 (1963)

103. Linares-Silano A., Mahajan O.P., and Walker P.L.Jr., Fuel 58 327 (1979)

104. Neavel R.C., p. 122